frontiers | Research Topics

Animal-derived foods: Authenticity and traceability, quality and safety control

Edited by
Hao Dong, Yan Zhao, Jinxuan Cao and Hongshun Yang

Published in
Frontiers in Nutrition

ISSN 1664-8714
ISBN 978-2-8325-2659-0
DOI 10.3389/978-2-8325-2659-0

About Frontiers

Frontiers is more than just an open access publisher of scholarly articles: it is a pioneering approach to the world of academia, radically improving the way scholarly research is managed. The grand vision of Frontiers is a world where all people have an equal opportunity to seek, share and generate knowledge. Frontiers provides immediate and permanent online open access to all its publications, but this alone is not enough to realize our grand goals.

Frontiers journal series

The Frontiers journal series is a multi-tier and interdisciplinary set of open-access, online journals, promising a paradigm shift from the current review, selection and dissemination processes in academic publishing. All Frontiers journals are driven by researchers for researchers; therefore, they constitute a service to the scholarly community. At the same time, the *Frontiers journal series* operates on a revolutionary invention, the tiered publishing system, initially addressing specific communities of scholars, and gradually climbing up to broader public understanding, thus serving the interests of the lay society, too.

Dedication to quality

Each Frontiers article is a landmark of the highest quality, thanks to genuinely collaborative interactions between authors and review editors, who include some of the world's best academicians. Research must be certified by peers before entering a stream of knowledge that may eventually reach the public - and shape society; therefore, Frontiers only applies the most rigorous and unbiased reviews. Frontiers revolutionizes research publishing by freely delivering the most outstanding research, evaluated with no bias from both the academic and social point of view. By applying the most advanced information technologies, Frontiers is catapulting scholarly publishing into a new generation.

What are Frontiers Research Topics?

Frontiers Research Topics are very popular trademarks of the *Frontiers journals series*: they are collections of at least ten articles, all centered on a particular subject. With their unique mix of varied contributions from Original Research to Review Articles, Frontiers Research Topics unify the most influential researchers, the latest key findings and historical advances in a hot research area.

Find out more on how to host your own Frontiers Research Topic or contribute to one as an author by contacting the Frontiers editorial office: frontiersin.org/about/contact

Animal-derived foods: Authenticity and traceability, quality and safety control

Topic editors

Hao Dong — Zhongkai University of Agriculture and Engineering, China
Yan Zhao — Chinese Academy of Agricultural Sciences (CAAS), China
Jinxuan Cao — Beijing Technology and Business University, China
Hongshun Yang — Jiangnan University (Shaoxing) Industrial Technology Research Institute, China

Citation

Dong, H., Zhao, Y., Cao, J., Yang, H., eds. (2023). *Animal-derived foods: Authenticity and traceability, quality and safety control*. Lausanne: Frontiers Media SA.
doi: 10.3389/978-2-8325-2659-0

Table of contents

04 Study on the physicochemical indexes, nutritional quality, and flavor compounds of *Trichiurus lepturus* from three representative origins for geographical traceability
Shitong Wang, Pingya Wang, Yiwei Cui, Weibo Lu, Xuewei Shen, Huimin Zheng, Jing Xue, Kang Chen, Qiaoling Zhao and Qing Shen

17 Origin of static magnetic field induced quality improvement in sea bass (*Lateolabrax japonicus*) during cold storage: Microbial growth inhibition and protein structure stabilization
Li Tong, Haiqing Tang, Jingyi Chen, Shangyuan Sang, Ruiping Liang, Zhepeng Zhang and Changrong Ou

31 Real-time qPCR for the detection of puffer fish components from *Lagocephalus* in food: *L. inermis*, *L. lagocephalus*, *L. gloveri, L. lunaris*, and *L. spadiceus*
Xinying Yin, Ranran Xing, Zhiru Li, Bing Hu, Lili Yang, Ruijie Deng, Jijuan Cao and Ying Chen

43 Biological function, mediate cell death pathway and their potential regulated mechanisms for post-mortem muscle tenderization of PARP1: A review
Rong Li, Ruiming Luo, Yulong Luo, Yanru Hou, Jinxia Wang, Qian Zhang, Xueyan Chen, Lijun Hu and Julong Zhou

54 Effects of hydrodynamic cavitation on physicochemical structure and emulsifying properties of tilapia (*Oreochromis niloticus*) myofibrillar protein
Yucheng Hou, Xian'e Ren, Yongchun Huang, Kun Xie, Keyao Wang, Liyang Wang, Fengyan Wei and Feng Yang

65 Geographical traceability of gelatin in China using stable isotope ratio analysis
Shuang Li, Di Jiang, Jinglin Li, Yuhua Ma, Jian Yao, Lin Du, Yisheng Xu and Yuan Qian

73 Effect of compound dietary fiber of soybean hulls on the gel properties of myofibrillar protein and its mechanism in recombinant meat products
Song-Shan Zhang, Jun-Ya Duan, Teng-Teng Zhang, Meng Lv and Xiao-Guang Gao

82 Rise and metabolic roles of *Vibrio* during the fermentation of crab paste
Tian-Han Xiong, Ce Shi, Chang-Kao Mu, Chun-Lin Wang and Yang-Fang Ye

91 Effects of donkey milk on UVB-induced skin barrier damage and melanin pigmentation: A network pharmacology and experimental validation study
Anqi Li, Hailun He, Yanjing Chen, Feng Liao, Jie Tang, Li Li, Yumei Fan, Li Li and Lidan Xiong

103 Improvement of muscle quality in tilapia (*Oreochromis niloticus*) with dietary faba bean (*Vicia faba* L.)
Qingqing Li, Yao Huang, Xingqian Zhang, Cuiyun Zou and Li Lin

frontiers | Frontiers in Nutrition

TYPE Original Research
PUBLISHED 01 November 2022
DOI 10.3389/fnut.2022.1034868

OPEN ACCESS

EDITED BY
Yan Zhao,
Chinese Academy of Agricultural Sciences (CAAS), China

REVIEWED BY
Yongkang Luo,
China Agricultural University, China
Lei Qin,
Dalian Polytechnic University, China

*CORRESPONDENCE
Kang Chen
chenkangfood@163.com
Qiaoling Zhao
zs_qlzhao@163.com
Qing Shen
leonqshen@163.com;
sq@zjgsu.edu.cn

†These authors have contributed equaly to this work

SPECIALTY SECTION
This article was submitted to Food Chemistry, a section of the journal Frontiers in Nutrition

RECEIVED 02 September 2022
ACCEPTED 13 October 2022
PUBLISHED 01 November 2022

CITATION
Wang S, Wang P, Cui Y, Lu W, Shen X, Zheng H, Xue J, Chen K, Zhao Q and Shen Q (2022) Study on the physicochemical indexes, nutritional quality, and flavor compounds of *Trichiurus lepturus* from three representative origins for geographical traceability. *Front. Nutr.* 9:1034868. doi: 10.3389/fnut.2022.1034868

Study on the physicochemical indexes, nutritional quality, and flavor compounds of *Trichiurus lepturus* from three representative origins for geographical traceability

Shitong Wang[1†], Pingya Wang[2†], Yiwei Cui[1], Weibo Lu[1], Xuewei Shen[1], Huimin Zheng[1], Jing Xue[1], Kang Chen[1*], Qiaoling Zhao[2*] and Qing Shen[1*]

[1]Collaborative Innovation Center of Seafood Deep Processing, Zhejiang Province Joint Key Laboratory of Aquatic Products Processing, Institute of Seafood, Zhejiang Gongshang University, Hangzhou, China, [2]Zhoushan Institute of Food & Drug Control, Zhoushan Institute of Calibration and Testing for Quality and Technology Supervision, Zhoushan, China

Trichiurus lepturus (hairtail) is an important economic component of China's marine fishing industry. However, due to the difficulty in identifying the appearance of hairtail from different geographical distributions, hairtails with geographical indication trademarks were imitated by general varieties. In this study, the texture characteristics, color, basic nutrients, amino acids, mineral, fatty acids, and volatile flavor substances were used as indicators for multivariate statistical analysis to determine whether three origins of hairtails from the habitats of Zhoushan (East China Sea, T.Z), Hainan (South China Sea, T.N), and Qingdao (Yellow Sea, T.Q) in the market could be distinguished. The findings revealed that there were significant differences in amino acids composition, mineral composition, fatty acid composition in lipids, and volatile flavor substances among the hairtails of three origins ($P < 0.05$), but no differences in color, texture, protein content. T.Z had moisture, crude fat, essential amino acids (EAA), flavor amino acids (FAA), unsaturated fatty acids (UFA), and docosahexaenoic acids and dicosapentaenoic acids (ΣEPA + DHA) contents of 74.33, 5.4%, 58.25 mg·g^{-1}, 46.20 mg·g^{-1}, 66.84 and 19.38%, respectively, and the contents of volatile alcohols, aldehydes and ketones were 7.44, 5.30, and 5.38%, respectively. T.N contains moisture, crude fat, EAA, FAA, UFA and ΣEPA + DHA as 77.69, 2.38%, 64.76 mg·g^{-1}, 52.44 mg·g^{-1}, 65.52 and 29.45%, respectively, and the contents of volatile alcohols, aldehydes and ketones as 3.21, 8.92, and 10.98%, respectively. T.Q had the contents of moisture, crude fat, EAA, FAA, UFA, and ΣEPA + DHA 79.69, 1.43%, 60.9 mg·g^{-1}, and 49.42 mg·g^{-1}, respectively. The contents of unsaturated fatty acid and ΣEPA + DHA were 63.75 and 26.12%, respectively, while the volatile alcohols, aldehydes, and ketones were 5.14, 5.99, and 7.85%,

respectively. Partial least squares-discriminant analysis (PLS-DA) multivariate statistical analysis showed that volatile flavor compounds could be used as the most ideal indicators for tracing the source of hairtail. In conclusion, the findings of this study can distinguish the three hairtail origins using some basic indicators, providing ideas for hairtail geographical identification.

KEYWORDS

***Trichiurus lepturus*, geographical traceability, nutritional components, fatty acid, volatile flavor substances**

Introduction

Under the pressure of high intensity fishing and the global decline of marine fishery resources, Chinese *Trichiurus lepturus* (hairtail) has maintained high yield, ranking first in the output of single species of marine fishing in China. According to a World Food and Agriculture Organization (FAO) statistical survey, the average annual output of the world's hairtail from 2005 to 2016 was as high as 1.31 million tonnes, with approximately 80 percent caught in China's oceans.

Chinese hairtail is distributed in the Yellow Sea, East China Sea, Bohai Sea and South China Sea, among which Zhoushan hairtail (*Trichiurus japanicus*, T.Z) in the East China Sea, Qingdao hairtail (*Trichiurus japanicus*, T.Q) in the Yellow Sea and Nanhai hairtail (*Trichiurus nanhaiensis*, T.N) in the South China Sea are the most prevalent in the market in China. China's sea area is vast and the water quality conditions such as temperature, salinity, water mass, dissolved oxygen, substrate type, and feed organisms, varies from sea to sea, so the quality of hairtail caught in different sea areas will also vary (1). The population of T.Z is distributed along the mixed waters of the coastal water system, the Taiwan warm current, and the Yellow Sea cold water mass, and the continuous injection of continental current brings a large amount of plankton and seawater nutrients to the habitat. Taking these factors into account, T.Z have been considered preferable in fish quality and taste compared to those from other regions, and it has become the owner of China's first seafood geographical indication certification trademark. However, due to the morphology of hairtail is complex and changeable, and the differences in fishing season, location, growth stage and sample specifications, the morphological identification may get wrong results. In addition, the commercial hairtail is mostly sold in the form of a segment, which further aggravates the difficulty of traceability of hairtail. This phenomenon can lead to seafood fraud, and the consequences of intentional species substitution and mislabeling may lead to some illegal profiting behaviors (2), which damages the interests of consumers. Therefore, necessitating research into product-specific and generic analytical fish product traceability systems (3).

There have been some detecting methods established for authenticating seafood traceability and identificating seafood mislabeling and fraud. Emerging techniques for seafood authentication include polymerase chain reaction-restriction fragment length polymorphism (PCR-RFLP), real-time PCR, droplet digital PCR, isothermal amplification, PCR-enzyme-linked immunosorbent assay (ELISA), and high-throughput or next-generation sequencing (4, 5). However, the classification accuracy would be unpredictable for genotypic methods due to the DNA contamination or analytes complexity. Recently, lipidomics method has been proven to be an effective tool for seafood provenance due to the unique lipid profile of each source organism (6). Yu et al. reported that lipidomics fingerprints, detected by hydrophilic interaction chromatography/mass spectrometry (HILIC/MS), of rainbow trout and two salmons were distinct and specific (7). Lu et al. established an *in situ* and real-time authentication method that used iKnife rapid evaporative ionization mass spectrometry (REIMS) based lipidomics for distinguishing the seven shrimp species (8). Electronic-nose (e-nose) sensor technology have been primarily used for the purposes of detection, discrimination and recognition of simple and complex gaseous mixture, which has great potential in the application of seafood traceability. Karunathilaka et al. evaluated an e-nose sensor in combination with support vector machine (SVM) modeling for predicting the decomposition state of four types of shllets (9). Wu et al. conducted qualitative and quantitative analyses of flavor substances in fresh hairtail, traditional, and fermented dried hairtail using an electronic nose and headspace solid-phase microextraction (HS-SPME-GC-MS) (10). However, detection instruments for these technology are expensive and not easy to get access, moreover, the data analysis is time-consuming. The solution to the traceability problem of hairtail caught from different sources in the Chinese market has not been reported. There are currently no relevant reports that distinguish different regions hairtail based on basic biological and chemical parameters.

In this study, three different geographic groups of hairtail, including T.Q, T.Z, and T.N were collected and their textural characteristics, color, nutritional components, amino

and volatile flavor substances were compared to obtain a comprehensive and systematic understanding of the basic characteristics and nutritional values of hairtail from different origins. Besides, the classification ability of these indicators for the three origin hairtail was compared by multivariate statistical analysis, providing the optimal ideas for tracing to the source of fishing.

Materials and methods

Materials and reagents

As shown in **Figure 1**, in order to ensure the authenticity of the hairtail, all the hairtail purchased in this experiment were complete hairtail transported by the cold chain. Zhoushan hairtail was purchased from the aquatic products business department of Zhoushan Putuo Jimei (Zhoushan, Zhejiang). Qingdao Hengjie Agricultural Products Co., Ltd. supplied Qingdao hairtail (Qingdao, Shandong). Hainan hairtail was bought from Hainan Wanyue Trading Co., Ltd. (Haikou, Hainan). Merck provided chromatography-grade acetonitrile, chloroform, and methanol (Darmstadt, Germany). Anpel Laboratory Technologies Inc. provided the standard mixture of 37 fatty acid methyl esters (FAMEs) (Shanghai, China). Sinopharm Chemical Reagent Co., Ltd. provided the other analytical grade chemicals and solvents (Shanghai, China).

Determination of color difference value

A Hunter Lab colorimeter was used to measure the fish color difference values (Lab value) of hairtail lateral lines in the front, middle, and back positions (Colorquest II, Hunter Associates Laboratory Inc., Reston, VA, USA). The hairtail were dissected and skinned, and the muscles (3 × 3 × 2 cm) above the fish's anterior, middle, and posterior lateral lines were cut to measure the color difference (Lab value), with the average value of the three parts used as the result.

FIGURE 1
External morphology of three origin hairtail.

Texture profile analysis

Texture profile analysis (TPA) was performed with a texture analyzer (TA-XT2i, Stable Micro System, UK) and a TMS P5 flat bottom cylindrical probe, and the samples' norm was 2 × 2 × 2 cm above the lateral line. Pre-test rate was 1 mm·s^{-1}; test rate was 1 mm·s^{-1}; post-test rate was 1 mm·s^{-1}; deformation rate was 60%; time internal was 5 s; initial test force was 0.01 N; data collection rate was 200 pps. Parallel experiments were carried out with six fish tails per group.

Determination of water, ash, mineral, crude protein, crude fat, and amino acid contents

Muscle water content was determined using the direct drying method, as specified in GB5009.3–2016. The ash content was determined in accordance with GB5009.4–2016, using the muffle furnace burning method. The crude protein content was determined using an automatic Kjeldahl nitrogen analyzer in accordance with GB5009.5–2016. Soxhlet extraction method for determining crude fat content in accordance with GB5009.6–2016. Mineral content was determined using inductively coupled plasma optical emission spectroscopy (ICP-OES) in accordance with GB5009.268–2016, and the dry digestion method was used for pretreatment. The hydrolysis amino acid method was used to determine the amino acid content in accordance with GB 5009.124–2016.

Analysis of fatty acids

A modified Folch method (11) was used to extract lipids. In a nutshell, 10 g of minced fish was accurately weighed and distributed in a mixture of chloroform and methanol (30 mL, 2:1, v/v) and distilled water (10 mL), which was then immersed in sonication (53 Hz, 350 W) for 20 min at room temperature. The mixture was then separated into two phases by centrifugation at 8000 rpm for 10 min (Thermo Scientific, Waltham, MA, USA). To remove organic reagents and obtain crude lipids, the lower organic phase was rotary evaporated at 70°C.

Fatty acid methyl esters (FAMEs) were created by esterifying crude lipids (12). In particular, 0.1 g of fish oil was precisely weighed and mixed with a 5 mL potassium hydroxide-methanol solution in a stoppered test tube at 65°C for 20 min. After naturally cooling to room temperature, boron trifluoride-methanol (700 μL, 55–60%) was added to shake at 65°C water bath for 3 min before being removed and naturally cooled to room temperature after 10 min of ultrasonication. The mixture was then extracted and washed with hexane (2 mL) and saturated sodium chloride solution (2 mL). After standing

the layers, the supernatant was aspirated, and a small amount of anhydrous sodium sulfate was added to remove the water. For gas chromatography, the supernatant was filtered through a 0.22 μm organic filter (GC).

The FAMEs were analyzed using an Agilent model 7890A capillary GC instrument with an HP-88 capillary column (Agilent Technologies Co. Ltd., Santa Clara, CA, USA) (100% cyanopropyl polysiloxane; 30 m × 0.25 mm, 0.2 μm membrane, Agilent Technologies Co. Ltd). Each time, high-purity nitrogen was used as the carrier gas, with a flow rate of 0.65 mg·min^{-1} and a sample volume of 1 μL. The temperature of the flame ionization detector (FID) was set to 250°C, and a gradient heating procedure was used. The temperature was set to 25°C for 5 min, then ramped to 120°C at a rate of 15°C per minute for 1 min, then to 175°C at a rate of 5°C per minute for 5 min, and finally to 220°C in 5 min and held for 5 min (7).

Determination of flavor substances

The volatile compounds in the three samples were analyzed using a headspace solid-phase microextraction gas chromatography-mass spectrometry (HS-SPME-GC/MS) with a TR-35MS elastic capillary column (30 m × 0.25 mm I.D., 0.25 μm film, Agilent Technologies Co. Ltd., DE, USA). The 4 g sample was placed in a 15 mL headspace vial and balanced in a water bath at 60°C for 20 min. The volatile was then adsorbed for 30 min with a divinylbenzene/carboxyl/polydimethylsiloxane (DVB/CAR/PDMS) extraction head and desorbed in a syringe (250°C, 1 min) at a flow rate of 1 mg·min^{-1} of helium (99.99%). The gradient procedure was set as follows: the initial temperature was 40°C, which was maintained for 3 min, then increased to 90°C at 5°C·min^{-1} which was maintained for 7 min, then continuously increased to 230°C at 20°C·min^{-1} which was maintained for 7 min. Electron bombardment ionization mode 70 eV, source temperature 250°C, interface temperature 280°C, and mass scanning range 33–450 m/z were the mass spectrometry conditions. Quantitative analysis with peak area normalization was used to calculate the relative content of each chemical component.

Statistical analysis

The experimental data were imported into Microsoft Excel 2016 (Microsoft Corp., Redmond, WA, USA), mean and standard deviation analysis were performed using SPSS version 26 (SPSS Inc., Chicago, IL, USA) that corresponding figures were drawn using OriginPro 2021 (OriginLab Corp., Northampton, MA, USA), and multivariate statistical analysis were processed at https://dev.metaboanalyst.ca/MetaboAnalyst/. When the difference was analyzed using one-way ANOVA, normality, equal variance, and *post hoc* Duncan's multiple range tests, $P < 0.05$ was considered statistically significant.

Results and discussion

Color

The color of fish is the result of long-term natural selection and adaptation to the ecological environment, and it is an essential criterion for assessing the freshness, quality, and acceptability of fish (13). Color can be used to identify hairtail in different sea areas and reflect the variation of their habitat environment to some extent. Therefore, the color of hairtail was studied, and the findings are shown in **Table 1**. The values of lightness (L*), redness (a*), and yellowness (b*) were obtained by employing a colorimeter with the aim of defining the surface color of the muscle sample. T.Q had the highest L* value (52.33) among these three hairtail samples, which was significantly higher ($P < 0.05$) than that of T.N. This could be explained by the high water content (79.64%) of muscle above the lateral-line of T.Q. Although T.Z has the lowest moisture content (74.81%) of the three hairtail samples, its high levels of oil content (5.38%) increased the intensity of light reflection from the muscle surface, which can explain why there is no statistically significant ($P > 0.05$) difference in the brightness of T.Z moisture. The a* values of hairtails were on a negative scale ranging from –1.71 (T.Z, control) to –1.52 (T.N, control), and the effect of sample origin was not statistically significant ($P > 0.05$). When compared to T.Z (4.44), the b* values of T.N (3.98) and T.Q (3.87) decreased significantly ($P < 0.05$). This variation could be attributed to the higher fat content of T.Z-fed nutrients, which promotes the absorption of pigments like astaxanthin and lutei (14, 15). Finally, the above findings demonstrated that the color of fish is not only determined primarily by genetic genes but is also closely related to its living environment and nutritional status.

TPA

TPA is a compression method that is widely used in the determination of food texture, which is an important index

TABLE 1 The color parameters of hairtails of the three origins.

Samples	L*	a*	b*
T.Z	51.52 ± 1.27^{ab}	-1.71 ± 0.13^{a}	4.44 ± 0.20^{a}
T.N	49.72 ± 0.99^{b}	-1.52 ± 0.11^{a}	3.98 ± 0.16^{b}
T.Q	52.33 ± 1.15^{a}	-1.68 ± 0.11^{a}	3.87 ± 0.13^{b}

$^{a-c}$Mean values in the same column (corresponding to the same parameter) not followed by a common letter differ significantly ($P < 0.05$). T.Z, Zhoushan hairtail; T.N, Hainan hairtail; T.Q, Qingdao hairtail.

TABLE 2 Texture profile analysis of three type hairtail.

Samples	T.Z	T.N	T.Q
Hardness (N)	5.16 ± 1.14^{a}	4.34 ± 0.70^{a}	5.83 ± 1.86^{a}
Cohesiveness (Ratio)	0.44 ± 0.03^{a}	0.32 ± 0.03^{b}	0.38 ± 0.07^{ab}
Springiness (mm)	6.72 ± 0.97^{a}	7.64 ± 0.81^{a}	5.55 ± 0.37^{b}
Gumminess (N)	2.24 ± 0.53^{ab}	1.36 ± 0.25^{b}	2.53 ± 1.11^{a}
Chewiness (mJ)	13.77 ± 3.32^{a}	9.87 ± 1.87^{a}	12.32 ± 3.91^{a}

$^{a-c}$Mean values in the same row (corresponding to the same parameter) not followed by a common letter differ significantly ($P < 0.05$). T.Z, Zhoushan hairtail; T.N, Hainan hairtail; T.Q, Qingdao hairtail.

for assessing fish freshness and sensory quality. Its theory is to simulate the occlude action of the human mouth cavity by squeezing the sample twice with the texture analyzer probe, hence the name "Two-bite test" (16). The advantage was that it could record the correlation between time and force using mechanical experiments on hairtail samples and obtain multiple physical properties at once, such as hardness, springiness, gumminess, and chewiness, as shown in Table 2. T.Q lump had the highest hardness (5.83 N) compared to T.Z (5.16 N) and T.N (4.34 N), but sea area difference had no significant ($P > 0.05$) effect on the hardness of these hairtails. This result was consistent with the findings of Ayala (17) that hairtail movement ability was similar in the three living environments, resulting in similar muscle fiber diameter and arrangement, and then similar hardness in macroscopically. When it comes to cohesiveness, there were differences in the binding ability between muscle cells due to the three origin hairtail' homologous motor ability, which revealed that the cohesiveness of T.Z sample (0.44) was slightly better than that of T.Q sample (0.38), but this advantage is not obvious. In the term of springiness, sample T.Q (5.55 mm) was weaker ($P < 0.05$) than samples T.Z (6.72 mm) and T.N (7.64 mm). Springiness is the deformation of a sample caused by an external force that is restored after the force is removed. Among the three main components of fish (myofibrillar protein, sarcoplasmin, and myostromal protein), the myofibrillar protein contains a lot of actin and myosin, and the myostromal protein has a lot of elastin which affects the springiness of hairtail. Gumminess is the property of being cohesive and sticky, whereas chewiness is the sensory "bite" that is positively related to taste. Protein, moisture, and fat content all have an impact on the texture of fish. The higher the fat content of fish, the more chewable it is.

Nutrition

Figure 2 depicts the basic nutrient composition values recorded for various hairtail samples. It is worth noting that the moisture and crude lipid content of the hairtail samples differed significantly. T.Q had the highest moisture percentage (79.69%).

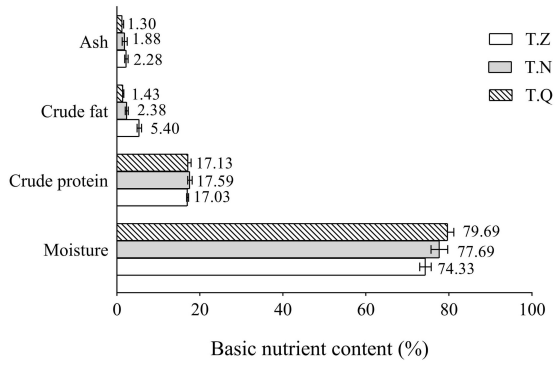

FIGURE 2
Hairtail muscle nutrient content from three different sources.

T.Z had the highest ash content (2.28%). The three samples had approximative protein percentages (17.03–17.59%). The protein content is thought to be determined by the species' genetic characteristics and unaffected by diet (18). The crude lipid content of hairtail was highest in T.Z (5.40%), followed by T.Q (2.38%), while lowest in T.Q. (1.43%). Normally, increased fat in the fish causes a decrease in moisture content (19), so it seems reasonable to assume that the real differences between the three hairtail were primarily due to fat content variability. T.Z were fatter, whereas the other hairtail were leaner, with the former being preferred by the general consumer due to the great taste and high nutritional qualities found in fat fish.

Amino acid

Amino acid content and composition are critical indicators for determining the nutritional value of proteins in foods (20). Table 3 shows the composition of 17 amino acids detected after acid hydrolysis of fish from three sources, with the exception of tryptophan, which was not detected because it is completely destroyed during protein acid hydrolysis. There were four flavor amino acids detected (aspartic acid, glutamate, glycine, alanine), seven essential amino acids detected (threonine, valine, methionine, phenylalanine, isoleucine, leucine, lysine), three half-essential amino acids detected (histidine, arginine, cystine), and three non-essential amino acids detected (serine, tyrosine, proline). T.N had a higher total amino acid content of 160.65 $mg{\cdot}g^{-1}$ than T.Q (141.41 $mg{\cdot}g^{-1}$) and T.Z (150.02 $mg{\cdot}g^{-1}$).

T.N had the highest essential amino acid content (64.76 $mg{\cdot}g^{-1}$), half-essential amino acid content (24.56 $mg{\cdot}g^{-1}$), umami amino acid content (52.44 $mg{\cdot}g^{-1}$), and non-essential amino acid content (64.08 $mg{\cdot}g^{-1}$) when compared to the other two hairtail samples. Despite being geographically diverse, the ratio of essential amino acids to

TABLE 3 The amino acids composition in muscle of hairtail (mg·g^{-1}).

Amino acid	T.Z	T.N	T.Q
Threonine+	6.06	6.82	6.30
Valine+	5.93	6.60	6.12
Methionine+	6.26	7.00	6.58
Isoleucine+	6.96	7.54	7.30
Leucine+	14.48	15.82	15.04
Phenylalanine+	6.16	7.08	6.60
Lysine+	12.40	13.90	12.96
Histidine*	3.12	3.64	3.30
Arginine*	17.56	20.92	18.98
Aspartic Acid^&	12.84	14.54	13.58
Glutamate^&	20.28	22.12	21.94
Glycine^&	5.32	7.00	5.70
Alanine^&	7.76	8.78	8.20
Proline&	4.10	4.82	4.54
Serine&	5.84	6.82	6.20
Cystine	0.10	0.14	0.10
Tyrosine	6.24	7.02	6.58
ΣTAA	141.41	160.56	150.02
ΣEAA	58.25	64.76	60.90
ΣHEAA	20.68	24.56	22.28
ΣFAA	46.20	52.44	49.42
ΣNEAA	56.14	64.08	60.16
EAA/TAA	0.41	0.40	0.41
EAA/(HEAA + NEAA)	0.76	0.73	0.74
FAA/TAA	0.33	0.33	0.33

+ Means essential amino acids (EAA); * means half-essential amino acids (HEAA); ^ means flavor amino acids (FAA); & means non-essential amino acids (NEAA). TAA, total amino acids; T.Z, Zhoushan hairtail; T.N, Hainan hairtail; T.Q, Qingdao hairtail.

total amino acids in these hairtail samples was close to 0.41, which was consistent with the discovery of Xu et al. (21). in Zhoushan hairtail muscle and fully conformed to FAO/WHO standard requirements (nearly 0.40). The essential amino acid to non-essential amino acid ratio ranged from T.N (0.73) to T.Q (0.76), which was higher than the FAO/WHO reference protein value of greater than 0.60. In flavor amino acids, glutamic acid and aspartic acid were the most umami, with glutamic acid being the most umami in particular, whereas glycine and alanine were the sweetest. T.N sample had a higher content of flavorful amino acids (52.44 mg·g^{-1}), with 20.12 mg·g^{-1} glutamate. However, the ratio of flavorful amino acids to total amino acids of the three hairtail samples was 0.33, indicating that these hairtail had a consistent sense of delicious taste.

Table 4 shows the amino acid score (AAS), chemical score (CS), and essential amino acid score (EAAI) calculated and evaluated using the FAO/WHO amino acid scoring standard model and the egg protein scoring standard model. According to the AAS model, the first limiting amino acid in hairtail muscle samples was valine, and the second limiting amino acid was threonine; similarly, the first and second limiting amino acids in hairtail muscle samples were valine and methionine + cystine, respectively. In other words, the valine, threonine, methionine, and cystine in hairtail muscle protein were deficient when compared to other essential amino acids. T.Z [72.68 mg·(g·pro)$^{-1}$], T.N [78.93 mg·(g·pro)$^{-1}$], and TQ [75.52 mg·(g·pro)$^{-1}$] had slightly higher lysine content than egg protein mode [70 mg·(g·pro)$^{-1}$], but significantly higher than FAO/WHO mode [55 mg·(g·pro)$^{-1}$]. Because lysine is the first limiting amino acid in wheat, corn, and other cereals, eating hairtail can compensate for the lack of lysine, greatly improving protein digestion and absorption (16). T.N (82.72) had a higher EAAI value than T.Z (76.95) and T.Q (79.84), indicating that the overall essential amino acids in T.N protein were more in line with human nutritional requirements, which may be influenced by physiological state, culture environment, water area, and water salinity. Except for the first and second limiting amino acids, the AAS value of essential amino acids was all greater than one, demonstrating that the essential amino acid composition of these three origin hairtail was in a suitable proportion and the nutritional value was abundant.

TABLE 4 Essential amino acid content, AAS, CS, and EAAI in hairtail muscle (mg·(g·pro)$^{-1}$).

EAA	FAO/WHO pattern	Egg protein pattern	T.Z	T.N	T.Q	AAS			CS		
						T.Z	T.N	T.Q	T.Z	T.N	T.Q
Isoleucine	40.00	54.00	40.80	42.82	42.54	1.02	1.07	1.06	0.76	0.79	0.79
Leucine	70.00	86.00	84.88	89.84	87.65	1.21	1.28	1.25	0.99	1.04	1.02
Lysine	55.00	70.00	72.68	78.93	75.52	1.32	1.44	1.37	1.04	1.13	1.08
Methionine + Cystine	35.00	57.00	37.28	40.55	38.93	1.07	1.16	1.11	0.65	0.71	0.68
Phenylalanine + Tyrosine	60.00	93.00	72.68	80.07	76.81	1.21	1.33	1.28	0.78	0.86	0.83
Threonine	40.00	47.00	35.52	38.73	36.71	0.89	0.97	0.92	0.76	0.82	0.78
Valine	50.00	66.00	34.78	37.45	35.64	0.70	0.75	0.71	0.53	0.57	0.54
EAAI			76.95	82.72	79.84						

T.Z, Zhoushan hairtail; T.N, Hainan hairtail; T.Q, Qingdao hairtail.

Mineral substance

Table 5 shows the concentrations of 12 essential mineral elements found in the muscle of hairtail. According to Afonso et al. (22) and Biandolino et al. (23), potassium, sodium, and phosphorus are the macrominerals with the highest concentrations in the three hairtail samples. In terms of the macroelements studied, potassium (3137.22 mg·kg^{-1}), sodium (1633.34 mg·kg^{-1}), and phosphorus (801.19 mg·kg^{-1}) concentrations were significantly higher in T.N than in the other two varieties. T.Z (243.31 mg·kg^{-1}) and T.N (296.17 mg·kg^{-1}) had the lowest and highest calcium concentrations, respectively. Potassium is the most abundant intracellular ion in fish and is essential for fish physiology (e.g., muscle function and membrane potential) (24). These hairtail have a diverse diet, feeding on everything from plankton crustaceans to swimming animals, allowing them to accumulate minerals from a variety of sources. Plankton, for example, is expected to be a good source of phosphorus for upper trophic levels, whereas crustaceans and fish, respectively, are good sources of calcium and potassium (22, 25). Iron (37.63–26.36 mg·kg^{-1}) and zinc (3.74–3.60 mg·kg^{-1}) had the highest concentrations of the microelements studied. Copper was the least abundant mineral studied, with 0.35 mg·g^{-1} (T.Z), 0.32 mg·kg^{-1} (T.N), and 0.27 mg·kg^{-1} (T.Q), respectively. Mineral content differences in hairtail of different source have been attributed to a combination of specific characteristics and physiological requirements, diet composition, and mineral bioavailability in the surrounding environment (water and sediments) (26).

TABLE 5 Mineral content of three hairtail muscles (mg·kg^{-1}, w/w).

Parameter		T.Z	T.N	T.Q
Macroelement	K	2881.55	3137.22	2660.89
	P	1552.86	1633.34	1269.69
	Na	679.99	801.19	571.80
	Mg	296.68	263.93	208.48
	Ca	253.41	296.17	243.31
Microelement	Fe	26.36	37.63	24.55
	Zn	3.60	3.66	3.74
	Al	1.96	1.01	2.11
	As	1.93	2.64	1.57
	Sr	1.48	0.54	0.79
	Cr	0.81	0.85	0.72
	Cu	0.35	0.32	0.27

T.Z, Zhoushan hairtail; T.N, Hainan hairtail; T.Q, Qingdao hairtail.

Fatty acid composition

The fatty acyl composition of the three hairtail samples was investigated to determine the effect of origin on fatty acid selectivity. The FAMEs were analyzed by GC after esterification; the characteristic chromatogram of each fatty acid molecular species is shown in Figure 3. Table 6 summarizes the detection and identification of 16 FAMEs. Overall, the most abundant fatty acid was oleic acid (C18:1) (26.38–28.86%). An OA-rich diet has been shown to improve inflammatory-related disorders, have anti-tumor activity, and lower hypercholesterolemia levels (27,

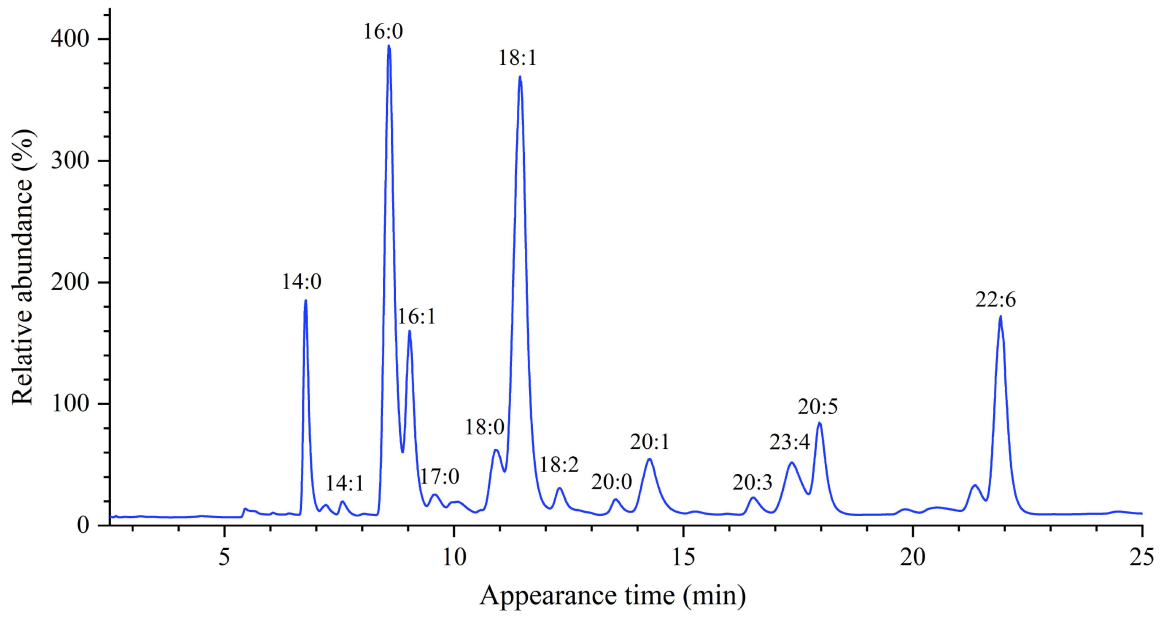

FIGURE 3
The representative GC chromatogram of hairtail muscle fatty acids.

TABLE 6 Hairtail muscle fatty acid composition from three different sources (%).

Fatty acid	T.Z	T.N	T.Q
C14:0	5.83 ± 0.11^{a}	3.56 ± 0.05^{b}	3.58 ± 0.02^{b}
C15:0	0.49 ± 0.07^{a}	n.d.	n.d.
C16:0	22.66 ± 0.21^{c}	24.19 ± 0.55^{b}	25.41 ± 0.51^{a}
C17:0	0.51 ± 0.01^{c}	1.26 ± 0.15^{b}	1.13 ± 0.01^{a}
C18:0	3.03 ± 0.06^{c}	5.47 ± 0.41^{b}	6.12 ± 0.10^{a}
C20:0	0.64 ± 0.02^{a}	n.d.	n.d.
SFA	33.16 ± 0.21^{c}	34.48 ± 0.07^{b}	36.23 ± 0.57^{a}
C14:1	0.24 ± 0.02^{b}	0.58 ± 0.02^{a}	0.55 ± 0.01^{a}
C16:1	7.65 ± 0.08^{b}	5.41 ± 0.33^{a}	6.09 ± 0.11^{a}
C18:1 *cis*	28.86 ± 0.39^{a}	28.11 ± 0.24^{a}	26.38 ± 0.51^{b}
C20:1	4.22 ± 0.10^{a}	n.d.	n.d.
C24:1	n.d.	n.d.	1.43 ± 0.08^{a}
MUFA	40.97 ± 0.35^{a}	34.10 ± 0.21^{b}	34.45 ± 0.43^{b}
C18:2 *cis*	1.26 ± 0.09^{a}	0.62 ± 0.02^{b}	0.63 ± 0.03^{b}
C20:3 n-3	0.88 ± 0.01^{c}	1.34 ± 0.08^{b}	2.55 ± 0.05^{a}
C20:4	4.35 ± 0.02^{a}	n.d.	n.d.
EPA n-3	5.48 ± 0.14^{a}	4.17 ± 0.23^{b}	3.80 ± 0.26^{b}
DHA n-3	13.90 ± 0.22^{c}	25.28 ± 0.45^{a}	22.32 ± 0.34^{b}
ΣEPA + DHA	19.38 ± 0.36^{c}	29.45 ± 0.45^{a}	26.12 ± 0.33^{b}
PUFA	25.87 ± 0.44^{c}	31.42 ± 0.36^{a}	29.30 ± 0.42^{b}
UFA	66.84 ± 0.21^{a}	65.52 ± 0.07^{b}	63.75 ± 0.57^{c}

$^{a-c}$Mean values in the same row (corresponding to the same parameter) not followed by a common letter differ significantly ($P < 0.05$). T.Z, Zhoushan hairtail; T.N, Hainan hairtail; T.Q, Qingdao hairtail.

28). The trans fatty acid (TFA), associated with the increased risk of coronary heart disease and altered prostaglandin metabolism, was not observed in these fishes (29).

For saturated fatty acid (SFA), it was similar in content and the main composition was palmitic acid (C16:0), myristic acid (C14:0), and stearic acid (C18:0). For monounsaturated fatty acid (MUFA), the major component of C18:1 in T.Z was slightly higher than the two others, which was in line with the situation of the content of MUFA, but the proportion in T.Z (40.97%) was prominently higher in T.N (34.10%) and T.Q (34.45%). For polyunsaturated fatty acids (PUFA), its proportion was varied in these fish, in the order of T.N (31.42%) > T.Q (29.30%) > T.Z (25.87%). Long-chain (≥ C20) omega-3 polyunsaturated fatty acids (LC-PUFA, e.g., EPA n-3 and DHA n-3) have health benefits against coronary heart disease, inflammatory diseases (e.g., rheumatoid arthritis and hypertension), some cancers as well as various mental disorders (e.g., schizophrenia, ADHD and Alzheimer's disease), and essential for the nutrition in brain and retina development of infant (30). Docosahexaenoic acid (DHA n-3) and eicosapentaenoic acid (EPA n-3) were the major component of LC-PUFA for hairtail as a research by Usydus et al. (31). It can be observed that the relative content of EPA and DHA of T.N (29.45%) and T.Q (26.12%) was significantly higher than T.Z (19.38%) in the total lipid profile. The fish do not synthesize these oils; rather, microalgae and other marine microorganisms (e.g., thraustochytrids and some bacteria) are the primary source of omega-3 LC-PUFA incorporated in higher marine animals and ultimately in humans through the consumption of seafood (32). The difference of LC-PUFA composition of the three hairtail samples may be related to their discrepant shift and expansion feeding ecology from zooplankton feeding to swimming feeding (25).

Flavor volatile compounds

Forty-four volatile compounds were detected, including alcohols (7), aldehydes (8), ketones (11), hydrocarbons (15), aromatic compounds (4). Among them, the compounds associated with fresh seafood flavors are mostly 6-, 8-, and 9-carbon aldehydes, ketones, and alcohols derived from the unsaturated fatty acid characteristic of seafood by lipoxygenase activities. As shown in **Table 7**, significant differences were observed in the molecular species and their concentrations between samples. The most abundant compounds in all samples were hydrocarbons, but they are generally minor contributors to food flavors because of their high odor threshold (33). Aldehydes showed a wide number of different compounds, characterized by low odor thresholds, which have been described as the main responsible of typical freshest most important contributors to the aroma of fish, associated with strong plastic, fatty, geranium, raw fish, and marine odor (34). Nonanal had the highest percentage of aldehydes volatiles among the samples: 1.92% (T.Z), 2.78% (T.N), and 2.80% (T.Q), respectively. The nonanal is the main volatile product of oleic acid oxidation, which can produce a special odor and is associated with a rotten odor. (E)-2-Octenal was derived from the oxidative breakdown of polyunsaturated fatty acids (PUFAs) of linoleic (C18:2) and linolenic (C18:3) acids producing fatty savory smell with 10.7 $lg{\cdot}kg^{-1}$ of the odor threshold value, which derived mainly from vegetable sources in fish diets. In these samples, (*E*)-2-octenal was only detected in T.N and its percentage content ranked second (2.00%) among the aldehydes of T.N. Furthermore, the flavor contribution of Hexanal, Octanal, and Heptanal in the three samples could not be ignored (concentrations, T.N > T.Q > T.Z): Hexanal is derived from linoleic acid oxidation, having a characteristic fruity odor and taste (35). Octanal could be related to the oxidation of n-9 MUFA and, generally, is associated with a soapy, oily, fatty, and citrus odor (36); while Heptanal has a very strong, fatty, harsh, pungent odor, which provides an unpleasant, fatty taste.

In fish, the relative mass fraction of ketones was slightly higher than that of aldehydes, but the threshold value was significantly higher than that of isomeric aldehydes. The ketones in T.N (10.98%), T.Q (7.85%), and T.Z (5.38%) primarily contribute to the aroma of fruits and lipids,

TABLE 7 Volatile compounds from three different sources were discovered in hairtail muscle (%).

Classify	Volatile compounds	T.Z	T.N	T.Q
Alcohol	1,3-Dioxan-5-ol, 4,4,5-trimethyl-	0.32 ± 0.02^{a}	n.d.	n.d.
	1-Hexanol	n.d.	n.d.	1.61 ± 0.90^{a}
	1-Octen-3-ol	0.86 ± 0.12^{b}	2.02 ± 1.10^{ab}	2.84 ± 0.62^{a}
	1-Penten-3-ol	n.d.	1.19 ± 0.25^{a}	0.69 ± 0.29^{b}
	2-Hexadecanol	0.25 ± 0.12^{a}	n.d.	n.d.
	4-Heptanol, 2,6-dimethyl-	0.63 ± 0.20^{a}	n.d.	n.d.
	Phenylethyl Alcohol	5.37 ± 0.65^{a}	n.d.	n.d.
	Subtotal	7.44 ± 0.91^{a}	3.21 ± 1.22^{b}	5.14 ± 1.43^{ab}
Aldehydes	2-Hexenal, (*E*)-	0.16 ± 0.04^{a}	0.18 ± 0.05^{a}	0.13 ± 0.01^{a}
	2-Octenal, (*E*)-	n.d.	2.00 ± 0.62^{a}	n.d.
	Butanal, 3-methyl-	0.42 ± 0.07^{a}	n.d.	n.d.
	Heptanal	0.61 ± 0.32^{ab}	0.90 ± 0.66^{a}	0.57 ± 0.25^{a}
	Hexanal	1.37 ± 0.81^{b}	1.80 ± 0.99^{a}	1.70 ± 0.70^{a}
	Nonanal	1.92 ± 0.49^{b}	2.78 ± 1.32^{a}	2.80 ± 1.19^{a}
	Octanal	0.82 ± 0.40^{b}	1.26 ± 0.78^{a}	0.79 ± 0.45^{b}
	Subtotal	5.30 ± 2.06^{b}	8.92 ± 4.16^{a}	5.99 ± 2.59^{b}
Ketones	2,3-Pentanedione	0.70 ± 0.16^{a}	0.47 ± 0.23^{ab}	0.26 ± 0.20^{b}
	2-Heptanone	0.97 ± 0.46^{b}	2.39 ± 0.29^{a}	1.55 ± 0.95^{ab}
	2-Hexanone	n.d.	0.23 ± 0.07^{a}	0.13 ± 0.09^{a}
	2-Nonanone	0.61 ± 0.15^{b}	2.89 ± 0.49^{a}	2.07 ± 0.72^{a}
	2-Pentanone	0.50 ± 0.34^{b}	1.35 ± 0.44^{a}	0.69 ± 0.58^{b}
	2-Undecanone	0.37 ± 0.01^{c}	1.57 ± 0.26^{a}	1.19 ± 0.17^{b}
	3,5-Octadien-2-one, (*E*,*E*)-	0.78 ± 0.01^{a}	n.d.	0.62 ± 0.07^{b}
	3-Octanone	n.d.	0.93 ± 0.46^{a}	0.50 ± 0.21^{b}
	3-Pentanone	0.70 ± 0.27^{a}	n.d.	n.d.
	5-Hepten-2-one, 6-methyl-	0.42 ± 0.01^{a}	0.46 ± 0.14^{a}	0.35 ± 0.06^{a}
	7-Octen-2-one	0.35 ± 0.03^{b}	0.69 ± 0.08^{a}	0.48 ± 0.14^{b}
	Subtotal	5.38 ± 1.41^{a}	10.98 ± 0.28^{a}	7.85 ± 2.67^{ab}
Hydrocarbons	Dodecane	1.75 ± 0.17^{a}	0.41 ± 0.06^{b}	0.41 ± 0.02^{b}
	Heptadecane	1.25 ± 0.75^{a}	n.d.	n.d.
	Hexadecane, 2,6,10-trimethyl-	n.d.	1.08 ± 0.60^{a}	n.d.
	Nonane	0.22 ± 0.05^{b}	1.35 ± 0.76^{a}	0.36 ± 0.14^{b}
	Octane	n.d.	2.74 ± 1.65^{a}	1.16 ± 0.42^{b}
	Pentadecane	2.28 ± 0.94^{b}	1.29 ± 0.40^{b}	5.24 ± 1.74^{a}
	Pentadecane, 2,6,10,14-tetramethyl-	n.d.	n.d.	2.94 ± 0.98^{a}
	Tetradecane	n.d.	n.d.	0.71 ± 0.06^{a}
	Tridecane	0.90 ± 0.26^{a}	0.63 ± 0.13^{b}	0.59 ± 0.12^{b}
	Undecane	0.70 ± 0.23^{a}	n.d.	n.d.
	1-Undecene	n.d.	n.d.	1.10 ± 0.64^{a}
	Benzene, 1-ethyl-3-methyl-	n.d.	0.42 ± 0.07^{a}	n.d.
	Ethylbenzene	1.38 ± 0.22^{a}	n.d.	1.18 ± 0.25^{a}
	p-Xylene	3.55 ± 0.62^{a}	2.36 ± 0.43^{b}	2.60 ± 0.64^{b}
	Styrene	1.94 ± 0.51^{a}	1.18 ± 0.17^{b}	1.97 ± 0.76^{a}
	Subtotal	13.97 ± 3.16^{ab}	11.46 ± 1.25^{b}	18.26 ± 3.90^{a}
Aromatic compounds	10-Heptadecen-8-ynoic acid, methyl ester, (*E*)-	0.23 ± 0.02^{b}	0.42 ± 0.12^{a}	0.28 ± 0.13^{b}
	Furan, 2-ethyl-	n.d.	0.35 ± 0.07^{a}	n.d.
	Hexadecanoic acid, ethyl ester	0.20 ± 0.03^{a}	0.24 ± 0.14^{a}	0.23 ± 0.04^{a}
	Pyrazine, 2,5-dimethyl-	0.90 ± 0.09^{a}	n.d.	n.d.
	Subtotal	1.32 ± 0.07^{a}	1.02 ± 0.23^{a}	0.51 ± 0.16^{b}

$^{a-c}$Mean values in the same row (corresponding to the same parameter) not followed by a common letter differ significantly ($P < 0.05$). T.Z, Zhoushan hairtail; T.N, Hainan hairtail; T.Q, Qingdao hairtail.

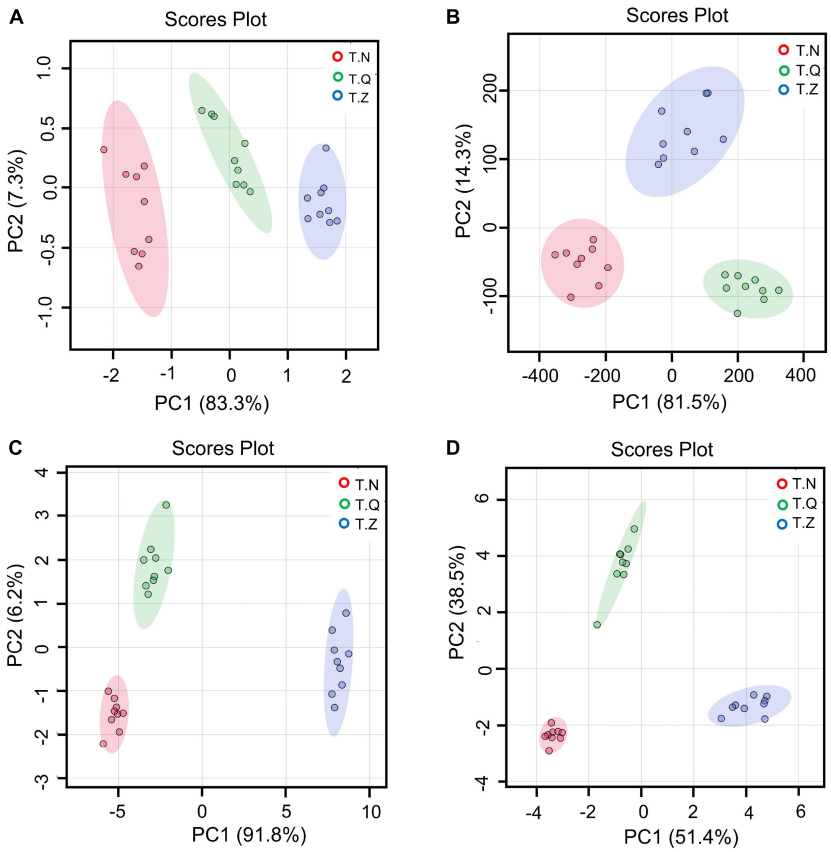

FIGURE 4
Score plots of PLS-DA of three origin hairtail: **(A)** mineral, **(B)** amino acid, **(C)** fatty acids, and **(D)** volatiles.

which were produced by thermal degradation of fatty acids with multiple unsaturated bonds, amino acid degradation, or microbial oxidation. 2-Heptanone has a cheesy ketonic, slightly green waxy, banana fruity aroma, and its relative percentage concentrations in T.N (2.89 percent) and T.Q (2.91 percent) were close but significantly higher ($P < 0.05$) than T.Z (0.61 percent). In terms of a rose- and tea-like flavor, 2-nonanone had a significant ($P < 0.05$) difference in T.N (2.93%) and T.Z (0.97%), and when compared to T.Q (0.69 percent) and T.Z (0.50 percent), 2-Pentanone, a colorless liquid ketone with the odor of fingernail polish or a strong fruity odor, had the highest relative percentage concentrations in T.N (1.35 percent). 3-Octanone has a strong, penetrating fruity odor that is reminiscent of lavender, mushroom, ketonic, cheesy, and moldy with fruity nuance, and its concentrations in T.N (0.93 percent) was significantly higher ($P < 0.05$) than T.Q. (0.50 percent). Because of high odor threshold, alcohols are generally minor contributors to food flavors unless they are unsaturated or present in high concentrations. T.Z had a higher volatile substance relative content of alcohol than the others, owing primarily to the affluent phenylethyl alcohol (5.37 percent) with a pleasant floral odor that was unique to T.Z. These findings, as well as the measured percentage of flavor volatile compounds derived from n-3 or n-6 fatty acids, were consistent with the fatty acid composition of the samples: T.N and T.Z were higher in n-3 fatty acids and PUFAs than T.Q.

Partial least squares-discriminant analysis

Because the color and TPA index could not well distinguish different sources of hairtail in this study, we selected amino acids, minerals, fatty acids and volatile substances as parameters for multivariate statistical analysis to try to find the indicators with the best classification ability. PLS-DA, a supervised discriminant analysis statistical method, uses partial least squares regression to establish a relationship model between the expression of features and sample categories to realize the model prediction of samples (37), showing the differences among three groups of samples. The results are shown in Figure 4. From Figure 4A, the first principal component (PC1) explained 83.3 cumulative percent (cum%) of the variance in the amino acid dataset. Similarly, PC2 explained 7.3 cum%, and PC3 explained

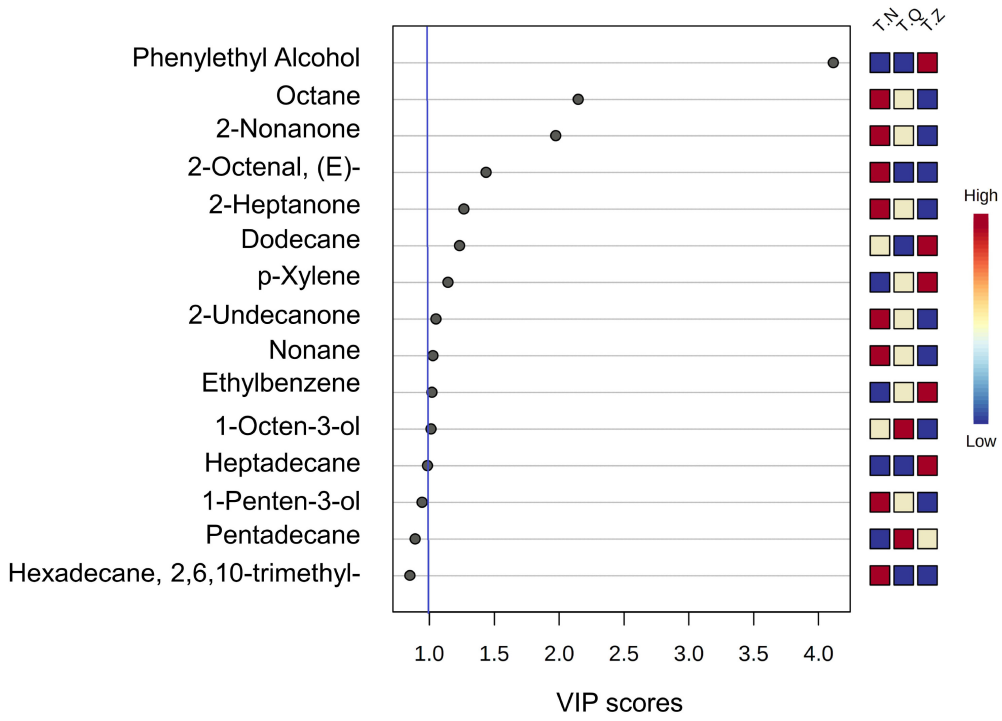

FIGURE 5
The VIP graph of PLS-DA of all relevant volatiles analyzed in the multivariate data set.

2.0 cum%. Figure 4B showed the PLS-DA of minerals, with PC1 explaining 81.5 cum%, PC2 explaining 14.3 cum%, and PC3 explaining 3.2cum%. From Figure 4C, the PC1 explained 91.8 cum% of the variance in the fatty acids dataset, PC2 explained 6.2 cum%, and PC3 explained 1.0 cum%. In the PLS-DA plot (Figure 4D) regarding flavor substances, the first three principal components could explain 92.7 cum% of the total variance (individual contributions include PC1 explained 51.4 cum%, PC2 explained 38.5 cum%, and PC3 explained 3.0 cum%). When the samples were distributed on different sides of the axis, it indicated that they had been successfully distinguished by the corresponding principal components. The first three principal components of all four sets of models could be considered adequate to demonstrate the variety of different hairtail samples, which shows that all four models can be distinguished well. The performance of the PLS-DA model depends on R^2 (evaluating the fitness) and Q^2 (indicating the predictive ability of the model). Generally, the value of Q^2 more than 0.5 is assigned well for the biological models (38). Among the four models for amino acids, minerals, fatty acids, and volatiles, the value of Q^2 (>0.5) were 0.9598, 0.98220, 97.45, 98.41, respectively; the value of R^2 were 0.9860, 0.9877, 0.9838, 0.9909, respectively. It can be seen that the separation effect of the four groups of model volatile groups was the most obvious, followed by the mineral group.

The most prominent variables can be obtained from the VIP plot, which was arranged in decreasing order of VIP, or importance or decreasing order of importance. The variables with VIP $>$ 1 were regarded as effective indicators of class separation (39). In the VIP plot for flavor substances (Figure 5), 11 volatiles, including two alcohols, one aldehyde, three ketones, and five hydrocarbons, were identified as effective in the discrimination of different source hairtail.

Conclusion

The basic characteristics of hairtail, such as color, texture, nutrient composition, amino acid composition, and volatile flavor substances, differed significantly in this study. T.Z fish caught in the East China Sea had the highest yellowness and crude fat content, with palmitic acid (C16:0) and monounsaturated fatty acids represented by oleic acid being the most abundant fatty acids in lipids (C18:1). T.N fish caught in the South China Sea had the highest concentration of macrominerals (e.g., potassium, sodium, phosphorus, and calcium) and amino acids, the most appropriate proportions of essential amino acids for human nutrition, and their lipids had a high content of PUFA, with the highest contribution of EPA and DHA. Furthermore, the analysis of flavor volatile compounds revealed some differences in the bouquet design of the three samples, particularly in the aroma compounds derived

from n-3 or n-6 fatty acids, with more pronounced oil and cheese notes in T.Z and clear and fishy notes in T.N and T.Q, which may influence consumer choice. Other analysis indices, such as fish texture, umami level, and protein content, were largely consistent across the three origin hairtail. In conclusion, the hairtails of three origins can be distinguished based on nutrition, fatty acids, and volatile aroma compounds, which is critical for combating counterfeiting inferiority products and establishing the hairtail brand status in different regions. The classification ability of different indexes for different sources of hairtail were compared and analyzed by multivariate statistical analysis, and it was found that the method of detecting volatile flavor substances by GC-MS was the best way to trace the origin of hairtail. In this study, the most effective method was found among many simple and convenient methods, which enriches the traceability and identification technology of hairtail fish and has high importance to food quality and safety.

Data availability statement

The original contributions presented in the study are included in the article/supplementary material, further inquiries can be directed to the corresponding authors.

Ethics statement

The studies involving animals were reviewed and approved by the Ethics Committee of Zhejiang Gongshang University. All applicable international, national, and/or institutional guidelines for the care and use of animals were followed.

Author contributions

SW: methodology and writing. PW: validation. XS: data curation. HZ: formal analysis. JX: software and validation. KC: conceptualization. QZ, YC, and WL: data curation. QS: conceptualization and funding acquisition. All authors contributed to the article and approved the submitted version.

Funding

This work was supported by the Eyas Program Incubation Project of Zhejiang Provincial Administration for Market Regulation (CY2022232).

Conflict of interest

The authors declare that the research was conducted in the absence of any commercial or financial relationships that could be construed as a potential conflict of interest.

Publisher's note

All claims expressed in this article are solely those of the authors and do not necessarily represent those of their affiliated organizations, or those of the publisher, the editors and the reviewers. Any product that may be evaluated in this article, or claim that may be made by its manufacturer, is not guaranteed or endorsed by the publisher.

References

1. Randall J, Busby MS, Spear AH, Mier KL. Spatial and temporal variation of late summer ichthyoplankton assemblage structure in the eastern Chukchi Sea: 2010–2015. *Polar Biol.* (2019) 42:1811–24. doi: 10.1007/s00300-019-02555-8

2. Young M. International trade law compatibility of market-related measures to combat illegal, unreported and unregulated (IUU) fishing. *Marine Policy.* (2016) 69:209–19. doi: 10.1016/j.marpol.2016.01.025

3. Hoque MZ, Akhter N, Chowdurhy MSR. Consumers' preferences for the traceability information of seafood safety. *Foods.* (2022) 11:1675. doi: 10.3390/foods11121675

4. Silva A, Hellberg R. DNA-based techniques for seafood species authentication. *Adv Food Nutr Res.* (2020) 95:207–55. doi: 10.1016/bs.afnr.2020.09.001

5. Sharma L, Watts E, Singh P. High resolution real-time PCR melting curve assay for identification of top five Penaeidae shrimp species. *Lebensmittel Wissenschaft Technol.* (2020) 133:109983. doi: 10.1016/j.lwt.2020.109983

6. Cui Y, Wang H, Zhao Q, Zhu X, Wang P, Xue J, et al. Real-time detection of authenticity and adulteration of krill phospholipids with soybean phospholipids using rapid evaporative ionization mass spectrometry: application on commercial samples. *Food Control.* (2021) 121:107680. doi: 10.1016/j.foodcont.2020.107680

7. Yu X, Li L, Wang H, Song G, Wang J, Li S, et al. Lipidomics study of rainbow trout (Oncorhynchus mykiss) and salmons (Oncorhynchus tshawytscha and Salmo salar) using hydrophilic interaction chromatography and mass spectrometry. *Lebensmittel Wissenschaft Technol.* (2020) 121:108988. doi: 10.1016/j.lwt.2019.108988

8. Lu W, Wang P, Ge L, Chen X, Guo S, Zhao Q, et al. Real-time authentication of minced shrimp by rapid evaporative ionization mass spectrometry. *Food Chem.* (2022) 383:132432. doi: 10.1016/j.foodchem.2022.132432

9. Karunathilaka SR, Ellsworth Z, Yakes B. Detection of decomposition in mahi-mahi, croaker, red snapper, and weakfish using an electronic-nose sensor and chemometric modeling. *J Food Sci.* (2021) 86:4148–58. doi: 10.1111/1750-3841.15878

10. Wu Y, Wang Y, Li L, Wang X, Yang X, Cai Q, et al. Based on electronic nose and HS-SPME-GC-MS technology, volatile flavor components of dried hairtail with different processing methods were analyzed. *J Fish China.* (2016) 40:1931–40.

11. Folch J, Lee S, Sloane-Stanley GH. A simple method for the isolation and purification of total lipids from animal tissues. *J Biol Chem.* (1957) 226:497–509. doi: 10.1016/S0021-9258(18)64849-5

12. Fournier V, Juaneda P, Destaillats F, Dionisi F, Lambelet P, Sebedio JL, et al. Analysis of eicosapentaenoic and docosahexaenoic acid geometrical isomers

formed during fish oil deodorization. *J Chromatogr A*. (2006) 1129:21–8. doi: 10.1016/j.chroma.2006.06.089

13. Nilsson Sköld H, Aspengren S, Wallin M. Rapid color change in fish and amphibians-function, regulation, and emerging applications. *Pigment Cell Melanoma Res.* (2012) 26:29–38. doi: 10.1111/pcmr.12040

14. Choubert G, Baccaunaud M. Colour changes of fillets of rainbow trout (Oncorhynchus mykiss W.) fed astaxanthin or canthaxanthin during storage under controlled or modified atmosphere. *LWT Food Sci Technol.* (2006) 39:1203–13. doi: 10.1016/j.lwt.2005.06.017

15. Quoc Toan T, Dang V, Pham Q, Nguyen PH, Trinh T, Tran T, et al. Effects of dietary inclusion of Canthaxanthin- and α-Tocopherol-loaded liposomes on growth and muscle pigmentation of rainbow trout (*Oncorhynchus mykiss*). *J Food Qual.* (2021) 2021:1–11. doi: 10.1155/2021/6653086

16. Ran X, Lou X, Zheng H, Gu Q, Yang H. Improving the texture and rheological qualities of a plant-based fishball analogue by using konjac glucomannan to enhance crosslinks with soy protein. *Innov Food Sci Emerg Technol.* (2022) 75:102910. doi: 10.1016/j.ifset.2021.102910

17. Ayala M, Albors OL, Blanco A, Alcáza GA, Abellán E, Zarzosa GR, et al. Structural and ultrastructural changes on muscle tissue of sea bass, *Dicentrarchus labrax* L., after cooking and freezing. *Aquaculture.* (2005) 250:345–58. doi: 10.1016/j.aquaculture.2005.04.057

18. Bogard JR, Thilsted SH, Marks GC, Wahab MA, Hossain MA, Jakobsen J, et al. composición nutricional de las especies de peces importantes en Bangladesh y la contribución potencial a la ingesta de nutrientes recomendados. *J Food Compos Anál.* (2015) 42:120–33.

19. Yan J, Liao K, Wang T, Mai K, Xu W, Ai Q. Dietary lipid levels influence lipid deposition in the liver of large yellow croaker (*Larimichthys crocea*) by regulating lipoprotein receptors, fatty acid uptake and triacylglycerol synthesis and catabolism at the transcriptional level. *PLoS One.* (2015) 10:e0129937. doi: 10.1371/journal.pone.0129937

20. Ren Z, Chen Z, Zhang Y, Lin X, Li Z, Weng W, et al. Effect of heat-treated tea water-insoluble protein nanoparticles on the characteristics of Pickering emulsions. *LWT Food Sci Technol.* (2021) 149:111999. doi: 10.1016/j.lwt.2021.111999

21. Xu D, Ding G, Fang Y, Yan Z, Huang L, Chen Y. Analysis and evaluation of nutrient composition in different parts of 7 kinds of seafood. *Chin J Nutr.* (2008) 40:409–11+414.

22. Afonso C, Cardoso C, Lourenço H, Anacleto P, Bandarra N, Carvalho M, et al. Evaluation of hazards and benefits associated with the consumption of six fish species from the Portuguese coast. *J Food Compos Anal.* (2013) 32:59–67. doi: 10.1016/j.jfca.2013.06.008

23. Biandolino F, Di Leo A, Parlapiano I, Papa L, Giandomenico S, Spada L, et al. Nutritional quality of edible marine bivalves from the southern coast of Italy, Mediterranean Sea. *Polish J Food Nutr Sci.* (2019) 69:71–81.

24. Partridge G, Lymbery A. The effect of salinity on the requirement for potassium by barramundi (Lates calcarifer) in saline groundwater. *Aquaculture.* (2008) 278:164–70.

25. Garrison T, Ellis R. *Oceanography An Invitation to Marine Science*. 9th ed. Boston, MA: Cengage Learning (2016).

26. Manuel J, Flávio F, Filipe M, Lina C, Maria E, Pereira J, et al. Essential mineral content variations in commercial marine species induced by ecological and taxonomical attributes. *Food Compos Anal.* (2021) 103:104118.

27. Farag M, Gad M. Omega-9 fatty acids: potential roles in inflammation and cancer management. *J Genet Eng Biotechnol.* (2022) 20:48. doi: 10.1186/s43141-022-00329-0

28. Smith S, Lunt D, Smith D, Walzem R. Producing high-oleic acid beef and the impact of ground beef consumption on risk factors for cardiovascular disease: a review. *Meat Sci.* (2020) 163:108076. doi: 10.1016/j.meatsci.2020.108076

29. Saerens M, Fouss F, Yen L, Dupont P. The principal components analysis of a graph, and its relationships to spectral clustering. In: Boulicaut JF, Esposito F, Giannotti F, and Pedreschi D, editors. *Machine Learning: ECML 2004. ECML 2004. Lecture Notes in Computer Science*. (Vol. 3201), Berlin: Springer (2005). p. 371–83.

30. Nichols P, Mansour P, Robert S, Frampton D, Blackburn S, Petrie J, et al. Alternate sources of long-chain omega-3 oils. *Asia Pacif. J. Clin. Nutr.* (2005) 14:S112.

31. Usydus Z, Szlinder-Richert J, Adamczyk M, Szatkowska U. Marine and farmed fish in the polish market: comparison of the nutritional value. *Food Chem.* (2011) 126:78–84. doi: 10.1016/j.chemosphere.2011.09.019

32. Shahidi F. Omega-3 oils: sources, applications, and health effects. In: Barrow C, Shahidi F, editors. *Marine Nutraceuticals and Functional Foods*. Boca Raton, FL: CRC Press (2008). p. 23–61. doi: 10.1201/9781420015812.ch2

33. Hosoglu MI. Aroma characterization of five microalgae species using solid-phase microextraction and gas chromatography-mass spectrometry/olfactometry. *Food Chem.* (2018) 240:1210–8. doi: 10.1016/j.foodchem.2017.08.052

34. Fuentes A, Fernandez-Segovia I, Escriche I, Serra AJ. Comparison of physico-chemical parameters and composition of mussels (*Mytilus galloprovincialis* Lmk.) from different Spanish origins. *Food Chem.* (2009) 112:295–302. doi: 10.1016/j.foodchem.2008.05.064

35. Turchini G, Giani I, Caprino F, Moretti V, Valfré F. Discrimination of origin of farmed trout by means of biometrical parameters, fillet composition and flavour volatile compounds. *Italian J Anim Sci.* (2010) 3:123–40. doi: 10.4081/ijas.2004.123

36. Wu S, Yang J, Dong H, Liu Q, Li X, Zeng X, et al. Key aroma compounds of Chinese dry-cured Spanish mackerel (*Scomberomorus niphonius*) and their potential metabolic mechanisms. *Food Chem.* (2021) 342:128381. doi: 10.1016/j.foodchem.2020.128381

37. Guitton Y, Dervilly-Pinel G, Jandova R, Stead S, Takats Z, Le Bizec B. Rapid evaporative ionisation mass spectrometry and chemometrics for high-throughput screening of growth promoters in meat producing animals. *Food Addit. Contam Part A Chem Anal Control Expo Risk Assess.* (2018) 35:900–10. doi: 10.1080/19440049.2017.1421778

38. Blasco H, Błaszczynski J, Billaut JC, Nadal-Desbarats L, Pradat PF, Devos D, et al. Comparative analysis of targeted metabolomics: dominance-based rough set approach versus orthogonal partial least square-discriminant analysis. *J Biomed Inform.* (2015) 53:291–9. doi: 10.1016/j.jbi.2014.12.001

39. Kosek V, Uttl L, Jírù M, Black C, Chevallier O, Tomaniová M, et al. Ambient mass spectrometry based on REIMS for the rapid detection of adulteration of minced meats by the use of a range of additives. *Food Control.* (2018) 104:50–6. doi: 10.1016/j.foodcont.2018.10.029

frontiers | Frontiers in Nutrition

TYPE Original Research
PUBLISHED 16 November 2022
DOI 10.3389/fnut.2022.1066964

OPEN ACCESS

EDITED BY
Jinxuan Cao,
Beijing Technology and Business University, China

REVIEWED BY
Bin Zhang,
Zhejiang Ocean University, China
Xuepeng Li,
Bohai University, China

*CORRESPONDENCE
Changrong Ou
ouchangrong@nbu.edu.cn

SPECIALTY SECTION
This article was submitted to Food Chemistry, a section of the journal Frontiers in Nutrition

RECEIVED 11 October 2022
ACCEPTED 31 October 2022
PUBLISHED 16 November 2022

CITATION
Tong L, Tang H, Chen J, Sang S, Liang R, Zhang Z and Ou C (2022) Origin of static magnetic field induced quality improvement in sea bass (*Lateolabrax japonicus*) during cold storage: Microbial growth inhibition and protein structure stabilization. *Front. Nutr.* 9:1066964. doi: 10.3389/fnut.2022.1066964

Origin of static magnetic field induced quality improvement in sea bass (*Lateolabrax japonicus*) during cold storage: Microbial growth inhibition and protein structure stabilization

Li Tong[1], Haiqing Tang[2], Jingyi Chen[1], Shangyuan Sang[1,3], Ruiping Liang[1], Zhepeng Zhang[1] and Changrong Ou[1,3]*

[1]College of Food and Pharmaceutical Sciences, Ningbo University, Ningbo, China, [2]Faculty of Food Science, Zhejiang Pharmaceutical University, Ningbo, China, [3]Key Laboratory of Animal Protein Food Deep Processing Technology of Zhejiang Province, Ningbo University, Ningbo, China

To explore the potential application of static magnetic field (SMF) treatment in marine fish preservation, the sea bass (*Lateolabrax japonicus*) was exposed to SMF (5 mT) and its quality changes during cold storage were evaluated by total viable counts, water holding capacity, pH, color, and textural properties. Characteristics of the protein in the presence of SMF were investigated by measuring total sulfhydryl (SH) content, Ca^{2+}-ATPase activity, secondary structure, and muscle microstructure. SMF treatment exhibited positive effects on fish quality, showing favorable performance on the most quality indicators, especially a significant reduction in the Microbial Counts. Furthermore, higher total SH content and Ca^{2+}-ATPase activity were observed in SMF-treated samples, demonstrating that the oxidation and denaturation of myofibrillar protein (MP) were delayed due to SMF treatment. The transformation of α-helix to random coil was prevented in SMF-treated samples, indicating that the secondary structure of MP was stabilized by SMF treatment. The above changes in protein structures were accompanied by changes in muscle microstructure. More intact and compact structures were observed in SMF-treated samples, characterized by well-defined boundaries between myofibers. Therefore, our findings suggest that under the conditions of this article, SMF treatment could maintain the quality of fish mainly by inhibiting the growth of microorganisms and enhancing the stability of protein structures, and could be a promising auxiliary technology for preservation of aquatic products.

KEYWORDS

sea bass, static magnetic field, myofibrillar protein, total viable counts, cold storage, protein structure

Introduction

Fish and fish products play an increasingly important role in human diet due to their delicious taste, rich nutrients, and widely recognized health benefits (1). However, the presence of relatively large amounts of protein and polyunsaturated fatty acids in fish, although with recognized benefits for health, is a significant obstacle for fish preservation due to their instability in the presence of external spoilage microorganisms and endogenous proteolytic enzymes (2, 3). Preservation of aquatic products has become a quite challenging and urgent issue. It is well known that low-temperature storage has been extensively used in aquatic products to extend shelf life and ensure quality. Thereinto, frozen and cold storage are considered to be the most common and effective methods to prolong the freshness lifetime of food by controlling the growth of pathogenic and spoilage microorganisms and slowing down the activity of endogenous enzymes (4). During the freezing process and frozen storage, the free water in fish muscle would undergo a liquid-solid transition to form ice crystals, which would severely damage the cell structure and thus lead to the quality deterioration of fish (5, 6). Consumers express personalized and diversified desires for organoleptic and nutritional quality in fish (7). Fish with compromised quality after frozen storage could not meet consumer demand for premium quality fish. Unlike the subzero temperature of frozen storage, temperatures in cold storage rooms range from 0 to 4°C. In this temperature zone, the water in food often exists in a liquid state. However, the relatively high storage temperature corresponds to a shorter shelf life, depending upon the type of products (8). Thus, researches on extending the fresh-keeping period of non-frozen aquatic products have attracted increasing attention.

For the above purpose, many emerging approaches, alone or combined, have been developed and applied, including nanoparticles, cold plasma, active packaging and so on (2, 9, 10). According to preservation mechanisms, these available technologies could be classified into chemical, biological, and physical approaches. Regrettably, while chemical and biological treatments are effective measures to inactivate spoilage bacteria and inhibit enzyme activity in aquatic products, consumers are concerned about the flavor changes and foodborne illnesses that these treatments might bring (11). As a result, many non-thermal physical methods have been applied to the preservation of fish, such as high-pressure processing (12), pulsed electric field (13), and cold plasma (9). However, there are still some unresolved issues with the above technologies, such as the difficulty of high-pressure processing for continuous production, the unsuitability of pulsed electric field for complex food systems (14), and the significant changes in food sensory quality after cold plasma treatment (15).

Static magnetic field (SMF) treatment is a novel physical preservation method characterized by high penetration depth and no reagent residue (16, 17). SMF treatment was initially proposed for the medical cryopreservation of biological organs and tissues and the germination of seeds (18, 19), and introduced into food preservation in recent years (20, 21). The major components in food are diamagnetic substances, of which functional properties were influenced by the external magnetic field. For instance, the SMF treatment has proven to strengthen intramolecular-hydrogen bonds and depress self-diffusion coefficient, thereby increasing the water activity and promoting a reduction in drip loss and a delay in tissue softening (22).

To date, few published researches mainly concentrated on the field of SMF-assisted frozen storage (23, 24). Nevertheless, given the above-mentioned disadvantages of frozen storage, the combined treatment of SMF and cold storage appears to be a more promising approach for maintaining freshness and obtaining better sensory quality in fish. According to the study of Lin et al. (25), SMF treatment (7.98–8.15 mT) combined with supercooling storage extended the shelf life of beef without adverse effects on other quality characteristics. Moreover, Bajpai et al. (26) found that SMF treatment (100 mT) effectively inhibited the growth of *Staphylococcus epidermidis* (gram-positive bacteria) and *Escherichia coli* (gram-negative bacteria) by disrupting the integrity of bacterial cell membranes. Interestingly, some studies have also found that SMF treatment had no positive effect on the preservation of food, and SMF treatment even promoted the growth of certain microorganisms, such as *Pseudomonas aeruginosa* (27). Hence results published in the literature are apparently contradictory. Further studies should find some clear evidence that SMF treatment is beneficial for food preservation and elucidate the underlying mechanism of action.

Magnetic fields (MFs) could be classified as time-varying magnetic field or SMF according to time interval (28). The time-varying magnetic field, which is associated with changes in electrical current, has strict requirements on voltage and current, so applying it as an auxiliary technology may significantly increase equipment costs and operating conditions. In practice, the heat generated by current coils of time-varying magnetic field could not be ignored (29). The SMF produced by a steady current in the surrounding space has constant magnetic field intensity and direction. Since the voltage and current requirements of SMF treatment could be easily met, it can be more suitable to be an adjunct on existing cryogenic storage systems such as refrigerators. In addition, considering the biological effects caused by SMF, it is accordingly classified as weak (<1 mT), moderate (1 mT–1 T), strong (1–5 T), and ultra-strong (>5 T). Zhao et al. (30) indicated that strong magnetic fields may damage the properties of cells and tissues and should not be applied to preserve fresh food. Moreover, a very weak magnetic field was also ineffective for food preservation. As reported by Zhu et al. (31), the effects of SMF treatment on retarding the deterioration of shrimp (*Litopenaeus vannamei*) could already be observed at an intensity of 5 mT. Hence in this

study we focus on the effects of exposure to SMF of 5 mT on fish quality during cold storage, considering the reasonable energy requirements and future commercial applications.

The present study aims to investigate the effects of SMF treatment on the quality of sea bass during cold storage by evaluating microbial quality, physicochemical properties, and protein structure, and provide theoretical support for the further application of SMF treatment in the aquatic product industry.

Materials and methods

Sample preparation

A total number of 14 live sea bass (weight 600 ± 35 g, length 31.5 ± 3.5 cm) were purchased from a local aquatic market (Ningbo, Zhejiang, China) in October, and transported to the laboratory in a box filled with water containing dissolved oxygen. Once arrival, the live sea bass was killed immediately by a physical blow to the head with a wooden hammer and then peeled, headed, and gutted. The dorsal muscle of sea bass was cut into fillets, which were individually packaged with polyethylene bags, and finally the fillets were randomly divided into two equal batches. The fish fillet subjected to SMF treatment (5 ± 0.1 mT) in a magnetic field-assisted refrigerator (MFI-Fm-x1, INDUC Scientific Co., Ltd., Wuxi, Jiangsu, China), and the temperature was set at 4 ± 0.1°C. The magnetic field-assisted refrigerator consisted of a magnetic field generator, a biological sample chamber, and a temperature control and monitoring system. A power supply and a pair of Helmholtz coils (80 cm × 80 cm square; 400 turns) constituted the magnetic field generator, which can produce a uniform magnetic field of 0–5 mT at an excitation current of 0–8 A. The magnetic field uniformity was 99%, verified by Maxwell Software simulation. The biological sample chamber had a volume of 50 L, and the temperature ranged from −20 ± 0.1 to 40 ± 0.1°C. The control treatment conditions were consistent with those of the experimental group. The control treatment condition was consistent with the experimental group except for exposure to SMF. The fillets were taken each day during storage for subsequent analyses.

Determination of total viable counts

Total viable counts (TVC) of the sea bass fillet were performed by the method of Hernandez et al. (32). An aliquot of 10 g minced sea bass fillet was placed in a sterile homogeneous bag with 90 ml of 0.9% normal saline and homogenized with a Masticator paddle blender (basic panoramic, IUL S.A., Spain). The homogenate was diluted with 0.9% normal saline and inoculated on the medium. TVC were determined by the pouring method in plate count agar (PCA) mediums. The PCA medium was purchased from Hangzhou Microbial Reagent Co., Ltd. (Hangzhou, China). The inoculated plates were incubated at 30 ± 0.5°C for 72 h. Results were recorded as $\log_{10}$ CFU (colony forming units)/g.

Determination of water holding capacity

Water holding capacity (WHC) was expressed as a percentage of weight loss of the initial sea bass fillet. Approximately 5 g of non-minced fillet was wrapped with filter paper, and centrifuged at 4,000 × *g* for 15 min at 4°C. Then, the water was poured out of the centrifuge tube and the remaining fillet was weighed again. The measurement was carried out in triplicate. The WHC was calculated by the Equation 1:

$$\mathrm{WHC}\,(\%) = \left[1 - \frac{(m_1 - m_2)}{m_1}\right] \times 100\% \qquad (1)$$

where m_1 is the weight of the sea bass fillet before centrifugation, and m_2 is the weight of the fillet after centrifugation.

Determination of pH

An aliquot of 5 g minced sea bass fillet was homogenized with a homogenizer (NANOJ H10, ATS Engineering Inc., Germany) in 50 ml of 0.1 M KCl (pH = 7.0). The pH of the homogenate was determined by a pH meter (PHS-2F, Shanghai INESA Scientific Instrument CO., Ltd, Shanghai, China).

Determination of color

The color of the fish fillet was measured by a colorimeter (NR110, Shenzhen 3nh Technology CO., LTD., Shenzhen, China) according to the method proposed by Chmiel et al. (33). Each fillet (50 mm × 20 mm × 10 mm) was measured at three typical positions (anterior, middle, and posterior) with recording L* (lightness), a* (redness/greenness), and b* (yellowness/blueness). All measurements were analyzed in five replicates, from which an average was calculated. The absolute color difference (ΔE) was calculated by the Equation 2:

$$\Delta E = \sqrt{\left(L_i^* - L_0^*\right)^2 + \left(a_i^* - a_0^*\right)^2 + \left(b_i^* - b_0^*\right)^2} \qquad (2)$$

where L_0^*, a_0^*, and b_0^* represent the color parameters of the fresh sea bass fillet. L_i^*, a_i^*, and b_0^* represented the color parameters of the fillet during storage.

Texture profile analysis

The texture profile analysis (TPA) was measured by a texture analyzer (TA-XT plus, Stable Micro Systems, Surrey, UK). The

fish fillet was cut into cubes (30 mm × 20 mm × 10 mm) and equilibrated at room temperature (25°C), then compressed to 40% of its initial thickness using a spherical probe having a one-inch diameter (P/1S), with a trigger force of 5 g and a test speed of 1 mm/s. Texture performances were expressed as hardness, springiness, cohesiveness, and chewiness. The hardness was defined as the maximum positive force of the first compression, expressed in grams. The cohesiveness was defined as the ratio of the positive area of the second compression to the positive area of the first compression. The springiness was defined as the ratio of the height detecting of the second compression to the first compression distance. The chewiness was defined as the product of hardness × cohesiveness × springiness. At least five replicates were performed for each treatment, once for each sample, and the mean was calculated.

Scanning electron microscopy

The scanning electron microscopy (SEM) analysis of the sea bass muscle was performed according to the method described by Liu et al. (34). The fillet was cut into 5 mm × 5 mm × 2 mm pieces, fixed with 2.5% glutaraldehyde solution at 4°C for 24 h, then rinsed with 0.1 M phosphate buffer (pH = 7.2) for 15 min, repeated three times. The washed sample was gradient dehydration with ethanol (50, 70, 80, 90, and 100%). Thereinto, the sample was dipped in anhydrous ethanol for 20 min twice, for 15 min in others. After freeze-drying and coating with gold, the specimen was observed using a Hitachi S-3400N scanning electron microscope (Hitachi S-3400N, Hitachi, Ltd., Tokyo, Japan).

Extraction of myofibrillar protein

Myofibrillar protein (MP) was extracted from sea bass using the method described by Ding et al. (35). Briefly, the white muscle from the fillet was minced and rinsed with four times the weight of low-salt buffer (0.05 M NaCl, 0.02 M Tris–HCl, pH = 7.5) and homogenized using a homogenizer (NANOJ H10, ATS Engineering Inc., Germany) for 2 min. The homogenate was centrifuged at 5,000 × *g* at 4°C for 10 min. After separating the supernatant containing the sarcoplasmic proteins, the precipitate was rinsed twice using the low-salt buffer. Afterward, the obtained precipitate was extracted at 4°C for 20 h with four times the weight of high-salt buffer (0.45 M NaCl, 0.02 M Tris–HCl, pH = 7.5). After centrifugation (12,000 × *g*, 15 min, 4°C), the supernatant was poured into ten times the weight of precool deionized water and the mixture was incubated for 30 min at 4°C to precipitate MP. Finally, the resulting precipitate (MP) was collected by centrifugation (12,000 × *g*, 10 min, 4°C), and dissolved with 0.6 M NaCl, 0.02 M Tris–HCl buffer (pH = 7.5) to prepare MP mother solution. The concentration of MP was determined by the BCA method employing bovine serum albumin as the standard.

Determination of total sulfhydryl content and Ca^{2+}-ATPase activity

A total SH measurement kit (Nanjing Jiancheng Bioengineering Institute, China) was used to measure the total SH content of MP according to its instruction. The MP solution was diluted to 2.5–4 mg/ml with 0.6 M NaCl (pH = 7.0). In order to denature the protein, the diluted MP solution (0.5 ml) was added to 4.5 ml of 0.2 M Tris–HCl buffer (pH = 6.8) containing 8 M urea, 2.0% SDS and 0.01 M EDTA. To determine the total SH content, 0.4 ml of 0.1% 5, 5-dithiobis (2-nitrobenzoic acid) (DTNB) in 0.2 M Tris–HCl buffer (pH = 8.0) was added to 4 ml of the mixture containing denatured proteins and incubated at 40°C for 25 min. The absorbance of the reaction mixture at 412 nm was determined using an UV-5200 spectrophotometer (Shanghai Metash Instruments Co., Ltd, Shanghai, China), and SH concentration was calculated by the Equation 3. The results of total SH content were expressed as μmol/g prot.

$$\text{SH concentration } (\mu\text{mol/g prot}) = A \times D/(B \times C) \quad (3)$$

where A is the measured absorbance, B is the concentration of MP solution, C is the molar extinction coefficient of 13,600 M^{-1} cm^{-1}, and D is the dilution volume.

A Ca^{2+}-ATPase kit (Nanjing Jiancheng Bioengineering Institute, China) was applied to determine the Ca^{2+}-ATPase activity of MP according to its instruction. An aliquot (1 ml) of the diluted MP solution (2.5–8 mg/ml) was added to 0.6 ml of 0.5 M Tris-maleate buffer (pH = 7.0), and 1 ml of 0.1 M calcium chloride. The total volume of the reaction solution was supplemented with deionized waster to 9.5 ml. The reaction was initiated by the addition of 0.5 ml of ATP (0.02 M). After incubation at 25°C for 8 min, the reaction was terminated by adding 5 ml of 15% (w/v) trichloroacetic acid (TCA), and the reaction mixture was centrifuged at 3,500 × *g* for 5 min. The blank was carried out by adding 15% TCA before the diluted MP solution (2.5–8 mg/ml) was added. The inorganic phosphate liberated in the supernatant was measured by the method of Benjakul et al. (36). The results of Ca^{2+}-ATPase activity were expressed by the concentration of released inorganic phosphate (Pi) indicated as μmol Pi/mg prot/h.

Circular dichroism spectroscopy

The secondary structure of MP was investigated by a circular dichroism (CD) spectropolarimeter (Jasco J-1500-150, Jasco Corp., Tokyo, Japan). The MP solution was put into a dialysis bag and dialyzed for 12 h at 4°C. A 300 μl aliquot of the

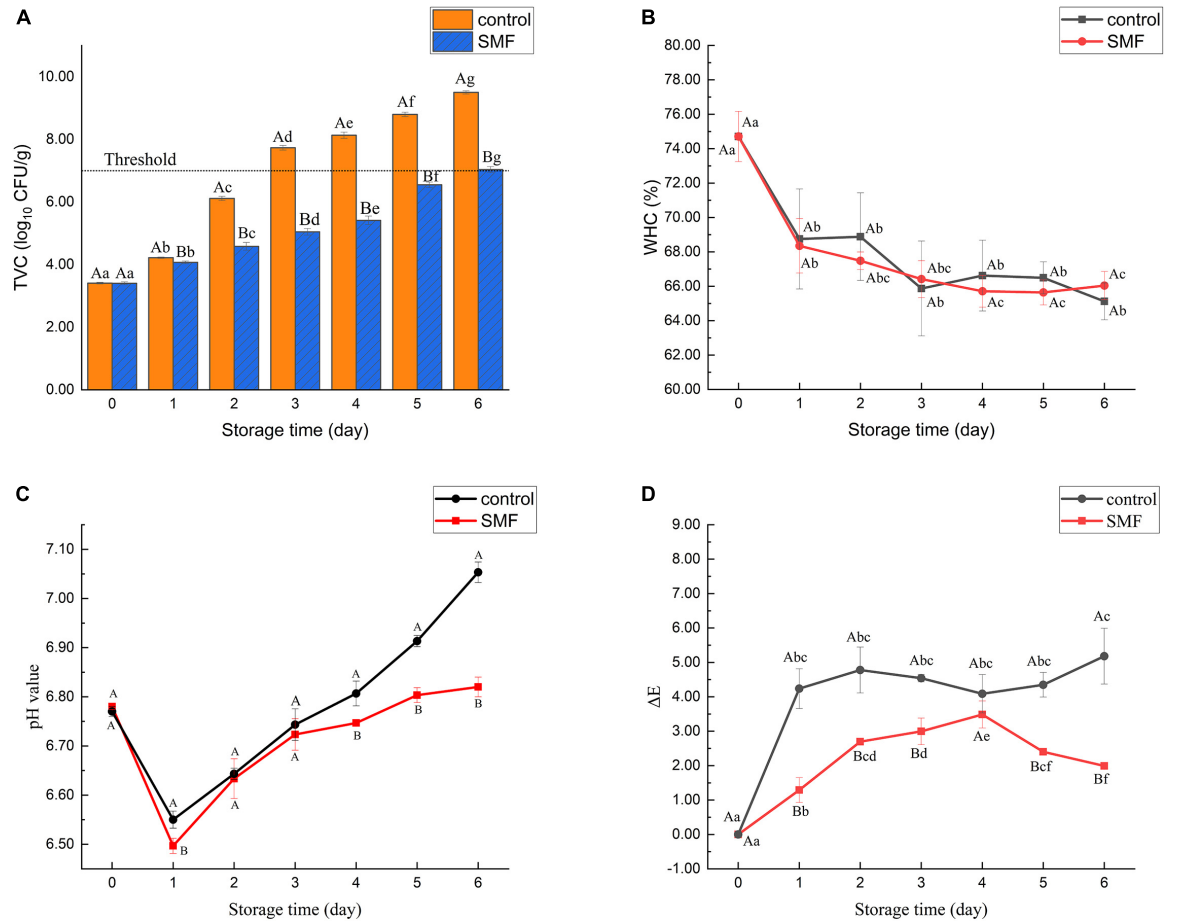

FIGURE 1
Changes in TVC **(A)**, WHC **(B)**, pH value **(C)**, and color differences **(D)** of sea bass fillets with different treatments. The dotted line in panel **(A)** shows the upper acceptable limit (7.0 $\log_{10}$ CFU/g). SMF: treated with static magnetic field (5 mT) at 4°C, control: storage at 4°C without SMF. Different capital letters indicate statistically significant differences between samples with different treatments on the same day ($p < 0.05$), and different lowercase letters indicate statistically significant differences between samples with different storage time under the same treatment ($p < 0.05$), the same below.

dialyzed MP solution (0.2 mg/ml) was placed in a 1 mm quartz CD cell (Hellma, Muellheim, Baden, Germany). The main parameters were set as follows: 1.0 nm bandwidth, 1 s D.I.T., 200 mdeg/1.0 dOD of CD and FL scale, 50 nm/min scan speed and 0.1 nm/data step resolution. The spectral scanning range was from 190 to 260 nm. Three scans were averaged to obtain one spectrum. Circular dichroism of MP structure was expressed by the mean specific ellipticity [θ] (deg·cm^2·dmo^{l-1}). The percentage of the secondary structure of MP was evaluated by Yang et al. (37) method.

Statistical analysis

Statistical data were subjected to analysis of one-way ANOVA followed by the Duncan procedure between means (significance was defined at $p < 0.05$) using IBM SPSS Statistics 25 (SPSS Inc., Chicago, IL, USA). Unless otherwise stated, all results were presented as the means ± standard deviation (SD). The figures were drawn by Origin 2019b (Origin Lab, Northampton, MA, USA).

Results and discussion

Effect of static magnetic field treatment on total viable counts

Changes in TVC of the sea bass fillet with different treatments are shown in **Figure 1A**. The initial count in the sample was 3.4 $\log_{10}$ CFU/g, indicating excellent quality of fresh fish. This load was similar to that of Japanese sea bass (*Lateolabrax japonicus*) reported by Li et al. (2). After 3 days of storage, it was observed that TVC of the control exceeded

TABLE 1 Effect of static magnetic field on color of the sea bass fillet during cold storage at 4°C.

	L*		a*		b*	
Storage time (day)	**Control**	**SMF**	**Control**	**SMF**	**Control**	**SMF**
0	44.19 ± 1.05^{a}	41.11 ± 0.95^{a}	-0.66 ± 0.47^{a}	-1.69 ± 0.09^{a}	-3.24 ± 0.18^{a}	-4.16 ± 0.27^{a}
1	39.99 ± 0.50^{bc}	40.21 ± 0.79^{ab}	-0.45 ± 0.41^{ab}	-0.96 ± 0.28^{b}	-2.9 ± 0.72^{a}	-3.62 ± 0.62^{ab}
2	39.53 ± 1.81^{b}	38.80 ± 1.33^{b}	-0.09 ± 0.41^{b}	-0.78 ± 0.34^{bc}	-2.54 ± 0.74^{ab}	-3.33 ± 0.90^{ab}
3	40.11 ± 1.12^{bc}	39.25 ± 0.91^{b}	0.66 ± 0.46^{c}	0.27 ± 0.41^{d}	-1.82 ± 0.74^{bc}	-2.89 ± 0.63^{b}
4	40.68 ± 0.92^{bc}	38.20 ± 1.02^{b}	-0.66 ± 0.40^{a}	-0.28 ± 0.79^{c}	-1.29 ± 1.10^{c}	-3.03 ± 0.79^{b}
5	41.03 ± 1.09^{c}	38.93 ± 1.09^{b}	-0.73 ± 0.28^{a}	-0.86 ± 0.40^{b}	-0.06 ± 0.74^{d}	-3.67 ± 0.44^{ab}
6	42.49 ± 0.55^{d}	39.59 ± 1.10^{ab}	-0.78 ± 0.46^{a}	-0.72 ± 0.38^{bc}	1.65 ± 0.86^{e}	-3.36 ± 0.33^{ab}

Results are presented as the mean ± SD. Different lowercase letters in a column indicate statistically significant differences between samples with different storage time ($p < 0.05$). SMF: treated with static magnetic field (5 mT) at 4°C, control: storage at 4°C without SMF.

the maximum acceptable level of TVC (7.0 $\log_{10}$ CFU/g) of freshwater and marine fish (38). By contrast, microbial counts in sea bass fillets treated with SMF for 6 days exceeded the edible limits. Therefore, these results reveal that SMF treatment could effectively extend the shelf life of the sea bass fillet from a microbiological point of view. Lins et al. (39) reported that 1 Hz pulsed magnetic field treatment (PMF, 10 mT), a type of time-varying magnetic field, for 2 h could reduce microbial counts in fresh beef during cold storage, while continuing exposure to PMF for 12 days did not significantly inhibit the growth of bacteria. They suggested that the surviving bacteria might have adapted to the PMF. In the present study, similar or even better bacteriostatic effects could be achieved by SMF treatment of 5 mT, while the energy required was lower.

Previous studies have suggested that the antimicrobial effect of SMF may rely on alterations in membrane calcium ion flux, which would result in the deformation of imbedded ion channels, thereby altering their activation kinetics and influencing several biological systems (40, 41). In addition, the inactivation efficacy of microorganisms depends on magnetic field process parameters (such as type, intensity, frequency, and duration of action), microorganism properties (such as types, growth phase, and density) (28). Consequently, the window effect hypothesis has been proposed for the different effects of magnetic field on the growth of microorganisms, that is, specific parameters correspond to specific microorganisms (42, 43).

Effect of static magnetic field treatment on water holding capacity

Water holding capacity is a crucial attribute reflecting fish quality, and it may represent the ability of muscle protein to prevent water from being released under external forces. As shown in **Figure 1B**, a decrease in WHC was observed in the sea bass fillet treated with and without SMF, and no significant difference was observed between them during the entire cold storage. Some studies confirmed that the WHC was often related to protein structures (44, 45). During storage, the denaturation of myosin will alter the water distribution in the fish, resulting in a considerable loss of the free water content in fish and a significant decrease in the WHC. Therefore, our results suggest that significant protein denaturation may occur in sea bass fillets. Yang et al. (46) found that the direct current magnetic field (DC-MF) treatment could improve WHC of MP gels, and this might be attributed to protein unfolding, re-crosslinking and aggregation induced by DC-MF. The results of the present study are inconsistent with these. It is possible that, due to the differences in biological characteristics between raw materials, differences in WHC of sea bass fillets are more difficult to detect during exposure to SMF.

Effect of static magnetic field treatment on pH

Figure 1C shows the changes of pH in the sea bass fillet with different treatments. The pH of all samples decreased in the early stage of storage and then increased gradually, while the pH of the SMF-treated samples remained consistently lower than that of the control ($p < 0.05$). One possible explanation for the initial decrease in pH could be the accumulation of lactic acid, a product of glycolysis (47). In glycolysis, glucose is metabolized to the final product pyruvate, which is converted to lactic acid by lactate dehydrogenase (48). However, there are no published data showing that lactate dehydrogenase activity is directly modulated by SMF, so further exploration is required. In addition, the accumulation of alkaline substances such as amines and ammonia produced by spoilage bacteria may be responsible for the increase of pH value of fish samples in the late period of storage (28, 49, 50). Thus, this result is consistent with the change of microbial counts stated in section "Effect of static magnetic field treatment on total viable counts," and demonstrate that SMF treatment not only inhibits the growth of microorganisms but also restrains other autolytic processes that generate alkaline substances.

TABLE 2 Effect of static magnetic field on texture of the sea bass fillet during cold storage at 4°C.

Storage time (day)	Hardness (g)		Springiness		Cohesiveness		Chewiness	
	Control	SMF	Control	SMF	Control	SMF	Control	SMF
0	$2{,}304.0 \pm 143.3^{Aa}$	$2{,}288.0 \pm 124.3^{Aa}$	0.57 ± 0.06^{Aa}	0.58 ± 0.05^{Aa}	0.42 ± 0.04^{Aa}	0.42 ± 0.04^{Aa}	786.8 ± 133.2^{Aa}	786.8 ± 175.2^{Aa}
1	$1{,}796.8 \pm 113.5^{Ab}$	$1{,}968.1 \pm 91.4^{Ab}$	0.48 ± 0.03^{Ab}	0.49 ± 0.03^{Abc}	0.41 ± 0.04^{Aa}	0.40 ± 0.04^{Aa}	350.7 ± 31.9^{Ab}	382.3 ± 54.0^{Ab}
2	$1{,}417.3 \pm 141.0^{Ac}$	$1{,}641.0 \pm 163.6^{Ac}$	0.43 ± 0.04^{Ab}	0.46 ± 0.02^{Abc}	0.38 ± 0.03^{Aa}	0.38 ± 0.02^{Aa}	225.0 ± 28.2^{Ac}	291.5 ± 51.8^{Abc}
3	$1{,}386.8 \pm 79.0^{Bc}$	$1{,}568.5 \pm 32.6^{Acd}$	0.46 ± 0.01^{Ab}	0.46 ± 0.03^{Abc}	0.39 ± 0.02^{Aa}	0.38 ± 0.02^{Aa}	248.1 ± 18.6^{Abc}	276.2 ± 24.2^{Abc}
4	$1{,}249.7 \pm 121.2^{Acd}$	$1{,}355.5 \pm 56.1^{Ade}$	0.46 ± 0.04^{Ab}	0.46 ± 0.01^{Abc}	0.38 ± 0.02^{Aa}	0.39 ± 0.01^{Aa}	218.8 ± 45.0^{Ac}	260.1 ± 24.0^{Abc}
5	$1{,}135.9 \pm 157.4^{Ad}$	$1{,}191.5 \pm 119.6^{Aef}$	0.42 ± 0.03^{Ab}	0.45 ± 0.03^{Abc}	0.39 ± 0.03^{Aa}	0.40 ± 0.02^{Aa}	189.8 ± 35.9^{Acd}	216.0 ± 29.6^{Ac}
6	702.0 ± 66.9^{Be}	$1{,}132.4 \pm 96.42^{Af}$	0.43 ± 0.02^{Ab}	0.41 ± 0.01^{Ac}	0.34 ± 0.07^{Aa}	0.40 ± 0.03^{Aa}	104.5 ± 29.9^{Bd}	186.6 ± 20.6^{Ac}

Results are presented as the mean ± SD. Different capital letters in a row indicate statistically significant differences between samples with different treatments ($p < 0.05$); different lowercase letters in a column indicate statistically significant differences between samples with different storage time ($p < 0.05$). SMF: treated with static magnetic field (5 mT) at 4°C, control: storage at 4°C without SMF.

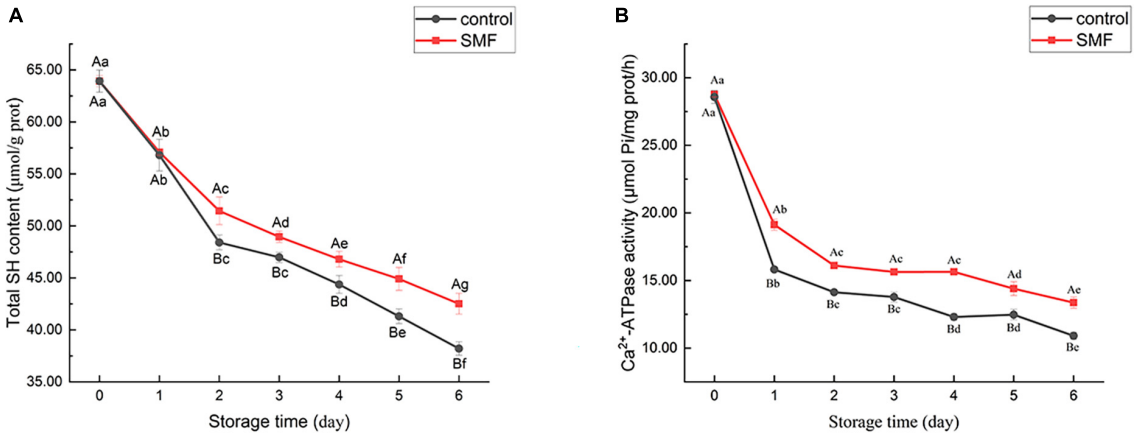

FIGURE 2
Changes in total SH content **(A)** and Ca^{2+}-ATPase activity **(B)** of sea bass fillets with different treatments.

Effect of static magnetic field treatment on color

Color is one of the most direct and satisfactory indicators for consumers to evaluate the freshness of fish (51). **Figure 1D** shows changes in absolute color difference (ΔE) of the sea bass fillet with different treatments. The values of ΔE presented an increasing trend during storage, and the ΔE value of the control sample was higher than that in the SMF-treated sample ($p < 0.05$). Color differences larger than 2–4 are considered perceptible to consumers (52). In our data, the sea bass fillet treated with SMF would be perceived as less color change than the control fillet by consumers, indicating that SMF treatment could delay the discoloration of fish fillets. As recorded in **Table 1**, the increase in ΔE value may be due to changes in a* and b* values, since changes in L* value of the SMF-treated samples were similar to those of the control. Hence the color variation between samples is mainly reflected in redness and yellowness, and the reasons for these changes are discussed below. In addition, the changes in the refractive index of the fish surface caused by decreased WHC could directly affect the L* value of fish (21). As discussed in section "Effect of static magnetic field treatment on water holding capacity," SMF treatment did not cause significant enhancement in WHC, which was reflected in the similar changes in L* value between the SMF-treated and control samples.

The a* value of meat is determined by the rate of oxymyoglobin oxidation and metmyoglobin reducing activity (53, 54). Oxymyoglobin is redness in color and is produced when myoglobin is oxygenated or exposed to oxygen, while methemoglobin is brown in color and occurs when oxygen concentration is between 0.5 and 1% or when meat is exposed to air for a long time (55). The initial a* value for SMF-treated fillet was lower than that in the control at day 0, which may be due to the inherent color differences between individuals. In the early stage of storage, the a* value of the fillet treated with SMF increased more, indicating that the myoglobin in

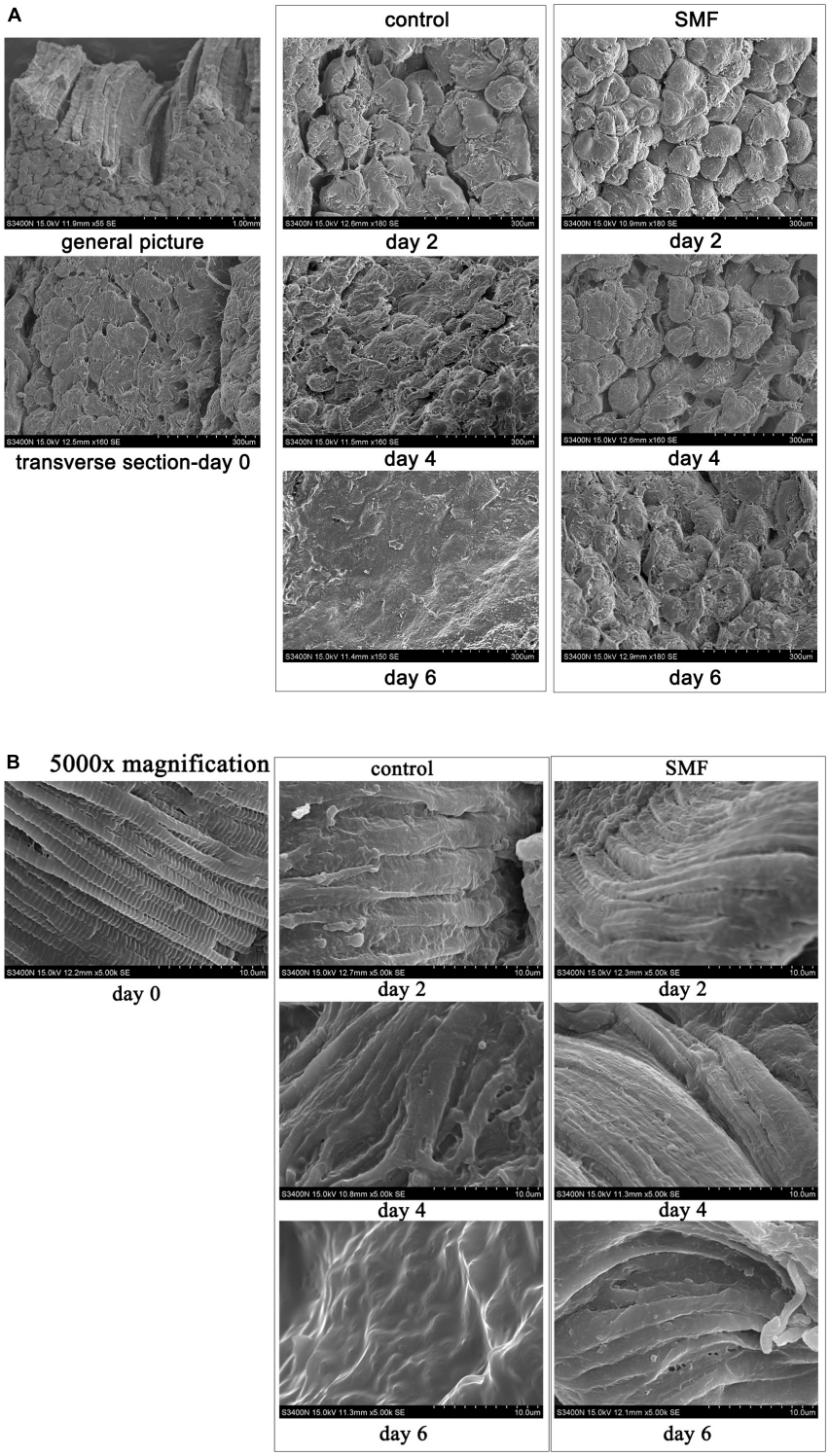

FIGURE 3
Microstructure of the sea bass muscle observed by SEM. **(A)** Transverse sections, **(B)** transverse sections at 5,000× magnification.

the fillet was accelerated to form oxymyoglobin, which may be related to the fact that magnetic field treatment could promote the unfolding of myoglobin structure (56). Myoglobin would be more susceptible to oxidative attack due to the unfolded structure. In the later stage of storage, decreased a* values were observed in both SMF-treated and control fillets, while

the decrease trend was relatively slighter in the fillets treated with SMF. The similar tendency of a* value for the SMF-treated fish was also found for other refrigerated meat products, such as static magnetic field extended supercooling (SM-ES) treated beef (25). This is not surprising since longer-stored fish fillets were expected to contain high levels of methemoglobin, which cause the surface color of the fillet to shift toward brown. Previous results in the literature have proven that low frequency magnetic field treatments (3, 6, 9, 12 mT, 50 Hz) for 10 h could effectively inhibit the increase of methemoglobin content in the solution of horse skeletal muscle myoglobin (57). Therefore, these results confirm that SMF treatment could stabilize the redness of the fish fillet.

The b* values in all sea bass fillets showed an increasing tendency during cold storage, expressing an evolution toward gray yellow tones as the fillets aged. Our results are consistent with data reported by Cai et al. (58), showing a significant increase in the b* parameter of Japanese sea bass fillets stored under refrigerated conditions. On the other hand, the b* value of the sea bass fillet increased more slowly when treated with SMF, suggesting the yellowish of SMF-treated fillets was not pronounced. Yellow color is often associated with lipid and protein oxidation (59). Therefore, the significant decrease detected in the b* value of the SMF-treated fillet might be attributed to SMF-induced antioxidant effects.

Effect of static magnetic field treatment on textural properties

Textural properties are valued quality indicators reflecting sensory and functional properties of fish. The variations in texture parameters of the sea bass fillet with different treatments are presented in **Table 2**. The TPA results showed that after 6 days of storage, the hardness, springiness, cohesiveness, and chewiness of the control sample decreased by 69.5, 24.6, 19.0, and 86.7%, respectively. These results indicated that the fish fillet began to soften and lose its elasticity. However, the corresponding values for the SMF-treated sample decreased by 50.5, 29.3, 4.8, and 76.3%, respectively. The evaluation results of texture properties showed that the SMF-treated sea bass fillet had a better texture than the control. A similar phenomenon was reported by Zhu et al. (31), who found that alternating magnetic field treatment (AMF, 5 mT), a type of time-varying magnetic field, could further delay the texture deterioration of ultra-high pressure treated shrimp, while AMF treatment had an adverse effect on the color of shrimp.

Muscle texture in fish is determined by several intrinsic biological parameters, such as the density of muscle fiber and the content of fat and collagen (32). Besides, autolysis is triggered by the death of the fish, softening the muscles under the combined effect of microbial activity (60). In our study, it was observed that microbial activity was inhibited by SMF treatment, which resulted in lower bacterial load and slighter protein degradation in the SMF-treated fillet. Therefore, the SMF-treated fillet exhibited significant improvements in textural properties, probably due to the magnetic field-induced inactivation of microorganisms and changes in the autolysis process.

Effect of static magnetic field treatment on total sulfhydryl content of myofibrillar protein

Sulfhydryl groups are present in MP, mainly in the head of myosin (61). The content of SH groups is recognized as an important indicator of the integrity of myosin (36). Changes in the total SH content of MP extracted from sea bass muscles with different treatments are shown in **Figure 2A**. Compared with fresh muscle, the final content of total SH in SMF-treated and control samples were 42.52 and 38.21 μmol/g prot, which decreased by 33.5 and 40.2%, respectively. The reduction in SH group content has been reported to be due to the formation of disulfide bonds through oxidation of SH groups or disulfide interchanges (62). As can be seen, SMF-treated samples tended to show less decrease in total SH content, particularly in later stage of storage. In other words, SMF treatment could suppress the oxidation of SH groups in MP during cold storage. Protein oxidation would modify the amino acid sidechains and alter the protein polypeptide backbone, resulting in structural changes in the protein (63, 64). The ion–protein dissociation proposed by Bingi and Savin (65) might explain the effect of magnetic field on protein oxidation, when an ion enters a protein cavity containing a ligand, it would undergo directional movement under the influence of the magnetic field. Such directional movement may induce the formation of local micro-electric fields, which disturb the original equilibrium distribution in the ion cloud, thereby causing different biological responses (16).

Effect of static magnetic field treatment on Ca^{2+}-ATPase activity of myofibrillar protein

The Ca^{2+}-ATPase activity is an important indicator of the integrity of myosin. Any change in the conformation of myosin would lead to a decrease in enzyme activity (66, 67). A notable decrease in Ca^{2+}-ATPase activity was observed in all samples (**Figure 2B**), indicating that myosin underwent denaturation. Thus, the denaturation of myofibrillar proteins during cold storage may account for the reduction in WHC. Myofibrillar proteins, which are primarily responsible for water-binding properties, suffered severe denaturation and, consequently, significantly reduced WHC was observed in both control and SMF samples.

It is noteworthy that the decrease of Ca^{2+}-ATPase activity was remarkably lower in the presence of SMF than in their absence ($p < 0.05$). Loss of Ca^{2+}-ATPase activity is postulated to be the conformational changes and aggregation in the globular head of myosin (61, 68). Moreover, the loss of Ca^{2+}-ATPase activity could also be caused by the oxidation of SH_1 and SH_2 on the active site of actomyosin (36, 69). In our study, the decrease in Ca^{2+}-ATPase activity was in agreement with the decrease in total SH content (**Figure 2A**). In addition, protein rearrangements *via* protein–protein interactions are also considered to be responsible for the loss in Ca^{2+}-ATPase activity (70). Overall, the above researches demonstrated that the loss in Ca^{2+}-ATPase activity is associated with the denaturation and oxidation of protein, and alteration in protein conformation, and our results suggest that SMF treatments could effectively retard these processes and stabilize the structure of protein.

Effect of static magnetic field on muscle microstructure

The microstructural changes in the transverse direction of the sea bass muscle with different treatments are shown in **Figure 3**. At day 0, single myofiber could be easily distinguished in the transverse fiber fracture, and the boundary between the myofibers was clear (**Figure 3A**). From the micrographs of control samples, clear changes in the cross-sectional structure of myofibers were visible. The boundaries between the adjacent myofibers were not visible any longer, and myofibers had largely agglomerated into lamellae. Compared with the controls, SMF treatment could reduce the structural changes of myofibers in the sea bass muscle during storage. No significant change was apparent in the myofibers, and the boundary between the myofibers was clearly identified, under SMF treatment of 5 mT for 2 and 4 days, respectively. After 6 days of SMF treatment, distorted myofibers were also observed, but to a lesser extent, suggesting a slower development of the structural changes under SMF treatment.

In addition, higher magnification of sea bass muscle was used to examine the myofiber structure in more detail. The sarcomere is the basic contractile unit of the striated muscle and is arranged in a stacked fashion throughout the muscle tissue (71). The defined brick structure of the sarcomere, intact and compact, was obviously observed in the fresh sample at day 0 (**Figure 3B**). After 6 days of storage at 4°C, it was not possible to identify the individual sarcomere or even transverse elements, and the striated structure of the myofibers disappeared and the contractile elements of the muscle fibers disintegrated. Applying SMF of 5 mT stabilized the structure of sarcomere, where Z-band (the dividing line between the sarcomeres) was visible (day 2), although the sarcomere structure appeared to be disrupted in samples treated with SMF for 6 days. These might suggest that SMF treatment partly protects sea bass muscle fibers from damage caused by aging and microbial associated proteolysis, as shown in sea bass (72).

Effect of static magnetic field treatment on the secondary structure of myofibrillar protein

The CD spectrums of MP extracted from sea bass muscles with different treatments are shown in **Figures 4A,B**. The CD spectrum of all samples exhibited two main minima at around 208 and 222 nm. The two bands were rationalized by the n-π^* transition in the peptide bond of α-helix, therefore, corresponding to the changes in α-helical structure (73). Secondary structure analysis of MP is exhibited in **Figures 4C,D**. The percentages of α-helix, β-turn, and random coil in SMF-treated samples had no significant decrease from day 0 to day 6 ($p > 0.05$), implying that the secondary structure of MP did not undergo severe damage. Conversely, the percentages of α-helix in the controls decreased whilst the percentages of random coil increased, suggesting a gradual loss of the helical structure in MP. The α-helix component was likely transformed into the random coil. Similar results were also shown in a study reported by Zhang et al. (74), in which the secondary structure of grouper (*Epinephelus coioides*) protein transformed from α-helix to random coil during cold storage. These results suggest that SMF treatment was effective in preserving the α-helix structure.

The gradual deletion of α-helix in MP was related to structural changes in myosin, including the unfolding of the α-helix structure of the myosin rod portion (75). As described in section "Effect of static magnetic field treatment on total sulfhydryl content of myofibrillar protein" and "Effect of static magnetic field treatment on Ca^{2+}-ATPase activity of myofibrillar protein," myosin was subjected to severe oxidation and denaturation during cold storage and, consequently, the decrease in the content of α-helix was detected. In addition, the content of α-helical structure is also related to the hydrogen bond stability between the carbonyl oxygen and amino hydrogen of the polypeptide chain (34). Enhanced strength of hydrogen bonds after magnetic field treatment has been previously reported in some bacteria and cells (76, 77). She et al. (77) described the transition of random coils to α-helices, and intermolecular β-sheets to intramolecular ones in the secondary structure of proteins in *E. coli* after SMF treatment at 10 T for 30 min, and they suggested that this may be due to the destruction of intermolecular cohesion and the enhancement of intramolecular hydrogen bonds. Thus, differences in the stability of α-helical structures between SMF-treated and control samples could be attributed to SMF-induced effects, including antioxidant effects and enhancement of intramolecular hydrogen bonds.

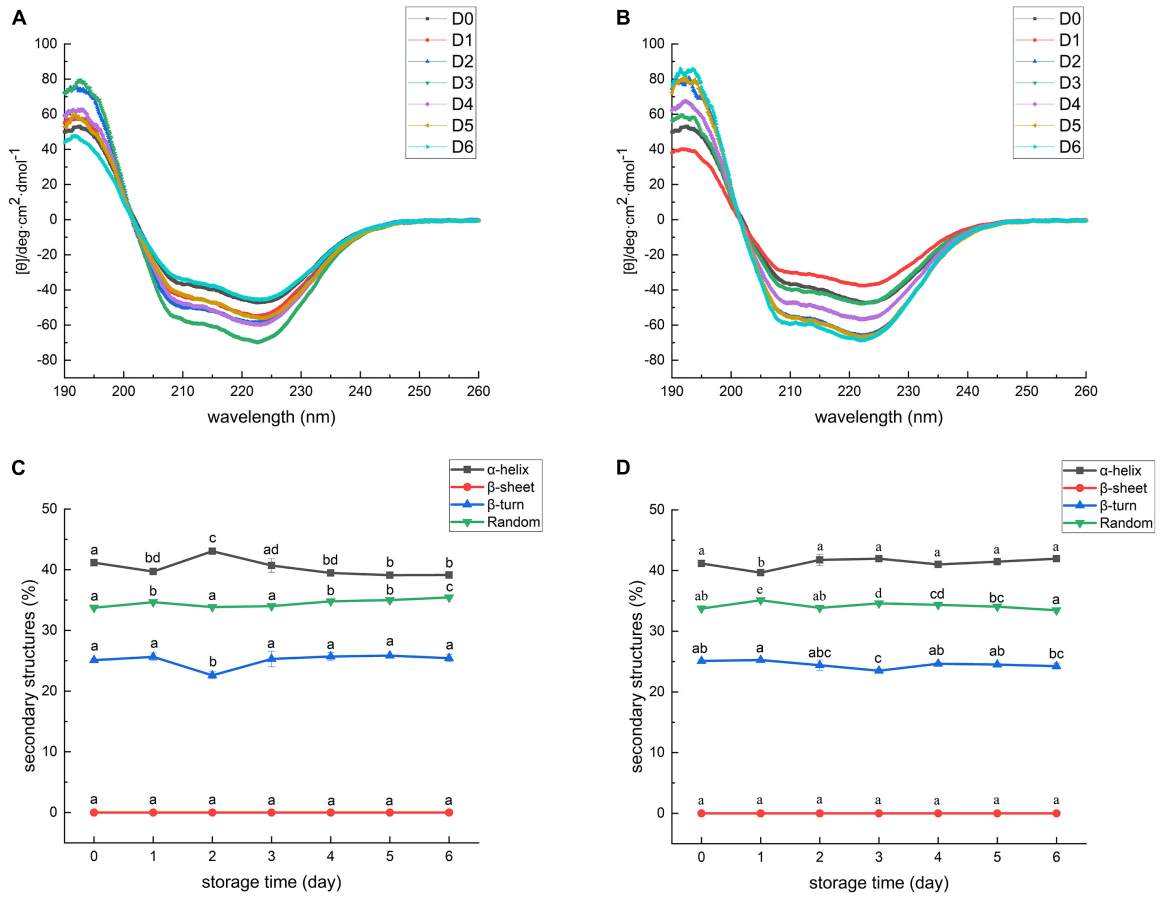

FIGURE 4
Circular dichroism spectra of myofibrillar protein from sea bass. **(A)** Control; **(B)** SMF. D0, 1, 2, 3, 4, 5, 6 represent day 0, 1, 2, 3, 4, 5, 6, respectively. Secondary structure of myofibrillar protein from sea bass. **(C)** Control; **(D)** SMF. Different lowercase letters on the top of bars indicated statistically significant differences between samples ($p < 0.05$).

Conclusion

This study investigated the feasible application of SMF treatment (5 mT) in mitigating the quality deterioration of the sea bass fillet during cold storage. The results of microbiological and physicochemical properties showed that SMF treatment could effectively slow down the rate of quality deterioration of the sea bass fillet. SMF treatment not only inhibited microbial growth, but also suppressed the protein structural changes. The inhibition of microbial metabolism and the stabilization of protein structure under SMF treatment resulted in lower pH and ΔE values, and the better texture in SMF-treated samples. Therefore, our results show that SMF treatment could be utilized as an effective approach for maintaining the quality of fish. In this study, the beneficial effects of SMF treatment on maintaining the quality of sea bass fillets may be limited, which is associated with magnetic field parameters, whereas the mechanism of SMF-induced effects is also worth exploring. Thus, future research working on SMF-assisted fish preservation should include optimal intensity, operating time, distribution of SMF, as well as whether the responses of different fish species are consistent.

Data availability statement

The original contributions presented in this study are included in the article/supplementary material, further inquiries can be directed to the corresponding author.

Author contributions

LT: methodology, validation, investigation, data curation, formal analysis, visualization, and writing—original draft and review and editing. HT: supervision, resources, and writing—review. JC: investigation and writing—review and editing. SS: conceptualization. RL: data curation. ZZ: methodology. CO: conceptualization, supervision,

project administration, resources, funding acquisition, and writing—review and editing. All authors contributed to the article and approved the submitted version.

Funding

This study was supported by the National Key Research and Development Program under Grant 2019YFD0901705.

Acknowledgments

We are grateful to the reviewers for their constructive comments on the manuscript.

Conflict of interest

The authors declare that the research was conducted in the absence of any commercial or financial relationships that could be construed as a potential conflict of interest.

Publisher's note

All claims expressed in this article are solely those of the authors and do not necessarily represent those of their affiliated organizations, or those of the publisher, the editors and the reviewers. Any product that may be evaluated in this article, or claim that may be made by its manufacturer, is not guaranteed or endorsed by the publisher.

References

1. Franceschelli L, Berardinelli A, Dabbou S, Ragni L, Tartagni M. Sensing technology for fish freshness and safety: a review. *Sensors (Basel).* (2021) 21:1373. doi: 10.3390/s21041373

2. Li P, Peng Y, Mei J, Xie J. Effects of microencapsulated eugenol emulsions on microbiological, chemical and organoleptic qualities of farmed Japanese sea bass (*Lateolabrax japonicus*) during cold storage. *LWT Food Sci Technol.* (2020) 118:108831. doi: 10.1016/j.lwt.2019.108831

3. Shi L, Yin T, Xiong GQ, Ding AZ, Li X, Wu WJ, et al. Microstructure and physicochemical properties: effect of pre-chilling and storage time on the quality of channel catfish during frozen storage. *LWT Food Sci Technol.* (2020) 130:109606. doi: 10.1016/j.lwt.2020.109606

4. Zhang MC, Xia XF, Liu Q, Chen Q, Kong BH. Changes in microstructure, quality and water distribution of porcine longissimus muscles subjected to ultrasound-assisted immersion freezing during frozen storage. *Meat Sci.* (2019) 151:24–32. doi: 10.1016/j.meatsci.2019.01.002

5. Lu H, Zhang L, Shi J, Wang Z, Luo Y. Effects of frozen storage on physicochemical characteristics of bighead carp (*Aristichthys nobilis*) fillets. *J Food Process Preserv.* (2019) 43:e14141. doi: 10.1111/jfpp.14141

6. Hu R, Zhang M, Liu WC, Mujumdar AS, Bai BS. Novel synergistic freezing methods and technologies for enhanced food product quality: a critical review. *Compr Rev Food Sci Food Saf.* (2022) 21:1979–2001. doi: 10.1111/1541-4337.12919

7. Smichi N, Abdelmalek BE, Kharrat N, Sila A, Bougatef A, Gargouri Y, et al. The effects of storage on quality and nutritional aspects of farmed and wild sea bass (*Dicentrachus labrax*) muscle: in vitro oils digestibility evaluation. *Fish Res.* (2017) 188:74–83. doi: 10.1016/j.fishres.2016.12.003

8. Kang, T, You Y, Jun S. Correction to: supercooling preservation technology in food and biological samples: a review focused on electric and magnetic field applications. *Food Sci Biotechnol.* (2020) doi: 10.1007/s10068-020-00786-8

9. Olatunde OO, Benjakul S, Vongkamjan K. Cold plasma combined with liposomal ethanolic coconut husk extract: a potential hurdle technology for shelf-life extension of Asian sea bass slices packaged under modified atmosphere. *Innov Food Sci Emerg Technol.* (2020) 65:102448. doi: 10.1016/j.ifset.2020.102448

10. Valizadeh S, Naseri M, Babaei S, Hosseini SMH. Shelf life extension of fish patty using biopolymer-coated active paper sheets. *Food Packag Shelf Life.* (2020) 26:100603. doi: 10.1016/j.fpsl.2020.100603

11. Yu DW, Regenstein JM, Xia WS. Bio-based edible coatings for the preservation of fishery products: a review. *Crit Rev Food Sci Nutr.* (2019) 59:2481–93. doi: 10.1080/10408398.2018.1457623

12. Wang, Y, Zhou Y, Wang XX, Ma F, Xu BC, Li PJ, et al. Origin of high-pressure induced changes in the properties of reduced-sodium chicken myofibrillar protein gels containing CaCl2: physicochemical and molecular modification perspectives. *Food Chem.* (2020) 319:126535. doi: 10.1016/j.foodchem.2020.126535

13. Zhang J, Tang T, Jiang Z, Liu YY, Jiang AM. The modification of ovalbumin surface properties treated by pulsed electric field combined with divalent metal ions. *Food Chem.* (2019) 293:455–62. doi: 10.1016/j.foodchem.2019.05.016

14. Pan JY, Zhang ZL, Mintah BK, Xu HN, Dabbour M, Cheng Y, et al. Effects of nonthermal physical processing technologies on functional, structural properties and digestibility of food protein: a review. *J Food Process Eng.* (2022) 45:e14010. doi: 10.1111/jfpe.14010

15. Rathod NB, Ranveer RC, Bhagwat PK, Ozogul F, Benjakul S, Pillai S, et al. Cold plasma for the preservation of aquatic food products: an overview. *Compr Rev Food Sci Food Saf.* (2021) 20:4407–25. doi: 10.1111/1541-4337.12815

16. Miñano HLA, Silva ACDS, Souto S, Costa EJX. Magnetic fields in food processing perspectives, applications and action models. *Processes.* (2020) 8:814. doi: 10.3390/pr8070814

17. Guo LN, Azam SMR, Guo YT, Liu DD, Ma HL. Germicidal efficacy of the pulsed magnetic field against pathogens and spoilage microorganisms in food processing: an overview. *Food Control.* (2022) 136:108496. doi: 10.1016/j.foodcont.2021.108496

18. Otero L, Rodriguez AC, Perez-Mateos M, Sanz PD. Effects of magnetic fields on freezing: application to biological products. *Compr Rev Food Sci Food Saf.* (2016) 15:646–67. doi: 10.1111/1541-4337.12202

19. Shine MB, Guruprasad KN, Anand A. Enhancement of germination, growth, and photosynthesis in soybean by pre-treatment of seeds with magnetic field. *Bioelectromagnetics.* (2011) 32:474–84. doi: 10.1002/bem.20656

20. Kaur M, Kumar M. An innovation in magnetic field assisted freezing of perishable fruits and vegetables: a review. *Food Rev Int.* (2020) 36:761–80. doi: 10.1080/87559129.2019.1683746

21. Lin H, He X, Liu C, Meng J, Guan W, Hou C, et al. Static magnetic field-assisted supercooling preservation enhances water-holding capacity of beef during subzero storage. *Innov Food Sci Emerg Technol.* (2022) 80:103106. doi: 10.1016/j.ifset.2022.103106

22. Jha PK, Xanthakis E, Jury V, Le-Bail A. An overview on magnetic field and electric field interactions with ice crystallisation; application in the case of frozen food. *Crystals.* (2017) 7:229. doi: 10.3390/cryst7100299

23. Wei H, Fu R, Lin X, Feng A. Effect of magnetic field-assisted freezing on water migration, fractal dimension, texture, and other quality changes in tilapia. *J Food Process Preserv.* (2021) 45:e15940. doi: 10.1111/jfpp.15940

24. Leng D, Zhang H, Tian C, Xu H, Li P. The effect of magnetic field on the quality of channel catfish under two different freezing temperatures. *Int J Refrig.* (2022) 140:49–56. doi: 10.1016/j.ijrefrig.2022.05.008

25. Lin H, Zhao S, Han X, Guan W, Liu B, Chen A, et al. Effect of static magnetic field extended supercooling preservation on beef quality. *Food Chem.* (2022) 370:131264. doi: 10.1016/j.foodchem.2021.131264

26. Bajpai i, Saha N, Basu B. Moderate intensity static magnetic field has bactericidal effect on E. coli and S. epidermidis on sintered hydroxyapatite. *J Biomed Mater Res B Appl Biomater.* (2012) 100:1206–17. doi: 10.1002/jbm.b.32685

27. Raouia H, Hamida B, Khadidja A, Ahmed L, Abdelwaheb C. Effect of static magnetic field (200 mT) on biofilm formation in *Pseudomonas aeruginosa*. *Arch Microbiol.* (2020) 202:77–83. doi: 10.1007/s00203-019-01719-8

28. Filipic J, Kraigher B, Tepus B, Kokol V, Mandic-Mulec I. Effects of low-density static magnetic fields on the growth and activities of wastewater bacteria *Escherichia coli* and *Pseudomonas putida*. *Bioresour Technol.* (2012) 120:225–32. doi: 10.1016/j.biortech.2012.06.023

29. Tang JY, Shao SQ, Tian CQ. Effects of the magnetic field on the freezing process of blueberry. *Int J Refrig.* (2020) 113:288–95. doi: 10.1016/j.ijrefrig.2019.12.022

30. Zhao HX, Zhang F, Hu HQ, Liu S, Han JT. Experimental study on freezing of liquids under static magnetic field. *Chin J Chem Eng.* (2017) 25:1288–93. doi: 10.1016/j.cjche.2016.10.026

31. Zhu C, Chen L, Zeng X, Sun Y, Jiao D, Liu M, et al. Effects of ultra high pressure-magnetic field treatment on protein properties and quality characteristics of stored shrimp (*Litopenaeus vannamei*). *LWT.* (2022) 170:114070. doi: 10.1016/j.lwt.2022.114070

32. Hernandez MD, Lopez MB, Alvarez A, Ferrandini E, Garcia BG, Garrido MD. Sensory, physical, chemical and microbiological changes in aquacultured meagre (*Argyrosomus regius*) fillets during ice storage. *Food Chem.* (2009) 114:237–45. doi: 10.1016/j.foodchem.2008.09.045

33. Chmiel M, Słowiński M, Dasiewicz K, Florowski T. Use of computer vision system (CVS) for detection of PSE pork meat obtained from m. Semimembranosus. *LWT Food Sci Technol.* (2016) 65:532–6. doi: 10.1016/j.lwt.2015.08.021

34. Liu R, Zhao SM, Xiong SB, Xie BJ, Qin LH. Role of secondary structures in the gelation of porcine myosin at different pH values. *Meat Sci.* (2008) 80:632–9. doi: 10.1016/j.meatsci.2008.02.014

35. Ding Y, Liu R, Rong J, Liu Y, Zhao S, Xiong S. Rheological behavior of heat-induced actomyosin gels from yellowcheek carp and grass carp. *Eur Food Res Technol.* (2012) 235:245–51. doi: 10.1007/s00217-012-1750-7

36. Benjakul S, Seymour TA, Morrissey MT, An HJ. Physicochemical changes in Pacific whiting muscle proteins during iced storage. *J Food Sci.* (1997) 62:729–33. doi: 10.1111/j.1365-2621.1997.tb15445.x

37. Yang JT, Wu CS, Martinez HM. Calculation of protein conformation from circular dichroism. *Methods Enzymol.* (1986) 130:208–69. doi: 10.1016/0076-6879(86)30013-2

38. Icmsf. Sampling plans for fish and shellfish. In: Elliott RP, Clark DS, Lewis KH, Lundenbeck H, Olsen JC, Simonjen JB editors. *Microorganisms in Foods, Sampling for Microbiological Analysis: principles and Specific Applications*. (Vol. 2), (Toronto, ON: Toronto Press, University of Toronto) (1986). p. 181–96.

39. Lins PG, Silva AA, Pugine SMP, Arce AIC, Costa EJX, De Melo MP. Effect of exposure to pulsed magnetic field on microbiological quality, color and oxidative stability of fresh ground beef. *J Food Process Eng.* (2017) 40:e12405. doi: 10.1111/jfpe.12405

40. Rosen AD. Mechanism of action of moderate-intensity static magnetic fields on biological systems. *Cell Biochem Biophys.* (2003) 39:163–73. doi: 10.1385/CBB:39:2:163

41. He R, Ma H, Wang H. Inactivation of E. coli by high-intensity pulsed electromagnetic field with a change in the intracellular Ca2+ concentration. *J Electromagn Waves Appl.* (2014) 28:459–69. doi: 10.1080/09205071.2013.874539

42. Harte F, San Martin MF, Lacerda AH, Lelieveld HLM, Swanson BG, Barbosa-Canovas GV. Potential use of 18 tesla, static and pulsed magnetic fields on *Escherichia coli* and *Saccharomyces cerevisiae*. *J Food Process Preserv.* (2001) 25:223–35. doi: 10.1111/j.1745-4549.2001.tb00456.x

43. Haile M, Pan Z, Gao M, Luo L. Efficacy in microbial sterilization of pulsed magnetic field treatment. *Int J Food Eng.* (2008) 4:1–14. doi: 10.2202/1556-3758.1177

44. Jeon YJ, Kamil JYVA, Shahidi F. Chitosan as an edible invisible film for quality preservation of herring and Atlantic cod. *J Agric Food Chem.* (2002) 50:5167–78. doi: 10.1021/jf011693l

45. Guo JJ, Zhou YH, Yang K, Yin XL, Ma J, Li ZS, et al. Effect of low-frequency magnetic field on the gel properties of pork myofibrillar proteins. *Food Chem.* (2019) 274:775–81. doi: 10.1016/j.foodchem.2018.09.028

46. Yang K, Wang L, Guo J, Wu D, Wang X, Wu M, et al. Structural changes induced by direct current magnetic field improve water holding capacity of pork myofibrillar protein gels. *Food Chem.* (2021) 345:128849. doi: 10.1016/j.foodchem.2020.128849

47. Li TT, Li JR, Hu WZ, Zhang XG, Li XP, Zhao J. Shelf-life extension of crucian carp (*Carassius auratus*) using natural preservatives during chilled storage. *Food Chem.* (2012) 135:140–5. doi: 10.1016/j.foodchem.2012.04.115

48. Wang GM, Fu JP, Mo WC, Zhang HT, Liu Y, He RQ. Shielded geomagnetic field accelerates glucose consumption in human neuroblastoma cells by promoting anaerobic glycolysis. *Biochem Biophys Res Commun.* (2022) 601:101–8. doi: 10.1016/j.bbrc.2022.01.114

49. Angsupanich K, Ledward DA. High pressure treatment effects on cod (*Gadus morhua*) muscle. *Food Chem.* (1998) 63:39–50. doi: 10.1016/S0308-8146(97)00234-3

50. Liu JL, Lan WQ, Sun XH, Xie J. Effects of chitosan grafted phenolic acid coating on microbiological, physicochemical and protein changes of sea bass (*Lateolabrax japonicus*) during refrigerated storage. *J Food Sci.* (2020) 85:2506–15. doi: 10.1111/1750-3841.15329

51. Song Y, Luo Y, You J, Shen H, Hu S. Biochemical, sensory and microbiological attributes of bream (*Megalobrama amblycephala*) during partial freezing and chilled storage. *J Sci Food Agric.* (2012) 92:197–202. doi: 10.1002/jsfa.4572

52. Otero L, Perez-Mateos M, Holgado F, Marquez-Ruiz G, Lopez-Caballero ME. Hyperbaric cold storage: pressure as an effective tool for extending the shelf-life of refrigerated mackerel (*Scomber scombrus*. L.). *Innov Food Sci Emerg Technol.* (2019) 51:41–50. doi: 10.1016/j.ifset.2018.05.003

53. Hersleth HP, Andersson KK. How different oxidation states of crystalline myoglobin are influenced by X-rays. *Biochim Biophys Acta Proteins Proteom.* (2011) 1814:785–96. doi: 10.1016/j.bbapap.2010.07.019

54. Zheng ZX, Lin SS, Xue J, Shen Q, Feng JL, Jin RY, et al. The characterization of myoglobin and myoglobin-induced lipid oxidation in frigate mackerel. *J Food Process Preserv.* (2016) 40:1438–47. doi: 10.1111/jfpp.12729

55. Seideman SC, Durland PR. The utilization of modified gas atmosphere packaging for fresh meat: a review. *J Food Qual.* (1984) 6:239–52. doi: 10.1111/j.1745-4557.1984.tb00827.x

56. Xia MQ, Chen YX, Ma J, Yin XL, Li ZS, Xiong GQ, et al. Low frequency magnetic fields modification on hydrogen peroxide oxidized myoglobin-isolate and mechanisms underlying the chain reaction process. *Food Chem.* (2020) 312:126069. doi: 10.1016/j.foodchem.2019.126069

57. Xia MQ, Chen YX, Ma J, Yin XL, Wang L, Wu WJ, et al. Effects of low frequency magnetic field on myoglobin oxidation stability. *Food Chem.* (2020) 309:125651. doi: 10.1016/j.foodchem.2019.125651

58. Cai LY, Cao AL, Bai FL, Li JR. Effect of epsilon-polylysine in combination with alginate coating treatment on physicochemical and microbial characteristics of Japanese sea bass (*Lateolabrax japonicas*) during refrigerated storage. *LWT Food Sci Technol.* (2015) 62:1053–9. doi: 10.1016/j.lwt.2015.02.002

59. Ginés R, Valdimarsdottir T, Sveinsdottir K, Thorarensen H. Effects of rearing temperature and strain on sensory characteristics, texture, colour and fat of Arctic charr (*Salvelinus alpinus*). *Food Qual Prefer.* (2004) 15:177–85. doi: 10.1016/S0950-3293(03)00056-9

60. Olafsdottir G, Nesvadba P, Di Natale C, Careche M, Oehlenschager J, Tryggvadottir SV, et al. Multisensor for fish quality determination. *Trends Food Sci Technol.* (2004) 15:86–93. doi: 10.1016/j.tifs.2003.08.006

61. Sompongse W, Itoh Y, Obatake A. Effect of cryoprotectants and a reducing reagent on the stability of actomyosin during ice storage. *Fish Sci.* (1996) 62:73–9. doi: 10.2331/fishsci.62.73

62. Shigeru H, Shuryo N. Contribution of hydrophobicity, net charge and sulfhydryl groups to thermal properties of ovalbumin. *Can Inst Food Technol J.* (1985) 18:290–5. doi: 10.1016/S0315-5463(85)71960-8

63. Zhang WG, Xiao S, Ahn DU. Protein oxidation: basic principles and implications for meat quality. *Crit Rev Food Sci Nutr.* (2013) 53:1191–201. doi: 10.1080/10408398.2011.577540

64. Koddy JK, Miao W, Hatab S, Tang L, Xu H, Nyaisaba BM, et al. Understanding the role of atmospheric cold plasma (ACP) in maintaining the quality of hairtail (*Trichiurus lepturus*). *Food Chem.* (2021) 343:128418. doi: 10.1016/j.foodchem.2020.128418

65. Bingi VN, Savin AV. Effects of weak magnetic fields on biological systems: physical aspects. *Phys Uspekhi.* (2003) 46:259–91. doi: 10.1070/pu2003v046n03abeh001283

66. Binsi PK, Shamasundar BA, Dileep AO. Physico-chemical and functional properties of proteins from green mussel (*Perna viridis*) during ice storage. *J Sci Food Agric.* (2007) 87:245–54. doi: 10.1002/jsfa.2706

67. Mehta NK, Chouksey MK, Balange AK, Tripathi G, Nayak BB. Physicochemical and gel properties of myofibrillar protein from sin croaker (*Johnius dussumieri*) fish during ice storage. *J Aquat Food Prod Technol.* (2017) 26:71–85. doi: 10.1080/10498850.2015.1092485

68. Okada T, Inoue N, Akiba M. Electron microscopic observation and biochemical properties of carp myosin B during frozen storage. *Nippon Suisan Gakkai.* (1986) 52:345–53. doi: 10.2331/suisan.52.345

69. Jiang S-T, Hwang D-C, Chen C-S. Effect of storage temperatures on the formation of disulfides and denaturation of milkfish actomyosin (*Chanos chanos*). *J Food Sci.* (1988) 53:1333–5. doi: 10.1111/j.1365-2621.1988.tb09270.x

70. Benjakul S, Bauer F. Physicochemical and enzymatic changes of cod muscle proteins subjected to different freeze–thaw cycles. *J Sci Food Agric.* (2000) 80:1143–50. doi: 10.1002/1097-0010(200006)80:8

71. Roco T, Torres MJ, Briones-Labarca V, Reyes JE, Tabilo-Munizaga G, Stucken K, et al. Effect of high hydrostatic pressure treatment on physical parameters, ultrastructure and shelf life of pre- and post-rigor mortis palm ruff (*Seriolella violacea*) under chilled storage. *Food Res Int.* (2018) 108:192–202. doi: 10.1016/j.foodres.2018.03.009

72. Chéret R, Chapleau N, Delbarre-Ladrat C, Verrez-Bagnis V, Lamballerie MD. Effects of high pressure on texture and microstructure of sea bass (*Dicentrarchus labrax* L.) Fillets. *J Food Sci.* (2005) 70:e477–83. doi: 10.1111/j.1365-2621.2005.tb11518.x

73. Neumann E, Katchalsky A. Long-lived conformation changes induced by electric impulses in biopolymers. *Proc Natl Acad Sci USA.* (1972) 69:993–7. doi: 10.1073/pnas.69.4.993

74. Zhang XC, Huang WB, Xie J. Effect of different packaging methods on protein oxidation and degradation of grouper (*Epinephelus coioides*) during refrigerated storage. *Foods.* (2019) 8:325. doi: 10.3390/foods8080325

75. Ren L, Xu YS, Jiang QX, Xia WS, Qiu CJ. Investigation on structural changes of myofibrillar proteins from silver carp (*Hypophthalmichthys molitrix*) during frozen storage. *Food Sci Technol Res.* (2013) 19:1051–9. doi: 10.3136/fstr.19.1051

76. Calabro E. Competition between hydrogen bonding and protein aggregation in neuronal-like cells under exposure to 50 Hz magnetic field. *Int J Radiat Biol.* (2016) 92:395–403. doi: 10.1080/09553002.2016.1175679

77. She Z, Hu X, Zhao X, Ren Z, Ding G. FTIR investigation of the effects of ultra-strong static magnetic field on the secondary structures of protein in bacteria. *Infrared Phys Technol.* (2009) 52:138–42. doi: 10.1016/j.infrared.2009.06.002

frontiers | Frontiers in Nutrition

TYPE Original Research
PUBLISHED 05 December 2022
DOI 10.3389/fnut.2022.1068767

OPEN ACCESS

EDITED BY
Yan Zhao,
Chinese Academy of Agricultural Sciences (CAAS), China

REVIEWED BY
Ailiang Chen,
Chinese Academy of Agricultural Sciences (CAAS), China
Wenjie Zheng,
Tianjin Normal University, China

*CORRESPONDENCE
Ruijie Deng
drj17@scu.edu.cn
Jijuan Cao
caojijuan@dlnu.edu.cn
Ying Chen
chenyingcaiq@163.com

†These authors have contributed equally to this work

SPECIALTY SECTION
This article was submitted to Food Chemistry, a section of the journal Frontiers in Nutrition

RECEIVED 13 October 2022
ACCEPTED 21 November 2022
PUBLISHED 05 December 2022

CITATION
Yin X, Xing R, Li Z, Hu B, Yang L, Deng R, Cao J and Chen Y (2022) Real-time qPCR for the detection of puffer fish components from *Lagocephalus* in food: *L. inermis*, *L. lagocephalus*, *L. gloveri*, *L. lunaris*, and *L. spadiceus*. *Front. Nutr.* 9:1068767. doi: 10.3389/fnut.2022.1068767

Real-time qPCR for the detection of puffer fish components from *Lagocephalus* in food: *L. inermis*, *L. lagocephalus*, *L. gloveri*, *L. lunaris*, and *L. spadiceus*

Xinying Yin[1,2†], Ranran Xing[3†], Zhiru Li[1†], Bing Hu[1], Lili Yang[1], Ruijie Deng[2*], Jijuan Cao[1*] and Ying Chen[3*]

[1]Key Laboratory of Biotechnology and Bioresources Utilization of Ministry of Education, Dalian Minzu University, Dalian, China, [2]Healthy Food Evaluation Research Center, College of Biomass Science and Engineering, Sichuan University, Chengdu, China, [3]Chinese Academy of Inspection and Quarantine, Beijing, China

Puffer fish is a type of precious high-end aquatic product, is widely popular in Asia, especially in China and Japan, even though it naturally harbors a neurotoxin known as tetrodotoxin (TTX) that is poisonous to humans and causes food poisoning. With the increasing trade demand, which frequently exceeds existing supply capacities, fostering fraudulent practices, such as adulteration of processed products with non-certified farmed wild puffer fish species. To determine the authenticity of puffer fish processed food, we developed a real-time qPCR method to detect five common puffer fish species in aquatic products: *Lagocephalus inermis*, *Lagocephalus lagocephalus*, *Lagocephalus gloveri*, *Lagocephalus lunaris*, and *Lagocephalus spadiceus*. The specificity, cross-reactivity, detection limit, efficiency, and robustness of the primers and probes created for five species of puffer fish using TaqMan technology have been determined. No cross-reactivity was detected in the DNA of non-target sample materials, and no false-positive signal was detected; the aquatic products containing 0.1% of a small amount of wild puffer fish materials without certification can be reliably tracked; the statistical *p*-value for each method's *Ct* value was greater than 0.05. The developed qPCR method was sensitive, highly specific, robust, and reproducibility, which could be used to validate the authenticity of wild puffer fish in aquatic products sold for commercial purposes.

KEYWORDS

food authenticity, food adulteration, *Lagocephalus*, qPCR, puffer fish

Introduction

Puffer fish (Tetraodontidae) generally belongs to the genera of *dontidae*, *Tetraodontiformes*, and *Actinopterygii*. Despite its recognized potential toxicity caused by Tetrodotoxin (TTX), puffer fish is a long-standing delicacy in China, Japan, and other Asian nations, and is regarded as the "top of dishes" (1). TTX is the naturally occurring toxin harbored in puffer fish's ovaries, liver, kidneys, eyes, and blood (2). Therefore, improper handling or accidental consumption of puffer fish can result in severe toxicity and even death. In addition, TTX is present in the muscles of a number of puffer fish, and because the TTX content in the muscles of some puffer fish is lethal, many poisoning occurrences have been caused by the consumption of processed and cooked puffer fish (3). In Japan, the preparation of puffer fish needs special training. In China, the sale of fresh puffer fish is banned. However, since 2016, the latest regulations permit *Takifugu rubripes* and *Takifugu obscurus* to be farmed by certified companies and sold after processing, with a code on the package to track the products' origin. Since 2016, both species have become available in China's local markets, and approximately 70% of the annual production is exported (1, 4, 5). The rapid expansion of the high-end aquatic product trade has led to an increase in demand, which is conducive to food fraud, such as incorrect labeling and the substitution of non-certified cultured puffer fish for wild puffer fish goods. In addition, because the morphological characteristics of puffer fish are highly similar (6, 7), it is difficult for inexperienced consumers to correctly identify morphologically, particularly after the fish has been processed (8). Due to their similar appearance, using the wrong species puffer fish may lead to poisoning risk to consumers (9).

Food authenticity identification technology has been developed to ensure food safety and quality control. However, processed foods have often been destroyed in their morphological features and cannot effectively identify in terms of morphology (8). To evaluate food authenticity, a significant amount of research has been conducted in recent years on omics-based food authenticity recognition technologies, including genomics, proteomics, and metabolomics. Proteomics studies the existence state and activity rules of proteins at the overall level under specific conditions, which cannot only identify protein species but also quantify proteins. Proteomics is based on protein databases for species identification, origin tracing, quality identification, and other food authenticity identification (10–13). However, protein-based methods can hardly find target protein in heat-treated foods due to the denaturation of proteins at high temperatures. The examination of metabolites based on metabolomics is primarily separated into target analysis and non-target analysis, including vibration spectrum, chromatography-mass spectrum, nuclear magnetic resonance, etc. (14). Omics-based methods have become a comprehensive solution for food fraud (15, 16).

PCR-based methods for the detection and differentiation of species have usually been applied due to their high specificity, sensitivity, and speed, including qPCR (17), digital PCR (18, 19), gene chip (20), and DNA barcode (21) which can quickly distinguish all animals and plants raw materials used in food and has attracted international attention and developed rapidly. TaqMan-based real-time quantitative polymerase chain reaction (qPCR) plays an important role in food authenticity identification. This method is highly sensitive, specific and DNA is stable at a high temperature and can be extracted in most cells. Such methods have been successfully developed to detect different materials affected by fraud. DNA-based molecular biology methods are still considered the most effective method for food authenticity identification (22). By selecting appropriate target genes based on the characteristics of gene evolution, it is possible to achieve satisfactory species and strain distinction. Even with certain biologically distinct individuals (23–26).

Here, we developed a real-time PCR method based on the TaqMan probe to identify the components of puffer fish of the genus *Lagocephalus* in food, including *Lagocephalus inermis*, *Lagocephalus lagocephalus*, *Lagocephalus gloveri*, *Lagocephalus lunaris,* and *Lagocephalus spadiceus*. This method is based on the amplification of the *cytochrome oxidase subunit I* (*COI*) gene. Due to the high variability of *COI*, it was selected to qualitatively identify the species of puffer fish of the genus *Lagocephalus*. The specificity of this method is determined by detecting cross-reactivity with other puffer fish family members and common fish species. The limit of detection (LOD) and stability of the method were evaluated.

Materials and methods

Materials

Complete samples of puffer fish have been identified by morphology. All puffer fish samples were provided by the Fisheries Research Institute of Fujian, including *Lagocephalus inermis*, *Lagocephalus lagocephalus*, *Lagocephalus gloveri*, *Lagocephalus lunaris*, *Lagocephalus spadiceus*, *Takifugu vermicularis*, *Takifugu fasciatus*, *Takifugu xanthopterus*, *Takifugu bimaculatus*, *Takifugu flavidus*, *Takifugu rubripes*, *Takifugu oblongus*, *Takifugu alboplumbeus*. Other fish samples used for the specificity test have also been identified in morphology, including *Limanda aspera*, *Verasper variegatus*, *Verasper moseri*, *Platichthys stellatus*, *Paralichthys lethostigma*, *Oncorhynchus gorbuscha*, *Gadus macrocephalus*, *Sebastes schlegelii*, *Trachurus japonicus* were obtained from Dalian Tianzheng Industrial Co., Ltd (Dalian, China). All fish materials information was listed in **Supplementary Tables 1**, **2**. DNA oligonucleotides were synthesized by TaKaRa (Dalian, China) and set out

in Supplementary Table 3. All sequences were purified by polyacrylamide gel electrophoresis (PAGE).

Deoxyribonucleic acid extraction

Fish meat samples were pulverized using a high-speed tissue masher (34BL99, Waring Blender dynamics Corp., New Hartford, CT, USA). Ground sample (200 mg) was taken for DNA extraction. DNA Extraction Kit (Code No. 9766, TaKaRa Co., Ltd., Dalian, China) was used according to the manufacturer's recommendations. The operations were as follows: 10 mg sample materials were taken for low-temperature grinding by adding liquid nitrogen, then added 200 μL PBS buffer. Briefly, 200 μL VGB buffer, 20 μL proteinase K, and 1.0 μL carrier RNA were added and fully mixed in a 56°C water bath for 10 min. Then 200 μL 96–100% ethanol was added, and fully mixed. Placed the spin column on the collection tube, transferred the solution to the spin column, centrifuge at 12,000 × g for 2 min, and discarded the filtrate. Then, 500 μL RWA buffer was added to the spin column, 12,000 × g centrifuge for 1 min, and discarded the filtrate. And then, 700 μL buffer RWB was added to the spin column, 12,000 × g centrifuge for 1 min, and discard the filtrate. Repeat the previous step. Placed the spin column on the collection tube, and 12,000 × g centrifuge for 2 min. Placed the spin column in a new 1.5 ml RNase-free collection tube, and added 30–50 μL RNase-free dH_2O, standing at room temperature for 5 min. Centrifugation at 12,000 rpm for 5 min. The products were dissolved in H_2O.

Sequence retrieval and analysis

Puffer fish *COI* gene sequences of mitochondrial were retrieved from the official National Center for Biotechnology Information (NCBI) database GenBank.[1] And then, these sequences as the template used for Blast analysis. In addition, the specificity of the primer and probes was tested by Blast. MEGA 4.0 software (27) was used to perform sequence alignment to screen high variability DNA fragments, examine the specificity of primers and probes, and guarantee that the primers and probes cannot theoretically amplify genes from related species. All sequence accession numbers were listed in Supplementary Table 2.

Quantitative polymerase chain reaction primers and probes design

Arrange the *COI* sequence of the target species and the DNA sequence of the most relevant species (such as the common puffer fish species of the genus Fugu) and screen for the fragments with the greatest variability.

Considering the impact of food processing on DNA quality, the amplification efficiency of real-time qPCR analysis was improved by designing primer pairs to amplify relatively short DNA fragments. The nucleotide sequences chosen for primer design were introduced into the program "Oligocalc" (28), and the length was optimized for the resulting "salt-adjusted" annealing temperature. Then, the annealing temperatures calculated by "Oligocalc" applying the "salt-adjusted" algorithm were used as starting values for the qPCR. Four qPCR methods were based on the TaqMan probe, modified with the reporter fluorophore, 6-carboxyfluorescein (FAM), and quencher fluorophore black hole quencher (BHQ_1) at 5' and 3' end, respective. *L. inermisand* and *L. lagocephalus* amplification fragment sizes were 196 bp, *L. gloveri* was 174 bp, *L. lunaris* was 150 bp, and *L. spadiceus* was 173 bp. Finally, 18SrRNA was used as the control gene to design primer and probe for detecting DNA of all sample materials to ensure no inhibitory contaminants. All primers and probes oligonucleotide sequences were listed in Supplementary Table 3 and synthesized by TaKaRa (Dalian, China).

Real-time quantitative polymerase chain reaction

Real-Time qPCR analysis was carried out in QuantStudio 7 Real-time fluorescent quantitative PCR system (Applied Biosystems, VA, USA). Real-time qPCR reaction was carried in a volume of 25 μL containing 16 μL Probe qPCR Mix (Code No. 391A, TaKaRa, Dalian, China), 1 μL forward primer (0.4 pmol/μL), 1 μL reverse primer (0.4 pmol/μL), 1 μL probe (0.4 pmol/μL), and 2 μL target DNA. The reaction blend was then subjected to 45 cycles at 95°C for 5 s and 60°C for 30 s, with fluorescence acquisition at each cycle. Each sample was analyzed three times.

Specificity and cross-reactivity

The specificity and cross reactivity of the detection methods were evaluated by qPCR analysis. Undiluted sample material DNA obtained from 13 closely related different puffer fish species and 9 other unrelated fish species listed in Supplementary Table 3 was used. DNA analysis of each species was repeated no less than 3 times. All sample DNA used for the test was detected with primers and probes of internal reference 18 S rRNA to avoid inhibitory substance.

1 https://www.ncbi.nlm.nih.gov/genbank/

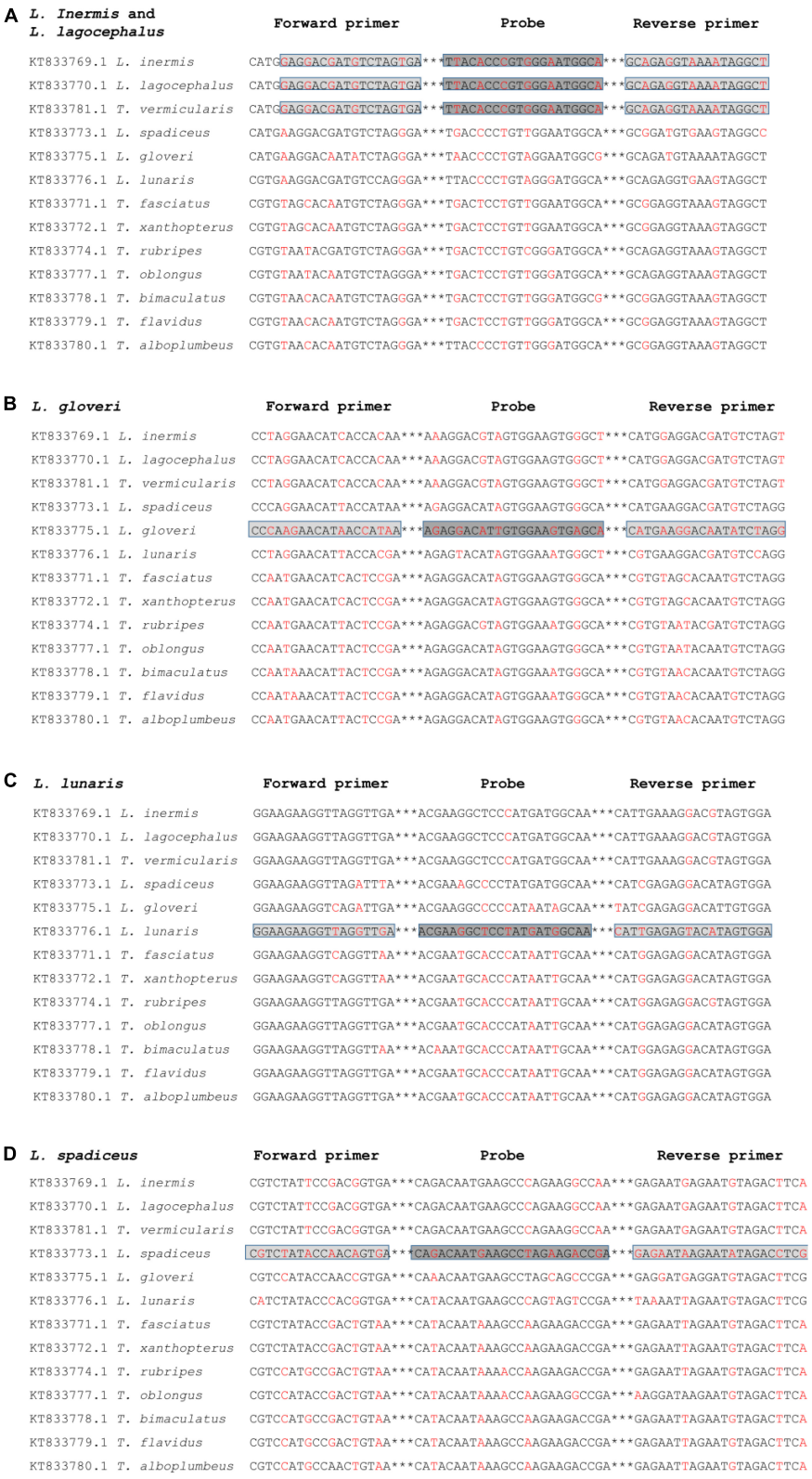

FIGURE 1
Alignment of a segment of the *COI* gene region of different puffer fish species for the development of the specific qPCR method for *L. inermis* and *L. lagocephalus* **(A)**, *L. gloveri* **(B)**, *L. lunaris* **(C)**, and *L. spadiceus* **(D)**. The location and orientation of primers and probes are indicated by lightgray and darkgray boxes, respectively. Differential bases are indicated by red. ***Represents the omitted part in oligonucleotide sequence.

Amplification efficiency (*E*)

In order to calculate the amplification efficiency (*E*) of qPCR, 8 series of dilution levels were prepared using the sample DNA of *Lagocephalus inermis*, *Lagocephalus lagocephalus*, *Lagocephalus gloveri*, *Lagocephalus lunaris*, and *Lagocephalus spadiceus*, including 100, 50, 20, 10, 5, 2, 1, and 0.1%. All samples were analyzed three times. Mean *Ct* values obtained for each point were plotted against the Log (DNA concentration (ng/μL), and a linear regression analysis was performed. Using the slope of the regression line, the qPCR efficiency was calculated using the equation $E = 100\ (10^{-1/\text{slope}} - 1)$ and expressed in percent. For each target, the slope of the regression curve should be between 3.9 and 2.9 corresponding to PCR efficiencies ranging from 80 to 120%. Additionally, the correlation coefficient R^2 of the curve is a measure of the linearity of the PCR reaction. The R^2 for each target should be greater than 0.98.

Sensitivity tests

The LOD was experimentally determined according to accepted guidelines (28). DNA was extracted from *Lagocephalus inermis*, *Lagocephalus lagocephalus*, *Lagocephalus gloveri*, *Lagocephalus lunaris*, and *Lagocephalus spadiceus*, respectively, and diluted by *Limanda aspera* DNA extracted from slices of fish meat. Therefore, 8 series of dilution levels were prepared to simulate real samples for qPCR analysis and determine LOD, including: 100, 50, 20, 10, 5, 2, 1 and 0.1%. LOD_6 of the qPCR method represents six replicate analyses performed for each dilution point of serial dilution. At least three times must be performed under repeat conditions, yielding a total of 18 results per dilution point. The lowest dilution level at which all 18 replicates show a specific positive amplification was considered as the LOD_6. The analytical sensitivity of the qPCR method was present by $LOD_{95\%}$. The $LOD_{95\%}$ refers to the use of the corresponding LOD_6 level, one higher dilution level, and one lower dilution level, and each level is tested 60 times. All 60 replicates showed specific positive amplification, and the lowest dilution level was considered as $LOD_{95\%}$ with a 95% confidence level. Statistical significance $LOD_{95\%}$ was calculated by Semi logarithmic regression analysis (PRISM, Graphpad Software Inc., San Diego, CA, United States), input of the corresponding number of sample materials, the number of repetitions, and the number of positive results in qPCR detection.

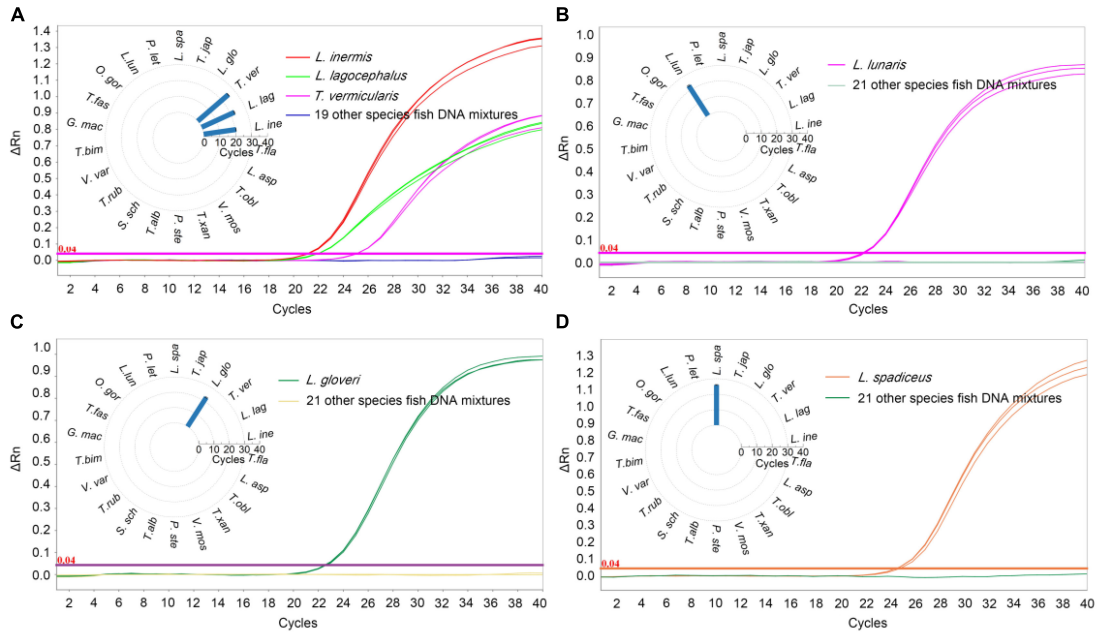

FIGURE 2
Specificity results of real-time qPCR methods. qPCR *Ct* value corresponding to puffer fish and other meat DNA, **(A)** *L. inermis*, *L. lagocephalus*, and *T. vermicularis* was detected and the *Ct* value was 20.58 ± 0.09, 22.61 ± 0.24, and 25.43 ± 0.11, respectively. Other 19 species fish were undetected. **(B)** *L. gloveri* was detected and the *Ct* value was 22.71 ± 0.38. **(C)** *L. lunaris* was detected and the *Ct* value was 22.99 ± 0.47. **(D)** *L. spadiceus* was detected and the *Ct* value was 25.98 ± 0.28. Inner: the *Ct* value for the samples with 22 species of fish. *L. ine*, *Lagocephalus inermis*; *L. lag*, *Lagocephalus lagocephalus*; *T. ver*, *Takifugu vermicularis*; *L. glo*, *Lagocephalus gloveri*; *T. jap*, *Trachurus japonicus*; *L. spa*, *Lagocephalus spadiceus*; *P. let*, *Paralichthys lethostigma*; *L. lun*, *Lagocephalus lunaris*; *O. gor*, *Oncorhynchus gorbuscha*; *T. fas*, *Takifugu fasciatus*; *G. mac*, *Gadus macrocephalus*; *T. bim*, *Takifugu bimaculatus*; *V. var*, *Verasper variegatus*; *T. rub*, *Takifugu rubripes*; *S. sch*, *Sebastes schlegelii*; *T. alb*, *Takifugu alboplumbeus*; *P. ste*, *Platichthys stellatus*; *V. mos*, *Verasper moseri*; *T. xan*, *Takifugu xanthopterus*; *T. obl*, *Takifugu oblongus*; *L. asp*, *Limanda aspera*; *T. fla*, *Takifugu flavidus*.

Robustness evaluation

The robustness of puffer fish detection was checked by changing conditions of the qPCR reaction such as the qPCR instrument (CFX 96 Real-Time qPCR System, Bio-Rad Co., Ltd, Hercules, CA, USA), the concentration of primers and probes (±25%), and the annealing temperature S6. In each combination, a template in an amount of four times the LOD_6 was added to the assay, at least repeat three times in one run. Regression analysis was carried out with SPSS (statistical product and service solutions, IBM Inc.) software, and the Kruskal Wallis H test was used to evaluate the significance level of difference in results obtained by orthogonal design combination of each method. When the $p > 0.05$, there was no significant difference in results.

Results and discussion

Development of the specific quantitative polymerase chain reaction method for five specific of puffer fish in *Lagocephalus*

The DNA fragment of the mitochondrial *Cytochrome Oxidase Sub-unit I* (*COI*) gene was selected as the target of the developed real-time qPCR method for puffer fish species identification. The base sequence of the *COI* gene region has a large genetic variation among species, but a small genetic variation within species, was stable and has high identification ability, and has been widely used for fish species identification (29–31). We have searched almost all the genus *Lagocephalus* in

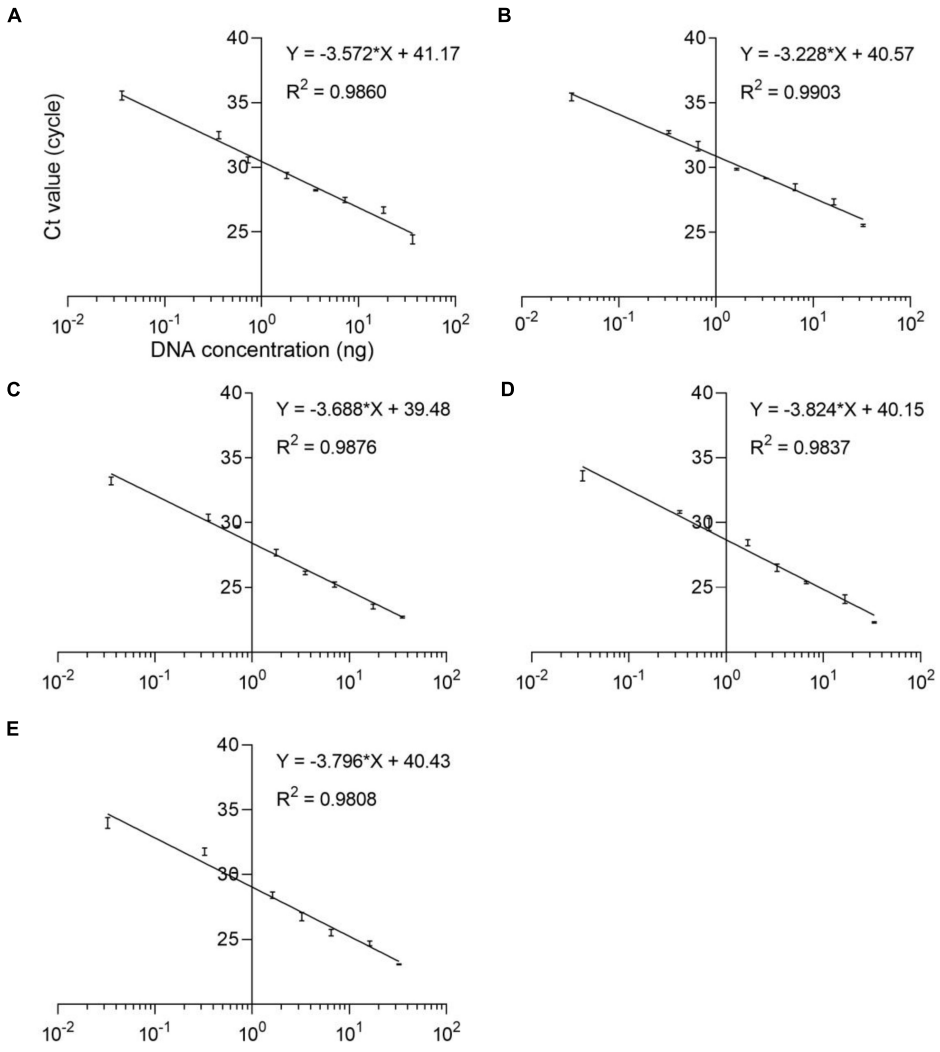

FIGURE 3
Standard curves of the analyses of eight dilution levels for the real-time qPCR assays. **(A)** *L. inermis*, **(B)** *L. lagocephalus*, **(C)** *L. gloveri*, **(D)** *L. lunaris*, **(E)** *L. spadiceus*. All samples were analyzed three times.

NCBI, there are 18 accession numbers of *COI* gene sequences of *Lagocephalus inermis* and 9 accession numbers of *COI* gene sequences of *Lagocephalus lagocephalus*. The homology of *COI* genes between these two species is 100%. In addition, there are 15 accession numbers of *Lagocephalus gloveri*, 19 accession numbers of *Lagocephalus lunaris,* and 41 accession numbers of *Lagocephalus spadiceu* in NCBI. They have differences in nucleic acid sequences, which can realize the identification of each species. The DNA sequences of 5 species of puffer fish in the genus *Lagocephalus* and 8 species of puffer fish in the genus *Takifugu* were aligned (Figure 1), and primer sequences that could distinguish the DNA sequences of 5 species of puffer fish in the genus lepidocephalus from those of other species were searched. The sequences of five *Lagocephalus* and eight *Takifugu* were comparable to search primers that can distinguish the DNA sequences of five species of *Lagocephalus*, *Takifugu* and other puffer fish species (Figure 1). All the designed primers could theoretically exclude other species of puffer fish. However, it was

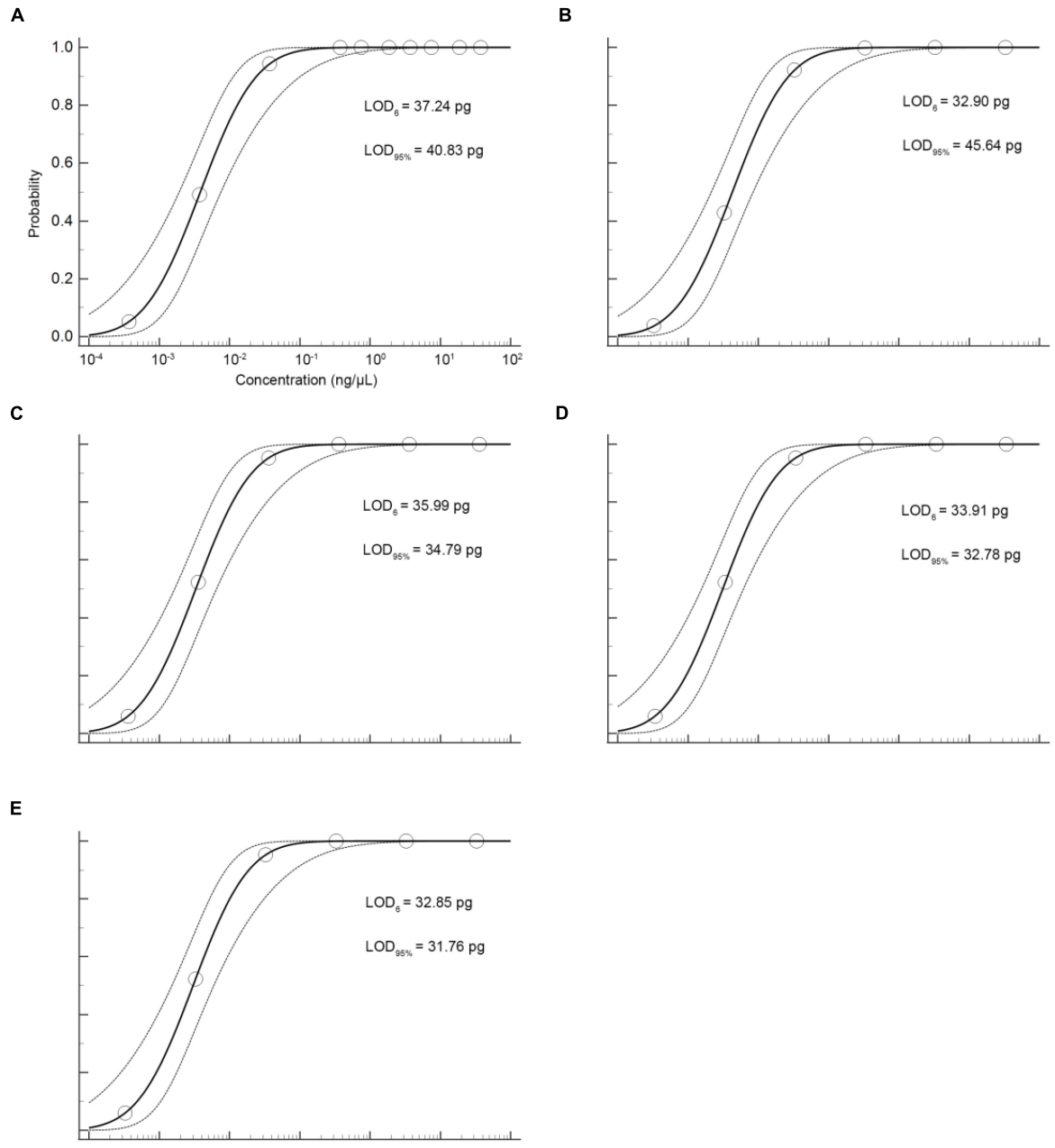

FIGURE 4
Probit regression analysis using MedCalc Software was performed on data of 6 replicates (m = 6, n = 3) from serial dilutions by the specific qPCR methods. **(A)** *L. inermis*, **(B)** *L. lagocephalus*, **(C)** *L. gloveri*, **(D)** *L. lunaris*, **(E)** *L. spadiceus*.

worth noting that the *COI* sequence of *Takifugu vermicularis* with three accession numbers in NCBI has 100% homology with that of *Lagocephalus inermis* and *Lagocephalus lagocephalus*. It is impossible to distinguish these three species based on the *COI* sequence. Nevertheless, it has been revealed that the homology analysis results of the 18 S rRNA, *Cytb*, and *COI* DNA fragment sequences of *Takifugu vermicularis* all belong to the same group as the genus *Lagocephalus*, with a homology of 99–100% (32).

Specificity and cross-reactivity

In order to determine the specificity of the qPCR method, the DNA of target sample materials (*L. inermis*, *L. lagocephalus*, *L. gloveri*, *L. lunaris*, and *L. spadiceus*) and non-target sample materials were analyzed. To exclude possible inhibitory effects in DNA preparations, samples were analyzed by qPCR using the primers and probe of internal reference of 18 SrRNA. All target and non-target fish species sample were successfully amplified on tested (**Supplementary Table 4**), confirming the suitability of sample DNA for qPCR assays. In the qPCR detection method of *L. inermis* and *L. lagocephalus*, the two species puffer fish could be detected at the same time, and had cross reactivity with the *T. vermicularis*, no false-positive signal was detected in other tested samples. The results of specificity test also verified that the sequence homology of the *COI* gene of *L. inermis*, *L. lagocephalus*, and *T. vermicularis*, indicating that the genus classification of *T. vermicularis* needs further exploration. In addition, in the respective qPCR detection methods of *L. gloveri*, *L. lunaris* and *L. spadiceus*, no cross reactivity was found in the DNA of non-target sample materials, and no false-positive signal was detected (**Figure 2**). These qPCR analysis results confirmed the accuracy and specificity of the detection method.

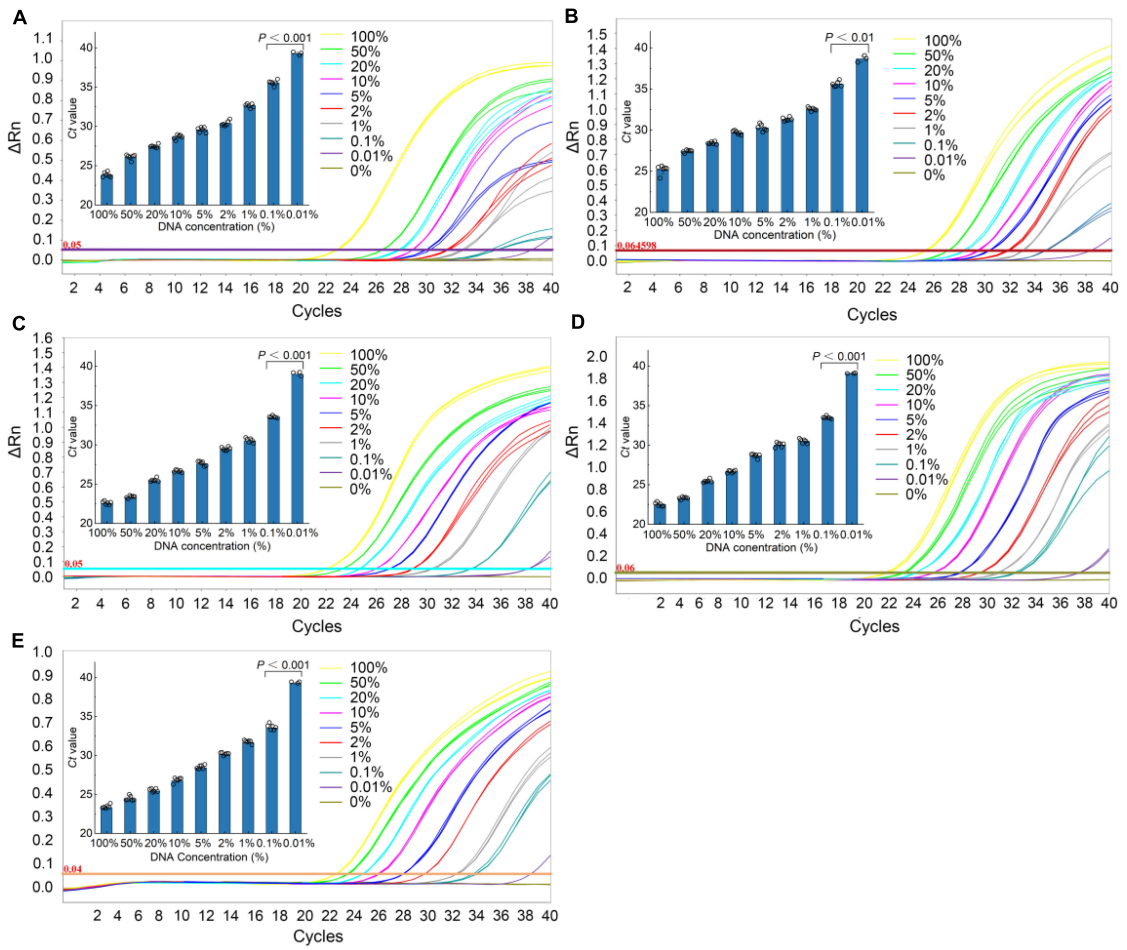

FIGURE 5
Real-time qPCR results of the sensitivity analyses. Typical fluorescence curves of qPCR method corresponding to the addition of different percentage of different species puffer fish added into mixture meat ranging from 0 to 100% (0, 0.001, 0.1, 1, 2, 5, 10, 20, 50, and 100%). Inner: the *Ct* value for the samples with 0.001–100% puffer fish. **(A)** *L. inermis*, **(B)** *L. lagocephalus*, **(C)** *L. gloveri*, **(D)** *L. lunaris*, **(E)** *L. spadiceus*. All values are presented as mean ± s.d. Statistical significances were obtained by the Mann Whitney test.

Amplification efficiency (*E*) and linearity (R^2)

The qPCR efficiency of these four methods was analyzed by qPCR at eight consecutive dilution levels (m = 8) of DNA samples from five species puffer fish in the genus *Lagocephalus* including *L. inermis*, *L. lagocephalus*, *L. gloveri*, *L. lunaris*, and *L. spadiceus*. Each dilution level is tested at least three times. The threshold cycle value (*Ct* value) was compared with the DNA concentration (pg/μL) to draw a linear regression curve.

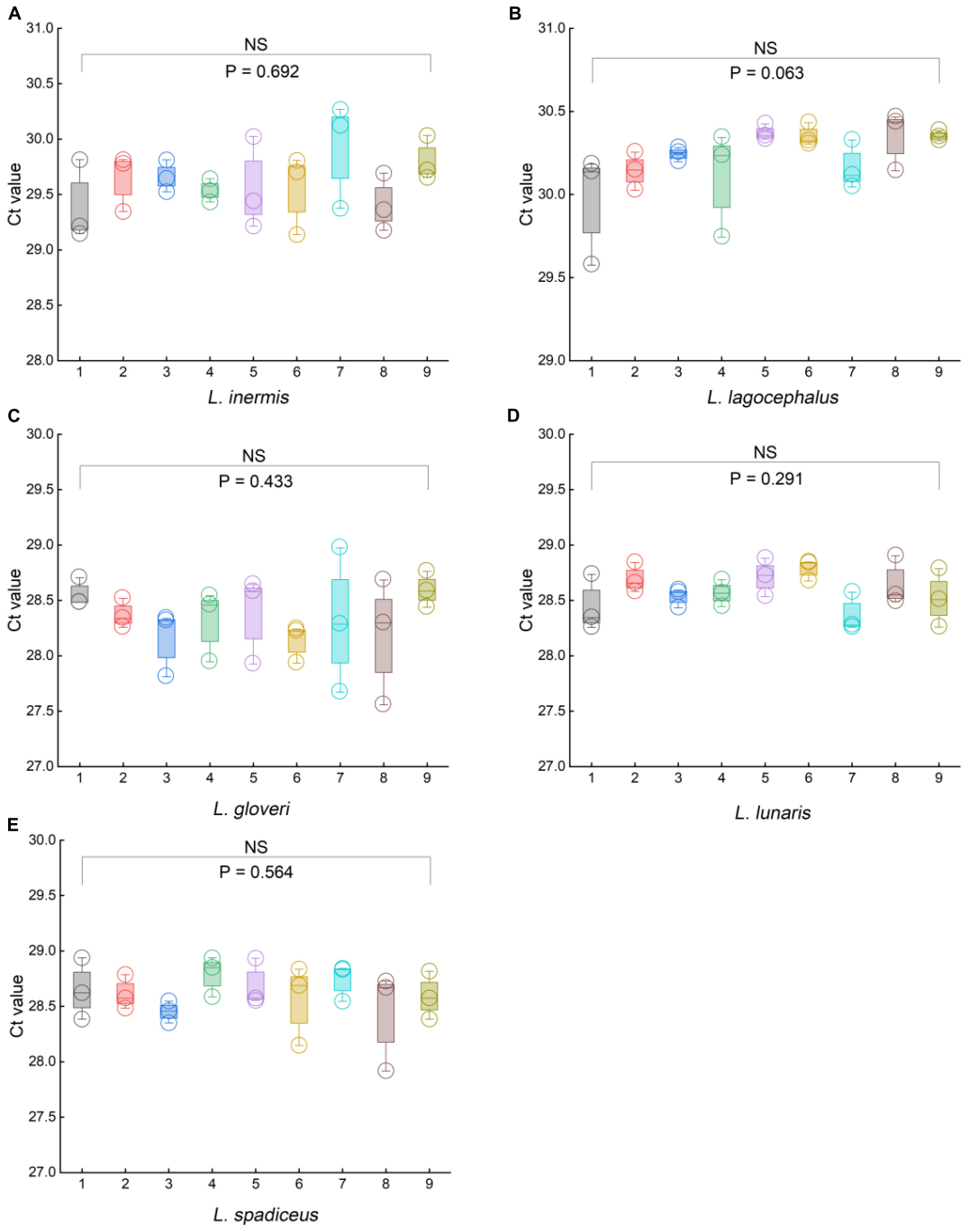

FIGURE 6
Results of the robustness experiments for the specific of qPCR methods. **(A)** *L. inermis*, **(B)** *L. lagocephalus*, **(C)** *L. gloveri*, **(D)** *L. lunaris*, **(E)** *L. spadiceus*. In **(A–E)**, box plots are centered around the median. Minima and maxima are shown as the bottom and top of the box plots, respectively. All values are presented as mean ± s.e.m. Kruskal Wallis H test was used. NS, not significant.

According to the equation $E = 100\ (10^{-1/\text{slope}} - 1)$, the analysis efficiency is determined as the slope of the regression line, which shows a good linear relationship between *Ct* value and DNA concentration (Figure 3). The correlation coefficient R^2 of these qPCR methods is 0.9808–0.9903, the slope of the regression curve is −3.824 to −3.228, and the efficiency *E* is 82.60–104.07% (Supplementary Table 5). These results match the specifications of the common qPCR validation guidelines, with a required linearity (R^2) should be ≥ 0.98, the slope of the regression curve should be between −3.9 and −2.9 corresponding to an efficiency (*E*) from 80 to 120%.

Sensitivity

The sensitivity of the qPCR method was an important parameter that needs to be evaluated, especially considering the regulations that wild puffer fish were not allowed to eat cultured by unauthorized certification companies, and the detection of species that may contain low concentrations. In this study, the sensitivity of the qPCR LOD was expressed by LOD_6 and $LOD_{95\%}$. It is determined by measuring the serial dilution level of DNA of five kinds of puffer fish samples in their respective detection. The LOD_6 of *L. inermis* and *L. lagocephalus* was 37.24 pg and 32.90 pg, and the $LOD_{95\%}$ was 40.83 pg (17.31–233.44 pg, 95% CI) and 45.64 pg (19.25–265.22 pg, 95% CI), respectively. For *L. gloveri*, *L. lunaris*, and *L. spadiceus* the LOD_6 was 35.99, 33.91, and 32.85 pg, and the $LOD_{95\%}$ was 34.79 pg (14.70–207.20 pg, 95% CI), 32.78 pg (13.85–195.23 pg, 95% CI), and 31.76 pg (13.41–189.13 pg, 95% CI), all of the five qPCR methods had highly sensitive (Supplementary Table 6 and Figure 4). This highly sensitive indicates that when the aquatic products contain 0.1% of a small amount of wild puffer fish materials without certification, they can be tracked reliably (Figure 5).

Robustness

To evaluate the robustness of the qPCR methods, we used orthogonal design to slightly change the principal different experimental conditions, such as the qPCR instruments, qPCR reagents, primer, and probe concentrations, and slight deviations of PCR annealing temperature. We used a 5% DNA template sample to examine the impact of the aforementioned variables on the stability of the results. In the orthogonal design combination of each method, there was no significant difference in the *Ct* values of the five species of puffer fish in the genus *Lagocephalus* (Figure 6 and Supplementary Tables 7, 8). For *L. inermis*, the *Ct* value was 29.84 ± 0.43 ($p = 0.692$). For *L. lagocephalus* the *Ct* value was 30.23 ± 0.20 ($p = 0.063$). For *L. gloveri* the *Ct* value was 28.33 ± 0.34 ($p = 0.433$). For *L. lunaris* the *Ct* value was 28.59 ± 0.20 ($p = 0.291$). For *L. spadiceus* the *Ct* value was 28.61 ± 0.24 ($p = 0.564$). Data in above are mean ± s.d. ($n = 3$). Thus, it can be concluded that the statistical *p*-value >0.05 of each method's *Ct* values, these qPCR methods were stable, and can be transferred to other laboratories and used in routine analysis.

Conclusion

This study describes a method for detecting five common puffer fish species belonging to the genus *Lagocephalus*: *L. inermis*, *L. lagocephalus*, *L. gloveri*, *L. lunaris*, and *L. spadiceus*. These methods were able to detect as little as 0.1% (w/w) puffer fish content, and the statistical *p*-value for each method's *Ct* values was greater than 0.05. Each of these qPCR methods did not identify any cross-reactivity in the DNA of 21 non-target species sample materials nor detect any false-positive signals.

In summary, the developed qPCR methods were sensitive, highly specific, robust, and reproducible, which could be a viable tool for analyzing the authenticity of puffer fish aquatic goods. It is also universal, which means that it can be applied to detect any species-specific DNA sequence and thus detect other types of food fraud. This is attributed to the molecular recognition of the species-specific DNA sequences is carried out by hybridizing the analyzed DNA sequences with complementary oligonucleotide probes. This method can detect puffer fish species rapidly and end within 45 min, and also allows tracing the cause of poisoning after a food poisoning incident.

Data availability statement

The datasets presented in this study can be found in online repositories. The names of the repository/repositories and accession number (s) can be found in the article/Supplementary material.

Author contributions

JC, RD, and YC conceived and designed the experiments. XY and RX performed the experiments. ZL and LY analyzed the data. BH edited and wrote the manuscript. All authors contributed to the article and approved the submitted version.

Funding

This work was supported by the National Key R&D Program of China (2021YFF0601902).

Acknowledgments

We thank Ruijie Deng from the College of Biomass Science and Engineering, Healthy Food Evaluation Research Center, Sichuan University for helpful discussions during the writing of this manuscript.

Conflict of interest

The authors declare that the research was conducted in the absence of any commercial or financial relationships that could be construed as a potential conflict of interest.

Publisher's note

All claims expressed in this article are solely those of the authors and do not necessarily represent those of their affiliated organizations, or those of the publisher, the editors and the reviewers. Any product that may be evaluated in this article, or claim that may be made by its manufacturer, is not guaranteed or endorsed by the publisher.

Supplementary material

The Supplementary Material for this article can be found online at: https://www.frontiersin.org/articles/10.3389/fnut.2022.1068767/full#supplementary-material

References

1. Bi HY, Cai DD, Zhang RR, Zhu YW, Zhang DN, Qiao L, et al. Mass spectrometry-based metabolomics approach to reveal differential compounds in pufferfish soups: flavor, nutrition, and safety. *Food Chem.* (2019) 301:8. doi: 10.1016/j.foodchem.2019.125261

2. Xinying Yin LJ, Fan M, She QT, You RY, Lu YD, Lu DC, et al. Facilely self-assembled and dual-molecule calibration aptasensor based on SERS for ultra-sensitive detection of tetrodotoxin in pufferfish. *Spectroc Acta Molec Biomolec Spectr.* (2022) 279:8. doi: 10.1016/j.saa.2022.121275

3. Amano M, Takatani T, Sakayauchi F, Oi R, Sakakura Y. The brain of the wild toxic marine pufferfishes accumulates tetrodotoxin. *Toxicon.* (2022) 218:1–7. doi: 10.1016/j.toxicon.2022.08.015

4. Zhang N, Wang W, Li B, Liu Y. Non-volatile taste active compounds and umami evaluation in two aquacultured pufferfish (*Takifugu obscurus* and *Takifugu rubripes*). *Food Bioscience.* (2019) 32:100468. doi: 10.1016/j.fbio.2019.100468

5. Zhang Q, Jing R, Wang B, Cui P, Zhou C, Yan T, et al. Fast mode decision based on gradient information in 3D-HEVC. *IEEE Access.* (2019) 7:135448-56.

6. Giusti A, Guarducci M, Stern N, Davidovich N, Golani D, Armani A. The importance of distinguishing pufferfish species (*Lagocephalus* spp.) in the mediterranean sea for ensuring public health: evaluation of the genetic databases reliability in supporting species identification. *Fish Res.* (2019) 210:14–21. doi: 10.1016/j.fishres.2018.10.003

7. Giusti A, Ricci E, Guarducci M, Gasperetti L, Davidovich N, Guidi A, et al. Emerging risks in the European seafood chain: molecular identification of toxic *Lagocephalus* spp. In fresh and processed products. *Food Control.* (2018) 91:311–20. doi: 10.1016/j.foodcont.2018.04.013

8. Galimberti A, De Mattia F, Losa A, Bruni I, Federici S, Casiraghi M, et al. DNA barcoding as a new tool for food traceability. *Food Res Int.* (2013) 50:55–63. doi: 10.1080/07388551.2021.1874279

9. Jurges G, Sahi V, Rios Rodriguez D, Reich E, Bhamra S, Howard C, et al. Product authenticity versus globalisation-the tulsi case. *PLoS One.* (2018) 13:e0207763. doi: 10.1371/journal.pone.0207763

10. Danezis GP, Tsagkaris AS, Camin F, Brusic V, Georgiou CA. Food authentication: techniques, trends & emerging approaches. *TrAC Trends Analy Chem.* (2016) 85:123–32. doi: 10.1016/j.trac.2016.02.026

11. Caira S, Pinto G, Nicolai MA, Chianese L, Addeo F. Simultaneously tracing the geographical origin and presence of bovine milk in Italian water buffalo Mozzarella cheese using MALDI-TOF data of casein signature peptides. *Anal Bioanal Chem.* (2016) 408:5609–21. doi: 10.1007/s00216-016-9663-0

12. Fornal E, Montowska M. Species-specific peptide-based liquid chromatography-mass spectrometry monitoring of three poultry species in processed meat products. *Food Chem.* (2019) 283:489–98. doi: 10.1016/j.foodchem.2019.01.074

13. Stahl A, Schroder U. Development of a MALDI-TOF MS-based protein fingerprint database of common food fish allowing fast and reliable identification of fraud and substitution. *J Agric Food Chem.* (2017) 65:7519–27. doi: 10.1021/acs.jafc.7b02826

14. Cubero-Leon E, Peñalver R, Maquet A. Review on metabolomics for food authentication. *Food Res Int.* (2014) 60:95–107. doi: 10.1016/j.foodres.2013.11.041

15. Böhme K, Calo-Mata P, Barros-Velázquez J, Ortea I. Recent applications of omics-based technologies to main topics in food authentication. *TrAC Trends Analy Chem.* (2019) 110:221–32. doi: 10.1016/j.trac.2018.11.005

16. Creydt M, Fischer M. Omics approaches for food authentication. *Electrophoresis.* (2018) 39:1569–81. doi: 10.1002/elps.201800004

17. Wu Y, Yang Y, Liu M, Wang B, Li M, Chen Y. Molecular tracing of the origin of six different plant species in bee honey using real-time PCR. *J Aoac Int.* (2017) 100:744–52. doi: 10.5740/jaoacint.16-0265

18. Köppel R, Ganeshan A, Weber S, Pietsch K, Graf C, Hochegger R, et al. Duplex digital PCR for the determination of meat proportions of sausages containing meat from chicken, turkey, horse, cow, pig and sheep. *Eur Food Res Technol.* (2019) 245:853–62.

19. Noh ES, Park YJ, Kim EM, Park JY, Shim KB, Choi TJ, et al. Quantitative analysis of alaska pollock in seafood products by droplet digital PCR. *Food Chem.* (2019) 275:638–43. doi: 10.1016/j.foodchem.2018.09.093

20. Wu YY, Liu M, Wang B, Han J, Chen Y. A 15-plex/xMAP method to detect 15 animal ingredients by suspension array system coupled with multifluorescent magnetic beads. *J Aoac Int.* (2016). [Epub ahead of print]. doi: 10.5740/jaoacint.15-0216

21. Haynes E, Jimenez E, Pardo MA, Helyar SJ. The future of NGS (next generation sequencing) analysis in testing food authenticity. *Food Control.* (2019) 101:134–43. doi: 10.3390/foods11081108

22. Manikandan M. DNA as a biomaterial in diagnosis of food adulteration and food safety assurance. *Res Dev Material Sci.* (2017) 2:3.

23. Ali ME, Amin MA, Razzak MA, Abd Hamid SB, Rahman MM, Abdul Rashid N, et al. Short amplicon-length PCR assay targeting mitochondrial cytochrome b gene for the detection of feline meats in burger formulation. *Food Analy Methods.* (2015) 9:571–81.

24. Doosti A, Ghasemi Dehkordi P, Rahimi E. Molecular assay to fraud identification of meat products. *J Food Sci Technol.* (2014) 51:148–52. doi: 10.1007/s13197-011-0456-3

25. Marieschi M, Torelli A, Beghe D, Bruni R. Authentication of *Punica granatum* L.: development of SCAR markers for the detection of 10 fruits potentially used in economically motivated adulteration. *Food Chem.* (2016) 202:438–44. doi: 10.1016/j.foodchem.2016.02.011

26. Schiefenhovel K, Rehbein H. Differentiation of sparidae species by DNA sequence analysis. PCR SSCP and IEF of sarcoplasmic proteins. *Food Chem.* (2013) 138:154–60. doi: 10.1016/j.foodchem.2012.10.057

27. Tamura SKGSaK. MEGA7: molecular evolutionary genetics analysis version 7.0 for bigger datasets. *Mol Biol Evol.* (2016) 33:1870–4. doi: 10.1093/molbev/msw054

28. Broeders S, Huber I, Grohmann L, Berben G, Taverniers I, Mazzara M, et al. Guidelines for validation of qualitative real-time PCR methods. *Trends Food Sci Technol.* (2014) 37:115–26. doi: 10.1016/j.tifs.2014.03.008

29. Asis AM, Lacsamana JK, Santos MD. Illegal trade of regulated and protected aquatic species in the philippines detected by DNA barcoding. *Mitochondrial DNA DNA Mapp Seq Anal.* (2016) 27:659–66. doi: 10.3109/19401736.2014.913138

30. Goncalves PF, Oliveira-Marques AR, Matsumoto TE, Miyaki CY. DNA barcoding identifies illegal parrot trade. *J Hered.* (2015) 106:560–4. doi: 10.1093/jhered/esv035

31. Stein FM, Wong JCY, Sheng V, Law CSW, Schröder B, Baker DM. Erratum to: first genetic evidence of illegal trade in endangered European eel (anguilla anguilla) from Europe to Asia. *Conservat Genet Res.* (2016) 8:539.

32. Wenbing Chen TM, Weng G, Chen R, Shao B, Peng J, Jiang S. Analysis of partial DNA sequence of COI gene and its application for species identification of thirteen species pufferfish. *Chin Food Sci.* (2018) 39:145–8.

frontiers | Frontiers in Nutrition

TYPE Review
PUBLISHED 15 December 2022
DOI 10.3389/fnut.2022.1093939

OPEN ACCESS

EDITED BY
Jinxuan Cao,
Beijing Technology and Business University, China

REVIEWED BY
Tong Xing,
Nanjing Agricultural University, China
Rui Liu,
Yangzhou University, China

*CORRESPONDENCE
Yulong Luo
18247120609@163.com

SPECIALTY SECTION
This article was submitted to Food Chemistry, a section of the journal Frontiers in Nutrition

RECEIVED 09 November 2022
ACCEPTED 30 November 2022
PUBLISHED 15 December 2022

CITATION
Li R, Luo R, Luo Y, Hou Y, Wang J, Zhang Q, Chen X, Hu L and Zhou J (2022) Biological function, mediate cell death pathway and their potential regulated mechanisms for post-mortem muscle tenderization of PARP1: A review. *Front. Nutr.* 9:1093939. doi: 10.3389/fnut.2022.1093939

Biological function, mediate cell death pathway and their potential regulated mechanisms for post-mortem muscle tenderization of PARP1: A review

Rong Li[1,2], Ruiming Luo[1,2], Yulong Luo[1,2]*, Yanru Hou[1,2], Jinxia Wang[1,2], Qian Zhang[1,2], Xueyan Chen[1,2], Lijun Hu[1] and Julong Zhou[1]

[1]School of Food and Wine, Ningxia University, Yinchuan, China, [2]National R & D Center for Mutton Processing, Yinchuan, China

Tenderness is a key attribute of meat quality that affects consumers' willingness to purchase meat. Changes in the physiological environment of skeletal muscles following slaughter can disrupt the balance of redox homeostasis and may lead to cell death. Excessive accumulation of reactive oxygen species (ROS) in the myocytes causes DNA damage and activates poly ADP-ribose polymerase 1 (PARP1), which is involved in different intracellular metabolic pathways and is known to affect muscle tenderness during post-slaughter maturation. There is an urgent requirement to summarize the related research findings. Thus, this paper reviews the current research on the protein structure of PARP1 and its metabolism and activation, outlines the mechanisms underlying the function of PARP1 in regulating muscle tenderness through cysteine protease 3 (Caspase-3), oxidative stress, heat shock proteins (HSPs), and energy metabolism. In addition, we describe the mechanisms of PARP1 in apoptosis and necrosis pathways to provide a theoretical reference for enhancing the mature technology of post-mortem muscle tenderization.

KEYWORDS

PARP1, apoptosis and necrosis pathway, Caspase-3, tenderization, energy metabolism

1 Introduction

Tenderness is an important indicator to evaluate the edible value of meat. Surveys have reported that consumers have a strong desire to buy meat with better tenderness. Muscle includes muscle fibers, intermuscular fat and connective tissue (1). Its structure and complex relationship are the material basis of tenderness. Myofibrillar protein

hydrolyzed by endogenous enzymes in muscle fibers is the most important factor affecting meat tenderness (2). Calpain can catalyze the degradation of myofibrils, improve the tenderness of postmortem muscles, and enhance meat quality. Huang et al. (3) used Calpain inhibitor to study its effect on chicken breast tenderness confirming that Calpain catalyzed myogenic fiber degradation is the primary reason for increased muscle tenderness and meat maturation after slaughter. During postmortem maturation, muscle triggers a series of cascade reactions due to environmental changes. Mitochondria in myocytes not only respond to ATP depletion in myocytes by accelerating the glycolytic process but also release different regulatory factors to induce apoptosis and regulate muscle tenderness. These factors include cytochrome c (cyt-c) (4), endonuclease G (Endo G), and apoptosis inducing factor (AIF) (5). At the same time, mitochondria are damaged, the body produces too much ROS, and the body is in a state of oxidative stress due to imbalance in oxygen radical metabolism in response to environmental change (6).

Poly ADP-ribose polymerase 1 is a DNA repair enzyme that has been implicated in DNA damage repair, apoptosis, necrosis, chromosome modification, and transcription (7). It can interact with Calpain and Caspase to catalyze the degradation of myogenic fibronectin, which in turn regulates muscle tenderness. However, the influence of PARP1 on meat tenderness and its related mechanism are poorly known. Therefore, this paper reviews the molecular structure characteristics and metabolic mechanism of PARP1, and summarizes the related mechanism of PARP1 in postmortem muscles participating in the pathway of apoptosis and necrosis and affecting muscle tenderness. The paper further focuses on the skeletal protein degradation and apoptosis processes to provide directions for postmortem muscle tenderization research.

2 PARP family and PARP1 activity

2.1 PARP family

Poly ADP-ribose polymerase is a family of poly ADP-ribose polymerases with 17 members identified that are largely distributed in the nucleus of eukaryotic cells, and responsible for catalyzing ADP-ribose modification in cells (8). The current family members, namely, PARP1, PARP2, and PARP3 are DNA-dependent and their common tryptophan-glycine-arginine (WGR) structural domain is a major regulator of catalytic activity, which can interact with damaged DNA to repair it in a timely manner (9). PARP1 is the most abundant and well-studied protease in the PARP family, which plays a significant role in apoptosis and DNA repair. PARP2 is responsible for base excision and single-strand break repair in DNA; it can bind specifically to damaged DNA end gaps and form a catalytic conformation. Chen et al. (10) demonstrated that PARP2 synthesizes a new poly-ADP ribose chain through the N-terminus with PARP1 located at the site of DNA damage. The N-terminal binding domain of PARP3 consists of only 40 amino acids and has a partial PARP1 N-terminal binding domain function; the WGR structural can bind to the DNA and transmits the information to the C-terminal structural domain (11). Vyas et al. (12) and Rulten et al. (13), respectively, demonstrated that PARP3 can modify the target proteins *via* the mono ADP-ribose (MAR) activity, which is different from the poly-ADP-ribose (PAR) activity of PARP1 and PARP2.

2.2 Structure of PARP1

Poly ADP-ribose polymerase 1, 1,014 amino acids long, consists of an N-terminal DNA-binding domain (DBD), automodification domain (AMD), and C-terminal catalytic domain (CAT), as shown in **Figure 1**. The DBD domain contains three zinc finger (Zn) structures, one nuclear localization signal (NLS), and an aspartate-glutamate-valine-aspartic acid (DEVD) structural related to apoptosis (14). Eustermann et al. (15) reported that Zn1 and Zn2 of the DBD domain can specifically recognize DNA damage gaps by binding to the 5′ and 3′ ends, respectively, which are distributed on both sides of DNA break sites, whereas Zn3 links the structural domains to activate the target protein. Zhou verified that NLS can recognize the Caspase cleavage site at DNA strand breaks and localize PARP1 in the nucleus. Subsequently, the two zinc finger structures can bind to and repair the DNA damage site (16). The AMD structural domain is adjacent to the WGR structural and contains a breast cancer type 1 (BRCT) structural that catalyzes PARP1-mediated synthesis of poly-ADP ribose chains. The CAT structural domain, a crucial region for linking NAD+ and catalyzing PAR synthesis, consists of the α-helical subdomain (HD) and ADP-ribosyl transferase (ART) subdomain, which contains a nicotinamide adenine dinucleotide (NAD+) binding site and a PAR catalytic site (17, 18). Rudolph et al. (19) reported that WGR, a core component of the CAT structural domain in PARP1, can interact with DNA, Zn1, Zn3, and CAT to form an inter-regional network linking the damaged DNA to the CAT structural domain. Furthermore, the Arginine (Arg) 591 site of the WGR structural domain can interact with the HD structural domain of PARP1.

2.3 PARP1 metabolism and activation

2.3.1 PARP1 metabolism

Metabolism of intracellular PARP1 occurs *via* PAR metabolism, including the formation and degradation of PAR multimers. In the absence of DNA damage, PARP1 activity is very low. In the presence of DNA damage, PARP1

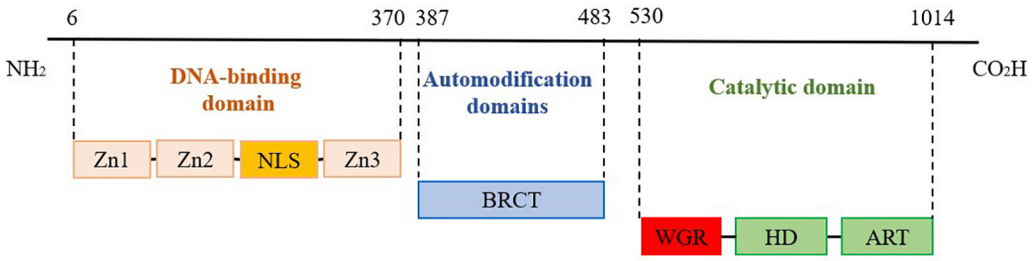

FIGURE 1
Poly ADP-ribose polymerase 1 (PARP1) structure.

is activated and its activity increases more than 500-fold. Excessive activation of PARP1 can produce an abundance of PAR, thereby inducing the release of AIF in mitochondria after polymerization (20). Gibson and Kraus (21) suggested that PARP1 synthesized by PARP1 in the nucleus could serve as a scaffold for DNA repair and recruit DNA repair proteins to the damaged site.

Poly ADP-ribose polymerase 1 cleaves the substrate NAD+ to ADP ribose and niacinamide, further catalyzes ADP ribose transfer, and polymerizes to glutamate residues of nuclear proteins, thus synthesizing large homopolymer PARs with more than 200 PARs and high branching (22). Buch-Larsen et al. (23) reported that PARP1 covalently binds adenosine diphosphate-ribose units *via* lipid exchange reactions to active modification sites of glutamate (Glu) and serine (Ser) residues, including Glu 488 and 491 and Ser 499, 507, and 519, which are subsequently and repeatedly catalyzed by PARP1 to form PAR chains on PARP1 itself or target proteins (**Figure 2**). PAR is degraded rapidly after synthesis by poly ADP-ribose glycohydrolase (PARG), whereas the binding activity of PARP1 to DNA is reactivated after PAR degradation.

2.3.2 PARP1 activation

The Zn or WGR structure in PARP1 protein binds to DNA to activate PARP1, which in turn participates in DNA repair. The activation of PARP1 is primarily caused by DNA damage. Intracellular oxidative stress can precipitate mitochondria to produce excessive reactive oxygen species (ROS, H_2O_2, NO, etc.) to induce DNA damage, and subsequently activate PARP1 with negative feedback. In the presence of slight DNA damage, PARP1 activation will timely repair the DNA break. In the presence of moderate damage, intracellular Caspase-3 and Caspase-7 would cleave PARP1 into PARP1-89 kDa and PARP1-24 kDa fragments to initiate cell apoptosis. However, when DNA is severely damaged, PARP1 will be overactivated and use the excess of intracellular NAD+, resulting in NAD+ depletion, reduced ATP levels, and eventually leading to cell necrosis (24). The activation of PARP1 accelerates the depletion of intracellular energy,

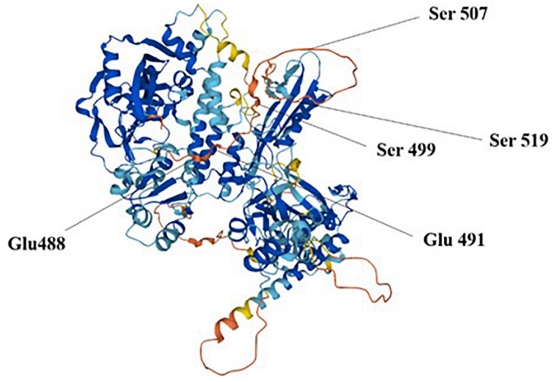

FIGURE 2
Poly ADP-ribose polymerase 1 (PARP1) modification sites.

decreases the ATP content, reduces NAD+ content, and alters the internal environment to accelerate cell death (25). In addition, the activation degree of PARP1 determines whether cells undergo apoptosis or necrosis by altering the levels of intracellular ATP (26).

3 PARP1 mediates cell death

Apoptosis and necrosis are the major death modes of postmortem myocytes, which are inter convertible and share similar characteristics. Cao et al. (27) observed that muscle cells of postmortem beef displayed necrosis characteristics such as vitrification of muscle fibers, lax cell nucleus and cytoplasm, and disappearance of the nucleus and cytoplasm, proving that apoptosis and necrosis of muscle cells coexisted. Similarly, Degterev et al. (28) believe that apoptosis and necrosis are two extreme types of cell death, and the two modes of death can be transformed into each other, and there will be coexistence of apoptosis and necrosis characteristics. Intracellular enzymes exist in cell apoptosis and necrosis and affect muscle tenderization by acting on cytoskeleton proteins.

3.1 PARP1 mediates apoptosis

After animal slaughter, the physiological activity of muscle tissue did not stop immediately. Under ischemia, hypoxia, and nutrient disruption apoptosis inducing factors can trigger myocytes to initiate the apoptotic program *via* coordinated control of multiple genes (29). As shown in **Figure 3**, the main cell-initiated apoptotic pathways include the exogenous death receptor pathway, endogenous mitochondrial pathway, PARP1 can all be involved in the onset of apoptosis through these pathways (30).

The death receptor pathway is activated by the cleavage of specific substrates by apoptotic effector enzymes. Death receptors on the cell surface bind to death ligands to recruit the Fas-associating protein with a novel death domain (FADD), which further binds to Caspase-8 precursors and activates Caspase-8 by FADD, which further binds to Caspase-8 precursor and activates Caspase-8 by forming a death-inducing signaling complex (DISC) (31). Activated Caspase-8, in turn, activates downstream Caspase-3, Caspase-6, and Caspase-7 through a cascade reaction, thus completing the apoptotic process (32). PARP1 is a substrate of Caspase, which is cleaved by Caspase-3 and Caspase-7 into PARP1 fragments (24 kDa N-terminal and 89 kDa C-terminal) in the Zn3 region, thereby losing PARP1 activity, which can retain ATP for subsequent energy consumption during apoptosis (33). Using DNA fragmentation, Lu et al. (34) demonstrated that Caspase-3 in the activated state cleaves PARP1 at specific sites into a binding structural domain (24 kDa) and a catalytic structural domain (89 kDa), leading to PARP1 inactivation. The 24 kDa PARP1 fragment is associated with DNA damage, which can bind to DNA ports and prevent the binding of intact PARP1 and DNA damage, ensuring that repair proteins are not recruited to chromosomes, resulting in DNA strand repair, and finally, complete apoptosis mediated by Caspase-3 (35). Mortusewicz et al. (36) reported that PARP1 recruited at the site of DNA damage could be cleaved, dissociating the 89 kDa fragment after cleavage and retaining the 24 kDa fragment at the site of DNA damage. The 89 kDa PARP1 fragment does not contain the DBD structural domain, and damaged DNA cannot activate it, thereby reducing intracellular energy consumption and providing sufficient energy to support apoptosis. In addition, the 89 kDa fragment catalyzes ADP ribosylation on RNA polymerase III (Pol III) complexes, activating innate immune responses and promoting apoptosis (37). Qin (38) used a high glucose-induced oxidative stress model to activate PARP1 and then inhibited PARP1 activity by ABT888. Moreover, Qin (38) confirmed that PARP1 reduced high glucose-induced cardiomyocyte apoptosis by activating the IGF-1R/Akt pathway. In conclusion, PARP1 participates in the occurrence of cell apoptosis by producing Caspase-3-mediated cleavage products of 24 kDa and 89 kDa fragments.

The mitochondrial pathway initiates in the mitochondria and is usually activated in response to injury or stress in cells within the body. When the mitochondria receive apoptotic signals, the mitochondrial membrane permeability transition pore (MPTP) is opened. Apoptotic factors, such as Cyt-c, AIF, and Endo G, are released from the mitochondria into the cytoplasm. Cyt-c released into the cytoplasm oligomerizes with apoptosis protease-activating factor (Apaf-1), leading to the conformational change in Apaf-1 to generate a heptameric apoptotic complex, which activates the apoptosis-initiating enzyme Caspase-9, thereby activating the downstream apoptosis effector enzymes Caspase-3 and Caspase-7 and initiating the apoptotic cascade response (39). However, AIF and Endo G can act directly on the nucleus, constituting another apoptotic pathway independent of apoptotic enzymes (40). Chen et al. (5) stated that gallic acid can induce apoptosis by AIF and Endo G released from the mitochondrial pathway in NCI-H292 cells. During apoptosis in the mitochondrial pathway, AIF mediates the onset of non-Caspase-dependent apoptosis by recruiting downstream nucleases that interact with cyclophilin A (Cyp A) to form active nucleases causing DNA damage by cleavage (41). After the DNA is cleaved by AIF, PARP1 functions as a protease to repair the damaged DNA and prevent chromosome shrinkage and DNA fragmentation. When large amounts of DNA are damaged, PARP1 fragments interact with AIF in the cytoplasm through the PAR polymer. PARP1 activation mediates AIF-dependent apoptosis, causing it to translocate from the mitochondria to the nucleus where apoptosis occurs. Sun et al. (42) reported that ionizing radiation can induce the death of HepG2 cells, thus releasing AIF from the mitochondria and transferring it to the nucleus by ionizing radiation, causing DNA breakage and leading to cell apoptosis. This finding indicates that ionizing radiation can induce HepG2 cell apoptosis through the AIF pathway. Yu et al. (43) demonstrated that AIF enters the mitochondria through the N-terminal mitochondrial localization signal, which is truncated by Calpain and cathepsin into a 57 kDa fragment and released into the cytoplasm in response to the death signal.

When the endoplasmic reticulum is strongly stimulated, the number of error proteins or unfolded proteins in the endoplasmic reticulum rapidly increases, beyond the range that the endoplasmic reticulum can handle, thereby disrupting the internal homeostasis and causing apoptosis (44). Calcium depletion is the primary cause of apoptosis induced by endoplasmic reticulum stress (ERS). When ERS occurs, a large amount of Ca^{2+} in the ER enters the cytosol, and activates Calpain and Caspase-12, further activating the downstream effector Caspase-3, ultimately leading to apoptosis (45). In the absence of DNA damage, the release of Ca^{2+} from the inositol triphosphate (IP3) receptor in the ER activates PARP1. Homburg et al. (46) studied nerve cells and contractile cardiomyocytes and reported that the release of intracellular stored Ca^{2+} could mediate PARP1 activation. After activation, PARP1 synthesizes excessive PAR to consume energy in cells. Caspase can timely bind to the active site of PARP1 and cleave it

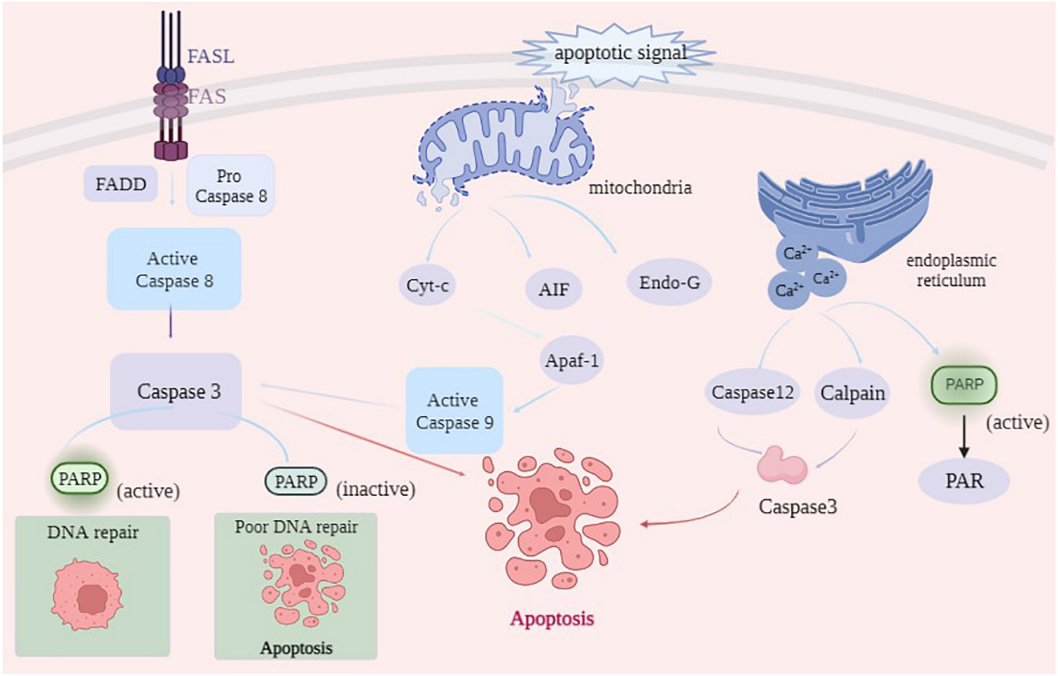

FIGURE 3
The main pathways of apoptosis.

into fragments to destroy the PARP1 activity and provide energy for the subsequent occurrence of apoptosis.

3.2 PARP1 mediates necrosis

Regulatory cell necrosis is characterized by increased membrane permeability, irregular changes in the appearance of certain cells, cell membrane fragmentation, cell contents leakage, and severe inflammatory reaction (47). Cell necrosis includes programmed necrosis, iron necrosis, and cyclophilin D-dependent necrosis, Parthanatos et al. (48). Among them, Parthanatos occurs mediated by PARP1, where cells lose their integrity, phospholipid bilayer exfoliates, nucleus shrinks, mitochondrial depolarization and chromatin agglutination occurs, and the DNA is broken into fragments of approximately 50 kb, in a Caspase-independent manner.

The hallmarks of the occurrence of Parthanatos include excessive activation of PARP1, PAR accumulation, and AIF nuclear translocation. Oxidative stress can cause DNA damage, and PARP1, a DNA damage receptor, is over-activated causing the occurrence of Parthanatos (49, 50). As shown in **Figure 4**, PARP1 is rapidly activated after the occurrence of DNA damage, and PAR polymer accumulates in the cells and consumes a large amount of NAD+, thus inhibiting the activity of the mitochondrial oxidative respiratory chain complex enzyme, blocking the tricarboxylic acid cycle pathway, impairing mitochondrial energy metabolism, and inducing the release of AIF from the mitochondria and its transfer to the nucleus (51–53). After AIF enters the nucleus, the large DNA fragment is degraded to a 50 kb fragment. In the mode of death of Parthanatos, AIF can be combined with macrophage migration inhibitory factor (MIF) in the cytoplasm, and this complex then enters the nucleus (54). MIF can perform nuclease function to degrade 3′ ssDNA, the intermediate product in the repair process of double-strand break (DSB), leading to the failure of DNA damage repair, resulting in nuclear shrinkage, chromatin agglutination, and DNA cleavage into small fragments (43). Park et al. (55) reported that the knockout of the MIF gene protected the neurons from damage caused by necrosis, further confirming the indispensable importance of MIF in the occurrence of Parthanatos. Baritaud et al. (56) reported that AIF enters the nucleus and binds to histone H2AX and the nucleic acid endonuclease CypA, leading to the formation of DNA degradation complexes to cause chromatin agglutination and promote DNA breakage. Andrabi et al. (57) demonstrated that PARP1 fragments interact with AIF in the cytoplasm through PAR polymers. Park et al. (58) reported that β-Lapachone induced non-caspase-dependent death of hepatocytes, with significantly enhanced activity of PARP1. Simultaneously, nuclear translocation of AIF was observed. The analysis showed that β-Lapachone activated the PARP1 activity and promoted the emergence of AIF, which in turn induced hepatocyte necrosis.

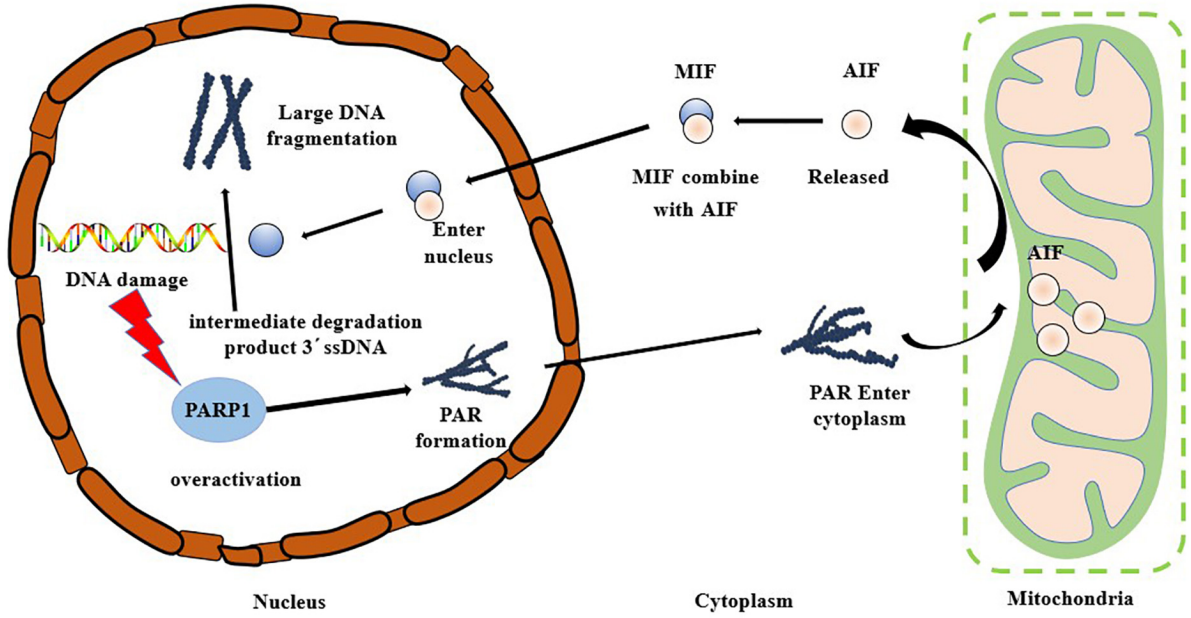

FIGURE 4
Molecular mechanism of Parthanatos.

4 PARP1 regulates the tenderization mechanism of postmortem muscles

Poly ADP-ribose polymerase 1, as a protease, can affect the structure of cytoskeleton proteins by acting on endogenous enzymes through cell apoptosis and cell necrosis, and can directly or indirectly participate in the muscle tenderization mechanism. D'Alessandro et al. (59) performed an integrated proteomics, interactomics and metabolomics analysis of Longissimus dorsi tender and tough meat samples from Chianina beef cattle. Indicating that tenderness was related to apoptosis through increase of HSPs and PARP fragment, that's because oxidative stress promoted meat tenderness and elicited heat shock protein responses, which in turn triggered apoptosis-like cascades along with PARP fragmentation. At present, the regulatory mechanism of muscle tenderness involves Caspase, Calpain endogenous enzymes, and energy metabolism.

4.1 Tenderness is influenced by the regulation of cytoskeletal protein degradation

Improvement in the post-slaughter tenderness of the meat is primarily attributed to the degradation of myogenic fibrous proteins, especially structural and cytoskeletal proteins (60). Proteins highly associated with meat tenderness largely include myosin (Titin), concomitant actin (Nebulin), and troponin-T (Troponin-T) (61). At present, there are many enzymes related to the degradation of cytoskeletal proteins, including Calpain, cathepsin, and apoptotic enzymes, whose hydrolysis of cytoskeletal proteins is closely related to the improvement of postmortem muscle tenderness (62, 63).

Caspase-3 is a terminal factor in the apoptotic cascade that affects muscle tenderization by disrupting the myofibrillar structure and degrading cytoskeletal proteins. Huang et al. (64) reported that Caspase-3 inhibitors inhibited the degradation of myofibrillar proteins in skeletal muscle cells, indirectly proving that Caspase-3 was involved in the degradation of myofibrillar proteins. Activated Caspase-3, an important protease, is involved in postmortem meat tenderization and has been implicated in myofibrillar degradation during muscle maturation. Huang et al. (65) incubated myofibrillar proteins of beef skeletal muscles with recombinant Caspase-3 *in vitro* and found that numerous myofibrillar protein degradation including titin, nebulin, troponin-T etc. Indicating the involvement of Caspase-3 in protein hydrolysis in muscles. PARP1 is a marker of hydrolytic skeletal muscle protein that is specifically recognized by Caspase-3 and cleaved into 89 kDa and 24 kDa fragments. It regulates the process of the death receptor pathway in apoptosis (66, 67). Cao et al. (68) reported that caspases cleave the PARP1 of 113 kDa to 24 kDa PARP1, which is also generated by the breakdown of PARP1 substrates of caspases. Huang et al. (69) reported that Caspase-3 activation sheared PARP1 protein, accelerated the apoptosis of muscle cells in duck meat, promoted the degradation of myofibrillar

proteins, and improved the tenderness of duck meat. Kemp et al. (70, 71) studied the protein hydrolysis in the skeletal muscles of pork after slaughter and reported that Caspase-3 cleaves PARP1 protein and degrades the cytoskeleton, which plays a key function in pork tenderization. Zhang (72) incubated dairy goat meat with calcium chloride and tea polyphenols during post-slaughter maturation and found that these significantly increased the protease activities of PARP1 and Caspase-3 in myocytes, resulting in increased degradation of interstitial line proteins. This finding suggested that apoptosis inducers can regulate muscle tenderness by promoting apoptosis in skeletal muscle cells (72). Saccà et al. (73) used the degradation pattern of PARP1 to assess the aging process in bovine muscles confirming that apoptotic processes occur in Longissimus lumborum (LL) and Infraspinatus (IS) during the early postmortem period and that may contribute to cell degradation of skeletal proteins. In conclusion, PARP1 is activated by caspase-3 cleavage to accelerate skeletal protein degradation (**Figure 5A**), thereby positively affecting the post-slaughter muscle tenderization of livestock.

Postmortem environmental changes result in excessive production of ROS in myocytes, such that the antioxidant defense system becomes insufficient to combat ROS, resulting in an imbalance between the oxidative and antioxidant systems and causing oxidative stress in the myocytes (74). Oxidative stress mediates protein oxidation, weakens the activity of proteolytic enzymes, and causes cross-linking and polymerization between protein molecules, thereby affecting the degradation of skeletal proteins, which is detrimental to the tenderization of muscles (75). Calpain degrades skeletal proteins, destroys the ultrastructure of muscle fibers, weakens the Z-line such that it disappears, causes fragmentation of myofibrils, and accelerates muscle tenderness. Carlin et al. (76) used Calpain to incubate porcine myofibrils supplemented with H_2O_2 and reported that oxidation changed the structure of myosin and actin and reduced the proteolytic activity of Calpain. Chen et al. (77) reported that packaging porcine dorsal longissimus muscle with high oxygen during storage enhanced the hydrophobicity of the protein surface, increased the carbonyl content, and enhanced protein oxidation. Protein oxidation inhibited the activity of μ-Calpain in the muscles, thereby delaying the degradation of skeletal proteins such as troponin-T and intercalary line proteins in pork. Silent information regulator 1 (Sirt1) enhances mitochondrial biogenesis, upregulates the activities of antioxidant enzymes superoxide dismutase (SOD) and succinate dehydrogenase (SDH) to play an antioxidant role and increases the expression of Sirt1, thus inhibiting the accumulation of ROS in myocytes (78). In contrast, excessive activation of PARP1 inhibits the expression of Sirt1, reduces the activity of mitochondrial complex I, inhibits the function of nicotinamide adenine dinucleotide (NADH) oxidase, induces the uncoupling of mitochondrial electron transport chain, induces the generation of superoxide anion radical ($O_2^{\cdot -}$), thus aggravating the oxidative stress in myocytes (79, 80). Cantó et al. (81) reported that over-activation of PARP1 can deplete large amounts of NAD+, thereby reducing intracellular NAD+ content to 20–30%, which in turn inhibits Sirt1 function and leads to increased levels of intracellular oxidative stress. Zhang et al. (82) enhanced the ubiquitination of PARP1 in mouse cells and found that the oxidative stress of cells was reduced following PARP1 proteasome degradation. As shown in **Figure 5A**, the overexpression of PARP1 inhibited Sirt1 activity, aggravated oxidative stress in myocytes, weakened the ability of proteolytic enzymes to degrade skeletal proteins, and reduced meat tenderness. Therefore, muscle tenderness can be improved by regulating PARP1 activity during postmortem maturation.

4.2 Tenderness is influenced by the regulation of apoptotic processes

Apoptosis enzyme belongs to cysteine protease and is mainly involved in cell apoptosis, which plays an important role in the transformation of muscle into meat. Therefore, the process of cell apoptosis is closely related to the tenderness of meat.

Heat shock proteins (HSPs) are a class of anti-apoptotic chaperone proteins, also known as heat stress proteins, that regulate the mitochondrial apoptotic pathway and can interact with apoptotic bodies (Apaf-1, Bax, Bcl-2, etc.), thereby preventing the activation of Caspase-3 and inhibiting the degradation of interstitial line proteins, and are molecular markers of meat tenderness (83, 84). As shown in **Figure 5A**, HSPs can bind to Caspase-3 to reduce its activity, which in turn affects the apoptotic process of cells. Ding et al. (85) reported that HSP27 binds to Caspase-3 during beef ripening and reduces the activity of Caspase-3, thereby inhibiting the degradation of myogenic fibrous proteins and thus hindering muscle tenderization. Balan et al. (86) observed the degradation of HSP27 in post-slaughter beef and reported that its degradation significantly correlated with the degradation of interstitial line proteins and troponin-T, and hypothesized that HSP27 degradation enhanced the hydrolysis of myogenic fibronectin by endogenous enzymes. Further studies demonstrated that HSPs not only bind the myofibrillar protein to act as a substitute for μ-Calpain, competitively inhibit μ-Calpain activity, and protect the integrity of myofibrils by reducing the enzymatic hydrolysis of myofibrillar protein, but also bind to the substrate site of Caspase-3 to inhibit its activity, followed by inhibiting the degradation of skeleton proteins (87). On the contrary, PARP1 is the activation substrate of Caspase-3, which can activate Caspase-3 and subsequently cleave PARP1 such that it loses its biological activity. Activated Caspase-3 can accelerate apoptosis and promote the degradation of skeletal proteins, which ameliorates muscle tenderness. Therefore, PARP1 can compete with HSPs for the Caspase-3 substrate site,

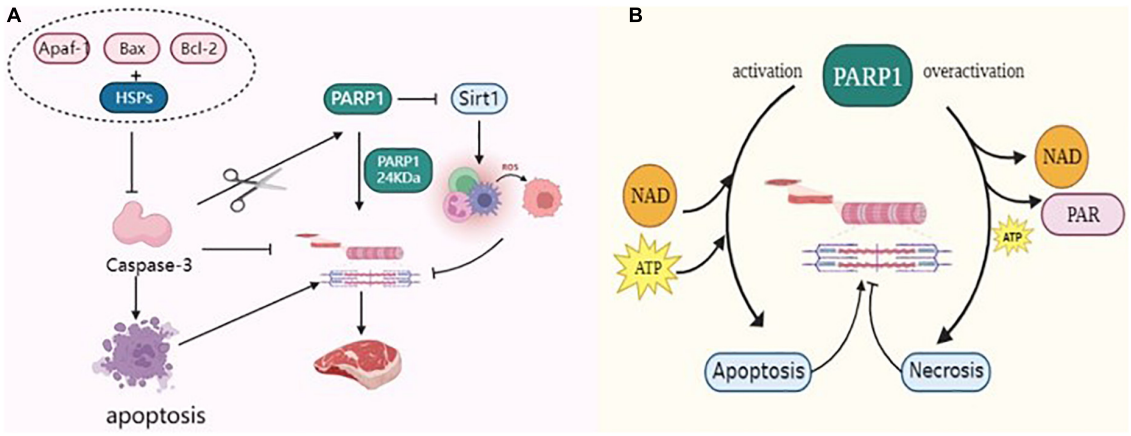

FIGURE 5
(A) PARP1 through Caspase-3, Sirt1, and HSPs regulates the tenderization mechanism of postmortem muscle. **(B)** PARP1 through energy metabolism regulates the tenderization mechanism of postmortem muscle.

promote the activation of Caspase-3, accelerate the degradation of myofibrillar protein, and facilitate the tenderization of postmortem muscles.

The ATP content in cells can affect cell apoptosis or necrosis, which is the crucial factor determining the cell death mode. Apoptosis requires energy consumption; ATP is required for the activation of Apaf-1 and Caspase precursors generated in the mitochondrial pathway (88). When energy is exhausted, apoptosis is inhibited, energy dependent life processes in myocytes stop, cell membranes are disrupted, and cytoplasm leaks out, leading to cell necrosis. Mitochondria are central regulators of apoptosis and provide sites for metabolic pathways such as oxidative phosphorylation, tricarboxylic acid cycle, energy conversion, and calcium ion storage under normal conditions (89, 90). After animal slaughter, the disruption of communication between muscle tissue and the outside world leads to tissue ischemia and hypoxia, which then leads to excessive ROS production in the metabolic processes of muscle cells. This cascade affects the functions of skeletal muscle mitochondria and damages the DNA structure in the cells, thus activating PARP1. The level of PARP1 activity is indirectly related to the mode of cell death, thus delaying or promoting muscle tenderization. The occurrence of necrosis is related to the decrease of intracellular NAD+ concentration. Excessive activation of PARP1 decreases NAD+ concentration, which is the primary factor causing the abnormal energy metabolism of cells. Simultaneously, PARP1 consumes a large amount of ATP while generating the PAR polymer, thus turning the cell death process from apoptosis to necrosis, which is not conducive to the tenderization of meat. However, NAD+ is a cofactor of glyceraldehyde 3-phosphate dehydrogenase (GAPDH), which participates in redox reactions. In addition, its depletion prevents ATP production by glycolysis in postmortem muscles. Chen et al. (91) used an acyl-CoA-binding domain containing 3 (ACBD3) to activate PARP1 and reported that a large amount of PAR was synthesized in the cytoplasm, which, in turn, reduced the intracellular NAD+ content. The introduction of mutant genes on the DEVD structural of PARP1 generates the mutant PARP1 that cannot be cleaved. The mutant PARP1 protein loses PAR activity and does not consume intracellular ATP and NAD+ (92). As shown in **Figure 5B**, PARP1 consumes large amounts of NAD+ and ATP, depleting intracellular energy and leading to cell necrosis, which in turn inhibits the activity of apoptosis enzymes. Caspase affects the tenderization of postmortem muscles, and inhibition of its activity delays the degradation of myogenic fibronectin in myocytes, which is negatively correlated with meat tenderness and is detrimental to post-slaughter meat tenderization (93).

5 Conclusion

This review details the structure and metabolic mechanism of PARP1, discusses the mechanism by which PARP1 mediates apoptosis and necrosis, and analyzes the potential mechanism by which it regulates muscle from the perspective of its ability to be activated by affecting oxidative stress and energy metabolism, get activated by Caspase-3 cleavage, and influence the competition for substrate sites by HSPs. PARP1 as a DNA damage receptor, in the presence of moderate DNA damage, PARP1 activation and participates in apoptosis through death receptors, mitochondria, and endoplasmic reticulum. In the presence of severe DNA damage it mediates the Parthanatos cell necrosis pathway. During the conversion of livestock from muscle to meat after slaughter, the mode of cell death affects the tenderness of the meat. Apoptosis activates Caspase-3, which destroys the structural integrity of muscle fibers and improves muscle tenderness, whereas cell necrosis exacerbates the accumulation of ROS and inhibits the activity

of apoptotic enzymes, which is detrimental to post-slaughter meat tenderness.

We believe that although studies on regulating meat tenderness by regulating PARP1 are scarce, PARP1 can provide novel ideas for subsequent muscle quality research. In the future, multiomics analyses such as metabolomics, transcriptomics, and proteomics can be used to study the link between PARP1 and meat tenderness. In addition, new ideas can be explored to improve meat tenderness after slaughter. The aim is to provide a theoretical reference for the development of high-quality and safe meat production technology.

Author contributions

YL: conceptualization, project administration, and funding acquisition. RLi, YH, JW, QZ, XC, LH, and JZ: resources. RLi: writing—original draft preparation. YL and RLu: writing—review and editing. All authors read and agreed to the published version of the manuscript.

Funding

This study was funded by the National Natural Science Foundation of China (32202135), the Ningxia Natural Science Foundation of Ningxia Hui Autonomous Region (2021AAC03098), the Key Research and Development Program of Ningxia Hui Autonomous Region (Talent Introduction Program) (2020BEB04023), and the Ningxia Youth Science and Technology Talent Support Project Ningxia Natural Science Foundation.

Conflict of interest

The authors declare that the research was conducted in the absence of any commercial or financial relationships that could be construed as a potential conflict of interest.

Publisher's note

All claims expressed in this article are solely those of the authors and do not necessarily represent those of their affiliated organizations, or those of the publisher, the editors and the reviewers. Any product that may be evaluated in this article, or claim that may be made by its manufacturer, is not guaranteed or endorsed by the publisher.

References

1. Holman B, van de Ven R, Mao Y, Coombs C, Hopkins D. Using instrumental (Cie and Reflectance) measures to predict consumers' acceptance of beef colour. *Meat Sci.* (2017). 127:57–62. doi: 10.1016/j.meatsci.2017.01.005

2. Wang T, Feng X, Li L, Luo J, Liu X, Zheng J, et al. Effects of quercetin on tenderness, apoptotic and autophagy signalling in chickens during post-mortem ageing. *Food Chem.* (2022) 383:132409. doi: 10.1016/j.foodchem.2022.132409

3. Huang J, Zhao L, Yang J, Zhang B, Xu X, Chen K, et al. The effect of μ/M-calpain on protein degradation of chicken breast meat. *J Food Sci.* (2019) 84:1054–9. doi: 10.1111/1750-3841.14596

4. Chen L, Chai Y, Luo J, Wang J, Liu X, Wang T, et al. Apoptotic changes and myofibrils degradation in post-mortem chicken muscles by ultrasonic processing. *LWT.* (2021) 142:110985. doi: 10.1016/j.lwt.2021.110985

5. Chen C, Shih Y, Yeh M, Liao N, Chung H, Liu K, et al. Ursolic acid induces apoptotic cell death through aif and endo G release through a mitochondria-dependent pathway in Nci-H292 human lung cancer cells in vitro. *In Vivo (Athens Greece).* (2019) 33:383–91. doi: 10.21873/invivo.11485

6. Chen C, Guo Z, Shi X, Guo Y, Ma G, Ma J, et al. H O -Induced oxidative stress improves meat tenderness by accelerating glycolysis via hypoxia-inducible factor-1α signaling pathway in postmortem bovine muscle. *Food Chem.* (2022) 16:100466. doi: 10.1016/j.fochx.2022.100466

7. Kumar V, Kumar A, Mir K, Yadav V, Chauhan S. Pleiotropic role of Parp1: an overview. *3 Biotech.* (2022) 12:3. doi: 10.1007/s13205-021-03038-6

8. Langelier M, Eisemann T, Riccio A, Pascal J. Parp family enzymes: regulation and catalysis of the poly(Adp-Ribose) posttranslational modification. *Curr Opin Struct Biol.* (2018) 53:187–98. doi: 10.1016/j.sbi.2018.11.002

9. Li X, Erden O, Li L, Ye Q, Wilson A, Du W. Binding to Wgr domain by salidroside activates Parp1 and protects hematopoietic stem cells from oxidative stress. *Antioxid Redox Signal.* (2014) 20:1853–65. doi: 10.1089/ars.2013.5600

10. Chen Q, Kassab M, Dantzer F, Yu X. Parp2 mediates branched poly adp-ribosylation in response to DNA damage. *Nat Commun.* (2018) 9:3233. doi: 10.1038/s41467-018-05588-5

11. Eustermann S, Videler H, Yang J, Cole P, Gruszka D, Veprintsev D, et al. The DNA-binding domain of human Parp-1 interacts with DNA single-strand breaks as a monomer through its second zinc finger. *J Mol Biol.* (2011) 407:149–70. doi: 10.1016/j.jmb.2011.01.034

12. Vyas S, Matic I, Uchima L, Rood J, Zaja R, Hay R, et al. Family-wide analysis of poly(Adp-Ribose) polymerase activity. *Nat Commun.* (2014) 5:4426. doi: 10.1038/ncomms5426

13. Rulten S, Fisher A, Robert I, Zuma M, Rouleau M, Ju L, et al. Parp-3 and aplf function together to accelerate nonhomologous end-joining. *Mol Cell.* (2011) 41:33–45. doi: 10.1016/j.molcel.2010.12.006

14. Liu L, Li J, Ke Y, Zeng X, Gao J, Ba X, et al. The key players of parthanatos: opportunities for targeting multiple levels in the therapy of parthanatos-based pathogenesis. *Cell Mol Life Sci.* (2022) 79:60. doi: 10.1007/s00018-021-04109-w

15. Eustermann S, Wu W, Langelier M, Yang J, Easton L, Riccio A, et al. Structural basis of detection and signaling of DNA single-strand breaks by human Parp-1. *Mol Cell.* (2015) 60:742–54. doi: 10.1016/j.molcel.2015.10.032

16. Lampart A, Sluzalska K, Czyrek A, Szerszen A, Otlewski J, Wiedlocha A, et al. Nuclear localization sequence of Fgf1 is not required for its intracellular anti-apoptotic activity in differentiated cells. *Cells.* (2022) 11:522. doi: 10.3390/cells11030522

17. Márton J, Fodor T, Nagy L, Vida A, Kis G, Brunyánszki A, et al. Parp10 (Artd10) modulates mitochondrial function. *PLoS One.* (2018) 13:e0187789. doi: 10.1371/journal.pone.0187789

18. Hottiger M, Hassa P, Lüscher B, Schüler H, Koch-Nolte F. Toward a unified nomenclature for mammalian adp-ribosyltransferases. *Trends Biochem Sci.* (2010) 35:208–19. doi: 10.1016/j.tibs.2009.12.003

19. Rudolph J, Muthurajan U, Palacio M, Mahadevan J, Roberts G, Erbse A, et al. The Brct domain of Parp1 binds intact DNA and mediates intrastrand transfer. *Mol Cell.* (2021) 81:4994–5006.e5. doi: 10.1016/j.molcel.2021.11.014

20. Regdon Z, Robaszkiewicz A, Kovács K, Rygielska Ż, Hegedűs C, Bodoor K, et al. Lps protects macrophages from aif-independent parthanatos by downregulation of Parp1 expression, induction of Sod2 expression, and a metabolic shift to aerobic glycolysis. *Free Radic Biol Med.* (2019) 131:184–96. doi: 10.1016/j.freeradbiomed.2018.11.034

21. Gibson B, Kraus W. New insights into the molecular and cellular functions of poly(Adp-Ribose) and parps. *Nat Rev Mol Cell Biol.* (2012) 13:411–24. doi: 10.1038/nrm3376

22. Amé J, Spenlehauer C, de Murcia G. The parp superfamily. *BioEssays.* (2004) 26:882–93. doi: 10.1002/bies.20085

23. Buch-Larsen S, Hendriks I, Lodge J, Rykær M, Furtwängler B, Shishkova E, et al. Mapping physiological adp-ribosylation using activated ion electron transfer dissociation. *Cell Rep.* (2020) 32:108176. doi: 10.1016/j.celrep.2020.108176

24. Herrmann G, Russell W, Garg N, Yin Y. Poly(Adp-Ribose) polymerase 1 regulates mitochondrial DNA repair in an Nad-dependent manner. *J Biol Chem.* (2021) 296:100309. doi: 10.1016/j.jbc.2021.100309

25. Gottschalk A, Timinszky G, Kong S, Jin J, Cai Y, Swanson S, et al. Poly(Adp-Ribosyl)ation directs recruitment and activation of an atp-dependent chromatin remodeler. *Proc Natl Acad Sci USA.* (2009) 106:13770–4. doi: 10.1073/pnas.0906920106

26. Bouchard V, Rouleau M, Poirier G. Parp-1, a determinant of cell survival in response to DNA damage. *Exp Hematol.* (2003) 31:446–54. doi: 10.1016/s0301-472x(03)00083-3

27. Cao J, Sun W, Zhou G, Xu X, Peng Z, Hu Z. Morphological and biochemical assessment of apoptosis in different skeletal muscles of bulls during conditioning. *J Anim Sci.* (2010) 88:3439–44. doi: 10.2527/jas.2009-2412

28. Degterev A, Huang Z, Boyce M, Li Y, Jagtap P, Mizushima N, et al. Chemical inhibitor of nonapoptotic cell death with therapeutic potential for ischemic brain injury. *Nat Chem Biol.* (2005) 1:112–9. doi: 10.1038/nchembio711

29. Musumeci G, Imbesi R, Szychlinska M, Castrogiovanni P. Apoptosis and skeletal muscle in aging. *Open J Apoptosis.* (2015) 4:41–6. doi: 10.4236/ojapo.2015.42004

30. Gupta S, Gollapudi S. Susceptibility of naïve and subsets of memory T cells to apoptosis via multiple signaling pathways. *Autoimmun Rev.* (2007) 6:476–81. doi: 10.1016/j.autrev.2007.02.005

31. Flusberg D, Sorger P. Surviving apoptosis: life-death signaling in single cells. *Trends Cell Biol.* (2015) 25:446–58. doi: 10.1016/j.tcb.2015.03.003

32. Salvesen G, Dixit V. Caspases: intracellular signaling by proteolysis. *Cell.* (1997) 91:443–6. doi: 10.1016/s0092-8674(00)80430-4

33. Mashimo M, Bu X, Aoyama K, Kato J, Ishiwata-Endo H, Stevens L, et al. Parp1 inhibition alleviates injury in Arh3-deficient mice and human cells. *JCI Insight.* (2019) 4:e124519. doi: 10.1172/jci.insight.124519

34. Lu A, Abo R, Ren Y, Gui B, Mo J, Blackwell D, et al. Enabling drug discovery for the parp protein family through the detection of mono-adp-ribosylation. *Biochem Pharmacol.* (2019) 167:97–106. doi: 10.1016/j.bcp.2019.05.007

35. Mashimo M, Onishi M, Uno A, Tanimichi A, Nobeyama A, Mori M, et al. The 89-Kda Parp1 cleavage fragment serves as a cytoplasmic par carrier to induce aif-mediated apoptosis. *J Biol Chem.* (2021) 296:100046. doi: 10.1074/jbc.RA120.014479

36. Mortusewicz O, Amé J, Schreiber V, Leonhardt H. Feedback-regulated poly(Adp-Ribosyl)ation by Parp-1 is required for rapid response to DNA damage in living cells. *Nucleic Acids Res.* (2007) 35:7665–75. doi: 10.1093/nar/gkm933

37. Chen Q, Ma K, Liu X, Chen S, Li P, Yu Y, et al. Truncated Parp1 mediates adp-ribosylation of rna polymerase iii for apoptosis. *Cell Discov.* (2022) 8:3. doi: 10.1038/s41421-021-00355-1

38. Qin W, Wei S, Wang X, Wang J, Wang W, Liu F, et al. Poly(Adp-Ribose) polymerase 1 inhibition protects against low shear stress induced inflammation. *Biochim Biophys Acta.* (2013) 1833:59–68. doi: 10.1016/j.bbamcr.2012.10.013

39. Wang H, Zhu J, Jiang L, Shan B, Xiao P, Ai J, et al. Mechanism of heshouwuyin inhibiting the Cyt C/Apaf-1/Caspase-9/Caspase-3 pathway in spermatogenic cell apoptosis. *BMC Complement Med Ther.* (2020) 20:180. doi: 10.1186/s12906-020-02904-9

40. Bu Q, Wang J, Zheng Y, Zou Y, Wei M. Mgl Induces nuclear translocation of endog and aif in caspase-independent T cell death. *Cell Mol Biol Lett.* (2015) 20:816–24. doi: 10.1515/cmble-2015-0051

41. Candé C, Vahsen N, Kouranti I, Schmitt E, Daugas E, Spahr C, et al. Aif and cyclophilin a cooperate in apoptosis-associated chromatinolysis. *Oncogene.* (2004) 23:1514–21. doi: 10.1038/sj.onc.1207279

42. Sun H, Yang S, Li J, Zhang Y, Gao D, Zhao S. Caspase-independent cell death mediated by apoptosis-inducing factor (Aif) nuclear translocation is involved in ionizing radiation induced Hepg2 cell death. *Biochem Biophys Res Commun.* (2016) 472:137–43. doi: 10.1016/j.bbrc.2016.02.082

43. Yu S, Wang Y, Frydenlund D, Ottersen O, Dawson V, Dawson T. Outer mitochondrial membrane localization of apoptosis-inducing factor: mechanistic implications for release. *ASN Neuro.* (2009) 1:e00021. doi: 10.1042/an20090046

44. Huang F, Wei Q, Li X, Liu C, Zhang C. Research progress on mechanisms of apoptosis to postmortem tenderization in muscle. *Sci Agric Sin.* (2021) 54:2192–202.

45. Wang L, Han L, Ma X, Yu Q, Zhao S. Effect of mitochondrial apoptotic activation through the mitochondrial membrane permeability transition pore on yak meat tenderness during postmortem aging. *Food Chem.* (2017) 234:323–31. doi: 10.1016/j.foodchem.2017.04.185

46. Homburg S, Visochek L, Moran N, Dantzer F, Priel E, Asculai E, et al. A fast signal-induced activation of poly(Adp-Ribose) polymerase: a novel downstream target of phospholipase C. *J Cell Biol.* (2000) 150:293–307. doi: 10.1083/jcb.150.2.293

47. D'Arcy M. Cell death: a review of the major forms of apoptosis, necrosis and autophagy. *Cell Biol Int.* (2019) 43:582–92. doi: 10.1002/cbin.11137

48. Jiang H, Yang Y, Zhang Y, Xie Z, Zhao X, Sun Y, et al. The dual role of poly(Adp-Ribose) polymerase-1 in modulating parthanatos and autophagy under oxidative stress in rat cochlear marginal cells of the stria vascularis. *Redox Biol.* (2018) 14:361–70. doi: 10.1016/j.redox.2017.10.002

49. Yang X, Zhang N, Yang Y, Xu T, An S. Recent progress in parthanatos—a new form of cell death. *Chine J Cell Biol.* (2021) 43:8. doi: 10.11844/cjcb.2021.01.0006

50. Fatokun A, Dawson V, Dawson T. Parthanatos: mitochondrial-linked mechanisms and therapeutic opportunities. *Br J Pharmacol.* (2014) 171:2000–16. doi: 10.1111/bph.12416

51. Herceg Z, Wang Z. Functions of poly(Adp-Ribose) polymerase (Parp) in DNA repair, genomic integrity and cell death. *Mutat Res.* (2001) 477:97–110. doi: 10.1016/s0027-5107(01)00111-7

52. Harraz M, Dawson T, Dawson V. Advances in neuronal cell death 2007. *Stroke.* (2008) 39:286–8. doi: 10.1161/strokeaha.107.511857

53. Mondal A, Roberge J, Gilleran J, Peng Y, Jia D, Akel M, et al. Bone morphogenetic protein inhibitors and mitochondria targeting agents synergistically induce apoptosis-inducing factor (Aif) caspase-independent cell death in lung cancer cells. *Cell Commun Signal.* (2022) 20:99. doi: 10.1186/s12964-022-00905-4

54. Wang Y, An R, Umanah G, Park H, Nambiar K, Eacker S, et al. A nuclease that mediates cell death induced by DNA damage and poly(Adp-Ribose) polymerase-1. *Science (New York NY).* (2016) 354:aad6872. doi: 10.1126/science.aad6872

55. Park H, Kam T, Dawson T, Dawson V. Poly (Adp-Ribose) (Par)-dependent cell death in neurodegenerative diseases. *Int Rev Cell Mol Biol.* (2020) 353:1–29. doi: 10.1016/bs.ircmb.2019.12.009

56. Baritaud M, Boujrad H, Lorenzo H, Krantic S, Susin S. Histone H2ax: the missing link in aif-mediated caspase-independent programmed necrosis. *Cell Cycle (Georgetown Tex).* (2010) 9:3166–73. doi: 10.4161/cc.9.16.12887

57. Andrabi S, Kim N, Yu S, Wang H, Koh D, Sasaki M, et al. Poly(Adp-Ribose) (Par) polymer is a death signal. *Proc Natl Acad Sci USA.* (2006) 103:18308–13. doi: 10.1073/pnas.0606526103

58. Park E, Min K, Lee T, Yoo Y, Kim Y, Kwon T. B-Lapachone induces programmed necrosis through the Rip1-parp-aif-dependent pathway in human hepatocellular carcinoma Sk-Hep1 cells. *Cell Death Dis.* (2014) 5:e1230. doi: 10.1038/cddis.2014.202

59. D'Alessandro A, Marrocco C, Rinalducci S, Mirasole C, Failla S, Zolla L. Chianina beef tenderness investigated through integrated omics. *J Proteomics.* (2012) 75:4381–98. doi: 10.1016/j.jprot.2012.03.052

60. Huff Lonergan E, Zhang W, Lonergan S. Biochemistry of postmortem muscle — lessons on mechanisms of meat tenderization. *Meat Sci.* (2010) 86:184–95. doi: 10.1016/j.meatsci.2010.05.004

61. Feng Y, Zhang S, Sun B, Xie P, Wen K, Xu C. Changes in physical meat traits, protein solubility, and the microstructure of different beef muscles during post-mortem aging. *Foods (Basel Switzerland).* (2020) 9:806. doi: 10.3390/foods9060806

62. Bhat Z, Morton J, Mason S, Bekhit A. Role of calpain system in meat tenderness: a review. *Food Sci Hum Wellness.* (2018) 7:196–204. doi: 10.1016/j.fshw.2018.08.002

63. Carlson K, Prusa K, Fedler C, Steadham E, Outhouse A, King D, et al. Postmortem protein degradation is a key contributor to fresh pork loin tenderness. *J Anim Sci.* (2017) 95:1574–86. doi: 10.2527/jas.2016.1032

64. Huang M, Huang F, Xue M, Xu X, Zhou G. The effect of active caspase-3 on degradation of chicken myofibrillar proteins and structure of myofibrils. *Food Chem.* (2011) 128:22–7. doi: 10.1016/j.foodchem.2011.02.062

65. Huang F, Huang M, Zhou G, Xu X, Xue M. In vitro proteolysis of myofibrillar proteins from beef skeletal muscle by caspase-3 and caspase-6. *J Agric Food Chem.* (2011) 59:9658–63. doi: 10.1021/jf202129r

66. Martire S, Fuso A, Rotili D, Tempera I, Giordano C, De Zottis I, et al. Parp-1 modulates amyloid beta peptide-induced neuronal damage. *PLoS One.* (2013) 8:e72169. doi: 10.1371/journal.pone.0072169

67. Kaufmann S, Desnoyers S, Ottaviano Y, Davidson N, Poirier G. Specific proteolytic cleavage of poly(Adp-Ribose) polymerase: an early marker of chemotherapy-induced apoptosis. *Cancer Res.* (1993) 53:3976–85.

68. Cao J, Ou C, Zou Y, Ye K, Zhang Q, Khan M, et al. Activation of caspase-3 and its correlation with shear force in bovine skeletal muscles during postmortem conditioning. *J Anim Sci.* (2013) 91:4547–52. doi: 10.2527/jas.2013-6469

69. Huang W, Cao J, Wang D, Xu W, Zhang M. Impact of caspase-3 activation on the tenderness of duck skeletal muscle during postmortem conditioning. *Sci Agric Sin.* (2012) 45:1372–9. doi: 10.3864/j.issn.0578-1752.2012.07.015

70. Kemp C, Bardsley R, Parr T. Changes in caspase activity during the postmortem conditioning period and its relationship to shear force in porcine longissimus muscle. *J Anim Sci.* (2006) 84:2841–6. doi: 10.2527/jas.2006-163

71. Kemp C, Parr T, Bardsley R, Buttery P. Comparison of the relative expression of caspase isoforms in different porcine skeletal muscles. *Meat Sci.* (2006) 73:426–31. doi: 10.1016/j.meatsci.2005.12.009

72. Zhang S. *The Mechanism of Apoptosis Inducers on Caspase-3 Activation Pathway During Matutation of Lamb.* Master's Thesis. Yangling: Northwest A&F University (2008).

73. Saccà E, Pizzutti N, Corazzin M, Lippe G, Piasentier E. Assessment of calpain and caspase systems activities during ageing of two bovine muscles by degradation patterns of αii spectrin and Parp-1. *Anim Sci J Nihon Chikusan Gakkaiho.* (2016) 87:462–6. doi: 10.1111/asj.12473

74. Wu J, Yang C, Yang M, Liang Z, Wu Y, Kong X, et al. The role of Er stress and Atp/Ampk in oxidative stress meditated hepatotoxicity induced by citrinin. *Ecotoxicol Environ Saf.* (2022) 237:113531. doi: 10.1016/j.ecoenv.2022.113531

75. Lametsch R, Lonergan S, Huff-Lonergan E. Disulfide bond within Mu-calpain active site inhibits activity and autolysis. *Biochim Biophys Acta.* (2008) 1784:1215–21. doi: 10.1016/j.bbapap.2008.04.018

76. Carlin K, Huff-Lonergan E, Rowe L, Lonergan S. Effect of oxidation, Ph, and ionic strength on calpastatin inhibition of Mu- and M-calpain. *J Anim Sci.* (2006) 84:925–37. doi: 10.2527/2006.844925x

77. Chen L, Zhou G, Zhang W. Effects of high oxygen packaging on tenderness and water holding capacity of pork through protein oxidation. *Food Bioproc Technol.* (2015) 8:2287–97. doi: 10.1007/s11947-015-1566-0

78. Zhou Y, Li K, Liu L, Li S. Microrna-132 promotes oxidative stress-induced pyroptosis by targeting sirtuin 1 in myocardial ischaemia-reperfusion injury. *Int J Mol Med.* (2020) 45:1942–50. doi: 10.3892/ijmm.2020.4557

79. Zhang F, Lau S, Monks TJA. Dual role for poly(Adp-Ribose) polymerase-1 during caspase-dependent apoptosis. *Toxicol Sci.* (2012) 128:103–14. doi: 10.1093/toxsci/kfs142

80. Magyar K, Deres L, Eros K, Bruszt K, Seress L, Hamar J, et al. A quinazoline-derivative compound with parp inhibitory effect suppresses hypertension-induced vascular alterations in spontaneously hypertensive rats. *Biochim Biophys Acta.* (2014) 1842:935–44. doi: 10.1016/j.bbadis.2014.03.008

81. Cantó C, Menzies K, Auwerx J. Nad(+) metabolism and the control of energy homeostasis: a balancing act between mitochondria and the nucleus. *Cell Metab.* (2015) 22:31–53. doi: 10.1016/j.cmet.2015.05.023

82. Zhang N, Zhang Y, Wu B, Wu S, You S, Lu S, et al. Deacetylation-dependent regulation of Parp1 by Sirt2 dictates ubiquitination of Parp1 in oxidative stress-induced vascular injury. *Redox Biol.* (2021) 47:102141. doi: 10.1016/j.redox.2021.102141

83. Kong F, Wang H, Guo J, Peng M, Ji H, Yang H, et al. Hsp70 suppresses apoptosis of Brl cells by regulating the expression of Bcl-2, cytochrome C, and caspase 8/3. *In Vitro Cell Dev Biol Anim.* (2016) 52:568–75. doi: 10.1007/s11626-016-0005-5

84. Malheiros J, Enríquez-Valencia C, da Silva Duran B, de Paula T, Curi R, de Vasconcelos Silva J, et al. Association of Cast2, Hsp90aa1, Dnaja1 and Hspb1 genes with meat tenderness in nellore cattle. *Meat Sci.* (2018) 138:49–52. doi: 10.1016/j.meatsci.2018.01.003

85. Ding Z, Huang F, Zhang C, Zhang L, Sun H, Zhang H. Effect of heat shock protein 27 on thein vitrodegradation of myofibrils by caspase-3 and M−calpain. *Int J Food Sci Technol.* (2017) 53:121–8. doi: 10.1111/ijfs.13565

86. Balan P, Kim Y, Blijenburg R. Small heat shock protein degradation could be an indicator of the extent of myofibrillar protein degradation. *Meat Sci.* (2014) 97:220–2. doi: 10.1016/j.meatsci.2014.01.019

87. Lomiwes D, Hurst S, Dobbie P, Frost D, Hurst R, Young O, et al. The protection of bovine skeletal myofibrils from proteolytic damage post mortem by small heat shock proteins. *Meat Sci.* (2014) 97:548–57. doi: 10.1016/j.meatsci.2014.03.016

88. Katoh I, Sato S, Fukunishi N, Yoshida H, Imai T, Kurata S. Apaf-1-deficient fog mouse cell apoptosis involves hypo-polarization of the mitochondrial inner membrane, Atp depletion and citrate accumulation. *Cell Res.* (2008) 18:1210–9. doi: 10.1038/cr.2008.87

89. Zhang J, Lautar S, Huang S, Ramsey C, Cheung A, Li J. Gpi 6150 prevents H O cytotoxicity by inhibiting poly(Adp-Ribose) polymerase. *Biochem Biophys Res Commun.* (2000) 278:590–8. doi: 10.1006/bbrc.2000.3816

90. Liu Y, Li Z, Zhang L, Wang D, Liu Y. Phenotypic plasticity of vascular smooth muscle cells in vascular calcification: role of mitochondria. *Front Cardiovasc Med.* (2022) 9:972836. doi: 10.3389/fcvm.2022.972836

91. Chen Y, Bang S, Park S, Shi H, Kim S. Acyl-Coa-binding domain containing 3 modulates Nad+ metabolism through activating poly(Adp-Ribose) polymerase 1. *Biochem J.* (2015) 469:189–98. doi: 10.1042/bj20141487

92. Herceg Z, Wang Z. Failure of poly(Adp-Ribose) polymerase cleavage by caspases leads to induction of necrosis and enhanced apoptosis. *Mol Cell Biol.* (1999) 19:5124–33. doi: 10.1128/mcb.19.7.5124

93. Saccà E, Corazzin M, Bovolenta S, Piasentier E. Meat qucccality traits and the expression of tenderness-related genes in the loins of young goats at different ages. *Animal.* (2019) 13:2419–28. doi: 10.1017/s1751731119000405

frontiers | Frontiers in Nutrition

TYPE Original Research
PUBLISHED 25 January 2023
DOI 10.3389/fnut.2023.1116100

OPEN ACCESS

EDITED BY
Jinxuan Cao,
Beijing Technology and Business University, China

REVIEWED BY
Zhongjiang Wang,
Northeast Agricultural University, China
Xi Huang,
Huazhong Agricultural University, China
Xinglian Xu,
Nanjing Agricultural University, China

*CORRESPONDENCE
Feng Yang
✉ yfyangfeng@hotmail.com

SPECIALTY SECTION
This article was submitted to Food Chemistry, a section of the journal Frontiers in Nutrition

RECEIVED 05 December 2022
ACCEPTED 09 January 2023
PUBLISHED 25 January 2023

CITATION
Hou Y, Ren X, Huang Y, Xie K, Wang K, Wang L, Wei F and Yang F (2023) Effects of hydrodynamic cavitation on physicochemical structure and emulsifying properties of tilapia (*Oreochromis niloticus*) myofibrillar protein. *Front. Nutr.* 10:1116100. doi: 10.3389/fnut.2023.1116100

Effects of hydrodynamic cavitation on physicochemical structure and emulsifying properties of tilapia (*Oreochromis niloticus*) myofibrillar protein

Yucheng Hou[1], Xian'e Ren[1,2], Yongchun Huang[1,2], Kun Xie[1], Keyao Wang[1], Liyang Wang[1], Fengyan Wei[1] and Feng Yang[1,2]*

[1]Guangxi Key Laboratory of Green Processing of Sugar Resources, Key Laboratory for Processing of Sugar Resources of Guangxi Higher Education Institutes, School of Biological and Chemical Engineering, Guangxi University of Science and Technology, Liuzhou, China, [2]Guangxi Liuzhou Luosifen Research Center of Engineering Technology, Liuzhou, China

The purpose of this research was to explore the different hydrodynamic cavitation (HC) times (0, 5, 10, 15, 20 min; power 550 W, pressure 0.14 MPa) on the emulsifying properties of tilapia myofibrillar protein (TMP). Results of pH, particle size, turbidity, solubility, surface hydrophobicity, and reactive sulfhydryl (SH) group indicated that HC changed the structure of TMP, as confirmed by the findings of intrinsic fluorescence and circular dichroism (CD) spectra. Furthermore, HC increased the emulsifying activity index (EAI) significantly ($P < 0.05$) and changed the emulsifying stability index (ESI), droplet size, and rheology of TMP emulsions. Notably, compared with control group, the 10-min HC significantly decreased particle size and turbidity but increased solubility ($P < 0.05$), resulting in accelerated diffusion of TMP in the emulsion. The prepared TMP emulsion showed the highest ESI (from 71.28 ± 5.50 to 91.73 ± 5.56 min), the smallest droplet size (from 2,754 ± 110 to 2,138 ± 182 nm) and the best rheological properties, as demonstrated by the microstructure photographs. Overall, by showing the effect of HC in improving the emulsifying properties of TMP, the study demonstrated HC as a potential technique for meat protein processing.

KEYWORDS

hydrodynamic cavitation, myofibrillar protein, physicochemical structure, rheology, emulsifying property

1. Introduction

Myofibrillar protein (MP), which mainly consists of myosin and actin (1), accounts for 55–65% of the total muscle proteins (2). The emulsifying properties of MP not only affects the quality and performance of emulsified-type meat products (3, 4), such as frankfurter-type sausage (5), but also contributes to the development of nutritive foods with bioactive ingredients as a potential emulsifier (6). However, due to the poor functional properties of natural MP,

MP-stabilized emulsions are usually easy to aggregate and flocculate, leading to the difficult in application of MP in the food industry (7). Furthermore, the emulsifying properties of MP are related to protein molecular size and protein conformational characteristics (8). Therefore, modification methods that can cause changes in the conformational characteristics or molecular size of MP may improve the emulsifying properties of MP, thus enhancing the quality of emulsified-type meat products.

In recent years, the physical modification of physicochemical structure of proteins by ultrasonic has attracted researchers' attention because of its non-toxicity, safety, and environmental friendliness (9). Some authors reported that ultrasonic was used to induce the modification of the functional properties of MP, especially the emulsifying properties (10–12). The underlying mechanism of ultrasonic modification is largely attributed to the cavitation phenomenon during ultrasonic treatment (13). Hydrodynamic cavitation (HC) can produce the same cavitation phenomenon as ultrasonic (14). In HC, cavitation bubbles are generated when the liquid flows through the compression region, and the volume of cavitation bubbles continues to increase as the local pressure continues to decrease (15). However, when the subsequent pressure increases, cavitation bubbles will collapse and explode (16), accompanied by the cavitation effects of instantaneous high temperature and pressure, high-speed micro-jet, strong shock wave, and active free radicals in local areas of the liquid (17). In addition, HC is easier to operate, more energy-efficient and more suitable for scale production than ultrasonic cavitation (18).

Recently, HC treatment, as a novel processing technique, has been reported to enhance the physicochemical and functional properties of proteins. For example, Ren et al. (19) found that HC improved the emulsifying activity index (EAI) and emulsifying stability index (ESI) of soybean protein isolate (SPI), and both increased with the extension of HC treatment time. Yang et al. (17) found that HC improved the EAI, ESI, and adsorbed protein percentage, but decreased the oil droplet size, flocculation index, and interfacial protein concentration, improving the emulsifying properties of SPI. Moreover, HC had some positive effects on the functional properties of soybean glycinin (15) and milk protein concentrate (20). However, the research on the properties of MP modified by HC has not been reported, and the effects of HC on the emulsifying properties of MP are unclear.

Therefore, the objective of this research was to study the effects of different HC times (5, 10, 15, and 20 min) on the physicochemical structure and emulsifying properties of tilapia (*Oreochromis niloticus*) tilapia MP (TMP). The experimental parameters of the pH, particle size, protein solubility, and structural changes in TMP and droplet size, microstructure, and rheological properties of emulsions were tested to elucidate the internal mechanism of HC affecting the emulsifying properties of TMP. The results of this study would provide a theoretical basis and technical support for further study on the functional modification of TMP and production of emulsified-type meat products.

Abbreviations: BPB, bromophenol blue; BSA, bovine serum albumin; CD, circular dichroism; DTNB, 5,5′-dithiobis-(2-nitrobenzoic acid); EAI, emulsifying activity index; ESI, emulsifying stability index; G′, storage modulus; G″, loss modulus; HC, hydrodynamic cavitation; H_0, surface hydrophobicity; MP, myofibrillar protein; SDS, sodium dodecyl sulfate; SH, sulfhydryl; SPI, soybean protein isolate; TMP, tilapia myofibrillar protein; λmax, maximum fluorescence emission wavelength.

2. Materials and methods

2.1. Materials

Tilapia, each weighing 750–900 g, were obtained from a local fresh food supermarket (Liuzhou, China). After removing the scales, viscera, skin and bones, the tilapia fish was frozen at −18°C until used. Soybean oil was provided by Kerry Grain and Oil Co., Ltd. (Fangchenggang, China). Bovine serum albumin (BSA) (98%) was purchased from Shanghai yuanye Bio-Technology Co., Ltd. (Shanghai, China). Bromophenol blue (BPB) indicator was purchased from Kermel Chemical Reagent Co., Ltd. (Tianjin, China). 5,5′-Dithiobis-(2-nitrobenzoic acid) (DTNB) (≥98%) was produced by Aladdin Biotechnology Co., Ltd. (Shanghai, China). The other reagents used in the experiment were all analytical grade.

2.2. Extraction of TMP

The TMP extraction procedures were adopted from a recent study (21), with slight modifications. Briefly, after small pieces of tilapia fish and a small amount of frozen isolation buffer (25 mmol/L KCl, 3 mmol/L $MgCl_2$, 0.1 mol/L NaCl, 4 mmol/L EDTA-2Na, 20 mmol/L phosphate buffer, pH 7.0) were ground in a meat grinder (ZG-L74A, Ningbo Zhao Ji Electric Appliance Co., Ltd., Ningbo, China), the cooling isolation buffer (4°C) was added until the total volume of isolation buffer was five times (w/v) the weight of the tilapia fish. Thereafter, the mixture was homogenized using a homogenizer (Ultra-Turrax T25, IKA, Staufen, Germany) at 9,000 r/min for 2 min (homogenizing for 30 s, then stopping for 30 s). The homogenized mixture was filtered through a layer of gauze to remove some skin and connective tissue, followed by centrifugation using a high-speed refrigerated centrifuge (JXN-26, Beckman Coulter Inc., Brea, CA, USA) at 3,220 × *g* at 4°C for 15 min. Then, the precipitate was homogenized and centrifuged twice under the same conditions with cooling five times (w/v) of isolation buffer (4°C) and four times (w/v) of 0.1 mol/L NaCl solution (4°C), respectively. The precipitate was then added to four times (w/v) of cooling phosphate buffer solution (20 mmol/L, pH 7.0, 4°C) and homogenized at 9,000 r/min for 2 min (homogenizing for 30 s, then stopping for 30 s). Thereafter, the mixture was filtered through three layers of gauze followed by centrifugation at 3,220 × *g* at 4°C for 15 min to obtain the precipitate. The protein concentration of TMP suspension was determined by the biuret method (22), using an ultraviolet-visible spectrophotometer (UV-5100, Shenzhen Ecorui Instrument Equipment Co. Ltd., Shenzhen, China) with BSA as the standard.

2.3. Treatment of TMP by HC

The HC treatment was carried out as described by previous studies with slight modifications (15, 19). As shown in **Figure 1**, V1 was used to adjust the flow of TMP suspension, V2 and V3 were used to adjust the upstream inlet pressure, which was measured by P1, and V4 was used to adjust the downstream recovery pressure. The TMP was dissolved in 0.6 mol/L NaCl buffer (0.6 mol/L NaCl, 20 mmol/L NaH_2PO_4/Na_2HPO_4, pH 6.5) and homogenized at 9,000 r/min for 30 s to prepare 10 mg/ml TMP suspension. After pouring 900 ml of TMP suspension into a storage tank and turning on the cooling water,

the HC treatment of TMP suspension was performed at a pressure of 0.14 MPa and a power of 550 W, using a single orifice plate (thickness 20 mm, orifice diameter 3 mm). After HC treatment for 0, 5, 10, 15, and 20 min, the TMP samples were stored at 4°C for further analysis.

2.4. Physicochemical properties

2.4.1. pH

The pH of TMP samples was measured as described by Wang et al. (21), using a pH meter (PHS-3E, INASE Scientific Instrument Co., Ltd., Shanghai, China).

2.4.2. Particle size

The TMP particle size was analyzed using the method of Chen et al. (6). The average particle sizes of diluted TMP (1 mg/ml) samples were determined at 25°C, using a Zetasizer (Nano-ZS90, Malvern Instrument Co. Ltd., Malvern, UK). The refractive index of particles, refractive index of dispersant, equilibrium time, and absorption parameter were 1.46, 1.33, 2 min, and 0.01, respectively.

2.4.3. Turbidity

A recent study was followed for turbidity measurement with slight modifications (23). Briefly, the absorbance of TMP was performed at 660 nm after the diluted TMP samples (1 mg/ml) were placed at room temperature for 30 min, using the UV-5100 spectrophotometer. A_{660} was used to indicate the turbidity of the TMP samples.

2.4.4. Protein solubility

The protein solubility of TMP samples was measured according to a published method (24), using BSA as the standard protein, with slight modifications. Briefly, 8 ml of the TMP samples (1 mg/ml) were taken and centrifuged at 10,000 × *g* for 10 min. Then, 1 ml of supernatant and 1 ml of TMP samples without centrifugation were added to 4 ml of biuret reagent, respectively. After mixing well, the absorbance was measured at 540 nm after reaction for 30 min in a dark chamber at room temperature. The protein solubility was expressed as follows:

$$S\,(\%) = \frac{C_a}{C_b} \times 100$$

Where S, C_b, and C_a represent the protein solubility of TMP samples (%), total protein content before centrifugation and protein content of the supernatant, respectively.

2.5. Secondary and tertiary structures

2.5.1. Surface hydrophobicity (H_0)

The H_0 was analyzed as described by Jia et al. (25). Briefly, 1 ml of TMP sample (5 mg/ml) was added to 200 μL of BPB solution (1 mg/ml) and mixed evenly, using a mixture of 200 μL of BPB solution (1 mg/ml) and 1 ml of 0.6 mol/L NaCl buffer as control. After standing at room temperature for 2 h and centrifuging at 6,000 × *g* for 15 min, 0.5 ml of supernatant was diluted into 4.5 ml of 0.6 mol/L NaCl buffer, and the absorbance of the diluted supernatant was measured at 595 nm using the UV-5100 spectrophotometer. The amount of BPB bound to TMP was used to represent the surface hydrophobicity of TMP, which was calculated as follows:

$$H_0(\mu g) = 200\mu g \times \frac{A_1 - A_2}{A_1}$$

Where A_1 and A_2 represent the absorbance value of control and TMP samples, respectively.

2.5.2. Reactive sulfhydryl (SH) group

The reactive sulfhydryl (SH) group of TMP samples was examined according to a previously published method (26). Briefly, after 50 μL of 10 mmol/L DTNB solution (phosphate buffer, pH 8.0) was mixed with 4 ml of TMP sample (1 mg/ml) and then incubated at 25°C for 20 min, the absorbance of the mixture was recorded at 412 nm using the UV-5100 spectrophotometer. The reactive SH group content was expressed as follows:

$$SH\,(\mu mol/100\ mg) = \frac{A_{412} \times D}{E_M \times C} \times 100,000$$

Where A_{412}, D, E_M, and C represent the absorbance of the mixture at 412 nm, dilution factor, molar extinction coefficient (13,600 $L{\cdot}mol^{-1}{\cdot}cm^{-1}$) and TMP concentration (mg/ml), respectively.

2.5.3. Intrinsic fluorescence spectroscopy

The intrinsic fluorescence spectra were analyzed using a Cary Eclipse fluorescence spectrophotometer (G9800A, Agilent Technologies Ltd., Santa Clara, CA, USA) with slight modifications (11). Briefly, after the TMP samples were dissolved in 0.6 mol/L NaCl buffer and adjusted to 0.2 mg/ml, the intrinsic fluorescence spectra of TMP samples were recorded at excitation wavelength, emission wavelength, excitation slit width, and emission slit width of 280, 300–400, 5, and 5 nm, respectively.

2.5.4. Circular dichroism (CD) spectroscopy

The circular dichroism (CD) spectra were measured using a CD spectropolarimeter (Chirascan, Applied Photophysics Ltd., Surrey, UK) with slight modifications (27). Briefly, after the TMP samples were diluted to 0.067 mg/ml and then injected into a quartz cuvette, the CD spectra were scanned in the far-UV range (200–260 nm) at room temperature. The results were described by the average of three scans, and the circle two data were expressed by the average molar ellipticity (θ) in $deg{\cdot}cm^2/dmol$. The scan rate, response time, bandwidth, and sensitivity were 100 nm/min, 0.5 s, 1.0 nm, and 20 mdeg, respectively. The proportions of four secondary structures were analyzed by CDNN software.

2.6. Emulsifying properties

2.6.1. Emulsion preparation

The preparation of O/W emulsion followed a recent report (6), with slight modifications. Briefly, 28 ml of TMP samples (10 mg/ml) were added to 7 ml of soybean oil, followed by homogenization at 8,000 r/min for 1 min.

2.6.2. EAI and ESI

The EAI and ESI of TMP emulsions were examined as reported (11). Briefly, immediately (0 min) and 10 min later after

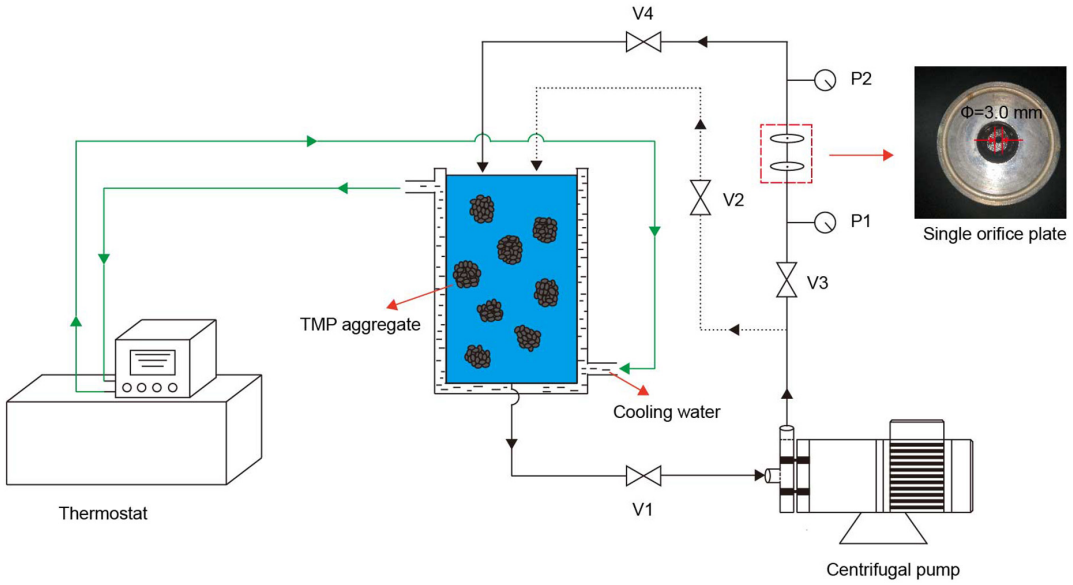

FIGURE 1
Schematic diagram of the hydrodynamic cavitation (HC) experimental setup. The HC device consists of a centrifugal pump (power 550 W), a storage tank, a thermostat, a single orifice plate (orifice diameter 3 mm, thickness 20 mm), two pressure gauges (P1 and P2), and four valves (V1, V2, V3, and V4).

homogenization, 50 μL of TMP emulsion of the bottom was diluted to 5 ml of 0.1% sodium dodecyl sulfate (SDS) (w/v) solution. After mixing well, the absorbance of the mixture was measured at 500 nm by the UV-5100 spectrophotometer, using SDS solution as blank. EAI and ESI were calculated as follows:

$$EAI\left(m^2/g\right) = \frac{2 \times 2.303 \times A_0 \times N}{C \times \theta \times 10000}$$

$$ESI\,(min) = \frac{A_0}{A_0 - A_{10}} \times 10$$

Where N, θ, and C represent the dilution factor (100), volume fraction of oil in emulsion (0.2) and initial concentration of TMP (g/ml), respectively, and A_0 and A_{10} represent the absorbance at 500 nm after 0 and 10 min, respectively.

2.6.3. Droplet size of the emulsions

The droplet size measurement was performed using the Nano-ZS90 Zetasizer according to the published method (11). Briefly, about 1 ml of fresh emulsion diluted 500-fold with 0.6 mol/L NaCl buffer was loaded into a quartz cuvette to measure droplet size.

2.6.4. Microstructure of the emulsions

The microstructure of TMP emulsions was observed using an optical microscope (DM-2000 LED, Leica Microsystems Co. Ltd., Wetzlar, Germany) (6). Briefly, 10 μL of the homogenized emulsion was dropped in the center of the slide and slowly covered with a cover glass to ensure no bubbles formed. The image was obtained by a 20× objective lens.

2.6.5. Dynamic rheological measurements of the emulsions

The rheology of TMP emulsions was examined using a rotational rheometer (MCR72, Antompa, Graz, Austria) with slight modifications (28). Briefly, using a 50 mm plate test, 3 ml of TMP emulsion was evenly coated on the test platform, and a layer of silicone oil was applied around TMP emulsion to prevent evaporation of TMP emulsion during the heating process. The frequency, strain, initial temperature, heating rate, termination temperature, and crack spacing were 0.1 Hz, 1%, 20°C, 1°C/min, 80°C, 1.0 mm, respectively. Storage modulus (G′) and loss modulus (G″) were analyzed as test indexes.

2.7. Statistical analysis

Each trial was conducted in triplicate independently and the data were presented as the mean ± standard deviation (SD). One-way analysis of variance (ANOVA) and Duncan's test were analyzed using SPSS statistical software (Version 26.0, IBM Corp., Armonk, NY, USA) to determine statistical differences ($P < 0.05$) among different groups.

3. Results and discussion

3.1. pH

The changes in the pH of TMP suspension as affected by HC treatment are shown in **Table 1**. Compared with control group (0 min), HC increased the pH of TMP suspension significantly ($P < 0.05$) by approximately 0.06 units (**Table 1**), indicating that HC induced a pH transition to alkaline, which was beneficial to the solubilization of TMP (**Table 1**) (21). However, with the extension of HC treatment time, pH only decreased slightly, indicating that pH was not the main factor in solubility reduction, which might be due to the thermal effect generated by long HC treatment time (17), resulting in TMP aggregation. The increase of pH might be because the cavitation effect produced by HC leaded to the denaturation

TABLE 1 Effect of hydrodynamic cavitation (HC) on the pH, average particle size, turbidity, and protein solubility of tilapia myofibrillar protein (TMP).

Time (min)	pH	Average particle size (nm)	Turbidity	Protein solubility (%)
0	6.33 ± 0.02^{b}	$1{,}026.2 \pm 25.9^{b}$	0.111 ± 0.001^{b}	57.65 ± 1.08^{c}
5	6.39 ± 0.01^{a}	719.3 ± 41.1^{c}	0.093 ± 0.001^{d}	63.07 ± 1.37^{ab}
10	6.39 ± 0.01^{a}	681.6 ± 13.6^{c}	0.089 ± 0.001^{d}	64.90 ± 0.34^{a}
15	6.38 ± 0.01^{a}	967.3 ± 27.8^{b}	0.105 ± 0.004^{c}	59.50 ± 0.41^{bc}
20	6.38 ± 0.01^{a}	$2{,}095.3 \pm 61.6^{a}$	0.227 ± 0.003^{a}	29.44 ± 5.10^{d}

Data are presented as mean ± standard deviation (SD) (n = 3). Different lowercase letters indicate that TMP had significant differences at different HC times ($P < 0.05$).

of TMP and the generation of free radicals, which reacted with protein side chains to reduce the acidic groups of protein. Similar speculations were reported in the results that ultrasonic treatment increased the pH of MP suspensions (10). In addition, a recent study reported that HC changed the pH of SPI suspension, and inferred that HC affected the exposure of acidic or basic amino acid residues (19). Therefore, the amount of acidic and basic amino acid residues exposed might be another important factor affecting the pH of the TMP suspension. However, there was no significant difference in pH between HC treatment groups ($P > 0.05$), which might be due to the similar amount of acidic and basic amino acid residues exposed. Nevertheless, Ren et al. (19) found that neither HC nor ultrasound treatment significantly changed the pH of SPI suspensions. The difference in results might be due to differences in the type of protein and cavitation.

3.2. Particle size, turbidity, and protein solubility

The average particle size of TMP decreased with the increase of HC treatment time within 0–10 min, as shown in **Table 1**. Furthermore, compared with 0, 15, and 20 min, HC for 5 min (from 1,026.2 ± 25.9 to 719.3 ± 41.1 nm) and 10 min (from 1,026.2 ± 25.9 to 681.6 ± 13.6 nm) decreased the average particle size of TMP significantly ($P < 0.05$), while no significant differences were observed between the two HC treatments ($P > 0.05$). This decrease might be attributed to cavitation effects during HC treatment, such as turbulence, high shear, and shock waves, which destroyed the non-covalent bonds between TMP molecules, such as hydrogen bonds and electrostatic interactions, causing the dissociation of TMP. Similar results have been reported that HC treatment decreased the particle size of SPI (17, 19) and soybean glycinin (15). However, the average particle size of TMP increased significantly ($P < 0.05$) with the extension of HC treatment time within 10–20 min. The increase in particle size of TMP might be due to high temperature and excessive free radicals caused by excessive HC, which leaded to the acceleration of movement and the increase of collision opportunities of TMP molecules, promoting aggregation of TMP. Similar results were observed for the effects of ultrasonic treatment on the particle size of MP (7, 12, 29). These results showed that appropriate HC could decrease effectively the formation of large aggregates, which might benefit the application of TMP in emulsification.

The turbidity of TMP as affected by HC is shown in **Table 1**. In general, higher turbidity corresponds to denser protein aggregation (6). HC for 10 min had lower turbidity (0.089 ± 0.001) compared to the other groups, which could be explained by a decrease in particle size, which resulted in less light scattering (30). However, with the further increase in HC treatment time (10–20 min), the turbidity of TMP increased significantly ($P < 0.05$), which might be due to the de-folding and reaggregation of protein molecules affecting light scattering, leading to an increase in turbidity (31). Additionally, excessive HC could decompose water and generate active free radicals (15), promoting intramolecular or intermolecular protein cross-linking, resulting in increased turbidity.

The solubility of TMP increased with the increase in HC treatment time (0–10 min), as shown in **Table 1**. Compared with 0, 15, and 20 min, HC for 10 min significantly increased the solubility of TMP ($P < 0.05$), which might be due to cavitation effects that dissociated TMP to form smaller aggregates with larger surface area and enhanced protein-water interaction, resulting in better solubility (32). However, as HC treatment time (10–20 min) continued to increase, protein solubility decreased significantly ($P < 0.05$), which might be caused by TMP aggregation (31). Therefore, appropriate HC could dissociate the TMP aggregate, resulting in increased solubility. In addition, the changes in particle size, turbidity, and solubility were consistent, confirming the significant influence of HC on the dissociation of TMP aggregates.

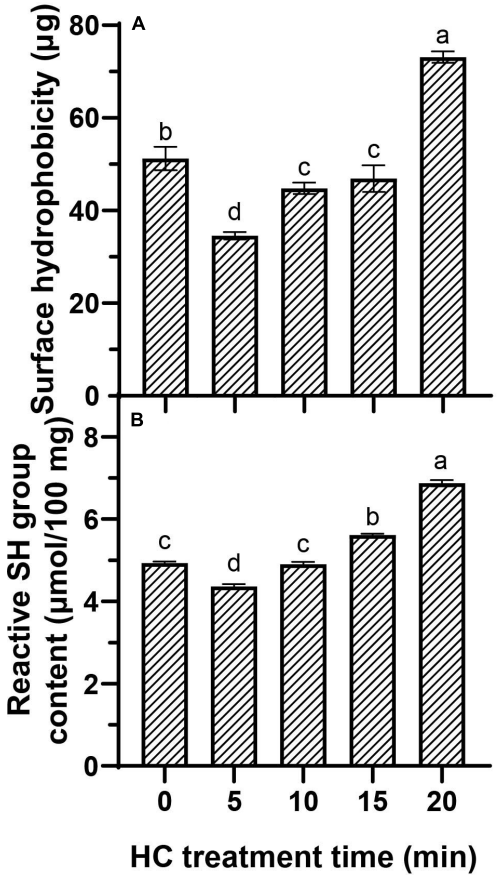

FIGURE 2
Effect of hydrodynamic cavitation (HC) on the surface hydrophobicity (H_0) **(A)** and reactive sulfhydryl (SH) group **(B)** of tilapia myofibrillar protein (TMP). Different lowercase letters indicate that TMP had significant differences at different HC times ($P < 0.05$).

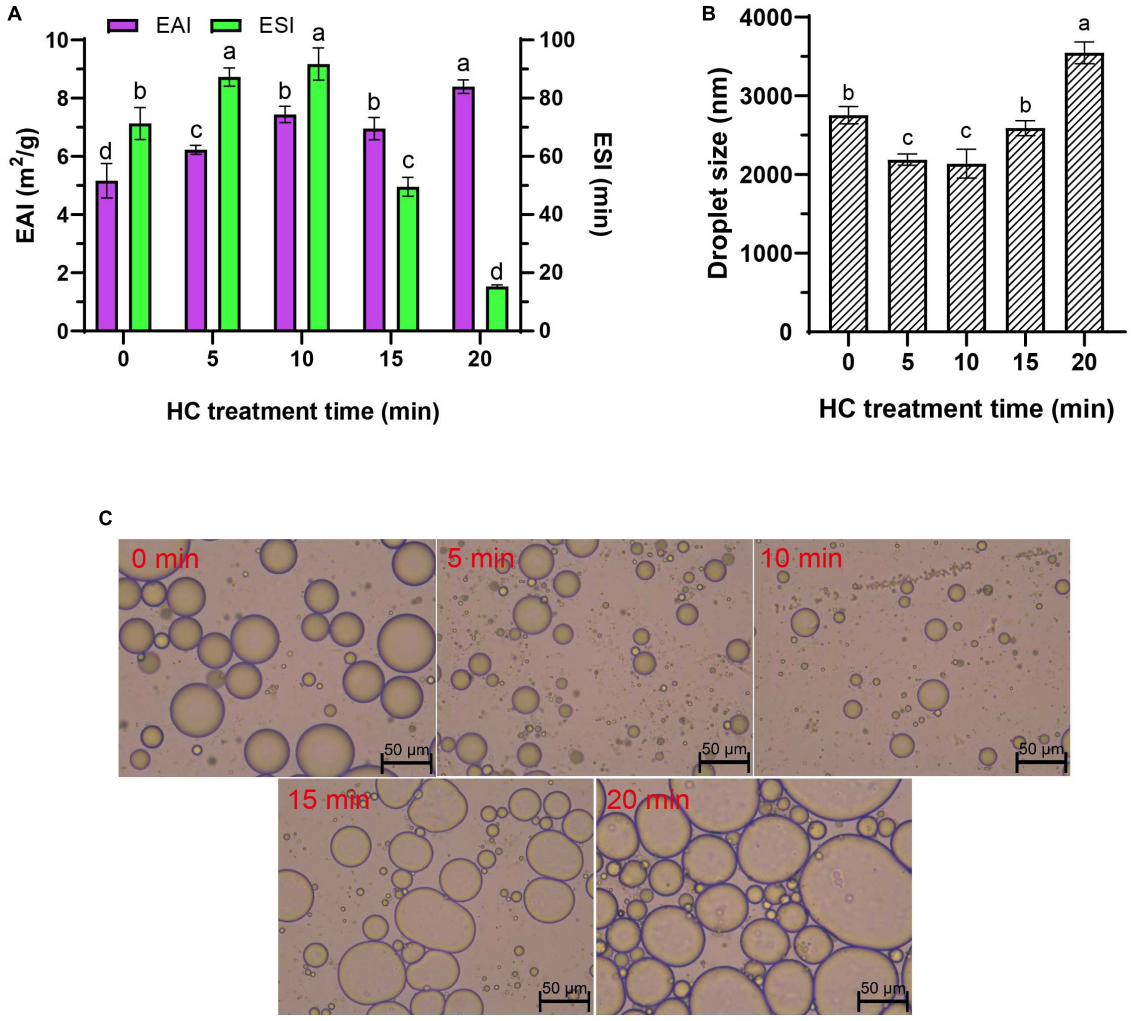

FIGURE 3
Effect of hydrodynamic cavitation (HC) on the emulsifying activity index (EAI) and emulsifying stability index (ESI) **(A)**, droplet size **(B)**, and microstructure **(C)** of tilapia myofibrillar protein (TMP) emulsions. In panels **(A,B)** different lowercase letters indicate that TMP emulsions had significant differences at different HC times ($P < 0.05$).

3.3. Tertiary structures

3.3.1. H_0

The H_0 represents the exposure of hydrophobic groups in protein molecules (29). This work is to determine the H_0 by analyzing the binding of hydrophobic amino acids of proteins to BPB. Compared with control group, HC for 5 min significantly decreased the binding amount of BPB ($P < 0.05$; **Figure 2A**). The decrease in H_0 was based on an increase in protein solubility (**Table 1**) (33), since the hydrophobic amino acids of TMP might be distributed inside the molecule by HC, leading to enhancing protein-water interactions and exposing less hydrophobic groups (34). With the further increase of HC treatment time (5–20 min), the H_0 of TMP increased significantly ($P < 0.05$), and reached the highest value (73.11 ± 1.23 μg) after HC treatment for 20 min. This was because the cavitation effect unfurled TMP structure and exposed hydrophobic groups, resulting in increased H_0. Similar to other physical modified MP studies (35–37). In addition, the temperature effect of HC in the local region of the suspension may be another important factor that causes the conformational change of TMP. Similarly, Pan et al. (30) suggested that the temperature effect of ultrasonic might alter the tertiary structure of MP due to the susceptibility of fish MP to thermal denaturation. These results suggested that HC changed the H_0 due to its influence on protein-water and protein intermolecular interactions and the exposure of hydrophobic groups.

3.3.2. Reactive SH group

The reactive SH groups refer to the SH groups located on the surface of the protein network, which can reflect MP tertiary structure conformational changes (7). Compared with control group, the reactive SH content was decreased significantly after HC treatment for 5 min ($P < 0.05$; **Figure 2B**), indicating that the structure of TMP and disulfide bond formation were changed, possibly because the reactive SH on TMP surface was converted to disulfide bonds by the HC-induced cavitation effects. Similarly, Yang et al. (17) reported that HC could lead to the conversion of free SH into disulfide bonds in SPI. However, compared with the 5 min, the reactive SH content increased significantly with the increase of HC treatment time ($P < 0.05$), indicating that HC accelerated the expansion and structural changes of protein molecules, leading to exposing more SH group hidden inside the protein molecules (19).

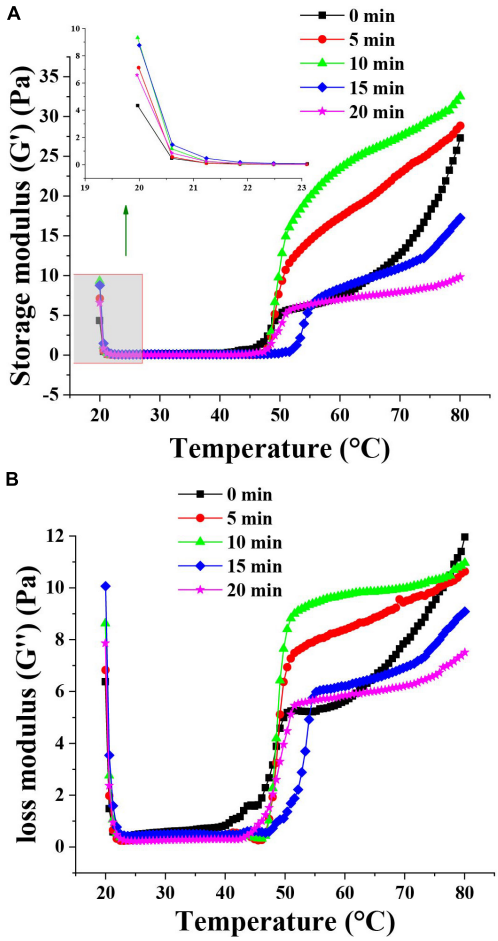

FIGURE 4
Effect of hydrodynamic cavitation (HC) on the storage modulus (G′) **(A)** and loss modulus (G″) **(B)** of tilapia myofibrillar protein (TMP) emulsions. The inserted figure is the enlarged part of the control and HC treatment groups.

3.4. Emulsifying properties

3.4.1. EAI and ESI

EAI and ESI represent the capacity of a protein to be adsorbed by the interface between the water phase and oil sphere during the formation of protein emulsion and the ability of a protein to maintain at the oil-water interface of emulsion after storage period, respectively (6, 24). Compared with control group (0 min), all HC treatments significantly increased the EAI of TMP emulsion ($P < 0.05$), and EAI was increased significantly with the increase of HC treatment time (except 10 and 15 min) ($P < 0.05$; **Figure 3A**). Different from EAI, ESI showed a trend of increasing first and then decreasing, that is, increasing gradually within 0–10 min of HC treatment and decreasing gradually with further treatment (10–20 min). The increase in EAI and ESI of TMP might be due to the cavitation effect generated by HC that decreases the particle size of TMP (**Table 1**), making more TMP easily adsorbed on the oil-water interface, resulting in the improvement of emulsifying capacity (17). Furthermore, lower protein turbidity and higher solubility (**Table 1**) accelerated the diffusion of TMP in the emulsion (6, 23). Interestingly, excessive HC treatment (20 min) increased particle size and turbidity and decreased solubility (**Table 1**) compared with the other groups, leading to a decrease in ESI but not in EAI as expected. This phenomenon might be attributed to an increase in H_0 (**Figure 2A**), which led to the enhancement of the interaction between adjacent molecules at the oil-water interface (7). Some other studies have reported that MP (10, 12) and SPI (17, 19) showed a good positive correlation between EAI and H_0, and increasing H_0 was conducive to improve EAI of proteins. This study showed that HC for 10 min could improve the EAI and ESI of TMP significantly.

3.4.2. Droplet size

Droplet size determines the rheology and stability of emulsion, and generally smaller droplet size is associated with higher emulsifying capacity (23, 38). The droplet size of TMP emulsion decreased significantly from 2,754 ± 110 nm (0 min) to 2,138 ± 182 nm (10 min) ($P < 0.05$) with the increase in HC treatment time (0–10 min), but no significant difference was observed between 5 min and 10 min treatments ($P > 0.05$; **Figure 3B**). However, with the continuous extension of HC treatment time (10–20 min), the droplet size of TMP emulsion increased significantly ($P < 0.05$), and this opposite trend was attributed to the overtreatment of the protein (7). These results indicated that appropriate HC could be conducive to decrease the droplet size of TMP emulsion and improve its emulsifying properties.

3.4.3. Microstructure of the emulsions

The microstructure of TMP emulsions as affected by HC was enlarged 200 times under an optical microscope, as shown in **Figure 3C**. The soybean oil droplets in the control group (0 min) were relatively large and unevenly distributed, which was attributed to the high interfacial tension between water and soybean oil (6). Compared with the untreated group, HC for 10 min had fewer large oil droplets, suggesting that HC induced TMP expansion and conformational changes, thereby decreasing the interfacial tension between water and soybean oil. Similar results have been reported in ultrasonic modification of MP (6). However, it was observed that the oil droplets size in the fresh emulsion increased, and the distribution was more uneven with the further extension of HC treatment time (10–20 min). The results of optical microscopic images could intuitively show the oil droplet size, corresponding to the previous results of the droplet size (**Figure 3B**). These results showed that compared with control group, HC for 10 min decreased the oil droplet size and improved the uniformity of emulsion.

3.4.4. Rheological properties of the emulsions

The rheological behavior of emulsions prepared with MP was analyzed to understand the viscoelastic properties of MP emulsions and the functionality of muscle protein in meat processing (39). The rheological properties of the TMP emulsions as affected by HC are shown in **Figure 4**. The G′ of TMP emulsion showed a decrease at the initial stage of heating (20–22°C), which might be attributed to the formation of weak and preliminary interactions of the protein aggregates prior to heating and destruction after initial heating (11). Compared with other groups, HC for 10 min had the highest G′ value at the initial stage and scanning end, indicating that HC for 10 min had the most robust gel structure of TMP emulsion (28). In addition, after HC treatment for 10 min, the particle size of TMP was decreased and an emulsion with more uniform and smaller oil droplets was formed. HC for 10 min decreased the particle size of TMP and formed smaller and more uniform oil droplets in the emulsion. Li et al. (11)

10.3389/fnut.2023.1116100

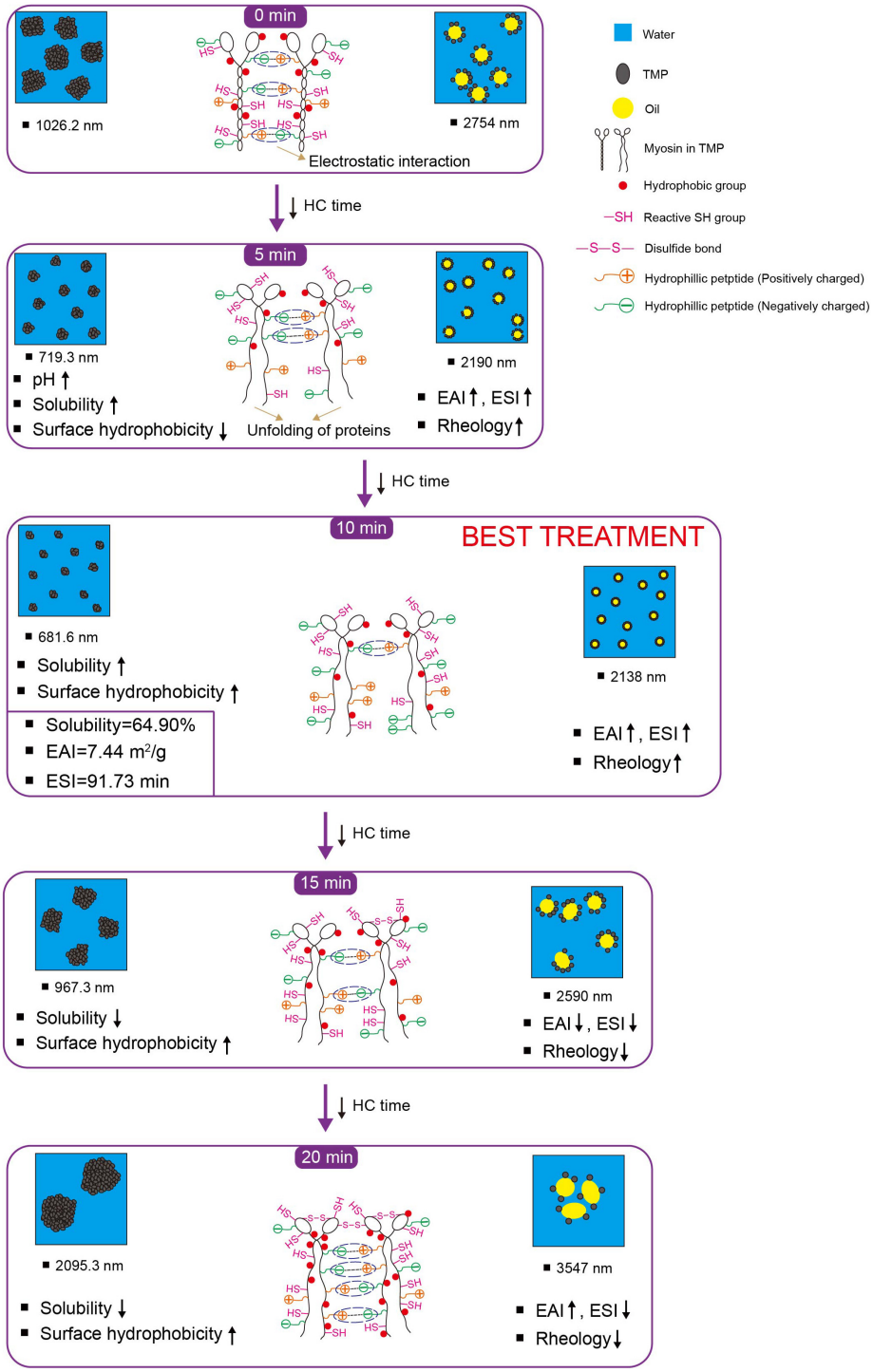

FIGURE 5
Schematic model illustrating the effects of hydrodynamic cavitation (HC) treatment on physicochemical structure and emulsifying properties of tilapia myofibrillar protein (TMP). ESI, emulsifying stability index; EAI, emulsifying activity index; reactive SH group, reactive sulfhydryl group. The chemical structure is not represented to actual scale, just to illustrate (For color references in this illustration, please refer to the online version of this article).

showed that smaller oil droplets could fill effectively and evenly into the network of MP gel during heating, resulting in better elasticity of MP emulsion gel. Therefore, HC for 10 min improved the elastic properties of TMP emulsion and prepared emulsion with stronger rheological properties. The changes in G″ of TMP emulsions were similar to that of G′. The G″ value of the TMP emulsion treated by HC for 10 min during about 50∼70°C heating was higher than that of the control (0 min). For all emulsions, the G″ values were substantially lower than that of G′ values indicating the formation of a gel-like behavior (39). The values of G′ and G″ increased with the increase of HC treatment time, indicating that HC promoted the formation of firm and dense gel structure of proteins. However, with the further extension of HC treatment time, the viscoelastic properties of the emulsion decreased, possibly due to the formation of

TABLE 2 Effect of hydrodynamic cavitation (HC) on the secondary structure contents (%) of tilapia myofibrillar protein (TMP).

Time (min)	Secondary structure of TMP			
	α-Helix	β-Sheet	β-Turn	Random coil
0	53.4 ± 0.7^{a}	9.9 ± 0.2^{b}	14.0 ± 0.2^{b}	22.7 ± 0.3^{b}
5	39.3 ± 2.6^{b}	14.8 ± 1.2^{a}	15.9 ± 0.4^{a}	30.0 ± 1.4^{a}
10	37.9 ± 2.1^{b}	15.3 ± 0.9^{a}	16.1 ± 0.3^{a}	30.7 ± 1.3^{a}
15	38.1 ± 0.4^{b}	15.2 ± 0.2^{a}	16.1 ± 0.2^{a}	30.6 ± 0.4^{a}
20	37.9 ± 0.5^{b}	15.2 ± 0.2^{a}	15.8 ± 0.4^{a}	31.1 ± 0.4^{a}

Data are presented as mean ± standard deviation (SD) (n = 3). Different lowercase letters indicate that TMP had significant differences at different HC times ($P < 0.05$).

uneven and rough gel structure. Rheological measurements showed that appropriate HC (10 min) improved the rheological properties of TMP-based emulsion as well as the structure of TMP.

3.5. Schematic model

Based on the results of physicochemical properties (sections "3.1. pH," and "3.2. Particle size, turbidity, and protein solubility"), tertiary structures (section "3.3. Tertiary structures"), and emulsifying properties (section "3.4. Emulsifying properties"), a schematic model (**Figure 5**) was proposed for the presentation of the modifications of HC-induced TMP. HC changed the particle size, turbidity, and solubility of TMP (**Table 1**) due to cavitation effects such as high shear, shock wave, and turbulence generated during HC treatment that affected covalent bonds such as disulfide bonds and non-covalent bonds such as electrostatic interactions between protein molecules (15, 17). Additionally, HC changed the tertiary structure of TMP (**Figure 2**) and partially expanded the TMP. These results led to changes in the interaction between protein and oil phases (7, 11, 40), thus affecting the emulsifying (**Figure 3**) and rheological (**Figure 4**) properties of TMP emulsions. Notably, HC for 10 min decreased the average particle size and turbidity and increased the solubility of TMP significantly ($P < 0.05$), which was conducive to the diffusion of TMP in the emulsion (6, 23). In addition, HC for 10 min increased the EAI and ESI significantly ($P < 0.05$), decreased the droplet size of TMP emulsion significantly ($P < 0.05$), and made its distribution more uniform, resulting in improved emulsifying and rheological properties of TMP emulsion. In summary, TMP treated by HC for 10 min had the capacity to form more uniform and smaller emulsion droplets. Interestingly, the decrease in emulsifying properties of TMP treated by HC for 20 min might be due to the excessive oxidation of TMP resulting in more reactive SH conversion to disulfide bonds (17), as well as the increase in particle size and decrease in solubility (**Table 1**). Therefore, this study showed that HC for 10 min enhanced the stability of emulsion stabilized by TMP and emulsifying properties of TMP.

3.6. Validation of the schematic model

3.6.1. Intrinsic fluorescence spectra

The tertiary and secondary structure changes of the HC-induced TMP were measured by intrinsic fluorescence spectra and CD

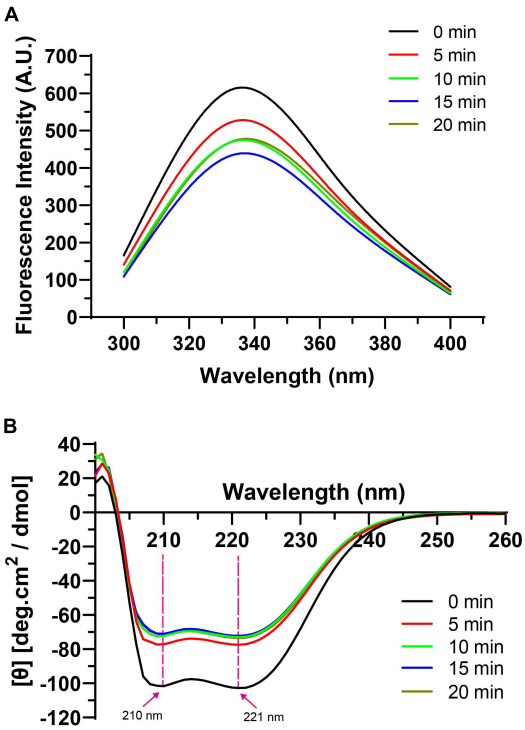

FIGURE 6
Effect of hydrodynamic cavitation (HC) on intrinsic fluorescence spectra **(A)** and circular dichroism (CD) spectra **(B)** of tilapia myofibrillar protein (TMP).

spectra, which reflected the changes in the physicochemical structure and emulsifying properties of TMP to verify the proposed schematic model. In general, intrinsic fluorescence spectroscopy is used to assess the local environment of certain chromophores, especially tryptophan residues, and can monitor tertiary structural changes in proteins (7). The fluorescence intensity of all treatment groups was lower than that of the control group (**Figure 6A**), suggesting that HC destroyed hydrophobic interactions, allowing the structure of TMP molecules to unfold, which caused the movement of tryptophan residues to more polar environments. Similar results have been reported in the ultrasonic treatment of MP (30, 31). For example, Jiang et al. (31) speculated that cavitation effects generated by ultrasound exposed the tryptophan group to the solvent, leading to a decrease in fluorescence intensity of MP. Pan et al. (30) pointed out that ultrasound disrupted hydrophobic interactions between MP molecules and moved tryptophan residues to a more polar environment. Interestingly, the fluorescence intensity of TMP decreased when HC treatment time increased from 0 to 15 min but increased after 20 min. This might be due to protein aggregation (**Table 1**), increased H_0 (**Figure 2A**), and specific modification of tryptophan residues in TMP, which combinedly resulted in less exposure of tryptophan residues to water (12).

In addition, in terms of the maximum fluorescence emission wavelength (λ_{max}), the λ_{max} of the control group (334 nm) was higher than 330 nm, indicating that tryptophan was in a polar environment (41). The larger the redshift of λ_{max}, the larger the conformational change of the protein. With the extension

of HC treatment time, λ_{max} of TMP redshifted from 334 to 338 nm, which might be due to the exposure of tryptophan and the microenvironment becoming more polar, causing the tertiary conformation of TMP to become looser (**Figure 5**) (12).

3.6.2. CD spectra

The CD spectra of TMP as affected by HC are shown in **Figure 6B**. In general, the α-helical structure is formed mainly by the hydrogen bond between the carbonyl oxygen (C=O) and amino hydrogen (NH^-) groups in the polypeptide chain (42). Two negative peaks of α-helical structures were detected at 210 and 221 nm, and HC decreased the intensity of these two peaks, indicating that HC destroyed the intramolecular hydrogen bond of TMP, thus promoting the unfolding of the protein (43). At the same time, **Table 2** also shows that HC significantly decreased the α-helix content ($P < 0.05$). Additionally, compared with control group, the β-sheet, β-turn, and random coil contents of all HC treatment groups were increased significantly ($P < 0.05$), but no significant differences were observed between HC treatment groups ($P > 0.05$). The transformation of secondary structure of TMP might be caused by the hydrogen bond change induced by HC. Similar conclusions have been reported in using other physical modification techniques to change the secondary structure of MP, such as ultrasound (44), high-pressure homogenization (23). Moreover, Yang et al. (17) reported that swirling cavitation increased β-sheet content and decreased α-helix content, which might improve the emulsifying properties of SPI. Consistent with the experimental results, HC increased the β-sheet content and decreased the α-helix content of TMP significantly ($P < 0.05$) compared with control group, which might be another important reason for the enhancement of emulsifying properties of TMP (**Figures 3**, **4**). However, the decrease in emulsifying properties after HC for 15 and 20 min might be attributed to the increase in particle size and turbidity as well as the decrease in solubility (**Table 1**).

4. Conclusion

The current study showed that different HC times (0, 5, 10, 15, 20 min; power 550 W, pressure 0.14 MPa) changed the physicochemical properties of TMP, thus affecting the emulsifying properties of TMP emulsions. The results showed that HC changed the structure of TMP, such as pH, particle size, turbidity, solubility, surface hydrophobicity, and reactive SH group. Furthermore, HC increased the EAI significantly ($P < 0.05$) and changed the ESI, droplet size, and rheology of TMP emulsions. Notably, appropriate HC treatment (10 min) decreased significantly particle size and turbidity and increased solubility of TMP ($P < 0.05$), resulting in a significant improvement in the emulsifying properties, according to measurements of ESI, droplet size, and rheology. In addition, HC induced TMP expansion and changed the physicochemical structure of TMP, as confirmed by the research findings of intrinsic fluorescence and CD spectra. This study suggested that HC is a feasible and potential technique, and the research results can provide theoretical basis and technical support for further research on functional modification of TMP and production of emulsified-type meat products.

Data availability statement

The original contributions presented in this study are included in this article/supplementary material, further inquiries can be directed to the corresponding author.

Author contributions

YuH: investigation, methodology, data curation, software, and writing—original draft. XR: investigation, resources, and writing—review and editing. YoH, KX, KW, LW, and FW: investigation. FY: conceptualization, methodology, supervision, funding acquisition, and writing—review and editing. All authors contributed to the article and approved the submitted version.

Funding

This research was funded by the National Natural Science Foundation of China (No. 31660473).

Conflict of interest

The authors declare that the research was conducted in the absence of any commercial or financial relationships that could be construed as a potential conflict of interest.

Publisher's note

References

1. Zhou Y, Liu J, Kang Y, Cui H, Yang H. Effects of acid and alkaline treatments on physicochemical and rheological properties of tilapia surimi prepared by pH shift method during cold storage. *Food Res Int.* (2021) 145:110424. doi: 10.1016/j.foodres.2021.110424

2. Ge G, Han Y, Zheng J, Zhao M, Sun W. Physicochemical characteristics and gel-forming properties of myofibrillar protein in an oxidative system affected by partial substitution of NaCl with KCl, MgCl2 or CaCl2. *Food Chem.* (2020) 309:125614. doi: 10.1016/j.foodchem.2019.125614

3. Zhou Y, Yang H. Effects of calcium ion on gel properties and gelation of tilapia (*Oreochromis niloticus*) protein isolates processed with pH shift method. *Food Chem.* (2019) 277:327–35. doi: 10.1016/j.foodchem.2018.10.110

4. Fu Q, Shi H, Zhou L, Li P, Wang R. Effects of ultrasound power on the properties of non-salt chicken myofibrillar protein emulsions. *Int J Food Sci Tech.* (2022) 57:2523–34. doi: 10.1111/ijfs.15626

5. Liu H, Zhang J, Wang H, Chen Q, Kong B. High-intensity ultrasound improves the physical stability of myofibrillar protein emulsion at low ionic strength by destroying and suppressing myosin molecular assembly. *Ultrason Sonochem.* (2021) 74:105554. doi: 10.1016/j.ultsonch.2021.105554

6. Chen J, Zhang X, Xue S, Xu X. Effects of ultrasound frequency mode on myofibrillar protein structure and emulsifying properties. *Int J Biol Macromol.* (2020) 163:1768–79. doi: 10.1016/j.ijbiomac.2020.09.114

7. Yu C, Li S, Sun S, Yan H, Zou H. Modification of emulsifying properties of mussel myofibrillar proteins by high-intensity ultrasonication treatment and the stability of O/W emulsion. *Colloid Surf A Physicochem Eng Asp.* (2022) 641:128511. doi: 10.1016/j.colsurfa.2022.128511

8. Guo X, Zhang Y, Jamali M, Peng Z. Manipulating interfacial behaviour and emulsifying properties of myofibrillar proteins by L-Arginine at low and high salt concentration. *Int J Food Sci Tech.* (2020) 56:999–1012. doi: 10.1111/ijfs.14752

9. Chen J, Zhang X, Chen Y, Zhao X, Anthony B, Xu X. Effects of different ultrasound frequencies on the structure, rheological and functional properties of myosin: significance of quorum sensing. *Ultrason Sonochem.* (2020) 69:105268. doi: 10.1016/j.ultsonch.2020.105268

10. Amiri A, Sharifian P, Soltanizadeh N. Application of ultrasound treatment for improving the physicochemical, functional and rheological properties of myofibrillar proteins. *Int J Biol Macromol.* (2018) 111:139–47. doi: 10.1016/j.ijbiomac.2017.12.167

11. Li K, Fu L, Zhao Y, Xue S, Wang P, Xu X, et al. Use of high-intensity ultrasound to improve emulsifying properties of chicken myofibrillar protein and enhance the rheological properties and stability of the emulsion. *Food Hydrocolloid.* (2020) 98:105275. doi: 10.1016/j.foodhyd.2019.105275

12. Deng X, Ma Y, Lei Y, Zhu X, Zhang L, Hu L, et al. Ultrasonic structural modification of myofibrillar proteins from *Coregonus peled* improves emulsification properties. *Ultrason Sonochem.* (2021) 76:105659. doi: 10.1016/j.ultsonch.2021.105659

13. Cichoski A, Silva M, Leães Y, Brasil C, De Menezes C, Barin J, et al. Ultrasound: a promising technology to improve the technological quality of meat emulsions. *Meat Sci.* (2019) 148:150–5. doi: 10.1016/j.meatsci.2018.10.009

14. Pathania S, Ho Q, Hogan S, McCarthy N, Tobin J. Applications of hydrodynamic cavitation for instant rehydration of high protein milk powders. *J Food Eng.* (2018) 225:18–25. doi: 10.1016/j.jfoodeng.2018.01.005

15. Hou Y, Yang F, Cao J, Huang Y, Li C, Li J, et al. Effects of hydrodynamic cavitation at different pH values on the physicochemical properties and aggregation behavior of soybean glycinin. *LWT.* (2022) 163:113615. doi: 10.1016/j.lwt.2022.113615

16. Gregersen S, Wiking L, Bertelsen K, Tangsanthatkun J, Pedersen B, Poulsen K, et al. Viscosity reduction in concentrated protein solutions by hydrodynamic cavitation. *Int Dairy J.* (2019) 97:1–4. doi: 10.1016/j.idairyj.2019.04.015

17. Yang F, Liu X, Ren X, Huang Y, Huang C, Zhang K. Swirling cavitation improves the emulsifying properties of commercial soy protein isolate. *Ultrason Sonochem.* (2018) 42:471–81. doi: 10.1016/j.ultsonch.2017.12.014

18. Asaithambi N, Singha P, Dwivedi M, Singh S. Hydrodynamic cavitation and its application in food and beverage industry: a review. *J Food Process Eng.* (2019) 42:e13144. doi: 10.1111/jfpe.13144

19. Ren X, Li C, Yang F, Huang Y, Huang C, Zhang K, et al. Comparison of hydrodynamic and ultrasonic cavitation effects on soy protein isolate functionality. *J Food Eng.* (2020) 265:109697. doi: 10.1016/j.jfoodeng.2019.109697

20. Li K, Woo M, Patel H, Metzger L, Selomulya C. Improvement of rheological and functional properties of milk protein concentrate by hydrodynamic cavitation. *J Food Eng.* (2018) 221:106–13. doi: 10.1016/j.jfoodeng.2017.10.005

21. Wang X, Feng T, Wang X, Zhang X, Xia S. Gelation and microstructural properties of fish myofibrillar protein gels with the incorporation of L-lysine and L-arginine at low ionic strength. *J Sci Food Agric.* (2021) 101:5469–77. doi: 10.1002/jsfa.11195

22. Shrivastaw K, Singh S, Sharma S, Sokhey J. Quantitation of protein content by biuret method during production of yellow fever vaccine. *Biologicals.* (1995) 23:299–300. doi: 10.1006/biol.1995.0048

23. Wu F, Shi X, Zou H, Zhang T, Dong X, Zhu R, et al. Effects of high-pressure homogenization on physicochemical, rheological and emulsifying properties of myofibrillar protein. *J Food Eng.* (2019) 263:272–9. doi: 10.1016/j.jfoodeng.2019.07.009

24. Sun Q, Zhang C, Li Q, Xia X, Kong B. Changes in functional properties of common carp (*Cyprinus carpio*) myofibrillar protein as affected by ultrasound-assisted freezing. *J Food Sci.* (2020) 85:2879–88. doi: 10.1111/1750-3841.15386

25. Jia N, Wang L, Shao J, Liu D, Kong B. Changes in the structural and gel properties of pork myofibrillar protein induced by catechin modification. *Meat Sci.* (2017) 127:45–50. doi: 10.1016/j.meatsci.2017.01.004

26. Li Z, Zheng Y, Sun Q, Wang J, Zheng B, Guo Z. Structural characteristics and emulsifying properties of myofibrillar protein-dextran conjugates induced by ultrasound Maillard reaction. *Ultrason Sonochem.* (2021) 72:105458. doi: 10.1016/j.ultsonch.2020.105458

27. Xu Y, Zhao Y, Wei Z, Zhang H, Dong M, Huang M, et al. Modification of myofibrillar protein via glycation: physicochemical characterization, rheological behavior and solubility property. *Food Hydrocoll.* (2020) 105:105852. doi: 10.1016/j.foodhyd.2020.105852

28. Gao T, Zhao X, Li R, Bassey A, Bai Y, Ye K, et al. Synergistic effects of polysaccharide addition-ultrasound treatment on the emulsified properties of low-salt myofibrillar protein. *Food Hydrocoll.* (2022) 123:107143. doi: 10.1016/j.foodhyd.2021.107143

29. Liu X, Sun X, Wei Y, Ma Y, Sun P, Li X. Effects of ultrasonic treatment on physicochemical properties and structure of tuna (*Thunnus tonggol*) myofibrillar proteins. *J Food Compos Anal.* (2022) 108:104438. doi: 10.1016/j.jfca.2022.104438

30. Pan J, Lian H, Jia H, Li S, Hao R, Wang Y, et al. Ultrasound treatment modified the functional mode of gallic acid on properties of fish myofibrillar protein. *Food Chem.* (2020) 320:126637. doi: 10.1016/j.foodchem.2020.126637

31. Jiang S, Zhang M, Liu H, Li Q, Xue D, Nian Y, et al. Ultrasound treatment can increase digestibility of myofibrillar protein of pork with modified atmosphere packaging. *Food Chem.* (2022) 377:131811. doi: 10.1016/j.foodchem.2021.131811

32. Zhang C, Liu H, Xia X, Sun F, Kong B. Effect of ultrasound-assisted immersion thawing on emulsifying and gelling properties of chicken myofibrillar protein. *LWT.* (2021) 142:111016. doi: 10.1016/j.lwt.2021.111016

33. Zhou Y, Yang H. Enhancing tilapia fish myosin solubility using proline in low ionic strength solution. *Food Chem.* (2020) 320:126665. doi: 10.1016/j.foodchem.2020.126665

34. Li X, Ma Y, Sun P, Liu H, Cai L, Li J. Effect of ultrasonic thawing on protein properties and muscle quality of Bonito. *J Food Process Preserv.* (2020) 45:e14930. doi: 10.1111/jfpp.14930

35. Xue S, Xu X, Shan H, Wang H, Yang J, Zhou G. Effects of high-intensity ultrasound, high-pressure processing, and high-pressure homogenization on the physicochemical and functional properties of myofibrillar proteins. *Innov Food Sci Emerg.* (2018) 45:354–60. doi: 10.1016/j.ifset.2017.12.007

36. Zhang Z, Yang Y, Zhou P, Zhang X, Wang J. Effects of high pressure modification on conformation and gelation properties of myofibrillar protein. *Food Chem.* (2017) 217:678–86. doi: 10.1016/j.foodchem.2016.09.040

37. Zhou L, Zhang J, Lorenzo J, Zhang W. Effects of ultrasound emulsification on the properties of pork myofibrillar protein-fat mixed gel. *Food Chem.* (2021) 345:128751. doi: 10.1016/j.foodchem.2020.128751

38. Ren Z, Chen Z, Zhang Y, Lin X, Li Z, Weng W, et al. Effect of heat-treated tea water-insoluble protein nanoparticles on the characteristics of Pickering emulsions. *LWT.* (2021) 149:111999. doi: 10.1016/j.lwt.2021.111999

39. Ren Z, Cui Y, Wang Y, Shi L, Yang S, Hao G, et al. Effect of ionic strength on the structural properties and emulsion characteristics of myofibrillar proteins from hairtail (*Trichiurus haumela*). *Food Res Int.* (2022) 157:111248. doi: 10.1016/j.foodres.2022.111248

40. Ren Z, Li Z, Chen Z, Zhang Y, Lin X, Weng W, et al. Characteristics and application of fish oil-in-water pickering emulsions structured with tea water-insoluble proteins/κ-carrageenan complexes. *Food Hydrocoll.* (2021) 114:106562. doi: 10.1016/j.foodhyd.2020.106562

41. Ma X, Yang D, Qiu W, Mei J, Xie J. Influence of multifrequency ultrasound-assisted freezing on the flavour attributes and myofibrillar protein characteristics of cultured large yellow croaker (*Larimichthys crocea*). *Front Nutr.* (2021) 8:779546. doi: 10.3389/fnut.2021.779546

42. Zhao X, Qi J, Fan C, Wang B, Yang C, Liu D. Ultrasound treatment enhanced the ability of the porcine myofibrillar protein to bind furan compounds: investigation of underlying mechanisms. *Food Chem.* (2022) 384:132472. doi: 10.1016/j.foodchem.2022.132472

43. Zhou Y, Hu M, Wang L. Effects of different curing methods on edible quality and myofibrillar protein characteristics of pork. *Food Chem.* (2022) 387:132872. doi: 10.1016/j.foodchem.2022.132872

44. Yu C, Wu F, Cha Y, Zou H, Bao J, Xu R, et al. Effects of high-pressure homogenization on functional properties and structure of mussel (*Mytilus edulis*) myofibrillar proteins. *Int J Biol Macromol.* (2018) 118:741–6. doi: 10.1016/j.ijbiomac.2018.06.134

frontiers | Frontiers in Nutrition

TYPE Original Research
PUBLISHED 16 February 2023
DOI 10.3389/fnut.2023.1116049

OPEN ACCESS

EDITED BY
Yan Zhao,
Chinese Academy of Agricultural Sciences, China

REVIEWED BY
Hao Dong,
Zhongkai University of Agriculture and Engineering, China
Tao Huang,
Ningbo University, China

*CORRESPONDENCE
Yisheng Xu
✉ yshxu@ecust.edu.cn
Yuan Qian
✉ qianyuan@sinap.ac.cn

†These authors have contributed equally to this work and share first authorship

SPECIALTY SECTION
This article was submitted to Food Chemistry, a section of the journal Frontiers in Nutrition

RECEIVED 05 December 2022
ACCEPTED 11 January 2023
PUBLISHED 16 February 2023

CITATION
Li S, Jiang D, Li J, Ma Y, Yao J, Du L, Xu Y and Qian Y (2023) Geographical traceability of gelatin in China using stable isotope ratio analysis. *Front. Nutr.* 10:1116049. doi: 10.3389/fnut.2023.1116049

Geographical traceability of gelatin in China using stable isotope ratio analysis

Shuang Li[1,2†], Di Jiang[2†], Jinglin Li[3], Yuhua Ma[3], Jian Yao[2], Lin Du[2], Yisheng Xu[1*] and Yuan Qian[2*]

[1]State Key Laboratory of Chemical Engineering, East China University of Science and Technology, Shanghai, China, [2]Department of Molten Salt Chemistry and Engineering, Shanghai Institute of Applied Physics, Chinese Academy of Sciences, Shanghai, China, [3]Department of Tritium Science and Engineering, Shanghai Institute of Applied Physics, Chinese Academy of Sciences, Shanghai, China

Geographical traceability is crucial to the quality and safety control of gelatin. However, currently, methods for gelatin traceability have not been established anywhere in the world. This study aimed to investigate the possibility of differentiating the geographical origins of gelatin from different regions in China using stable isotope technology. To achieve this objective, 47 bovine stick bone samples from three different regions (Inner Mongolia, Shandong, and Guangxi, respectively) in China were collected, and gelatin was extracted from these bones using the enzymatic method. The fingerprint characteristics of stable isotopes of $\delta^{13}C$, $\delta^{15}N$, and $\delta^{2}H$ of gelatin from different regions in China were studied. Moreover, isotopic changes from the bone to gelatin during the processing were examined to evaluate the effectiveness of these factors as origin indicators. The results of the one-way analysis of variance (ANOVA) showed that the $\delta^{13}C$, $\delta^{15}N$, and $\delta^{2}H$ of gelatin from different regions display significant differences, and using the linear discriminant analysis (LDA), the correct differentiation of origin reached 97.9%. Certain differences in stable isotope ratios were observed during the processing of bone to gelatin samples. Nonetheless, the fractionation effect caused by the processing of bone to gelatin samples was not sufficient to influence the identification of gelatin from different origins, which proves that $\delta^{13}C$, $\delta^{15}N$, and $\delta^{2}H$ are effective origin indicators of gelatin. In conclusion, the stable isotope ratio analysis combined with the chemometric analysis can be used as a reliable tool for identifying gelatin traceability.

KEYWORDS

stable isotope ratios, gelatin, geographical traceability, bone, processing

1. Introduction

Gelatin, a natural polymer extracted from the bones, skin, or connective tissue of animals, has been widely used in food, pharmaceuticals, cosmetics, and other industries due to its distinctive physicochemical property (1, 2). In recent years, a variety of gelatin safety incidents, such as animal epidemics, mislabeling, and adulteration, have occurred frequently, and consumers have increasingly focused on the origins of gelatin. Thus, laws and regulations were promulgated in many countries to regulate the sources of gelatin (3). However, related studies on the methods differentiating the origins of gelatin from different regions are limited at present. It is difficult for the government to ensure effective supervision of the source of gelatin, which not only greatly compromises public health and life safety but also highly restricts the development of the gelatin industry. Therefore, an effective method is urgently required to trace the geographical origins of gelatin.

Recently, various methods, such as stable isotope ratio analysis (4, 5), mineral element analysis (6), fatty acid analysis (7), near-infrared spectroscopy (NIRS) (8–10), high-performance liquid chromatography (HPLC) (11), mass spectroscopy (MS) (12), and DNA-based technology

(13, 14), have been applied to origin traceability and authentication of animal-derived products (15). However, these methods have a few shortcomings. For instance, the processing cost and experimental operation requirements of mineral element analysis are high. The sample pretreatment time for fatty acid analysis is prolonged, and is easily affected by feed, genetics, variety, and processing. The sensitivity of near-infrared spectroscopy is not high, and its data processing is difficult. HPLC has a limited capacity for qualitative determination and makes considerable use of hazardous solvents that are toxic to human health. The DNA-based technique requires numerous samples, and it is challenging to select effective molecular markers. At present, stable isotope ratio analysis is considered a more accurate and quicker method and has become the most commonly used technology for validating the traceability and authenticity of animal-derived foods. Geographical origins of some animal-derived products, such as meat, dairy products, seafood, and honey, were successfully traced using stable isotope ratio analysis (16–19). Meanwhile, research on the transformation law of stable isotopes from raw material to the terminal product during processing has also been carried out (20–22), which can further provide theoretical support for animal-derived product traceability.

Many studies on gelatin focused on species identification, and there are few related studies on traceability methods for gelatin are available at present. Jannat et al. successfully differentiated bovine, porcine, and fish sources of gelatin in commercially pure gelatin and gelatin-containing food and drug products using real-time polymerase chain reaction (PCR) and the analysis of mass spectrometry (MS)-based proteomic datasets (23). Sha et al. successfully identified fish gelatins in seven commercial cyprinid fishes using high-performance liquid chromatography (HPLC) and high-resolution mass spectrometry (HRMS) (24). Cai et al. presented a new strategy for the simultaneous rapid identification and quantification of gelatins from various species using ultrasound-assisted digestion-ultra-high performance liquid chromatography-tandem mass spectrometry (UPLC-MS/MS) (25). In our previous study, Jiang et al. successfully traced the origin of bone materials of gelatin in China using stable isotope analysis and mineral element analysis (26).

Based on the aforementioned studies, stable isotope ratio analysis coupled with chemometric analysis was first used to trace the geographical origin of gelatin in this study. The key aim of this study was to explore the regional differences in stable isotopes in gelatin from China and develop a reliable identification method. In addition, changes in $\delta^{13}C$, $\delta^{15}N$, and $\delta^{2}H$ from bone raw materials to gelatin during processing were also investigated to evaluate their effectiveness as geographical origin indicators. The results of the present study will provide a new idea and strategy for the origin traceability of gelatin.

2. Materials and methods

2.1. Sample information

A total of 47 bovine stick bone samples were sampled from three representative regions of China, including Mashan County of Guangxi Province (GX), Heze City of Shandong Province (SD), and Hulun Buir City of Inner Mongolia (NMG) (Table 1). Defatted bovine granules (d < 20 mm) were obtained using the conventional method (26) and then stored in a dryer.

TABLE 1 Region-wise information of bovine stick bone samples.

Region	Longitude and latitude	Sampling time	No.of samples
Mashan County of Guangxi Province (GX)	108°17′E, 23°72′N	November 2018	16
Hulun Buir City of Inner Mongolia (NMG)	115°31′-126°04′E, 47°05′-53°20′N	December 2018	15
Heze City of Shandong Province (SD)	114°45′-116°25′E, 34°39′-35°52′N	January 2019	16

GX, SD, and NMG are the abbreviations of Guangxi, Shandong, and Inner Mongolia, respectively.

2.2. Experimental methods

2.2.1. Bone gelatin extraction

Gelatin was extracted from defatted bovine granules using the enzymatic method (27), as shown in Figure 1. Defatted bovine granules were soaked in 1 M hydrochloric acid (HCl) (Sinopharm Chemical Reagent Co., Ltd., Shanghai, China) at 25°C for 3 h with continuous shaking at the solid-to-solvent ratio of 1:9 (w/v). The mixture was washed until a neutral or faintly basic mixture was obtained and dried at 65°C for 12 h to obtain defatted demineralized bovine granules. Then, the defatted demineralized bovine granules were mixed with pepsin at 40 U/g, deionized water (Millipore Milli-Q Advantage A10 Water Purification System, Millipore, USA) was added at the ratio of 1:9 (w/v) and adjusted to pH 2, and then the mixture was stirred for 3 h at 25°C. Subsequently, the mixture was washed with deionized water and adjusted to pH 5 to ensure that no pepsin remained in the mixture. Later, the pretreated bovine granules were mixed with deionized water at a ratio of 1:2 (w/v) and adjusted to pH 5 to extract the gelatin at 60°C for 3 h with continuous stirring; the gelatin extracted solution was obtained through centrifugation. Finally, the obtained solution was dried to 5 mL at 50°C in an oven (DHG-9140 A, Shanghai Huitai Instrument Manufacturing Co., Ltd., Shanghai, China) and vacuum freeze-dried (HXLG-10-50B, Shanghai Huxi Industrial Co., Ltd., Shanghai, China) for 3 days to obtain solid gelatin samples.

2.2.2. Characterization of bovine gelatin

2.2.2.1. Ultraviolet (UV) spectrum

Ultraviolet spectra of gelatin samples were obtained using a Hitachi U-3900 spectrophotometer (Hitachi Co., Ltd., China). Gelatin samples were dissolved in 0.5 M acetic acid to form a mixed solution at room temperature. The spectra were obtained at a resolution of 4 cm^{-1}, and the measurement range varied between 800 and 200 cm^{-1}.

2.2.2.2. Fourier transform infrared (FTIR) spectra

The FTIR spectrum (Bruker Optics TENSOR 27 FT-IR Spectrometer, Bruker Optics Inc., Billerica, MA, USA) of gelatin samples was recorded using the tablet method. Briefly, the bovine

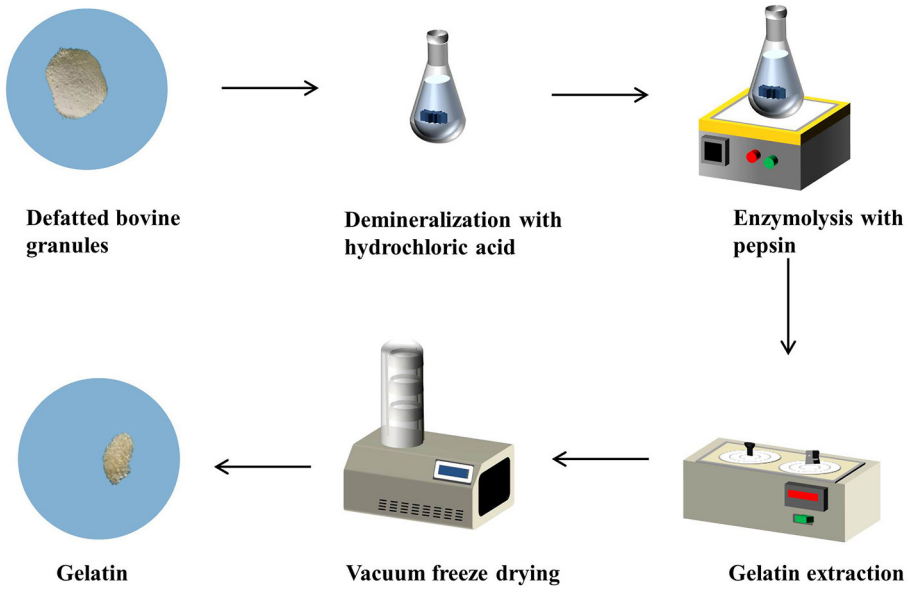

FIGURE 1
A flowsheet of gelatin extraction by the enzymatic method.

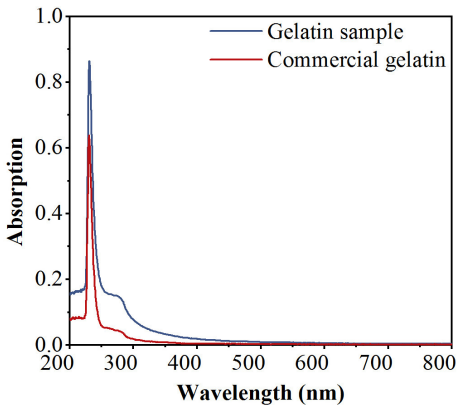

FIGURE 2
Ultraviolet (UV) spectra of the gelatin sample (GS) and commercial gelatin (CG).

gelatin samples were mixed and ground with potassium bromide (KBr) in the ratio of 1:100 to make a tablet; the spectra were obtained at a resolution of 4 cm^{-1} and the measurement range varied between 400 and 4,000 cm^{-1}. Automatic signals were collected in 32 scans at a resolution of 4 cm^{-1}.

2.2.3. Stable isotope ratio analysis

Stable isotope ratios were determined using an Elemental Analyzer (EA) (Flash 2000 HT, Thermo Fisher Scientific, USA) connected to an Isotope Ratio Mass Spectrometer (IRMS) (Delta V MAT 253, Thermo Fisher Scientific, USA). IAEA-600 ($\delta^{13}C = -27.771 \pm 0.043‰$ VPDB, $\delta^{15}N = 1.0 \pm 0.2‰$ air N_2), USGS24 ($\delta^{13}C_{VPDB} = -16.05 \pm 0.07‰$), USGS42 ($\delta^{15}N_{air} = 8.05 \pm 0.10‰$, $\delta^{2}H_{VSMOW} = -72.9 \pm 2.2‰$), and USGS43 ($\delta^{2}H_{VSMOW} = -44.4 \pm 2.0‰$) were performed to calibrate the stable isotope data.

For the $\delta^{13}C$ and $\delta^{15}N$ analysis, appropriate amounts of gelatin samples were weighed into tin capsules and placed into the EA using an autosampler. Carbon and nitrogen in the sample were converted into carbon dioxide (CO_2) and nitrogen gas (N_2) in an oxidation–reduction furnace at 980°C, and then, the gases were separated using the gas chromatography (GC) before being sent to the IRMS for analysis.

For the $\delta^{2}H$ analysis, appropriate amounts of gelatin samples were weighed into silver capsules and introduced into the EA using the autosampler. Hydrogen in the sample was converted into molecular hydrogen gas (H_2) in a pyrolysis furnace at 1,380°C, and then, the gases were separated using the GC before being sent to the IRMS for analysis.

Stable isotopic ratios ($^{13}C/^{12}C$, $^{15}N/^{14}N$, and $^{2}H/^{1}H$) were expressed in δ notation in parts per thousands (‰) and were calculated using the following equation:

$$\boldsymbol{\delta}\ ‰ = \frac{R_{sample} - R_{standard}}{R_{standard}} \times 1000, \quad (1)$$

where $\boldsymbol{R_{sample}}$ is the isotope ratio of the sample and $\boldsymbol{R_{standard}}$ is the isotope ratio of the international reference material.

2.3. Statistical analysis

The data were analyzed using SPSS 24.0. A *post-hoc* Duncan's test of a one-way analysis of variance (ANOVA) was performed to determine significant differences between the mean values of gelatin samples from different regions ($p < 0.05$) (28). A paired sample *t*-test and Pearson's correlation analysis were, respectively, used to analyze the variability and correlation in $\delta^{13}C$, $\delta^{15}N$, and

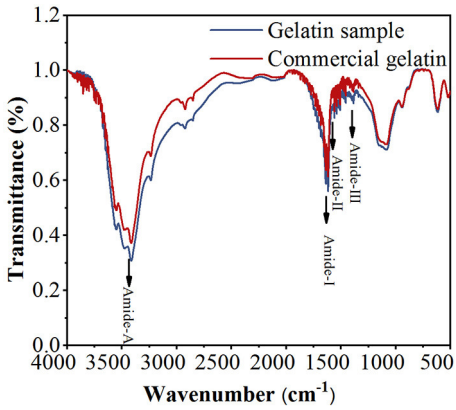

FIGURE 3
Fourier transform infrared (FTIR) spectra of the gelatin sample (GS) and commercial gelatin (CG).

δ^2H from bone to gelatin samples during processing to evaluate the effectiveness of these factors as geographical origin indicators ($p < 0.01$) (20, 29). The linear discriminant analysis (LDA) was used to establish a classification model, and its performance was assessed using cross-validation (30).

3. Results and discussion

3.1. UV spectra

The UV spectra of the gelatin sample (GS) and commercial gelatin (CG) (Shanghai Titan Technology Co., Ltd., Shanghai, China) are depicted in Figure 2. The GS is highly similar to the CG in the spectra. The absorption peak was recorded at 220–240 nm and was mostly associated with the presence of peptide bonds in the polypeptide chains of gelatin. Compared to CG, GS has a small hump at 270–280 nm, which may have been caused by a few aromatic residues, such as phenylalanine, tyrosine, and tryptophan (31). As the two substances show similar spectra, GS is likely to be gelatin.

3.2. FTIR spectra

The FTIR spectra were used to analyze the functional groups and secondary structure of gelatin. As shown in Figure 3, both GS and CG show four infrared (IR) peaks in their spectra, representing amide-A, amide-I, amide-II, and amide-III, respectively. The amide-A band is associated with the NH stretching vibration coupled with hydrogen bonding at the wavenumbers of 3,400–3,440 cm^{-1} (32). The amide-I band is assigned to the C=O stretching vibration coupled to contributions from the CN stretch, CCN deformation, and in-plane NH bending modes, ranging from 1,600 to 1,700 cm^{-1} (33). The amide-II band is attributed to the combination of the NH in-plane bend and the CN stretching vibration in the range of 1,500–1,560 cm^{-1} (34). The amide-III band appears at 1,200–1,300 cm^{-1}, due to CN stretching, NH in-plane bending, and wagging vibrations from the CH_2 groups (35). Amide-A, amide-I, amide-II, and amide-III of GS and CG are found at 3,415.76, 3,415.76, 1,617.23, 1,617.23, 1,559.37, 1,558.41, 1,384.82, 1,385.79 cm^{-1}, respectively. Amide-III of GS and CG is shifted to a higher wavenumber, indicating an increased random coil or disordered structure in gelatin (32). Similar peak locations appear for both GS and CG within the reasonable wavenumber range of these peaks, and the striking similarity of the GS and CG peak locations suggests that their secondary structures are similar. Combined with the UV spectra, it can be considered that the GS extracted from defatted bovine granules is gelatin.

TABLE 2 A comparison of the mean δ^{13}C, δ^{15}N, and δ^2H values and standard deviations of the gelatin samples from three regions.

Region	GX	NMG	SD
δ^{13}C (‰)	−12.27 ± 2.63a	−17.25 ± 4.04b	−13.27 ± 0.98a
δ^{15}N (‰)	6.52 ± 0.88a	6.38 ± 0.91a	4.20 ± 0.91b
δ^2H (‰)	−52.98 ± 3.90a	−84.19 ± 8.76c	−62.94 ± 3.97b

Different letters indicate significant differences at a p-value of < 0.05.

3.3. Stable isotope ratio analysis

Three stable isotope ratios (δ^{13}C, δ^{15}N, and δ^2H) and the distribution characteristics of gelatin samples from the three different regions in China are given in Table 2 and Figure 4. According to the results of the ANOVA and three-dimensional (3D) scatter plot of δ^{13}C, δ^{15}N, and δ^2H in the three regions, the stable isotope ratios are significantly different ($P < 0.05$) in gelatin samples from the regions.

The δ^{13}C of animal products is primarily related to animal feed, particularly the ratio of C_3 or C_4 plants (29). In this study, NMG has the lowest δ^{13}C (−17.25 ± 4.04‰) value in gelatin samples compared to GX (−12.27 ± 2.63‰) and SD (−13.27 ± 0.98‰). In a previous report, the δ^{13}C values of milk samples from Inner Mongolia were also significantly lower than those from Tianjin, Hebei, and Jiangsu (19). The two substances show a similar tendency. This may be because Inner Mongolia has large areas of C_3 pasture available as the primary fodder source. Another reason for the difference in δ^{13}C values between the two may be because of species differences. Guangxi is located in southwest China, which is suitable for C_3 and C_4 pasture growing. The cattle from Guangxi are mainly fed C_3 and C_4 pasture, but C_4 pasture is the dominant type. Shandong is located in Eastern China, where wheat and maize are the main products. In the majority of feed given to the cattle, there is a mixture of wheat and maize, with a high proportion of maize. Some studies showed that animals fed C_3 plants (e.g., wheat) have lower δ^{13}C in their tissues than those fed C_4 plants (e.g., maize) (36). Thus, the δ^{13}C values in gelatin samples from NMG are significantly lower than those in the other two regions.

The δ^{15}N in animal products is closely linked to the diet consumed by the animals and the regions of their habitat (37). In the present study, the δ^{15}N values in gelatin samples from SD (4.20 ± 0.91‰) are significantly lower than those in NMG (6.38 ± 0.91‰) and GX (6.52 ± 0.88‰). This may be due to the cattle from SD being mainly fed maize but the cattle from NMG and GX being mainly fed pasture. During the growing process, maize uses more chemical fertilizers, while pasture uses more organic fertilizers, which are then transferred to the cattle through feed. Compared to organic fertilizers, chemical fertilizers are depleted in δ^{15}N (38). Therefore, the δ^{15}N values of gelatin in SD are lower than those of the other two regions.

10.3389/fnut.2023.1116049

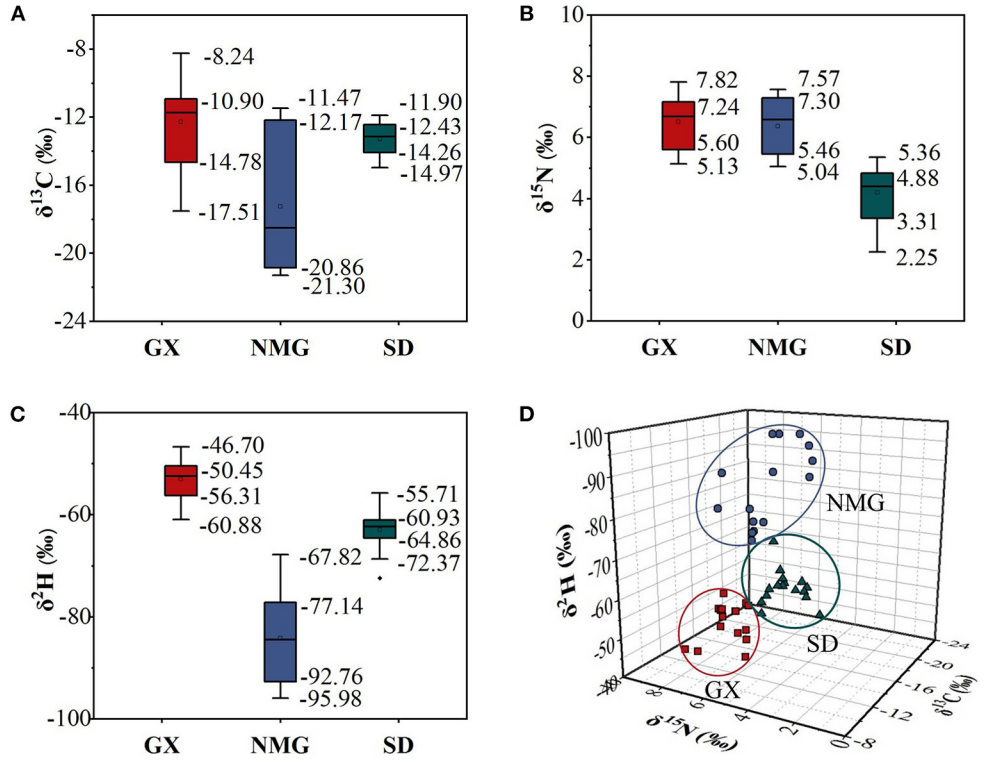

FIGURE 4
Boxplots of $\delta^{13}C$ **(A)**, $\delta^{15}N$ **(B)**, and $\delta^{2}H$ **(C)** values in gelatin samples from different regions. **(D)** Three-dimensional (3D) scatter plots of $\delta^{13}C$, $\delta^{15}N$, and $\delta^{2}H$ in three regions.

TABLE 3 A comparison of the mean $\delta^{13}C$, $\delta^{15}N$, and $\delta^{2}H$ values and standard deviations in gelatin samples and bone raw materials from different regions.

Sample		$\delta^{13}C$ (‰)	$\Delta^{13}C$	$\delta^{15}N$ (‰)	$\Delta^{15}N$	$\delta^{2}H$ (‰)	$\Delta^{2}H$
GX	Bone	−13.35 ± 2.54		6.08 ± 0.89		−61.09 ± 5.95	
	Gelatin	−12.27 ± 2.63	1.08	6.52 ± 0.88	0.44	−52.98 ± 3.90	8.11
NMG	Bone	−17.75 ± 3.71		5.96 ± 0.90		−82.86 ± 6.49	
	Gelatin	−17.25 ± 4.04	0.50	6.38 ± 0.91	0.42	−84.19 ± 8.76	−1.33
SD	Bone	−13.34 ± 0.94		3.60 ± 0.81		−72.87 ± 2.40	
	Gelatin	−13.27 ± 0.98	0.07	4.20 ± 0.91	0.60	−62.94 ± 3.97	9.93

The symbol Δ represents the difference in $\delta^{13}C$, $\delta^{15}N$, and $\delta^{2}H$ values between the gelatin samples and bone raw materials.

The $\delta^{2}H$ values of animal products are affected by drinking water and animal feed, which are related to latitude, altitude, and distance from the sea (28). In our study, the $\delta^{2}H$ values of gelatin are −84.19 ± 8.76‰ in NMG, −62.94 ± 3.97‰ in SD, and −52.98 ± 3.90‰ in GX, indicating a significant difference. Jiang et al. also found that the $\delta^{2}H$ values of bone samples from Inner Mongolia, Shandon, and Guangxi were in the order of NMG < SD < GX (26). Similar trends appear for both substances. This may be due to NMG having the highest altitude and GX having the lowest altitude among the three regions. The $\delta^{2}H$ values decrease with increasing latitude, altitude, and distance from the sea, so the $\delta^{2}H$ values are in the order of NMG < SD < GX.

A significant difference can be noticed in the $\delta^{13}C$, $\delta^{15}N$, and $\delta^{2}H$ values in gelatin samples from different regions. Therefore, $\delta^{13}C$, $\delta^{15}N$, and $\delta^{2}H$ can be good indicators for the traceability of gelatin.

3.4. Difference between gelatin and bone samples

All the data on bone samples are gathered from an article published by our research group (26). Table 3 shows the mean $\delta^{13}C$, $\delta^{15}N$, and $\delta^{2}H$ values and standard deviations in the gelatin samples and bone raw materials from different regions. In this study, the $\delta^{13}C$ values in gelatin samples are slightly higher than those in bone samples, indicating that $\delta^{13}C$ gets enriched during processing from bone to gelatin, which may be related to the acidification effect. The $\delta^{13}C$ values were lower when acidification eliminated the ^{13}C-enriched carbonate. The $\delta^{15}N$ values showed no significant variations. In a previous study, Tomaszewicz et al. found that acidification had a minimal effect on the $\delta^{13}C$ values, reducing marine turtle bone samples by <1‰, and acidification did not affect the $\delta^{15}N$ values of the

10.3389/fnut.2023.1116049

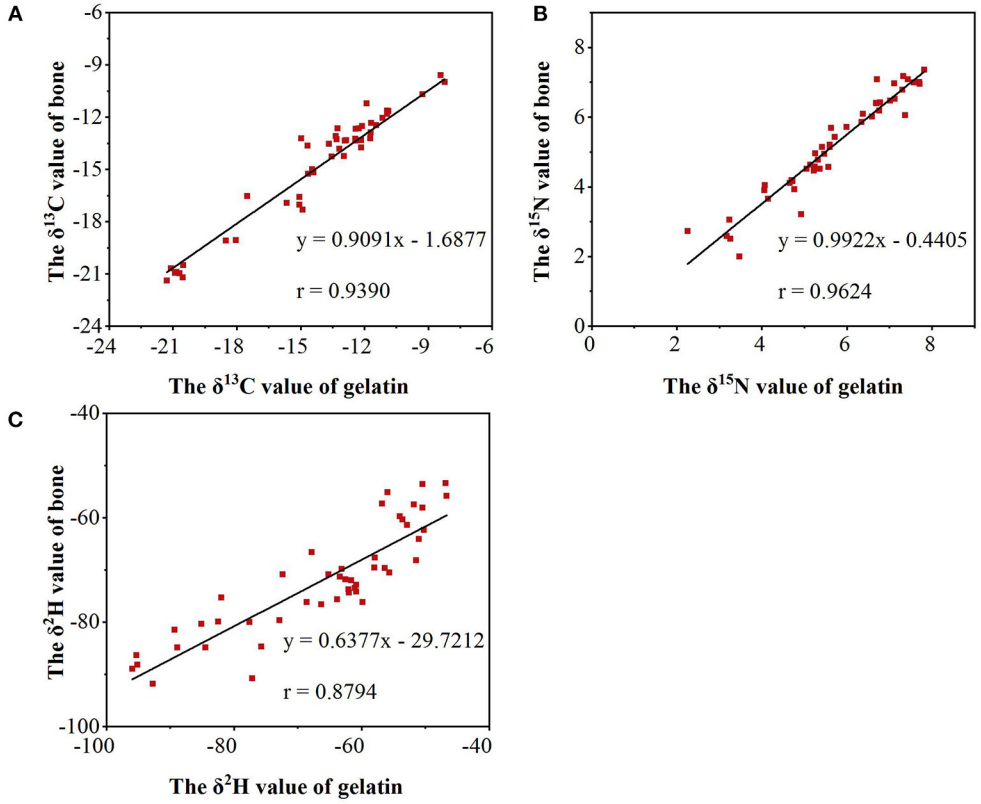

FIGURE 5
The correlation coefficients of $\delta^{13}C$ **(A)**, $\delta^{15}N$ **(B)**, and $\delta^{2}H$ **(C)** values between the gelatin samples and bone raw materials.

milled bone powder, which shows trends similar to the results of our study (39). The $\delta^{2}H$ values show significant differences, suggesting that the $\delta^{2}H$ values are significantly affected by processing. Because of the complexity of processing, this aspect needs to be further studied.

In summary, differences were found in $\delta^{13}C$, $\delta^{15}N$, and $\delta^{2}H$ values during the processing from bone to gelatin. However, compared with the differences in $\delta^{13}C$, $\delta^{15}N$, and $\delta^{2}H$ values of gelatin from different origins, the fractionation effect caused by processing is not sufficient to influence the identification of gelatin samples from different origins. Meanwhile, a significant correlation was observed among $\delta^{13}C$, $\delta^{15}N$, and $\delta^{2}H$ values between the gelatin and bone samples. As shown in Figure 5, the correlation coefficients of $\delta^{13}C$, $\delta^{15}N$, and $\delta^{2}H$ values between the gelatin samples and bone raw materials are 0.9390, 0.9624, and 0.8794, respectively ($P < 0.01$). Combined with Table 2, it indicates that $\delta^{13}C$, $\delta^{15}N$, and $\delta^{2}H$ can be used as good indicators for gelatin origin traceability.

3.5. Discriminant analysis

As single indicators, $\delta^{13}C$, $\delta^{15}N$, and $\delta^{2}H$ were not sufficient to identify gelatin samples from different origins; thus, the combination of these three indicators was used to improve the rate of correct classification. As shown in Table 4, the classification model was established using the LDA. Discrimination accuracies of the original classification and cross-validation of gelatin are 97.9 and 95.7%, respectively. Only a few samples from GX and NMG that are misclassified by origin are available. This misclassification may have occurred because the cattle fed on pasture from GX and NMG have a similar feed. These results indicate that the classification model could differentiate gelatin from different regions.

TABLE 4 Discriminant accuracies of the original classification and cross-validation of gelatin samples from different regions.

			Predicted group membership			
			GX	NMG	SD	Total
Original classification	Number	GX	16	0	0	16
		NMG	1	14	0	15
		SD	0	0	16	16
	%		100.0	93.3	100.0	97.9
Cross-validation	Number	GX	16	0	0	16
		NMG	1	14	0	15
		SD	1	0	15	16
	%		100.0	93.3	93.8	95.7

4. Conclusion

This study investigated the feasibility of using stable isotope ratio analysis combined with chemometric analysis to identify the origins of gelatin. The results show that stable isotopes ($\delta^{13}C$, $\delta^{15}N$, and $\delta^{2}H$) could be used as effective origin indicators for gelatin traceability, and the classification model also shows high discriminant ability. Therefore, stable isotope ratio analysis coupled with chemometric analysis can be used as an effective method for gelatin traceability. Furthermore, the results of this study may provide technical support for the quality and safety control of gelatin.

Data availability statement

The raw data supporting the conclusions of this article will be made available by the authors, without undue reservation.

Author contributions

SL: methodology, investigation, validation, and writing. DJ: methodology, formal analysis, reviewing, and editing. JL: software and formal analysis. YM, JY, and LD: formal analysis support. YX: supervision, reviewing, and editing. YQ: supervision, funding acquisition, review, and editing. All authors contributed to the article and approved the submitted version.

Funding

This study received funding from the Nuclear Energy Development Program Crop Varietal Improvement and Insect Pests Control by Nuclear Radiation of the State Administration of Science, Technology and Industry for National Defense (SASTIND), People's Republic of China (PRC).

Acknowledgments

The authors are grateful to Prof. Wei Liu (Shanghai Institute of Applied Physics, Chinese Academy of Sciences) for his support on the stable isotope analysis and Associate Prof. Bing Zhang (Technical Institute of Physics and Chemistry, Chinese Academy of Sciences) for her guidance on gelatin extraction.

Conflict of interest

The authors declare that the research was conducted in the absence of any commercial or financial relationships that could be construed as a potential conflict of interest.

Publisher's note

References

1. Djagny KB, Wang Z, Xu S. Gelatin: a valuable protein for food and pharmaceutical industries: review. *Crit Rev Food Sci Nutr.* (2001) 41:481–92. doi: 10.1080/20014091091904

2. Alipal J. Mohd Pu'ad NAS, Lee TC, Nayan NHM, Sahari N, Basri H, et al. A review of gelatin: properties, sources, process, applications, and commercialization. *Mater Today: Proc.* (2021) 42:240–50. doi: 10.1016/j.matpr.2020.12.922

3. Regenstein JM, Zhou P. "Collagen and gelatin from marine by-products," In: Shahidi F, editor. *Maximising the Value of Marine By-Products*. Sawston: Woodhead Publishing (2007). p. 279–303. doi: 10.1533/9781845692087.2.279

4. Zhao S, Liu H, Qie M, Zhang J, Tan L, Zhao Y. Stable isotope analysis for authenticity and traceability in food of animal origin. *Food Rev Int.* (2021). 1–21. doi: 10.1080/87559129.2021.2005087

5. Camin F, Perini M, Bontempo L, Galeotti M, Tibaldi E, Piasentier E. Stable isotope ratios of H, C, O, N and S for the geographical traceability of Italian rainbow trout (*Oncorhynchus mykiss*). *Food Chem.* (2018) 267:288–95. doi: 10.1016/j.foodchem.2017.06.017

6. Wang Q, Liu H, Zhao S, Qie M, Bai Y, Zhang J, et al. Discrimination of mutton from different sources (regions, feeding patterns and species) by mineral elements in Inner Mongolia, China. *Meat Sci.* (2021) 174:108415. doi: 10.1016/j.meatsci.2020.108415

7. Horcada A, López A, Polvillo O, Pino R. Cubiles-de-la-Vega D, Tejerina D, et al. Fatty acid profile as a tool to trace the origin of beef in pasture- and grain-fed young bulls of Retinta breed. *Span J Agric Res.* (2018) 15:1–11. doi: 10.5424/sjar/2017154-11032

8. Sun S, Guo B, Wei Y, Fan M. Classification of geographical origins and prediction of ^{13}C and ^{15}N values of lamb meat by near infared reflectance spectroscopy. *Food Chem.* (2012) 135:508–14. doi: 10.1016/j.foodchem.2012.05.004

9. Ghidini S, Varrà MO. Dall'Asta C, Badiani A, Ianieri A, Zanardi E. Rapid authentication of European sea bass (*Dicentrarchus labrax* L.) according to production method, farming system, and geographical origin by near infrared spectroscopy coupled with chemometrics. *Food Chem.* (2019) 280:321–7. doi: 10.1016/j.foodchem.2018.12.075

10. Varrà MO, Ghidini S, Ianieri A, Zanardi E. Near infrared spectral fingerprinting: A tool against origin-related fraud in the sector of processed anchovies. *Food Control.* (2021) 123:107778. doi: 10.1016/j.foodcont.2020.107778

11. Esteki M, Shahsavari Z, Simal-Gandara J. Food identification by high performance liquid chromatography fingerprinting and mathematical processing. *Food Res Int.* (2019) 122:303–17. doi: 10.1016/j.foodres.2019.04.025

12. Valletta M, Ragucci S, Landi N, Maro AD, Pedone PV, Russo R, et al. Mass spectrometry-based protein and peptide profiling for food frauds, traceability and authenticity assessment. *Food Chem.* (2021) 365:130456. doi: 10.1016/j.foodchem.2021.130456

13. Hu Y, Huang SY, Hanner R, Levin J, Lu X. Study of fish products in Metro Vancouver using DNA barcoding methods reveals fraudulent labeling. *Food Control.* (2018) 94:38–47. doi: 10.1016/j.foodcont.2018.06.023

14. Uncu AO, Uncu AT. A barcode-DNA analysis method for the identification of plant oil adulteration in milk and dairy products. *Food Chem.* (2020) 326:126986. doi: 10.1016/j.foodchem.2020.126986

15. Ye H, Yang J, Xiao G, Zhao Y, Li Z, Bai W. A comprehensive overview of emerging techniques and chemometrics for authenticity and traceability of animal-derived food. *Food Chem.* (2023) 402:134216. doi: 10.1016/j.foodchem.2022.134216

16. Nie J, Shao S, Xia W, Liu Z, Yu C, Li R, et al. Stable isotopes verify geographical origin of yak meat from Qinghai-Tibet plateau. *Meat Sci.* (2020) 165:108113. doi: 10.1016/j.meatsci.2020.108113

17. Zhao S, Zhao Y, Rogers KM, Chen G. Chen A, Yang S. Application of multi-element (C, N, H, O) stable isotope ratio analysis for the traceability of milk samples from China. *Food Chem.* (2020) 310:125826. doi: 10.1016/j.foodchem.2019.125826

18. Kang X, Zhao Y, Shang D, Zhai Y, Ning J, Ding H, et al. Identification of the geographical origins of sea cucumbers in China: the application of stable isotope ratios and compositions of C, N, O, and H. *Food Control.* (2020) 111:107036. doi: 10.1016/j.foodcont.2019.107036

19. Chen CT, Chen BY, Nai YS, Chang YM, Chen KH, Chen YW. Novel inspection of sugar residue and origin in honey based on the $^{13}C/^{12}C$ isotopic ratio and protein content. *J Food Drug Anal.* (2019) 27:175–83. doi: 10.1016/j.jfda.2018.08.004

20. Zhou J, Guo B, Wei Y, Zhang G, Wei S, Ma Y. The effect of different cooking processes on stable C, N, and H isotopic compositions of beef. *Food Chem.* (2015) 182:23–6. doi: 10.1016/j.foodchem.2015.02.116

21. Liu H, Wei Y, Wei S, Jiang T, Zhang S, Guo B. δ^2H of wheat and soil water in different growth stages and their application potentialities as fingerprints of geographical origin. *Food Chem.* (2017) 226:135–40. doi: 10.1016/j.foodchem.2017.01.029

22. Li H, Wu M, She S, Lin G, Zhou J. Chen L. Study on stable carbon isotope fractionation of rape honey from rape flowers (*Brassica napus L.*) to its unifloral ripe honey. *Food Chem.* (2022) 386:132754. doi: 10.1016/j.foodchem.2022.132754

23. Jannat B, Ghorbani K, Shafieyan H, Kouchaki S, Behfar A, Sadeghi N, et al. Gelatin speciation using real-time PCR and analysis of mass spectrometry-based proteomics datasets. *Food Control.* (2018) 87:79–87. doi: 10.1016/j.foodcont.2017.12.006

24. Sha X, Jiang W, Hu Z, Zhang L, Xie Z, Lu L, et al. Traceability and identification of fish gelatin from seven cyprinid fishes by high performance liquid chromatography and high-resolution mass spectrometry. *Food Chem.* (2023) 400:133961. doi: 10.1016/j.foodchem.2022.133961

25. Cai S, Jiang M, Zhao K, Huang X, Fei F, Cao B, et al. A quantitative strategy of ultrasound-assisted digestion combined UPLC-MS/MS for rapid identifying species-specific peptide markers in the application of food gelatin authentication. *Lwt-Food Sci Technol.* (2021) 147:111590. doi: 10.1016/j.lwt.2021.111590

26. Jiang D, Du L, Guo Y, Ma J, Li X, Han L, et al. Potential use of stable isotope and multi-element analyses for regional geographical traceability of bone raw materials for gelatin production. *Food Anal Method.* (2019) 13:762–9. doi: 10.1007/s12161-019-01687-1

27. Ma Y, Zeng X, Ma X, Yang R, Zhao W. A simple and eco-friendly method of gelatin production from bone: One-step biocatalysis. *J Clean Prod.* (2019) 209:916–26. doi: 10.1016/j.jclepro.2018.10.313

28. Zhaxi C, Zhao S, Zhang T, Dong H, Liu H, Zhao Y. Stable isotopes verify geographical origin of Tibetan chicken. *Food Chem.* (2021) 358:129893. doi: 10.1016/j.foodchem.2021.129893

29. Guo B, Wei Y, Pan J, Li Y. Stable C and N isotope ratio analysis for regional geographical traceability of cattle in China. *Food Chem.* (2010) 118:915–20. doi: 10.1016/j.foodchem.2008.09.062

30. Zhang X, Cheng J, Han D, Zhao X, Chen X, Liu Y. Geographical origin traceability and species identification of three scallops (*Patinopecten yessoensis*, *Chlamys farreri*, and *Argopecten irradians*) using stable isotope analysis. *Food Chem.* (2019) 299:125107. doi: 10.1016/j.foodchem.2019.125107

31. Chandra MV, Shamasundar BA. Rheological properties of gelatin prepared from the swim bladders of freshwater fish Catla catla. *Food Hydrocolloid.* (2015) 48:47–54. doi: 10.1016/j.foodhyd.2015.01.022

32. Sow LC, Yang H. Effects of salt and sugar addition on the physicochemical properties and nanostructure of fish gelatin. *Food Hydrocolloid.* (2015) 45:72–82. doi: 10.1016/j.foodhyd.2014.10.021

33. Ali AMMM, Kishimura H, Benjakul S. Physicochemical and molecular properties of gelatin from skin of golden carp (*Probarbus Jullieni*) as influenced by acid pretreatment and prior-ultrasonication. *Food Hydrocolloid.* (2018) 82:164–72. doi: 10.1016/j.foodhyd.2018.03.052

34. Benjakul S, Oungbho K, Visessanguan W, Thiansilakul Y, Roytrakul S. Characteristics of gelatin from the skins of bigeye snapper, *Priacanthus tayenus* and *Priacanthus macracanthus*. *Food Chem.* (2009) 116:445–51. doi: 10.1016/j.foodchem.2009.02.063

35. Ahmad T, Ismail A, Ahmad SA, Khalil KA, Awad EA, Leo TK, et al. Characterization of gelatin from bovine skin extracted using ultrasound subsequent to bromelain pretreatment. *Food Hydrocolloid.* (2018) 80:264–73. doi: 10.1016/j.foodhyd.2018.01.036

36. Bahar B, Monahan FJ, Moloney AP, O'Kiely P, Scrimgeour CM, Schmidt O. Alteration of the carbon and nitrogen stable isotope composition of beef by substitution of grass silage with maize silage. *Rapid Commun Mass Sp.* (2005) 19:1937–42. doi: 10.1002/rcm.2007

37. Sun S, Guo B, Wei Y. Origin assignment by multi-element stable isotopes of lamb tissues. *Food Chem.* (2016) 213:675–81. doi: 10.1016/j.foodchem.2016.07.013

38. Bateman AS, Kelly SD, Jickells TD. Nitrogen isotope relationships between crops and fertilizer: Implications for using nitrogen isotope analysis as an indicator of agricultural regime. *J Agric Food Chem.* (2005) 53:5760–5. doi: 10.1021/jf050374h

39. Tomaszewicz CNT, Seminoff JA, Ramirez MD, Kurle CM. Effects of demineralization on the stable isotope analysis of bone samples. *Rapid Commun Mass Sp.* (2015) 29:1879–88. doi: 10.1002/rcm.7295

frontiers | Frontiers in Nutrition

TYPE Original Research
PUBLISHED 23 February 2023
DOI 10.3389/fnut.2023.1129514

OPEN ACCESS

EDITED BY
Jinxuan Cao,
Beijing Technology and Business University, China

REVIEWED BY
Jin Guofeng,
Beijing Technology and Business University, China
Changyu Zhou,
Ningbo University, China

*CORRESPONDENCE
Xiao-Guang Gao
✉ gaoxiaoguang23@hotmail.com

SPECIALTY SECTION
This article was submitted to Food Chemistry, a section of the journal Frontiers in Nutrition

RECEIVED 22 December 2022
ACCEPTED 06 February 2023
PUBLISHED 23 February 2023

CITATION
Zhang S-S, Duan J-Y, Zhang T-T, Lv M and Gao X-G (2023) Effect of compound dietary fiber of soybean hulls on the gel properties of myofibrillar protein and its mechanism in recombinant meat products.
Front. Nutr. 10:1129514.
doi: 10.3389/fnut.2023.1129514

Effect of compound dietary fiber of soybean hulls on the gel properties of myofibrillar protein and its mechanism in recombinant meat products

Song-Shan Zhang[1], Jun-Ya Duan[2], Teng-Teng Zhang[2], Meng Lv[2] and Xiao-Guang Gao[2]*

[1]Institute of Animal Sciences, Chinese Academy of Agricultural Sciences, Beijing, China, [2]College of Food Science and Biology, Hebei University of Science and Technology, Shijiazhuang, Hebei, China

In this study, the compound dietary fiber composed of rice hull dietary fiber, soybean dietary fiber and inulin was added to meat products as a fat substitute. Response surface methodology was used to determine the optimum ratio of rice husk dietary fiber, soybean hull dietary fiber, and inulin as 1.40, 1.42, and 3.24%. The effects of compound and single dietary fiber on water holding capacity, gel strength, secondary structure, rheological properties, chemical action force, and microstructure of myofibrillar proteins (MP) gel were investigated. The application of composite dietary fiber significantly ($P < 0.05$) improved the gel strength, water holding capacity and storage modulus (G′) of MP gel. Fourier transform infrared spectrum analysis shows that the addition of compound dietary fiber can make the gel structure more stable. The effect of dietary fiber complex on the chemical action of MP gel was further studied, and it was found that hydrophobic interaction and disulfide bond could promote the formation of compound gel. By comparing the microstructure of the MP gel with and without dietary fiber, the results showed that the MP gel with compound dietary fiber had smaller pores and stronger structure. Therefore, the rice hull dietary fiber, the soybean hull dietary fiber and the inulin are compounded and added into the low-fat recombinant meat product in a proper proportion, so that the quality characteristics and the nutritional value of the low-fat recombinant meat product can be effectively improved, the rice hull dietary fiber has the potential of being used as a fat substitute, and a theoretical basis is provided for the development of the functional meat product.

KEYWORDS

compound dietary fibers, gel strength, water holding capacity, rheological properties, secondary structure, chemical force, microstructure

1. Introduction

Fat is a very important component in recombinant meat products, helping to maintain the original taste, texture and appearance of meat and increasing satiety during meals. Fats change the perception of taste compounds by affecting the balance, intensity and release of taste as well as their distribution and migration. However, excessive fat intake increases the

risk of obesity, certain cancers, and other diseases (1). In recent years, low-fat or non-fat meat products have become a hot research topic (2). But reducing fat in meat products can affect product appearance, flavor and texture (3). Many scholars have found that part of the fat can be replaced by non-meat components while offsetting the adverse effects of the low fat content due to its strong water holding capacity to (4). Studies have proved that dietary fiber can be used as a fat substitute with its excellent physical and chemical properties and functional characteristics (5).

The hulls of grains and beans contain a large amount of dietary fiber, which can cause a waste of resources if directly discarded (6, 7). At present, dietary fiber is mainly produced by physical methods (superfine grinding, high-pressure treatment, and extrusion), chemical methods (alkali method and acid method), and biological methods (fermentation method and enzyme method) (8, 9). Alkaline treatment is to use most of the impurities such as protein and starch can be dissolved in the alkali liquor, by controlling the appropriate reaction conditions to make dietary fiber. Studies have shown that alkali method can not only effectively produce dietary fiber, but also make part of the hemicellulose and cellulose hydrolysis modification into soluble dietary fiber. The cost of preparing dietary fiber by the alkali method is low, and the large-scale production is convenient to realize.

Inulin is derived from Jerusalem artichoke, onion and other plants, and is a natural water-soluble dietary fiber that can be added to meat products as a fat substitute (10). Generally, the gel-forming effect is good when the addition amount of inulin is more than 10 %, but excessive inulin can cause harm to the human body. Therefore, there is a need to maximize the quality of meat products while limiting the amount of inulin added. It is an effective solution to use multiple dietary fibers in combination to make them work synergistically. At present, there are few studies on the application of the combination of insoluble dietary fiber and soluble dietary fiber in meat products.

The quality of meat mainly depends on the properties of myofibrillar proteins (MP) (11). MP accounts for 55–60% of total muscle protein and 10–20% of skeletal muscle weight. It plays an important role in the water holding capacity, elastic properties and gel strength of meat products, and is an important structural protein affecting the quality of muscle food (12, 13). Therefore, the properties of MP were of great significance for studying the mechanism of meat products.

In this paper, the chaff and the soybean hull powder are treated by an alkali method to prepare the hull dietary fiber which is compounded with inulin, developing a low-fat recombinant meat product with high dietary fiber; by analyzing the effects of compound dietary fiber and single dietary fiber on protein components, gel properties, intermolecular chemical forces, the secondary structure and microstructure of protein of pork MP gel system, the interaction mechanism of compound dietary fiber and pork MP was explored in order to provide a theoretical basis for developing the application of dietary fiber in meat processing and improving the quality of low-fat recombinant meat products.

TABLE 1 Response surface experimental design.

Test number	A (Chaff dietary fiber)	B (Soybean hull dietary fiber)	C (Inulin)
1	1.00% (−1)	1.00% (−1)	3.34% (0)
2	2.00% (+1)	1.00% (−1)	3.34% (0)
3	1.00% (−1)	2.00% (+1)	3.34% (0)
4	2.00% (+1)	2.00% (+1)	3.34% (0)
5	1.00% (−1)	1.50% (0)	2.50% (−1)
6	2.00% (+1)	1.50% (0)	2.50% (−1)
7	1.00% (−1)	1.50% (0)	4.17% (+1)
8	2.00% (+1)	1.50% (0)	4.17% (+1)
9	1.50% (0)	1.00% (−1)	2.50% (−1)
10	1.50% (0)	2.00% (+1)	2.50% (−1)
11	1.50% (0)	1.00% (−1)	4.17% (+1)
12	1.50% (0)	1.00% (−1)	4.17% (+1)
13	1.50% (0)	1.50% (0)	3.34% (0)
14	1.50% (0)	1.50% (0)	3.34% (0)
15	1.50% (0)	1.50% (0)	3.34% (0)
16	1.50% (0)	1.50% (0)	3.34% (0)
17	1.50% (0)	1.50% (0)	3.34% (0)

2. Materials and methods

2.1. The dietary fiber from chaff by alkaline method

The chaff and soybean hull materials were cleaned from impurities and placed in a blast dryer (210 mm, Huawei Chemical Instruments, Wuhan, Hubei, China) and dry overnight. The two raw materials were crushed by a crusher (FSJ302-5, Taist, Tianjing, China) and sieved by a 60-mesh sieve to obtain raw material powder. Each treated raw material powder was individually vacuum packed in polyethylene bags and stored in a −20°C refrigerator (BCD-251WP3CX, Changhong Meiling, Hefei, Anhui, China) for use. A certain amount of raw material powder was accurately weighed, added with 20 g/L NaOH solution in the solid to liquid ratio of 1:15 (g:mL), and placed in a water bath (HH-4, Shengwei, Shanghai, China) at 60°C for extraction for 40 min. The mixed system was filtered and the filtrate was washed with water to neutral; the supernatant was precipitated by adding 4 times the volume of anhydrous ethanol for 6 h. The filter residues were obtained by centrifugation (HC-3018, Zhongke Zhongjia, Anhui, China) at 1,274 × *g*, and the pH was adjusted to neutral. The two filter residues were mixed and freeze-dried to produce dietary fiber.

2.2. Response surface methodology (RSM)

Response surface methodology (RSM) was used to determine the effect of the three independent variables, that is, the addition amount of chaff dietary fiber(A), the addition amount of soybean hull dietary fiber (B), and the addition amount of inulin (C).

Seventeen treatments were conducted based on the Box-Behnken design (BBD). Each run was done in triplicate. The designed response surface tests are presented in Table 1.

According to the preliminary experiment based on RSM, the optimum condition of the three dietary fibers was determined and was used in the following experiments, which was 1.40% chaff dietary fiber, 1.42% soybean hull dietary fiber, and 3.24% inulin, respectively.

2.3. Extraction of myofibrillar protein (MP)

Extraction of MP was carried out as described by Park et al. (14) with minor modifications. The longest muscle of pig back was thawed for 4 h at 4°C in advance, cleaned, and tidied, and the meat was cut into small pieces and weighed in a pre-cooled beaker. Buffer solution (containing 10 mmol/L Na_2HPO_4/NaH_2PO_4, 2 mmol/L $MgCl_2$, 1 mmol/L EGTA, 0.1 mmol/L NaCl, 7.0) was added in a volume ratio of 1: 4, and the mixture was stirred evenly with a glass rod (for about 1 min) and homogenized at high speed for 2 min. The connective tissue was filtered out with two layers of sterile gauze. The samples were centrifuged at 5,000 × g for 15 min at 4°C, and the precipitate was collected. Repeat the above procedure three times to obtain the precipitate as crude MP. The crude MP and 0.1 mmol/L NaCl solution were mixed in a volume ratio of 1:4, and centrifuged (H2050R, Xiangyi, Changsha, Hunan, China) (consistent with the centrifugal conditions during extraction) for three times. The obtained precipitate was purified MP, which was stored under seal at 4°C and used up within 48 h. The whole preparation process is carried out at 4°C. Bovine serum albumin was used as the standard, and the extracted MP concentration was determined by biuret method.

2.4. Sodium dodecyl sulfate–polyacrylamide gel electrophoresis (SDS–PAGE)

According to the method described by Lv et al. (15) with minor modifications, conduct sodium dodecyl sulfate polyacrylamide gel electrophoresis (SDS-PAGE) to observe protein cross-linking and polymerization, the extracted MP was diluted to a certain concentration with the loading buffer. And then cooled to room temperature after a water bath of 100°C for 10 min to produce the electrophoretic loading sample. The MP was analyzed by SDS-PAGE gel electrophoresis (WD-9413D, Liuyi, Beijing, China) and imaged in the gel imaging system.

2.5. Preparation of dietary fiber-MP composite gels

The MP was dissolved (0.6 mol/L NaCl,50 mmol/L NaH_2SO_4/Na_2HSO_4, pH 6.2) in the extract to adjust the protein concentration to 40 mg/mL. Different dietary fibers were added, respectively, homogenized at a low speed for 30 s by a homogenizer (FSH-2, Mengte, Changzhou, Jiangsu, China), and placed in a constant temperature water bath, which was gradually heated from room temperature to 75°C at a rate of 1°C/min and kept in the 75°C water bath for 10 min before being quickly removed and cooled in ice for 30 min, and finally stored overnight in a 4°C refrigerator for backup. All samples were equilibrated at room temperature for 30 min before testing.

According to the optimal proportion of the composite dietary fiber in the low-fat recombinant meat product obtained by the response surface method. Hull dietary fiber 1.40%, soybean hull dietary fiber 1.42%, inulin 3.24%, the experimental groups were divided into five groups: the control group (T0); added 6.06% chaff dietary fiber (T1); added 6.06% soybean hull dietary fiber (T2); added 6.06% inulin (T3); added 1.40% chaff dietary fiber +1.42% soybean hull dietary fiber +3.24 % inulin (T4).

2.6. Gel strength

According to the method described by Zhuang et al. (16) with minor modifications, the gel samples were cut into cylinders with a height of 2 cm, and the fracture strength and fracture distance were measured on a physical property analyzer (TA. XTPlus, Supertechnical, Fujian, China) using a spherical probe (P/5s). The fracture strength is the value corresponding to the first highest peak on the puncture curve, and the distance at which this peak is formed is the fracture distance. The gel strength value is the product of fracture strength and fracture distance. Specific parameters were set as follows: automatic trigger type, induced force of 5.0 g, and test speed of 1.0 mm/s. The maximum sustain force is that gel strength.

2.7. Water holding capacity (WHC)

A certain mass of gel sample (designated as W_1) was weighed, placed in a centrifuge tube (designated as W_0), and centrifuged at 10,000 × g for 15 min at 4°C, and weighed the final mass of the sample after centrifugation (17). Three parallel experiments were conducted for each group, and the sampling position as consistent as possible. The water holding capacity of composite gel was calculated according to Formula (1-1):

$$\mathrm{WHC} = \frac{w_2 - w_0}{w_1 - w_0} \times 100\% (1-1)$$

In the formula, W_0—centrifugal tube quality(g); W_1—quality before centrifugation(g); W_2—total mass of tube and sample after centrifugation (g).

2.8. Rheological measurements

According to the method described by Sun et al. (18) with minor modifications to determine the rheological properties (Viscotester iQ, Thermo Fisher Scientific Shier, Guangzhou, China) of the samples. Tests were performed in gradient warming oscillation mode using 50 mm plates. The samples were uniformly coated on the test platform. Before the test, the sample edges were sealed with silicone oil to keep closed. Then, the temperature was increased from 20 to 80°C at a rate of 1°C/min with a frequency of 0.1 Hz and a plate spacing of 0.6 mm.

2.9. Secondary structures

The gel samples were freeze-dried and pulverized, and KBr was added for milling. KBr sample tablets were prepared under the

pressure of 600 kg/cm^2 and scanned in the range of 4,000 cm^{-1}–500 cm^{-1} by using a Fourier transform infrared spectrometer (Nicolet6700, Thermo Fisher, USA) (19).

2.10. Determination of the intermolecular chemical forces

According to the method of Gómez-Guillén (20), weighing 2 g of the gel sample, adding 10 mL of S1 solution (0.05 mol/L NaCl, 10 ml), S2 solution (0.6 mol/L NaCl), S3 solution (0.6 mol/L NaCl + 1.5 mol/L urea), Solution S4 (0.6 mol/L NaCl + 8 mol/L urea), solution S5 (0.6 mol/L NaCl + 8 mol/L urea + 0.5 mol/L β- mercaptoethanol), homogenized at low speed for 2 min, placed in an environment at 4°C for 1 h, and centrifuged at 10,000 × *g* for 15 min at 4°C. The supernatant was collected, and the content of protein was determined by biuret method. The chemical acting force is calculated according to formulae 1-2)–1-5:

$$\text{Ionic bond} = \text{Protein content in S2 solution} - \text{protein content in S1 solution} (1-2)$$

$$\text{Hydrogen bond} = \text{Protein content in S3 solution} - \text{Protein content in S2 solution} (1-3)$$

$$\text{Hydrophobic interaction} = \text{Protein content in S4 solution} - \text{Protein content in S3 solution} (1-4)$$

$$\text{Disulfide bond} = \text{Protein content in S5 solution} - \text{Protein content in S4 solution} (1-5)$$

2.11. Scanning electron microscopy (SEM) of gel structures

According to the method described by Zhuang et al. (21) with minor modifications, the gel samples were cut into small cubes (5 mm × 5 mm × 5 mm) and fixed in 2.5% glutaraldehyde solution at 4°C for 1 day under protection from light. The 0.1 mol/L treated gel samples were washed three times with phosphate buffer (pH 7.4) for 10 min each. Dehydration was performed sequentially with a gradient of ethanol solution (60, 70, 80, 90, and 100%) for 15 min each time. The gel samples were immersed in isoamyl acetate for 15 min and repeated twice, and finally the samples were freeze-dried for 24 h, fixed with double-sided conductive adhesive and then sprayed with gold. The microstructure of the treated gel samples was observed using scanning electron microscopy (S-4800-I, HITACHI, Tokyo, Japan) at 2,500× and 4,000× magnification.

2.12. Statistical analyses

The experiment of each group was repeated three times, and the final result was expressed as means ± standard deviation. The optimum process conditions were obtained by software Design-Expert V8.0.6.1. The data was processed by SPSS 21.0 software. Analyze data for plotting with Origin 2019, Omnic and PeakFit.

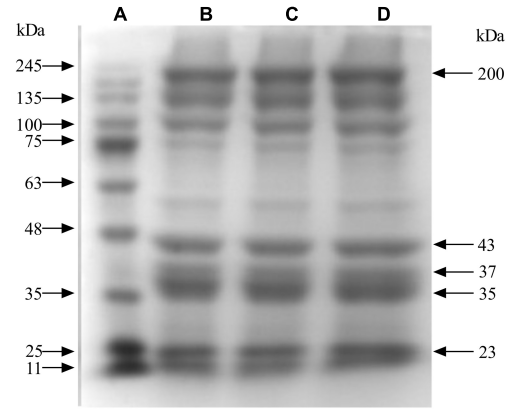

FIGURE 1
MP electrophoresis results. A is Marker; B, C, and D are MP.

3. Results and discussion

3.1. Component analysis of the MP

Myofibrillar protein is the protein of muscle myofibrils, which is composed of myosin, tropomyosin, myosin, and actin (22). According to the electrophoresis results in **Figure 1**, the MP extracted in this test contained the basic components of MP, such as myosin heavy chain (200 kDa), actin (43 kDa), troponin (37 kDa), tropomyosin (34–36 kDa), and myosin light chain (16–25 kDa). The bands in each group were clear and complete, and the results were basically the same as those reported by Li (23), indicating that the extracted MP could be used for subsequent studies.

3.2. Gel strength

Gel strength can reflect the gel-forming ability of protein, which is related to the gel network structure (24). The effect of different dietary fibers on the strength of MP gel is shown in **Figure 2**. Compared with the control T0 group, the gel strength was significantly increased in the T1 group added with chaff dietary fiber, the T2 group added with soybean hull dietary fiber, and the T4 group added with compound dietary fiber were increased significantly ($P < 0.05$). Based on the physicochemical properties of dietary fiber from gluten meal, it was speculated that the improvement of pork MP gel strength might be closely related to the strong water absorption and expansion of dietary fiber from gluten meal. During the thermal processing, the uniformly distributed dietary fibers are expanded and then filled into the MP gel network, resulting in the improvement of gel strength. Inulin has an effect on the gel strength of MP, which may be due to its own gel-forming property, making it possible to increase the number of gel molecules that can be formed per unit volume, strengthening the collision and cross-linking between dietary fiber and protein molecules, and the gel strength is improved (25). The adding effect of the composite dietary fiber is better than that of the single dietary fiber at the same concentration, probably due to the synergistic effect of the different types of dietary fiber on the MP gel, resulting in a significant increase in gel strength ($P < 0.05$).

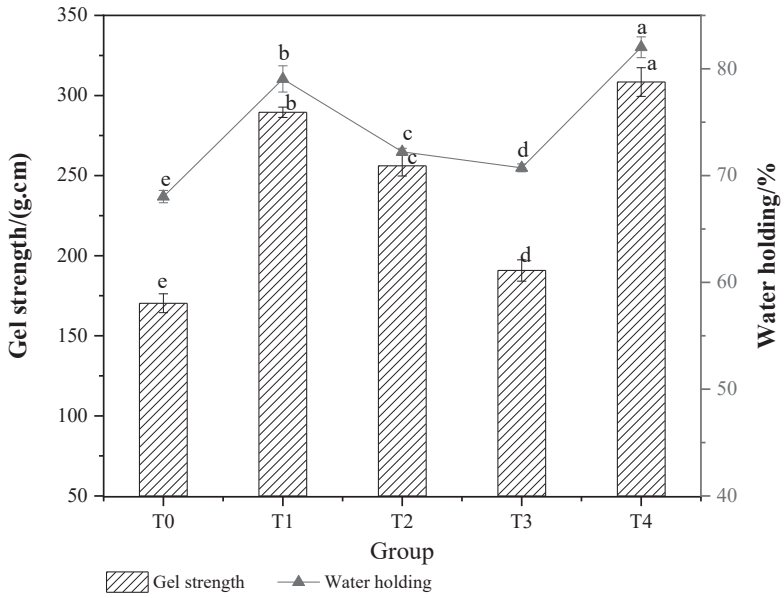

FIGURE 2
Effect of composite dietary fiber on MP gel strength and water retention. T0: control group; T1: 6.06% chaff dietary fiber; T2: 6.06% soybean hull dietary fiber; T3: 6.06% inulin; T4: 1.40% chaff dietary fiber +1.42% soybean hull dietary fiber +3.24% inulin; a–e: different letters indicated significant differences among the samples ($P < 0.05$).

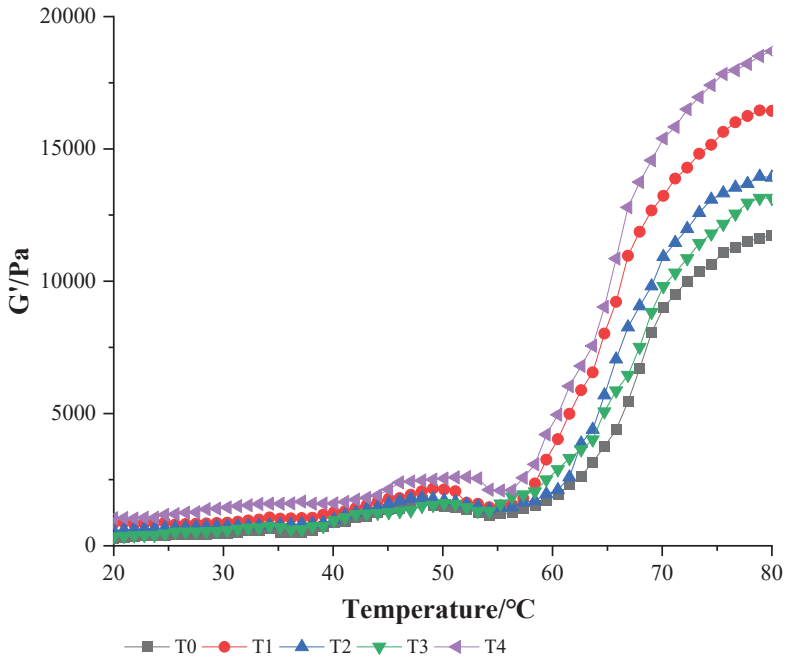

FIGURE 3
Effect of composite dietary fiber on rheological properties of MP gel. T0: control group; T1: 6.06% chaff dietary fiber; T2: 6.06% soybean hull dietary fiber; T3: 6.06% inulin; T4: 1.40% chaff dietary fiber +1.42% soybean hull dietary fiber +3.24% inulin.

3.3. WHC

The WHC of MP gel reflected the water binding capacity and gel degree of MP gel in the system, which had a very important effect on the quality of recombinant meat products (26). As shown in Figure 2, the WHC of the composite gel system was significantly ($P < 0.05$) improved with the addition of dietary fiber. The WHC of the T0 control group was (68.03 ± 0.58)%, and that of the T3 group added with inulin was (70.73 ± 0.36)%, which was 3.97 % higher than that of the T0 control group. This is because inulin can form a strong gel network structure with MP, blocking the free flow of water. The movement of the water molecules is constrained,

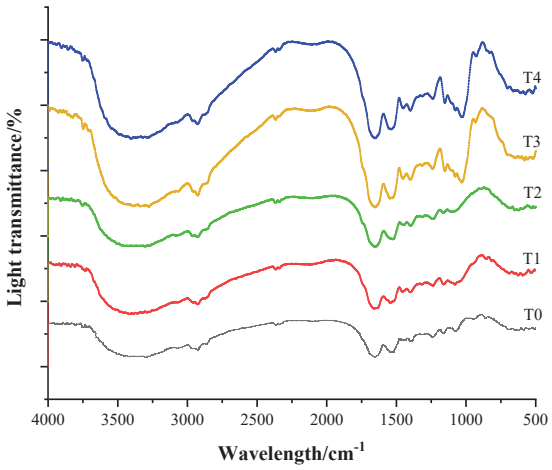

FIGURE 4
Infrared spectrum of composite dietary fiber-MP composite gel. T0: control group; T1: 6.06% chaff dietary fiber; T2: 6.06% soybean hull dietary fiber; T3: 6.06% inulin; T4: 1.40% chaff dietary fiber + 1.42% soybean hull dietary fiber + 3.24% inulin.

and the water contained in the water molecules is not easily separated from the MP even under the action of an external force. Therefore, the WHC of the gel is greatly improved. Compared with other groups, the WHC of T4 group with compound dietary fiber was the strongest, which was (82.02 ± 0.97)%, increased by 17.62% compared with the control T0 group. This indicated that the addition of compound dietary fiber could promote the cross-linking of MP during the heat-induced gel process and significantly improve the water binding capacity of the final gel structure (27).

3.4. Rheological property

Myofibrillar protein gel has unique viscoelasticity, and its physical and chemical properties can be reflected by rheology (28). The change of Storage modulus (G′) may reflect the expansion or aggregation of the protein with an increase in temperature, the process of forming an elastic gel network structure. A higher value of G′ indicates a stronger gel-forming ability of protein (19). As shown in **Figure 3**, the MP storage modulus G′ of dietary fiber increased when compared with that of the control group, and the storage modulus G′ of group T4 when dietary fiber was added was the largest. These results showed that compound dietary fiber could promote the formation of gel structure to the maximum extent. In the control group, the value of G′ gradually increased at 40–50°C, reached its peak at about 50°C and then gradually decreased, rising sharply at 55–80°C. This phenomenon reflected that the temperature began to rise and the protein gel network was initially formed. As the further increase of temperature, leading to the denaturation and recombination of protein molecules, the final stable protein gel is formed (29). The temperature at which the G′ value changed in the T4 group when dietary fiber was added was later than that in other groups, and it occurred at about 54°C. This might be because the three dietary fibers combined to produce a synergistic effect, fully absorbing water and swelling, blocking the development of protein molecules, leading to an increase in the denaturation temperature of protein. Wang et al. (30) believes that synergy between several different exogenous additives can significantly increase that G′ value of MP gel, resulting in higher gel strength, similar to the results of this test.

3.5. Changes of secondary structures

Fourier transform infrared spectrometer can selectively absorb infrared wavelengths and generate different characteristic absorption peaks according to the difference in the internal structure of the sample, so that the Fourier transform infrared spectrometer can be used for analyzing the change law of the secondary structure of the protein (31). **Figure 4** shows the infrared spectrum of the dietary fiber-MP composite gel. The amide I-band was located in the range of 1,700–1,600 cm^{-1}, and it characterized the C-O elastic vibration. The amide II band was located in the range of 1,600–1,500 cm^{-1}, and characterized by N–H bending vibration and C–N extensional vibration. The amide A-band, located in the range of 3,600–3,200 cm^{-1}, characterizes the O–H stretching vibration of water molecules, so it is also called "water zone" (32).

As shown in **Figure 4**, the infrared spectra of MP gel group added with dietary fiber were similar to those of T0 control group, indicating that the addition of dietary fiber would not change the protein skeleton structure. With the addition of dietary fiber, two new absorption peaks appeared in the infrared spectra of MP gel at 1,100–1,000 cm^{-1} and 3,700–3,600 cm^{-1}, and the peak intensity of the group added with compound dietary fiber increased the most. In addition, compared with the control group, the addition of dietary fiber enhanced the peak intensity at 2,933 and 1,531 cm^{-1}, and the wave number was slightly shifted.

The secondary structure of a protein is extremely sensitive to changes in the amide I band, so it can be used to analyze the

TABLE 2 Effect of composite dietary fiber on the secondary structure of MP gel.

Group	α-Helix	β-Fold	β-Rotation angle	Random coil
T0	41.68 ± 1.01^{a}	27.83 ± 0.40^{d}	17.29 ± 0.28^{ac}	13.20 ± 0.92^{a}
T1	34.24 ± 0.73^{b}	39.04 ± 0.19^{b}	18.51 ± 0.61^{ab}	8.21 ± 0.57^{c}
T2	35.42 ± 0.34^{b}	36.90 ± 0.47^{c}	17.41 ± 0.58^{bc}	10.27 ± 0.40^{b}
T3	31.84 ± 0.59^{c}	40.49 ± 0.46^{a}	16.68 ± 0.49^{c}	10.98 ± 0.13^{b}
T4	28.31 ± 0.54^{d}	40.97 ± 0.47^{a}	19.05 ± 0.71^{a}	11.67 ± 1.14^{ab}

T0: control group; T1: 6.06% chaff dietary fiber; T2: 6.06% soybean hull dietary fiber; T3: 6.06% inulin; T4: 1.40% chaff dietary fiber +1.42% soybean hull dietary fiber +3.24% inulin; Different letters in the same column indicated significant differences between the samples ($P < 0.05$).

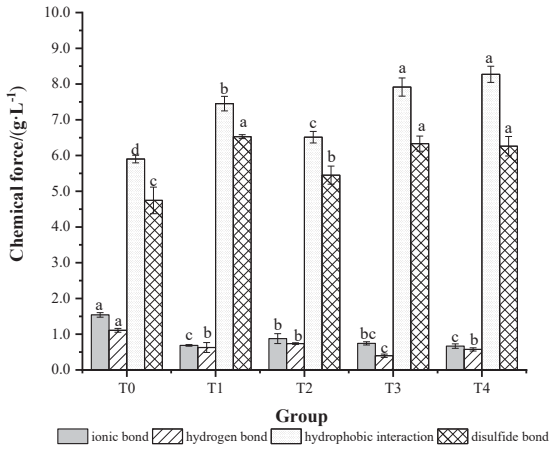

FIGURE 5
The effect of composite dietary fiber on the chemical force of MP gel. T0: control group; T1: 6.06% chaff dietary fiber; T2: 6.06% soybean hull dietary fiber; T3: 6.06% inulin; T4: 1.40% chaff dietary fiber + 1.42% soybean hull dietary fiber + 3.24% inulin. a–d: Different letters indicate that there are significant differences among the samples ($P < 0.05$).

secondary structure of a protein. The relationship between the secondary structure and the corresponding absorption peak was as follows: 1,650–1,660 cm^{-1} represented an α-helix structure, 1,600–1,640 cm^{-1} represented a β-fold structure, 1,660–1,695 cm^{-1} represented a β-turn and 1,640–1,650 cm^{-1} represented a random coil structure (33). The changes in the secondary structure of dietary fiber-MP composite gel are shown in Table 2. Compared with the MP gel of the control group, the α-helix and random coil contents of MP gel added with dietary fiber were decreased, while the β-sheet and β-corner contents were significantly increased. This indicates that the transformation from α-helix to β-fold and β-turn promotes the gelation of protein. In addition, in the α-helix content of MP gel decreased the most, while the β-sheet and β-corner contents increased the most in the compound dietary fiber group, which was conducive to the formation of a more stable gel structure of MP. This was consistent with the results reported by Liu (34). Therefore, the results of this study proved that the added of compound dietary fibers could effectively change the secondary structure of MP gel and enhance the gel-forming ability of protein, thereby improving the texture characteristics of recombinant meat products.

3.6. Determination of the intermolecular chemical forces

The process of MP gel formation is related to chemical forces such as ionic bonds, hydrophobic interactions, hydrogen bonds and disulfide bonds, which together lead to changes in the gel structure of the protein and thus affect the gel properties of the protein (35). The effect of dietary fiber on the chemical action of MP gel is shown in Figure 5. As shown in Figure 5, compared with the T0 control group, the ionic bonds and hydrogen bonds of the group added with dietary fiber were significantly reduced ($P < 0.05$). This may be due to the consumption of hydrogen bonds during

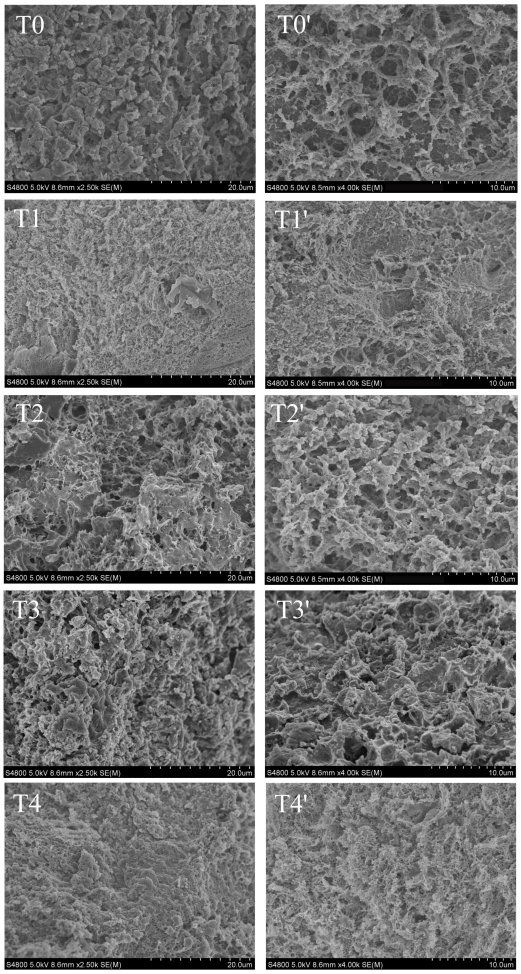

FIGURE 6
Effect of composite dietary fiber on the microstructure of MP gel. T0: control group; T1: 6.06% chaff dietary fiber; T2: 6.06% soybean hull dietary fiber; T3: 6.06% inulin; T4: 1.40% chaff dietary fiber + 1.42% soybean hull dietary fiber + 3.24% inulin. T0–T4: the sample is magnified by 2,500 times; T0′–T4′: the sample is magnified 4,000 times.

the transformation of the α-helix to β-fold during gel formation. The hydrophobic interaction and disulfide bond content were increased significantly ($P < 0.05$), suggesting that the hydrophobic interaction and disulfide bond could promote the formation of a more powerful and elastic three-dimensional network structure between protein molecules and promote the formation of gel (36). Compared with the T0 control group and the T1, T2, and T3 groups added with a single dietary fiber, the hydrophobic interaction and disulfide bond content of the T4 group added with the composite dietary fiber was higher, which indicates that there was a synergistic effect between the chaff dietary fiber, the soybean hull dietary fiber and inulin, which could improve the stability of the gel structure.

3.7. Scanning electron microscopy

The network structure of MP gel had an important effect on the texture properties and water holding capacity of recombinant meat products (37). As shown in Figure 6, compared with the

control group. The microstructure of pork MP gel added with dietary fiber was more compact, uniform and delicate. Compared with T0 control group, the gel structure of dietary fiber added is smaller, and the pores were decreased. Compared with the gel structure of the control group and the group added with the single dietary fiber, the structure is denser, the surface is smoother and the gap is smaller. This indicated that the protein structure formed by the combination of husk dietary fiber, soybean hull dietary fiber and inulin was superior to the protein gel structure of a single dietary fiber. The chaff dietary fiber and the soybean hull dietary fiber can play a filling role in the gel network. Inulin is uniformly dispersed in the gel structure without macropores. It can promote intermolecular covalent or non-covalent interactions, including disulfide bonds and hydrophobic interactions, can be promoted between protein-protein or protein-fibers. The inulin-MP mixed gel system formed a compact structure (38). The addition of inulin and dietary fiber from soybean hull into meat products could increase the total dietary fiber content and maintain the stability of the meat emulsion system. Therefore, the gel structure pores in the T1 and T2 groups were larger than those in the T4 group.

4. Conclusion

Response surface methodology was used to determine the optimum ratio of rice husk dietary fiber, soybean hull dietary fiber and inulin as 1.40, 1.42, and 3.24%. Compound dietary fibers can affect not only the network structure of MP gel, but also the chemical force between protein and change the gel characteristics. Compared with MP gel without dietary fiber and with single dietary fiber, the water holding capacity, gel strength and storage modulus G′ of the MP gel prepared with the compound dietary fibers added with chaff dietary fiber, soybean hull dietary fiber and inulin were significantly improved. Addition of complex dietary fibers promotes protein secondary structure in α- spiral direction β- fold and β- turn transformation, making the holes in the gel network smaller and the structure more uniformly dense. In addition, the addition of composite dietary fibers could reduce ionic and hydrogen bonds, increase hydrophobic interactions and disulfide bonds, and improve the stability of the gel structure.

In this study, it was found that the compound dietary fiber made of dietary fiber from chaff, dietary fiber from soybean hull and inulin affected the gel characteristics of pork MP, which was of great significance to improve the product quality. In the future, aiming at the changes in the tertiary structure of proteins, the mechanism of the effect of dietary fiber on low-fat recombinant meat products can be explored in depth, which will provide a theoretical support for the actual production.

Instrument summary

Blast dryer (210mm, Huawei Chemical Instruments, Wuhan, Hubei, China), crusher (FSJ302-5, Taist, Tianjing, China), refrigerator (BCD-251WP3CX, Changhong Meiling, Hefei, Anhui, China), water bath (HH-4, Shengwei, Shanghai, China), high-speed centrifuge (HC-3018, Zhongke Zhongjia, Anhui, China), high-speed freezing centrifuge (H2050R, Xiangyi, Changsha, Hunan, China), electrophoretic gel imaging system (WD-9413D, Liuyi, Beijing, China), homogenizer (FSH-2, Mengte, Changzhou, Jiangsu, China), physical property analyzer (TA. XTPlus, Supertechnical, Fujian, China), rheometer (Viscotester iQ, Thermo Fisher Scientific Shier, Guangzhou, China), fourier infrared spectrometer (Nicolet6700, Thermo Fisher, USA), scanning electron microscopy (S-4800-I, HITACHI, Tokyo, Japan).

Data availability statement

The original contributions presented in this study are included in the article/supplementary material, further inquiries can be directed to the corresponding author.

Author contributions

X-GG and S-SZ conceived, designed the experiments, and supervised the study. ML performed the experiments and contributed to data curation. J-YD and T-TZ edited and wrote the manuscript. All authors contributed to the article and approved the submitted version.

Funding

This work was supported by the Major Public Welfare Projects of Henan Province (No. 201300111200), the Agriculture Research System of China (No. CARS-37), Xinjiang Uygur Autonomous Region major scientific and technological projects, and Beef and Mutton Slaughter and Processing Key Technology Integration and Industrialization Demonstration (2021A02003-3).

Acknowledgments

We are grateful to the reviewers for their constructive comments on the manuscript.

Conflict of interest

The authors declare that the research was conducted in the absence of any commercial or financial relationships that could be construed as a potential conflict of interest.

Publisher's note

References

1. Cofrades S, Benedi J, Garcimartin A, Sanchez-Muniz F, Jimenez-Colmenero F. A comprehensive approach to formulation of seaweed-enriched meat products: from technological development to assessment of healthy properties. *Food Res Int.* (2017) 99:1084–94. doi: 10.1016/j.foodres.2016.06.029

2. Yessimbekov Z, Zinina O, Baryshnikova N, Tazeddinova D, Rebezov M, Okuskhanova E, et al. Stuart M. Enrichment of meat products with dietary fibers: a review. *Agron Res.* (2019) 4:1808–22. doi: 10.15159/ar.19.163

3. Han M, Clausen M, Christensen M, Vossen E, Van Hecke T, Bertram H. Enhancing the health potential of processed meat: the effect of chitosan or carboxymethyl cellulose enrichment on inherent microstructure, water mobility and oxidation in a meat-based food matrix. *Food Funct.* (2018) 7:4017–27. doi: 10.1039/c8fo00835c

4. Bis-Souza C, Henck J, Barretto A. Performance of low-fat beef burger with added soluble and insoluble dietary fibers. *Food Sci Technol.* (2018) 3:522–9. doi: 10.1590/fst.09217

5. Ma W, Yang Q, Fan X, Yao X, Kuang J, Min C, et al. Modification of myofibrillar protein gelation under oxidative stress using combined inulin and glutathione. *Food Chem X.* (2022) 14:100318. doi: 10.1016/j.fochx.2022.100318

6. Zhang X, Zhang M, Dong L, Jia X, Liu L, Ma Y, et al. Phytochemical profile, bioactivity, and prebiotic potential of bound phenolics released from rice bran dietary fiber during in vitro gastrointestinal digestion and colonic fermentation. *J Agric Food Chem.* (2019) 46:12796–805. doi: 10.1021/acs.jafc.9b06477

7. Dong J, Wang L, LÜc J, Y-Y Z, Shen R. Structural, antioxidant and adsorption properties of dietary fiber from foxtail millet (*Setaria italica*) bran. *J Sci Food Agric.* (2019) 99:3886–94. doi: 10.1002/jsfa.9611

8. Li S, Li J, Zhu Z, Cheng S, He J, Lamikanra O. Soluble dietary fiber and polyphenol complex in lotus root: preparation, interaction and identification. *Food Chem.* (2020) 14:126219. doi: 10.1016/j.foodchem.2020.126219

9. Zhang W, Zeng G, Pan Y, Chen W, Huang W, Chen H, et al. Properties of soluble dietary fiber-polysaccharide from papaya peel obtained through alkaline or ultrasound-assisted alkaline extraction. *Carbohydr Polym.* (2017) 172:102–12. doi: 10.1016/j.carbpol.2017.05.030

10. Kılınççeker O, Kurt S. Effects of inulin, carrot and cellulose fibres on the properties of raw and fried chicken meatballs. *South Afr J Anim Sci.* (2018) 48:39–47. doi: 10.4314/sajas.v48i1.5

11. Cao Y, Ma W, Huang J, Xiong Y. Effects of sodium pyrophosphate coupled with catechin on the oxidative stability and gelling properties of myofibrillar protein. *Food Hydrocoll.* (2020) 104:105722. doi: 10.1016/j.foodhyd.2020.105722

12. Xu Y, Xu X. Modification of myofibrillar protein functional properties prepared by various strategies: a comprehensive review. *Compr Rev Food Sci Food Saf.* (2021) 1:458–500. doi: 10.1111/1541-4337.12665

13. Cao Y, Li B, Fan X, Wang J, Zhu Z, Huang J, et al. Synergistic recovery and enhancement of gelling properties of oxidatively damaged myofibrillar protein by l-lysine and transglutaminase. *Food Chem.* (2021) 358:129860. doi: 10.1016/j.foodchem.2021.129860

14. Park D, Xiong Y. Oxidative modification of amino acids in porcine myofibrillar protein isolates exposed to three oxidizing systems. *Food Chem.* (2007) 2:607–16. doi: 10.1016/j.foodchem.2006.09.004

15. Lv Y, Chen L, Wu H, Xu X, Zhou G, Zhu B, et al. (-)-Epigallocatechin-3-gallate-mediated formation of myofibrillar protein emulsion gels under malondialdehyde-induced oxidative stress. *Food Chem.* (2019) 285:139–46. doi: 10.1016/j.foodchem.2019.01.147

16. Zhuang X, Jiang X, Zhou H, Han M, Liu Y, Bai Y, et al. The effect of insoluble dietary fiber on myofibrillar protein emulsion gels: oil particle size and protein network microstructure. *LWT.* (2019) 101:534–42. doi: 10.1016/j.lwt.2018.11.065

17. Jiang Y, Li D, Tu J, Zhong Y, Zhang D, Wang Z, et al. Mechanisms of change in gel water-holding capacity of myofibrillar proteins affected by lipid oxidation: the role of protein unfolding and cross-linking. *Food Chem.* (2021) 344:128587. doi: 10.1016/j.foodchem.2020.128587

18. Sun J, Yin G, Chen J, Li P. Gelling properties of myofibrillar protein–soy protein and k-carrageenan composite as affected by various salt levels. *Int J Food Prop.* (2019) 1:2047–56. doi: 10.1080/10942912.2019.1705482

19. Zhang Y, Zhang Q, Lu J, Xu J, Zhang H, Wang J. Physicochemical properties of Tremella fuciformis polysaccharide and its interactions with myofibrillar protein. *Bioact Carbohydr Diet Fibre.* (2017) 11:18–25. doi: 10.1016/j.bcdf.2017.06.002

20. Gómez-Guillén M, Borderìas A, Montero P. Chemical interactions of nonmuscle proteins in the network of sardine (*Sardina pilchardus*) muscle gels. *LWT Food Sci Technol.* (1997) 6:602–8. doi: 10.1006/fstl.1997.0239

21. Zhuang X, Han M, Bai Y, Liu Y, Xing L, Xu X. Insight into the mechanism of myofibrillar protein gel improved by insoluble dietary fiber. *Food Hydrocoll.* (2018) 74:219–26. doi: 10.1016/j.foodhyd.2017.08.015

22. Zhang Z, Xiong Z, Lu S, Walayat N, Hu C, Xiong H. Effects of oxidative modification on the functional, conformational and gelling properties of myofibrillar proteins from Culter alburnus. *Int J Biol Macromol.* (2020) 162:1442–52. doi: 10.1016/j.ijbiomac.2020.08.052

23. Li K, Liu J, Bai Y, Zhao Y, Zhang Y, Li J, et al. Effect of bamboo shoot dietary fiber on gel quality, thermal stability and secondary structure changes of pork salt-soluble proteins. *CyTA J Food.* (2019) 1:706–15. doi: 10.1080/19476337.2019.1641161

24. Zhuang X, Wang L, Jiang X, Chen Y, Zhou G. The effects of three polysaccharides on the gelation properties of myofibrillar protein: phase behaviour and moisture stability. *Meat Sci.* (2020) 170:108228. doi: 10.1016/j.meatsci.2020.108228

25. Zhang Y, Dong M, Zhang X, Hu Y, Han M, Xu X, et al. Effects of inulin on the gel properties and molecular structure of porcine myosin: a underlying mechanisms study. *Food Hydrocoll.* (2020) 108:105974. doi: 10.1016/j.foodhyd.2020.105974

26. Zhao Y, Zhou G, Zhang W. Effects of regenerated cellulose fiber on the characteristics of myofibrillar protein gels. *Carbohydr Polym.* (2019) 209:276–81. doi: 10.1016/j.carbpol.2019.01.042

27. Xu Y, Yan H, Xu W, Jia C, Peng Y, Zhuang X, et al. The effect of water-insoluble dietary fiber from star anise on water retention of minced meat gels. *Food Res Int.* (2022) 157:111425. doi: 10.1016/j.foodres.2022.111425

28. Wang Z, Sun Y, Dang Y, Cao J, Pan D, Guo Y, et al. Water-insoluble dietary fibers from oats enhance gel properties of duck myofibrillar proteins. *Food Chem.* (2021) 344:128690. doi: 10.1016/j.foodchem.2020.128690

29. Lv Y, Tang T, Xu L, Wang J, Su Y, Li J, et al. Influence of soybean dietary fiber with varying particle sizes and transglutaminase on soy protein isolate gel. *Food Res Int.* (2022) 161:111876. doi: 10.1016/j.foodres.2022.111876

30. Wang C, Jiang D, Sun Y, Gu Y, Ming Y, Zheng J, et al. Synergistic effects of UVA irradiation and phlorotannin extracts of Laminaria japonica on properties of grass carp myofibrillar protein gel. *J Sci Food Agric.* (2020) 7:2659–67. doi: 10.1002/jsfa.10890

31. Xiao Y, Li J, Liu Y, Peng F, Wang X, Wang C, et al. Gel properties and formation mechanism of soy protein isolate gels improved by wheat bran cellulose. *Food Chem.* (2020) 324:126876. doi: 10.1016/j.foodchem.2020.126876

32. Zhang Z, Liu P, Deng X, Guo X, Mao X, Guo X, et al. Effects of hydroxyl radical oxidation on myofibrillar protein and its susceptibility to μ-calpain proteolysis. *LWT.* (2021) 137:110453. doi: 10.1016/j.lwt.2020.110453

33. Liu R, Zhao S, Xie B, Xiong S. Contribution of protein conformation and intermolecular bonds to fish and pork gelation properties. *Food Hydrocoll.* (2011) 5:898–906. doi: 10.1016/j.foodhyd.2010.08.016

34. Liu J, Zhu K, Ye T, Wan S, Wang Y, Wang D, et al. Influence of konjac glucomannan on gelling properties and water state in egg white protein gel. *Food Res Int.* (2013) 2:437–43. doi: 10.1016/j.foodres.2013.01.002

35. Lv Y, Xu L, Su Y, Chang C, Gu L, Yang Y, et al. Effect of soybean protein isolate and egg white mixture on gelation of chicken myofibrillar proteins under salt/-free conditions. *LWT.* (2021) 149:111871. doi: 10.1016/j.lwt.2021.111871

36. Wang B, Kong B, Li F, Liu Q, Zhang H, Xia X. Changes in the thermal stability and structure of protein from porcine longissimus dorsi induced by different thawing methods. *Food Chem.* (2020) 316:126375. doi: 10.1016/j.foodchem.2020.126375

37. Zhuang X, Han M, Jiang X, Bai Y, Zhou H, Li C, et al. The effects of insoluble dietary fiber on myofibrillar protein gelation: microstructure and molecular conformations. *Food Chem.* (2019) 275:770–7. doi: 10.1016/j.foodchem.2018.09.141

38. Ullah I, Hu Y, You J, Yin T, Xiong S, Din ZU, et al. Influence of okara dietary fiber with varying particle sizes on gelling properties, water state and microstructure of tofu gel. *Food Hydrocoll.* (2019) 89:512–22. doi: 10.1016/j.foodhyd.2018.11.006

frontiers | Frontiers in Nutrition

TYPE Original Research
PUBLISHED 24 February 2023
DOI 10.3389/fnut.2023.1092573

OPEN ACCESS

EDITED BY
Jinxuan Cao,
Beijing Technology and Business University, China

REVIEWED BY
Wen-Liang Xiang,
Xihua University, China
Li Li,
Ocean University of China, China
Changle Qi,
Huzhou University, China

*CORRESPONDENCE
Yang-Fang Ye
✉ yeyangfang@nbu.edu.cn

SPECIALTY SECTION
This article was submitted to Food Chemistry, a section of the journal Frontiers in Nutrition

RECEIVED 08 November 2022
ACCEPTED 09 February 2023
PUBLISHED 24 February 2023

CITATION
Xiong T-H, Shi C, Mu C-K, Wang C-L and Ye Y-F (2023) Rise and metabolic roles of *Vibrio* during the fermentation of crab paste.
Front. Nutr. 10:1092573.
doi: 10.3389/fnut.2023.1092573

Rise and metabolic roles of *Vibrio* during the fermentation of crab paste

Tian-Han Xiong[1], Ce Shi[1], Chang-Kao Mu[1,2], Chun-Lin Wang[1] and Yang-Fang Ye[1]*

[1]School of Marine Sciences, Ningbo University, Ningbo, China, [2]Key Laboratory of Aquacultural Biotechnology, Ministry of Education, Ningbo University, Ningbo, China

Microbial community may systematically promote the development of fermentation process of foods. Traditional fermentation is a spontaneous natural process that determines a unique nutritional characteristic of crab paste of *Portunus trituberculatus*, However, rare information is available regarding the development pattern and metabolic role of bacterial community during the fermentation of crab paste. Here, using a 16S rRNA gene amplicon sequencing technology, we investigated dynamics of bacterial community and its relationship with metabolites during the fermentation of crab paste. The results showed that bacterial community changed dynamically with the fermentation of crab paste which highlighted by consistently decreased α-diversity and overwhelming dominance of *Vibrio* at the later days of fermentation. *Vibrio* had a positive correlation with trimethylamine, hypoxanthine, formate, and alanine while a negative correlation with inosine and adenosine diphosphate. In contrast, most of other bacterial indicators had a reverse correlation with these metabolites. Moreover, *Vibrio* presented an improved function potential in the formation of the significantly increased metabolites. These findings demonstrate that the inexorable rise of *Vibrio* not only drives the indicator OTUs turnover in the bacterial community but also has incriminated the quality of crab paste from fresh to perished.

KEYWORDS

crab paste, swimming crab, fermentation, *Vibrio*, bacterial community

1. Introduction

By giving the distinctive flavor and taste, traditional fermentation process has been conducted on a catalog of seafoods such as fish (1, 2), shrimp (3), and crab (4). On one hand, the physiologically active substances such as vitamins (3), amino acids (5), and organic acids (6) are produced during the fermentation of aquatic products. On the other hand, some undesirable substances such as hypoxanthine (Hx) and trimethylamine (TMA) could be simultaneously formed (7). Hx is the main cause of the bitter taste and unpleasant smell of aquatic products (8, 9) whereas TMA may induce cancer (10) and cardiovascular disease (11) if taken excessively. In this regard, fermented seafood quality is a hotspot for food safety, which play a vital role for human health.

Traditional fermentation of seafoods is a spontaneous natural process in which autolytic enzymes and microbes jointly develop a unique nutritional characteristic (12).

Among them, microbial community could be adaptive and metabolically diverse and may systematically promote the development of fermentation process (13). Particularly, some studies have explored the microbial metabolic functions in the production of volatile flavor compounds from shrimp paste (12) and fermented mandarin fish (14). Like Hx from adenosine triphosphate (ATP) (15), and TMA from trimethylamine N-oxide (TMAO) (16, 17). Therefore, comprehensively elucidating how the microbial community changes and its relationship with fermented substances over fermentation is fundamental for the seafood quality.

As a popular fermented aquatic product, crab paste is made by directly mixing fresh meat of the swimming crab, *Portunus trituberculatus*, with seasonings including salt, sugar, monosodium glutamate, and liquor (4). Twenty-eight metabolites such as amino acids, organic acids, and organic bases have been detected in crab paste based on our previous metabolomic work (7). Although some cultural bacteria such as *Staphylococcus*, *Arthrobacter*, and *Sphingobacterium* have been found in crab paste (18–21). Rare information is available regarding the succession of bacterial community in such an evolving, complex mixture of crab paste and its metabolic contribution to fermented substances, which might be important to the quality control of crab paste.

Therefore, in this study, a 16S rRNA gene amplicon sequencing technology was used to analyze the change of bacterial community structure across the fermentation of crab paste. Combining multivariate statistical analysis and PICRUSt2 functional prediction, we aimed to reveal the following: (1) the dynamics of α-diversity and composition of bacterial community with the fermentation of crab paste, (2) the relationships between bacterial taxa and fermented products of crab paste, (3) the functional potential of *Vibrio* in the formation of fermented products.

2. Materials and methods

2.1. Crab paste processing

Live seven swimming crabs (205.69 ± 17.25 g) were purchased from a crab aquafarm in Ningbo, China and anaesthetized on ice. Each crab was cleaned using tap water and cut into pieces immediately. For crab paste processing, the crab pieces were mixed with 4% sucrose, 2% salt, 1% monosodium glutamate, and 1% white liquor with 40% ethanol and were packaged in an airtight plastic bag for 7 days-fermentation at 4°C. The samples were respectively taken at 1, 3, 5, and 7 days of fermentation and the fresh crab samples were used as control. All samples were stored at −80°C for further analysis.

2.2. DNA extraction, 16S rRNA gene amplification, and illumina sequencing

Genomic DNA was extracted from 0.5 g of crab paste for each sample using the FastDNA Spin kit (MP Biomedicals, USA). The concentration and purity of DNA extracts were measured by a NanoDrop ND-1000 spectrophotometer. The V3–V4 region of 16S rRNA gene was amplified using the primer sets 341F (5′-CCTAYGGGRBGCASCAG-3′) and 806R (5′-GGACTACHVGGGTWTCTAAT-3′) with dual barcodes (21). To reduce the bias during amplification, PCR reactions were performed in triplicate for each sample. Following purification, assessment of fragment size, and quantification, PCR amplicons for each sample were aggregated in equimolar ratios and sequenced with the Illumina MiSeq platform (Illumina, USA) for generating paired end reads. Raw sequence data are available in the NCBI Sequence Read Archive under BigProject PRJNA808815.

2.3. Sequence processing

Paired-end reads were merged using FLASH (22). The merged sequences were quality filtered and processed using the QIIME2 pipeline (23). Following chimera detection using UCHIME (24), the remaining high-quality sequences without chimeras were sorted into the operational taxonomic units (OTUs) with a cutoff of 97% sequence similarity using UCLUST (25). To obtain the taxonomic information, the sequence with the highest abundance and coverage in each OTU was selected for assignment against the Greengenes database (release 13.8) using PyNAST (26). After removing the sequences which cannot be assigned to bacteria, a total of 3,288,164 clean reads (mean 93,948 reads per sample) were detected in the 35 crab paste samples. To avoid unequal sequencing depth, the OTU table was rarefied at 44,350 reads per sample for further analysis.

2.4. Statistical analysis

Shannon index, Richness, and phylogenetic diversity indices were calculated using QIIME. Pielou's evenness was calculated using the R package "vegan." Differences in α-diversity indices and bacterial populations were compared using the Kruskal-Wallis test in the "agricolae" package. A non-metric multidimensional scaling (NMDS) and a principal coordinate analysis (PCoA) were jointly used to visualize the differences in bacterial communities of crab paste between each fermentation time point, with three non-parametric multivariate analyses of dissimilarity based on Bray-Curtis distance using the "vegan" package, including MRPP, ANOSIM, and Adonis. To identify indicative bacteria that associated with fermentation time, the indicators at the OTU level were screened using the R "labdsv" package (27). The indicators of dominant bacteria at the OTU level (with average relative abundance > 0.01% in all samples) were screened with a significant difference between groups ($p < 0.05$) and indicator value (Indval) > 0.5 using the R package "labdsv." Spearman correlations between indicator OTUs and significantly changed metabolites (7) were calculated and visualized using the R "psych" and "pheatmap" packages, respectively.

To infer the functional potential of *Vibrio*, the OTU table of *Vibrio* was used for predicted 16S rRNA gene copy number by PICRUSt2 (Phylogenetic Investigation of Communities by Reconstruction of Observed States, v2.1.0-b) pipeline (28). Here, only genes involved in the metabolism pathways of significantly changed metabolites of crab paste were predicted. Functional

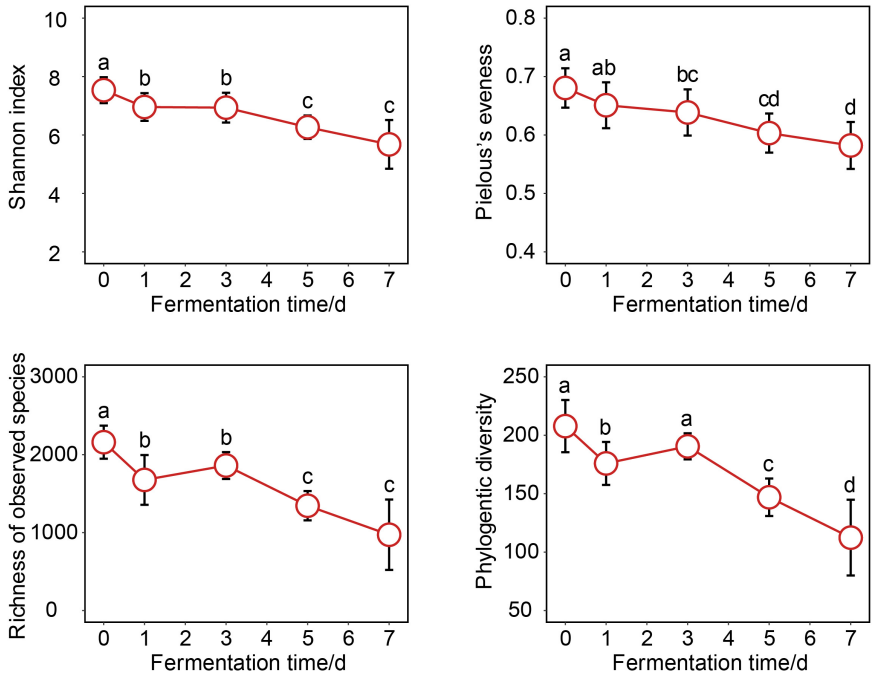

FIGURE 1
Changes of bacterial α-diversity indices over crab paste fermentation. Data present means ± standard deviation. Different letters indicate significant differences among groups ($p < 0.05$).

annotations of the genes were obtained according to the KEGG database.[1] Differences in functional genes were compared using the Kruskal-Wallis test in the "agricolae" package. All analyses and plots were completed in R 4.0.4 (R Foundation for Statistical Computing, Vienna, Austria).

3. Results

3.1. Change of bacterial community during fermentation

After the sequencing of 16S rRNA amplicons, a total of 3,288,164 high-quality sequences from 35 samples were obtained, with an average of 93,948 ± 21,784 reads per sample. Subsequent analysis was performed on a minimum of 44,350 reads per sample after normalization and homogenization.

To explore change in the bacterial community of crab paste during fermentation, changes of bacterial α-diversity indices were investigated. Bacterial α-diversity of crab paste was at the highest level before fermentation (at day 0), then decreased after fermentation (Figure 1). The Shannon index, richness of observed species, and phylogenetic diversity decreased sharply at the first day of fermentation ($p < 0.05$) while the Pielous's evenness index showed a significant drop from the third day of fermentation ($p < 0.05$). Although the bacterial α-diversity showed certain fluctuation at day 3, it finally reached the lowest level at the end of fermentation. Overall, bacterial α-diversity indices of crab paste were all reduced over fermentation time.

Next, we analyzed whether bacterial community composition of crab paste changed with fermentation time. We found that the bacterial community of crab paste presented a clear succession tendency along the first axis after fermentation if fresh crab samples were excluded (Figures 2A, B). Three non-parametric dissimilarity analyses including MRPP, ANOSIM, and Adonis showed a significant difference between fermentation time points ($p < 0.05$) except between day 0 and day 1 as well as between day 1 and day 3 (Table 1). These observations indicate that the main variation in the crab paste microbiota occurs at the later period of fermentation.

The changes in bacterial community composition of crab paste over fermentation time were detectable at the phylum/class level (Figure 2C). Seven dominant phyla/classes including Gammaproteobacteria, Bacteroides, Alphaproteobacteria, Actinobacteria, Tenericutes, Firmicutes, and Deltaproteobacteria all changed across time. Of note, the relative abundance of Gammaproteobacteria highly increased over fermentation time (Figure 2D). Among them, the relative abundance of Gammaproteobacteria continued to increase to the extreme dominance (71.9%) at day 7. In contrast, the relative abundances of Bacteroides, Alphaproteobacteria, and Deltaproteobacteria decreased over fermentation time (Supplementary Figure 1A). The bacterial changes in crab paste over fermentation time were also detectable at the genus level (Figure 2E). The average relative abundance of *Vibrio* markedly increased throughout the fermentation, reaching up to 48% at day 7 (Figure 2F). In contrast, the relative abundances of *Psychrobacter*, *Bizionia*, and *Roseovarius* significantly decreased over time (Supplementary Figure 1B).

1 http://www.genome.jp/kegg/

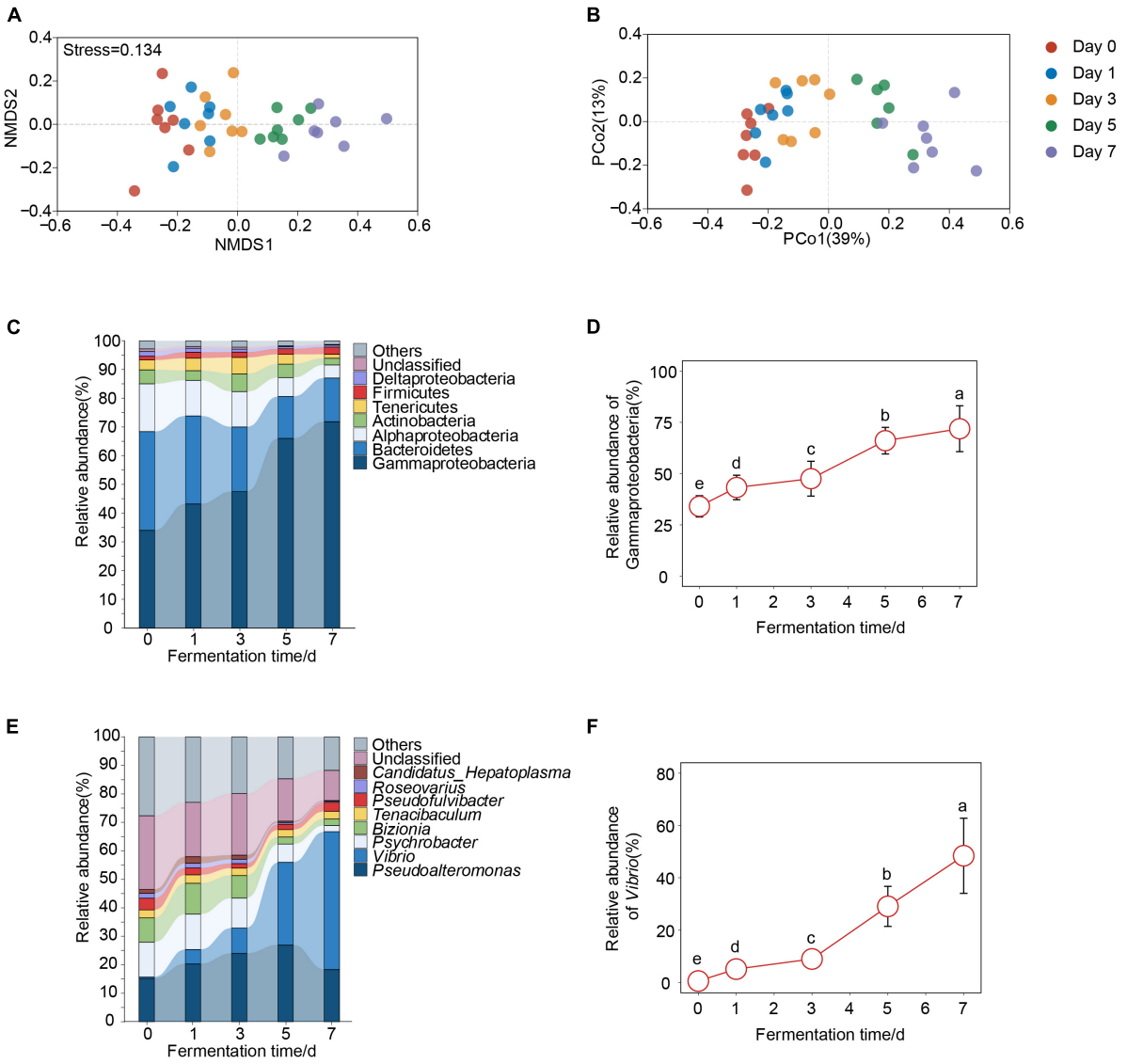

FIGURE 2
Changes of bacterial communities over crab paste fermentation. Non-metric multidimensional scaling (NMDS) plot **(A)** and principal coordinate analysis (PCoA) plot **(B)** based on Bray-Curtis dissimilarity visualizing compositional variations of bacterial communities of crab paste at day 0 (red), day 1 (blue), day 3 (orange), day 5 (green), and day 7 (purple). The relative abundances of bacterial communities at the phyla/proteobacterial classes **(C)** and genus **(E)** Level in crab paste during fermentation. Species with relative abundance < 1% were classified as "others". Significantly increased phyla/proteobacterial classes **(D)** and genera **(F)** over crab paste fermentation. Data present means ± standard deviation. Different letters indicate significant differences among groups ($p < 0.05$).

Taken together, these observations indicate a substantial rising of Gammaproteobacteria (mainly *Vibrio*) in the bacterial community of crab paste due to fermentation.

3.2. Indicator OTUs associated with fermentation time

The bacterial assemblages which characterized the discrete bacterial communities of crab paste due to fermentation were further examined. A total of 32 indicator OTUs were screened out at different fermentation time points (Figure 3). In detail, nearly half of the indicator OTUs were most abundant in the fresh crabs (at day 0), such as five OTUs belonging to Flavobacteriaceae (OTU 148, OTU 4657, OTU 6196, OTU 5946, and OTU 1499), three OTUs belonging to Gracilibacteria (OTU 194, OTU 455, and OTU 383), and two OTUs belonging to *Mesonia* (OTU 4231 and OTU 6680) (Figure 3A). As fermentation proceeded, indicators OTU 344 belonging to *Aequorivita viscosa* and OTU 338 belonging to *Halomonas* were most abundant in the crab paste at day 1 (Figure 3B). Further, only one indicator OTU 651 belonging to *Brachybacterium* presented the highest relative abundance at day 3 and one indicator OTU 329 belonging to *Vibrio* did at day 5 (Figure 3B). At day 7, 11 OTUs (OTU 35, OTU 28, OTU 26, OTU 24, OTU 7, OTU 140, OTU 14, OTU 275, OTU 77, OTU 8, and OTU 9) belonging to *Vibrio* dominated in the bacterial community of crab paste, accompanied by OTU 6592 belonging to Gammaproteobacteria (Figure 3A).

TABLE 1 Significance tests of the differences in bacterial communities of crab paste between fermentation time points.

Group	MRPP		ANOSIM		ADONIS	
	δ	*p*	*r*	*p*	*F*	*p*
Day 0-Day 1	0.007	0.277	0.062	0.253	1.373	0.190
Day 0-Day 3	0.067	0.003	0.370	0.003	3.005	0.003
Day 0-Day 5	0.227	0.003	0.909	0.004	10.130	0.004
Day 0-Day 7	0.275	0.003	0.983	0.003	13.670	0.003
Day 1-Day 3	0.007	0.277	0.050	0.288	1.271	0.201
Day 1-Day 5	0.175	0.003	0.873	0.003	7.420	0.003
Day 1-Day 7	0.245	0.003	0.983	0.003	11.630	0.003
Day 3-Day 5	0.101	0.003	0.510	0.003	4.234	0.003
Day 3-Day 7	0.216	0.003	0.934	0.003	9.713	0.003
Day 5-Day 7	0.077	0.014	0.381	0.009	3.312	0.016

MRPP, multiple response permutation procedure; ANOSIM, analysis of similarity; Adonis, permutational multivariate analysis of variance.

3.3. Relationships between indicator OTUs and metabolites

To understand how bacteria relate to metabolites during crab paste fermentation, we analyzed the relationships between indicator OTUs and significantly changed metabolites based on our previous metabolomic results (7). As expected, the heatmap shows a close correlation between bacteria and metabolites with red denoting positive correlation, whereas blue denoting negative correlation (Figure 4). Notably, almost all of indicator OTUs could be classified into two clusters according to the taxonomic information: cluster I (not *Vibrio*) and cluster II (*Vibrio*) except OTU6592 which could not be assigned to genus due to the limited 16S rRNA gene information. The cluster I was complex during the first three days of fermentation while cluster II tended to be simple and highlighted by one remarkable indicator OTU turnover since the fifth day of fermentation. Specifically, 12 *Vibrio* OTUs overwhelmingly dominated in cluster II with one OTU emerging at day 5. Moreover, the two clusters presented a complementary correlation with metabolites. In detail, most of OTUs in cluster I showed positive correlations with inosine, adenosine diphosphate (ADP), taurine, and 2-pyridinemethanol, whereas negative correlations with formate, Hx, and TMA. In contrast, most of OTUs in cluster II presented reverse correlations with metabolites which highlighted by positive correlations with alanine, formate, Hx, and TMA while negative correlations with lactate, inosine, ADP, taurine, trigonelline, and 2-pyridinemethanol. These observations indicate that the succession of bacterial community may play a vital role in the metabolite formation of crab paste during fermentation.

3.4. *Vibrio* function prediction analysis

Given the predominance of *Vibrio* in the bacterial community due to fermentation, large differences in functional profiles of the genus *Vibrio* between before and after fermentation were predicted by PICRUSt2. We found a significant increase in the abundances of nine predicted function genes of *Vibrio* ($p < 0.05$) (Table 2 and Figure 5), which were involved in the metabolic pathways of significantly changed metabolites of crab paste during fermentation (7). For example, the abundances of *torA* and *torZ* encoding trimethylamine-N-oxide reductase increased approximately 98-fold at day 7 compared to those at day 0. These results indicate

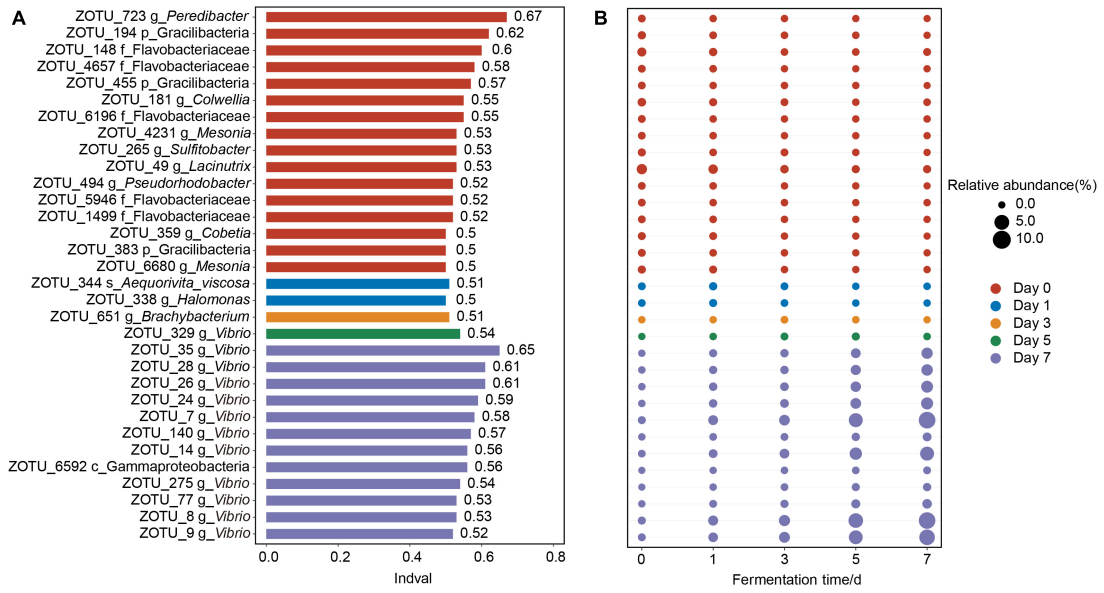

FIGURE 3
The 32 indicator operational taxonomic units (OTUs) values **(A)** and relative abundances **(B)** of crab paste at day 0 (red), day 1 (blue), day 3 (orange), day 5 (green), and day 7 (purple). The length of the bar in plot **(A)** represents Indval of one indicator OTU. The diameters of the circles in plot **(B)** are proportional to the relative abundances of the OTUs, with the red, blue, orange, green, and purple circles indicating the peak relative abundances at five fermentation time points, respectively.

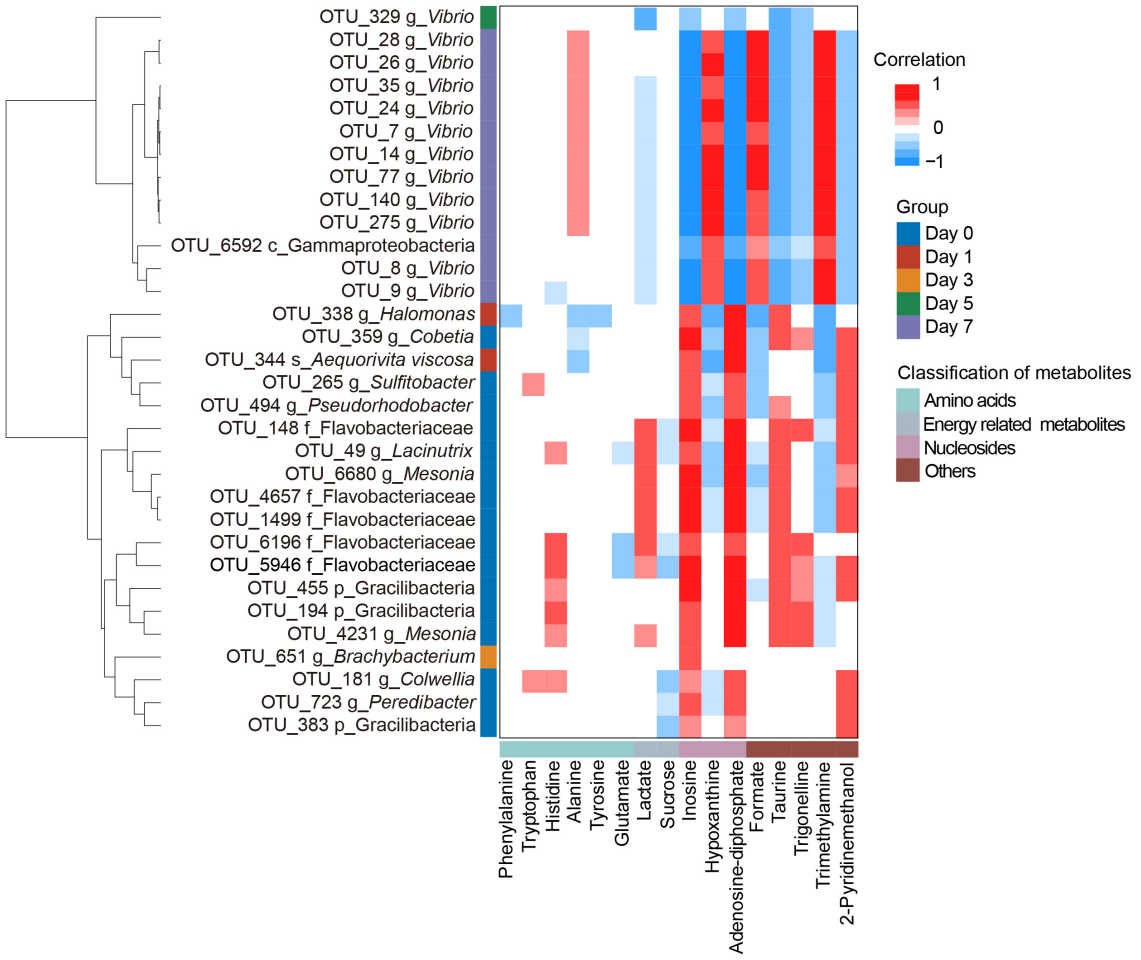

FIGURE 4
Clustering heatmap showing the Spearman's correlations between the indicative bacterial operational taxonomic units (OTUs) and the significantly changed metabolites, with red and blue indicating significant positive and negative correlations, respectively.

that *Vibrio* may play a critical role in the metabolite changes of crab paste during fermentation.

4. Discussion

Microorganisms impart crab paste a unique flavor and nutritional composition, but they may also lead to spoilage (18–20). Understanding the dynamic changes in the bacterial community may help in the quality control in seafood fermentation. Our microbial study across 7-day fermentation of crab paste allowed an in-depth look into the dynamics of a developing fermented seafood ecosystem. We observed a consistent decrease in bacterial α-diversity over fermentation (**Figure 1**). The decrease of bacterial α-diversity due to fermentation has been observed in fermented tempeh (29), kimchi (30), and fish (2). The reason why the great loss of bacterial α-diversity during fermentation may be the overabundance of Gamaproteobacteria which inexorably rising from the fifth day of fermentation (**Figures 2C, D**). Specifically, merely the relative abundance of Gamaproteobacteria (mainly *Vibrio*) continuously increased with fermentation which accompanied by a substantial decrease in the relative abundances of other phyla. Notably, only *Vibrio* became predominant in the later days of crab paste fermentation (**Figures 2E, F**, **3A, B**), which is consistent with the change characteristics of gut bacteria in the diseased swimming crab (31) and shrimp (32). *Vibrio* comprises about > 100 species (33). some *Vibrio* species such as *V. harveyi*, *V. alginolyticus*, and *V. parahaemolyticus* form pathogenic or symbiotic relationships with marine animals (34–37). This genus seemly had a robust competitive ability and physiological adaption in crab paste environment with high sugar, high salt, and high liquor contents. Such a characteristic change of bacterial community highlighted by an inexorable rise of *Vibrio* may drive the evolution of metabolomic profile of crab paste during fermentation as observed before (7).

Our correlation analysis and functional prediction can confirm this assertion. As we expected, the results of correlation analysis strongly support a vital role of *Vibrio* in the formation of TMA, Hx, formate, and alanine in the crab paste during fermentation (**Figure 4**). TMA is mainly responsible for the fishy odor and often associated with decomposition of aquatic animals, therefore this simple amine is regarded as well-known fish freshness index (38). An excessive intake of TMA will lead to a TMA poisoning (39) and it has been identified as a uremic toxin (40). TMA has been found

TABLE 2 The abundances of predicted functional genes in *Vibrio*.

KO	Group				
	Day 0	Day 1	Day 3	Day 5	Day 7
K00259	191.24 ± 68.72^{e}	1990.81 ± 813.89^{d}	3487.11 ± 1306.30^{c}	11221.26 ± 2888.51^{b}	18556.90 ± 5444.85^{a}
K09758	125.78 ± 46.89^{e}	1435.99 ± 608.33^{d}	2584.95 ± 947.47^{c}	8059.44 ± 2260.10^{b}	12935.29 ± 3749.88^{a}
K01081	239.46 ± 87.64^{e}	2429.31 ± 975.12^{d}	4317.18 ± 1607.31^{c}	14450.61 ± 3684.46^{b}	24546.12 ± 7115.68^{a}
K11751	253.56 ± 90.20^{e}	2852.81 ± 1216.23^{d}	4900.66 ± 1897.43^{c}	15194.42 ± 3800.12^{b}	24636.19 ± 7247.23^{a}
K03784	382.06 ± 137.09^{e}	3969.04 ± 1628.83^{d}	6943.80 ± 2613.25^{c}	22388.37 ± 5764.55^{b}	37102.81 ± 10889.60^{a}
K09913	189.82 ± 68.53^{e}	1987.66 ± 814.45^{d}	3487.11 ± 1306.30^{c}	11220.97 ± 2888.30^{b}	18556.76 ± 5444.73^{a}
K00656	268.77 ± 93.20^{e}	2932.22 ± 1239.96^{d}	5145.58 ± 1956.57^{c}	16189.7 ± 4127.10^{b}	26295.19 ± 7670.21^{a}
K07811	190.24 ± 68.23^{e}	1979.95 ± 814.39^{d}	3456.54 ± 1307.49^{c}	11166.83 ± 2876.03^{b}	18546.05 ± 5444.87^{a}
K07812	156.75 ± 56.79^{e}	1657.57 ± 689.89^{d}	2915.83 ± 1110.75^{c}	9391.07 ± 2307.23^{b}	15433.43 ± 4488.84^{a}

Different letters indicate significant differences among groups ($p < 0.05$).

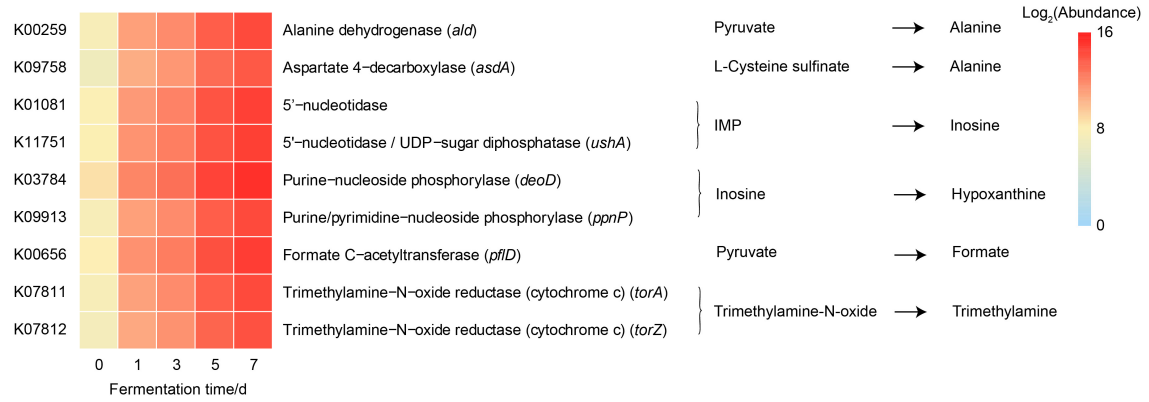

FIGURE 5
Heatmap showing the abundances of predicted function genes of *Vibrio* involved in the metabolic pathways of significantly changed metabolites of crab paste during fermentation. The data of gene abundances were log2 transformed.

to be a product of various types of bacteria such as *Escherichia*, *Shewanella*, *Photobacterium*, and *Vibrio via* the reduction of TMAO (16, 41–44). Of note, in this study, two genes K07811 (*torA*) and K07812 (*torZ*) encoding two isozymes of TMAO reductase (TorA and TorZ) were predicted in the genome of *Vibrio*. TMAO reductase is capable to reduce TMAO to TMA. Moreover, the abundances of these two genes were largely enhanced with the fermentation of crab paste (Figure 5). As such, we speculate that *Vibrio* contributes most to the TMA formation by TMAO reductase system and drives the spoilage of crab paste.

Moreover, *Vibrio* positively correlated to Hx but negatively correlated to ADP and inosine (Figure 4). These three compounds are intermediate metabolites in the pathway of ATP catabolism as observed in the postmortem muscle of the mud crab *Scylla paramamosain* (15, 45). Among them, inosine and Hx are two important determinants of various nucleotide freshness indicators such as *K* value, *Ki* value, and *H* value (46–48). It is generally believed that the breakdown from ATP to inosine monophosphate (IMP) results from autolysis enzyme action, while the further degradation of IMP to inosine and Hx probably results from microbial action (49). In this regard, the production of inosine and Hx may attribute to bacterial metabolism. Moreover, we predicted the genes including K01081 and *ushA* (K11751) which encoding 5′-nucleotidase/UDP-sugar diphosphatase involved in the conversion of IMP to inosine in *Vibrio*. We also predicted the genes including *deoD* (K03784) and *ppnP* (K09913) which encoding purine-nucleoside phosphorylase and purine-pyrimidine-nucleoside phosphorylase involved in the degradation of inosine to Hx in this genus. Notably, the abundances of these four genes were all highly elevated with the fermentation of crab paste (Figure 5). These observations strongly imply the crucial functional potentials of *Vibrio* in the ATP catabolism. Previous evidence supports this notion in which *Vibrio* can secrete extracellular hydrolases decomposing inosine to Hx (50). Given the importance of inosine and Hx in calculating the nucleotide indices, *Vibrio* is further inferred as an important driver in the spoilage of crab paste from the perspective of nucleotide freshness indicator.

In addition, our results suggest that *Vibrio* may contribute to the formate and alanine production in the crab paste (Figures 4, 5). This is in line with earlier observations in which formate and alanine can be produced from glucose and other carbohydrates under the action of *Vibrio* (51, 52). Although formate and alanine are not regarded as the freshness index of seafood, these observations indicate a more diverse metabolic potential of *Vibrio* during the fermentation of crab paste.

Collectively, these findings combined with our previous metabolomic findings demonstrate that the succession of bacterial community highlighted by the rise of *Vibrio* during the fermentation of crab paste could be Darwinism encouraging survival of the fittest by requiring extinction of the unfit. Such a change in microbial ecology indeed correlates with a changed metabolic activity of bacteria, which subsequently driving the quality switch from fresh to spoilt crab paste.

5. Conclusion

This study revealed a dynamic change of bacterial community with the fermentation of crab paste which highlighted by consistently decreased α-diversity and overwhelming dominance of *Vibrio* at the later days of fermentation. *Vibrio* had a positive correlation with TMA, Hx, formate, and alanine while a negative correlation with inosine and ADP. In contrast, most of other bacterial indicators had a reverse correlation with these metabolites. Moreover, *Vibrio* presented an improved function potential in the formation of the significantly increased metabolites. Collectively, these findings combined with our previous metabolomic findings demonstrate that the inexorable rise of *Vibrio* not only drives the indicator OTUs turnover in the bacterial community but also is implicated in the quality switch from fresh to spoilt crab paste. In fact, natural microbial fermentation can be a double-edged sword. How to control the microbial fermentation of seafood with great precision merits need to be studied in future.

Data availability statement

The original contributions presented in this study are publicly available. This data can be found here: https://www.ncbi.nlm.nih.gov/bioproject/PRJNA808815.

Ethics statement

The animal study was reviewed and approved by Animal Care and Use Committee of Ningbo University.

Author contributions

T-HX: conceptualization, validation, methodology, data curation, formal analysis, software, and writing—original draft. CS, C-KM, and C-LW: supervision and writing—review and editing. Y-FY: conceptualization, validation, methodology, data curation, formal analysis, funding acquisition, supervision, and writing—review and editing. All authors contributed to the article and approved the submitted version.

Funding

This research was supported by the Key Scientific and Technological Grant of Zhejiang for Breeding New Agricultural Varieties (2021C02069-6), 2025 Technological Innovation for Ningbo (2019B10010), China Agriculture Research System of MOF and MARA, and K. C. Wong Magna Fund in Ningbo University.

Conflict of interest

The authors declare that the research was conducted in the absence of any commercial or financial relationships that could be construed as a potential conflict of interest.

Publisher's note

All claims expressed in this article are solely those of the authors and do not necessarily represent those of their affiliated organizations, or those of the publisher, the editors and the reviewers. Any product that may be evaluated in this article, or claim that may be made by its manufacturer, is not guaranteed or endorsed by the publisher.

Supplementary material

The Supplementary Material for this article can be found online at: https://www.frontiersin.org/articles/10.3389/fnut.2023.1092573/full#supplementary-material

References

1. Yang Z, Liu S, Lv J, Sun Z, Xu W, Ji C, et al. Microbial succession and the changes of flavor and aroma in *Chouguiyu*, a traditional Chinese fermented fish. *Food Biosci.* (2020) 37:100725. doi: 10.1016/j.fbio.2020.100725

2. Li C, Zhao Y, Wang Y, Li L, Huang J, Yang X, et al. Contribution of microbial community to flavor formation in tilapia sausage during fermentation with *Pediococcus pentosaceus*. *LWT Food Sci Technol.* (2022) 154:112628. doi: 10.1016/j.lwt.2021.112628

3. Afifah D, Dewi U, Anggraeni R, Tsani A, Widyastuti N, Fulyani F, et al. Antioxidant activity, microbiological quality, and acceptability of spontaneously fermented shrimp sausage (*Litopenaeus vannamei*). *J Food Qual.* (2022) 2022:1–8. doi: 10.1155/2022/5553432

4. Ye Y, Zhang L, Tang H, Yan X. Survey of nutrients and quality assessment of crab paste by 1H NMR spectroscopy and multivariate data analysis. *Chin Sci Bull.* (2012) 57:3353–62. doi: 10.1007/s11434-012-5119-x

5. Kleekayai T, Pinitklang S, Laohakunjit N, Suntornsuk W. Volatile components and sensory characteristics of Thai traditional fermented shrimp pastes during fermentation periods. *J Food Sci Technol.* (2016) 53:1399–410. doi: 10.1007/s13197-015-2142-3

6. Shim K, Mok J, Jeong Y, Park K, Jang M. Effect of organic acids on the formation of biogenic amines in fermented anchovy sauce comprising raw anchovy materials with different levels of freshness. *J Food Sci Technol.* (2022) 59:703–14. doi: 10.1007/s13197-021-05065-w

7. Chen D, Ye Y, Chen J, Yan X. Evolution of metabolomics profile of crab paste during fermentation. *Food Chem.* (2016) 192:886–92. doi: 10.1016/j.foodchem.2015.07.098

8. Özogul F, Özden Ö, Özoğul Y, Erkan N. The effects of gamma-irradiation on the nucleotide degradation compounds in sea bass (*Dicentrarchus labrax*) stored in ice. *Food Chem.* (2010) 122:789–94. doi: 10.1016/j.foodchem.2010.03.054

9. Dervisevic M, Custiuc E, Çevik E, Durmus Z, Şenel M, Durmus A. Electrochemical biosensor based on REGO/Fe3O4 bionanocomposite interface for xanthine detection in fish sample. *Food Control.* (2015) 57:402–10. doi: 10.1016/j.foodcont.2015.05.001

10. Bulushi I, Poole S, Deeth H, Dykes G. Biogenic amines in fish: Roles in intoxication, spoilage, and nitrosamine formation—a review. *Crit Rev Food Sci Nutr.* (2009) 49:369–77. doi: 10.1080/10408390802067514

11. He S, Jiang H, Zhuo C, Jiang W. Trimethylamine/Trimethylamine-N-oxide as a key between diet and cardiovascular diseases. *Cardiovasc Toxicol.* (2021) 21:593–604. doi: 10.1007/s12012-021-09656-z

12. Lv X, Li Y, Cui T, Sun M, Bai F, Li X, et al. Bacterial community succession and volatile compound changes during fermentation of shrimp paste from Chinese Jinzhou region. *LWT Food Sci Technol.* (2020) 122:108998. doi: 10.1016/j.lwt.2019.108998

13. Bao R, Liu S, Ji C, Liang H, Yang S, Yan X, et al. Shortening fermentation period and quality improvement of fermented fish, *chouguiyu*, by co-inoculation of *Lactococcus lactis* M10 and *Weissella cibaria* M3. *Front Microbiol.* (2018) 9:3003. doi: 10.3389/fmicb.2018.03003

14. Shen Y, Wu Y, Wang Y, Li L, Li C, Zhao Y, et al. Contribution of autochthonous microbiota succession to flavor formation during Chinese fermented mandarin fish (*Siniperca chuatsi*). *Food Chem.* (2021) 348:129107. doi: 10.1016/j.foodchem.2021.129107

15. Lin W, He Y, Shi C, Mu C, Wang C, Li R, et al. ATP catabolism and bacterial succession in postmortem tissues of mud crab (*Scylla paramamosain*) and their roles in freshness. *Food Res Int.* (2022) 155:110992. doi: 10.1016/j.foodres.2022.110992

16. Dos Santos J, Iobbi-Nivol C, Couillault C, Giordano G, Méjean V. Molecular analysis of the trimethylamine N -oxide (TMAO) reductase respiratory system from a *Shewanella* species. *J Mol Biol.* (1998) 284:421–33. doi: 10.1006/jmbi.1998.2155

17. Kim K, Lee S, Chun B, Jeong S, Jeon C. *Tetragenococcus halophilus* MJ4 as a starter culture for repressing biogenic amine (cadaverine) formation during saeu-jeot (salted shrimp) fermentation. *Food Microbiol.* (2019) 82:465–73. doi: 10.1016/j.fm.2019.02.017

18. Ma C, Xu Z, Yang X. Studies on microbiological quality and safety characteristics of bottled crab paste in cold storage. *J Shanghai Fish Univ.* (2008) 2:222–6.

19. Zhang C, Chen Y, Quan J, Xu J, Su X, Zhang C, et al. Bacterial diversity of salted mudsnail and crab paste. *Food Sci.* (2011) 32:185–8.

20. Huang J, Chen Y, Quan J, Zhang C, Li Y, Qiu D, et al. Isolation of identification of cultivable microorganisms in bottled crab paste and salted mudsnail. *Food Sci.* (2011) 32:217–20.

21. Herlemann D, Labrenz M, Jürgens K, Bertilsson S, Waniek J, Andersson A. Transitions in bacterial communities along the 2000 km salinity gradient of the Baltic Sea. *ISME J.* (2011) 5:1571–9. doi: 10.1038/ismej.2011.41

22. Magoč T, Salzberg S. FLASH: Fast length adjustment of short reads to improve genome assemblies. *Bioinformatics.* (2011) 27:2957–63. doi: 10.1093/bioinformatics/btr507

23. Callahan B, McMurdie P, Rosen M, Han A, Johnson A, Holmes S. DADA2: High-resolution sample inference from Illumina amplicon data. *Nat Methods.* (2016) 13:581–3. doi: 10.1038/nmeth.3869

24. Edgar R, Haas B, Clemente J, Quince C, Knight R. UCHIME improves sensitivity and speed of chimera detection. *Bioinformatics* (2011) 27:2194–200. doi: 10.1093/bioinformatics/btr381

25. Edgar R. Search and clustering orders of magnitude faster than BLAST. *Bioinformatics.* (2010) 26:2460–1. doi: 10.1093/bioinformatics/btq461

26. DeSantis T, Hugenholtz P, Larsen N, Rojas M, Brodie E, Keller K, et al. Greengenes, a Chimera-Checked 16S rRNA gene database and workbench compatible with ARB. *Appl Environ Microbiol.* (2006) 72:5069–72. doi: 10.1128/AEM.03006-05

27. Dufrêne M, Legendre P. Species assemblages and indicator species: The need for a flexible asymmetrical approach. *Ecol Monogr.* (1997) 67:345–66. doi: 10.1890/0012-96151997067[0345:SAAIST]2.0.CO;2

28. Wang Y, Wang K, Huang L, Dong P, Wang S, Chen H, et al. Fine-scale succession patterns and assembly mechanisms of bacterial community of *Litopenaeus vannamei* larvae across the developmental cycle. *Microbiome* (2020) 8:106. doi: 10.1186/s40168-020-00879-w

29. Chen Y, Li P, He W, Liao L, Xia B, Jiang L, et al. Analysis of microbial community and the characterization of *Aspergillus flavus* in Liuyang *Douchi* during fermentation. *LWT Food Sci Technol.* (2022) 154:112567. doi: 10.1016/j.lwt.2021.112567

30. Yang Y, Fan Y, Li T, Yang Y, Zeng F, Wang H, et al. Microbial composition and correlation between microbiota and quality-related physiochemical characteristics in chongqing radish paocai. *Food Chem.* (2022) 369:130897. doi: 10.1016/j.foodchem.2021.130897

31. Xia M, Pei F, Mu C, Ye Y, Wang C. Disruption of bacterial balance in the gut of *Portunus trituberculatus* induced by *Vibrio alginolyticus* infection. *J Ocean Limnol.* (2018) 36:1891–8. doi: 10.1007/s00343-018-7121-x

32. Hou D, Zhou R, Zeng S, Wei D, Deng X, Xing C, et al. Intestine bacterial community composition of shrimp varies under low- and high-salinity culture conditions. *Front Microbiol.* (2020) 11:589164. doi: 10.3389/fmicb.2020.589164

33. Baker-Austin C, Oliver J, Alam M, Ali A, Waldor M, Qadri F, et al. *Vibrio* spp. infections. *Nat Rev Dis Primers.* (2018) 4:1–19. doi: 10.1038/s41572-018-0005-8

34. Liu Q, Li H, Wang Q, Liu P, Dai F, Li J. Identification and phylogenetic analysis of a strain of *Vibrio alginolyticus*, a pathogen in *Portunus trituberculatus* with toothpaste disease. *Mar Freshw Res.* (2007) 4:9–13.

35. Yildiz F, Visick K. *Vibrio* biofilms: So much the same yet so different. *Trends Microbiol.* (2009) 17:109–18. doi: 10.1016/j.tim.2008.12.004

36. Yan B, Qin G, Bao Z, Zhang X, Bi K, Qin L. Isolation and identification of *Vibrio parahaemolyticus* from diseased *Portunus trituberculatus* L. *Mar Sci Bull.* (2010) 29:560–6.

37. Zhang X, Bai X, Yan B, Bi K, Qin L. Vibrio harveyi as a causative agent of mass mortalities of megalopa in the seed production of swimming crab *Portunus trituberculatus*. *Aquacult Int.* (2014) 22:661–72. doi: 10.1007/s10499-013-9695-9

38. Prabhakar P, Vatsa S, Srivastav P, Pathak SS. A comprehensive review on freshness of fish and assessment: Analytical methods and recent innovations. *Food Res Int.* (2020) 133:109157. doi: 10.1016/j.foodres.2020.109157

39. Anthoni U, Christophersen C, Gram L, Nielsen N, Nielsen P. Poisonings from flesh of the Greenland shark *Somniosus microcephalus* may be due to trimethylamine. *Toxicon.* (1991) 29:1205–12. doi: 10.1016/0041-0101(91)90193-U

40. Duranton F, Cohen G, De Smet R, Rodriguez M, Jankowski J, Vanholder R, et al. Normal and pathologic concentrations of uremic toxins. *J Am Soc Nephrol.* (2012) 23:1258–70. doi: 10.1681/ASN.2011121175

41. Gram L, Huss H. Microbiological spoilage of fish and fish products. *Int J Food Microbiol.* (1996) 33:121–37. doi: 10.1016/0168-1605(96)01134-8

42. Santini C. A novel Sec-independent periplasmic protein translocation pathway in *Escherichia coli*. *EMBO J.* (1998) 17:101–12. doi: 10.1093/emboj/17.1.101

43. Dunn A, Stabb E. Genetic analysis of Trimethylamine *N* -Oxide reductases in the light organ symbiont *Vibrio fischeri* ES114. *J Bacteriol.* (2008) 190:5814–23. doi: 10.1128/JB.00227-08

44. Proctor L, Gunsalus R. Anaerobic respiratory growth of *Vibrio harveyi*, *Vibrio fischeri* and *Photobacterium leiognathi* with trimethylamine N-oxide, nitrate and fumarate: Ecological implications. *Environ Microbiol.* (2000) 2:399–406. doi: 10.1046/j.1462-2920.2000.00121.x

45. Zhang L, Guo L, Mu C, Ye Y, Wang C. Postmortem metabolite profile changes of mud crab (*Scylla paramamosain*) under different storage conditions. *J Ocean Univ China.* (2021) 20:608–18. doi: 10.1007/s11802-021-4558-x

46. Song Y, Luo Y, You J, Shen H, Hu S. Biochemical, sensory and microbiological attributes of bream (*Megalobrama amblycephala*) during partial freezing and chilled storage. *J Sci Food Agric.* (2012) 92:197–202. doi: 10.1002/jsfa.4572

47. Hong H, Regenstein J, Luo Y. The importance of ATP-related compounds for the freshness and flavor of post-mortem fish and shellfish muscle: A review. *Crit Rev Food Sci Nutr.* (2017) 57:1787–98. doi: 10.1080/10408398.2014.1001489

48. Garg D, Singh M, Verma N, Monika. Review on recent advances in fabrication of enzymatic and chemical sensors for hypoxanthine. *Food Chem.* (2022) 375:131839. doi: 10.1016/j.foodchem.2021.131839

49. Jia S, Liu Y, Zhuang S, Sun X, Li Y, Hong H, et al. Effect of ε-polylysine and ice storage on microbiota composition and quality of Pacific white shrimp (*Litopenaeus vannamei*) stored at 0 °C. *Food Microbiol.* (2019) 83:27–35. doi: 10.1016/j.fm.2019.04.007

50. Cai S, Cheng H, Pang H, Jian J, Wu Z. AcfA is an essential regulator for pathogenesis of fish pathogen *Vibrio alginolyticus*. *Vet Microbiol.* (2018) 213:35–41. doi: 10.1016/j.vetmic.2017.11.016

51. Shieh W, Chen A, Chiu H. *Vibrio aerogenes* sp. nov., a facultatively anaerobic marine bacterium that ferments glucose with gas production. *Int J Syst Evol Microbiol.* (2000) 50:321–9. doi: 10.1099/00207713-50-1-321

52. Hoffart E, Grenz S, Lange J, Nitschel R, Müller F, Schwentner A, et al. High substrate uptake rates empower *Vibrio natriegens* as production host for industrial biotechnology. *Appl Environ Microbiol.* (2017) 83:e1614–7. doi: 10.1128/AEM.01614-17

frontiers | Frontiers in Nutrition

TYPE Original Research
PUBLISHED 09 March 2023
DOI 10.3389/fnut.2023.1121498

OPEN ACCESS

EDITED BY
Yan Zhao,
Chinese Academy of Agricultural Sciences, China

REVIEWED BY
Lei Wang,
Ocean University of China, China
Ruijie Deng,
Sichuan University, China
Hao Dong,
Zhongkai University of Agriculture and Engineering, China

*CORRESPONDENCE
Li Li
✉ hxskincos2017@qq.com
Lidan Xiong
✉ xionglidan@wchscu.cn

SPECIALTY SECTION
This article was submitted to Food Chemistry, a section of the journal Frontiers in Nutrition

RECEIVED 11 December 2022
ACCEPTED 10 February 2023
PUBLISHED 09 March 2023

CITATION
Li A, He H, Chen Y, Liao F, Tang J, Li L, Fan Y, Li L and Xiong L (2023) Effects of donkey milk on UVB-induced skin barrier damage and melanin pigmentation: A network pharmacology and experimental validation study.
Front. Nutr. 10:1121498.
doi: 10.3389/fnut.2023.1121498

Effects of donkey milk on UVB-induced skin barrier damage and melanin pigmentation: A network pharmacology and experimental validation study

Anqi Li[1,2,3], Hailun He[1,2,3], Yanjing Chen[1,2,3], Feng Liao[4], Jie Tang[1,2], Li Li[5], Yumei Fan[4], Li Li[1,2,3]* and Lidan Xiong[1,2]*

[1]Cosmetics Safety and Efficacy Evaluation Center, West China Hospital, Sichuan University, Chengdu, Sichuan, China, [2]NMPA Key Laboratory for Human Evaluation and Big Data of Cosmetics, Chengdu, China, [3]Department of Dermatology, West China Hospital, Sichuan University, Chengdu, Sichuan, China, [4]National Engineering Research Center for Gelatin-based Traditional Chinese Medicine, Dong-E-E-Jiao Co. Ltd., Shandong, China, [5]Laboratory of Pathology, West China Hospital of Sichuan University, Chengdu, Sichuan, China

Introduction: Dairy products have long been regarded as a controversial nutrient for the skin. However, a clear demonstration of donkey milk (DM) on skincare is required.

Methods: In this study, spectrum and chemical component analyses were applied to DM. Then, the effects of DM on UVB-induced skin barrier damage and melanin pigmentation were first evaluated *in vitro* and *in vivo*. Cell survival, animal models, and expression of filaggrin (FLG) were determined to confirm the effect of DM on UVB-induced skin barrier damage. Melanogenesis and tyrosinase (TYR) activity were assessed after UVB irradiation to clarify the effect of DM on whitening activities. Further, a network pharmacology method was applied to study the interaction between DM ingredients and UVB-induced skin injury. Meanwhile, an analysis of the melanogenesis molecular target network was developed and validated to predict the melanogenesis regulators in DM.

Results: DM was rich in cholesterols, fatty acids, vitamins and amino acids. The results of evaluation of whitening activities *in vitro* and *in vivo* indicated that DM had a potent inhibitory effect on melanin synthesis. The results of effects of DM on UVB-induced skin barrier damage indicated that DM inhibited UVB-induced injury and restored skin barrier function *via* up-regulation expression of FLG (filaggrin). The pharmacological network of DM showed that DM regulated steroid biosynthesis and fatty acid metabolism in keratinocytes and 64 melanin targets which the main contributing role of DM might target melanogenesis, cell adhesion molecules (CAMs), and Tumor necrosis factor (TNF) pathway.

Discussion: These results highlight the potential use of DM as a promising agent for whitening and anti-photoaging applications.

KEYWORDS

donkey milk, UVB, skin barrier function, melanogenesis, network pharmacology

Introduction

Exposure to ultraviolet (UV) radiation from sunlight accounts for a global rise in premature skin aging and skin cancer (1). UV rays are separable into three types through wavelength: UVC is 200–280 nm, UVA is 320–400 nm and 280–320 nm is UVB (2). Since shorter UV wavelengths

bring about more terrific impairment to the human body, the impairment induced by UVC is more pernicious than that caused by UVA and UVB (3). UVC has been mostly absorbed by the ozone layer in the atmosphere. Therefore, UVB is the most dominant UV radiation for resulting in wrinkles, laxity, coarseness, and mottled pigmentation (4). In the sunburn response, vasodilation and increased blood flow, endothelial cell activation, formation of "sunburn cells" (i.e., keratinocytes undergoing p53-dependent apoptosis), and release of inflammatory mediators occur in the epidermis and dermis before erythema and edema (5, 6). Proinflammatory cytokines, i.e., TNF-α, PGE2, PGE3, COX-2, IL-6, and IL-8, may play several roles in UVB-induced inflammation, including activation of transcription factors, upregulation of endothelial adhesion molecules, and recruitment of neutrophils to the skin (7–9).

Acute skin damage due to tanning manifests as sunburn (4). Melanogenesis, on the other hand, may protect skin from the damages caused by UV irradiation (10). Exposure to UV radiation, keratinocytes secrete an important melanogenesis regulator, α-melanocyte stimulating hormones (α-MSH), which may trigger the microphthalmia-associated transcription factor (MITF) activation through the melanocortin 1 receptor (MC1R) signaling pathway in melanocytes (11). Then, the tyrosinase (TYR) activity and melanin production are subsequently upregulated in the melanosome. Finally, melanin, which is produced and stored in melanocytes, is transferred to their attached keratinocytes. UVB-mediated pigmentation (delayed tanning) can also be triggered by an inflammatory cascade, suggesting that inflammation and sunburn are also important in the tanning response (12–14). Furthermore, UV damage to the skin triggers inflammation that decreases the expression of genes associated with permeability barrier repair (15). Filaggrin (FLG), which is thought to be a major factor in the skin barrier, is reduced by sunburn (4, 16). During the past decade, safeguarding against UV radiation has been highly studied and was promoted in lots of public health education programs (17). Researchers have frequently concentrated on how to forbid excessive UV exposure, and seldom pay attention to sunburn repairing, post-basking recovery, and pigmentation mechanisms (14, 18).

Milk, one of the most significant provisions for mammals, is the preferred form of feed supplying nutrients and energy (19). Dairy products have been regarded as a conventional nutrient for the skin and milk bath remains popular. Dairy protein allergy, nevertheless, is the most prevailing food allergy in infants, that often experience crossed sensitivity to the present substitute formulae including sheep, goats, milk hydrolysate, and soya bean milk (20). Donkey milk (DM), as a valid natural substitute for cow milk, is similar to human milk in chemical components and organoleptic characteristics (21), which draws our attention. To our knowledge, no allergic reaction to DM has been reported so far. It is said that Cleopatra took DM for a shower to lighten the skin around 3,000 years ago (22). Many milk compositions have shown promise in preclinical studies and have been undergoing active clinical trials (23). DM may benefit overall skin health and cure some skin diseases because DM is rich in vitamin A, vitamin C, niacin, phosphorus, magnesium, zinc, glycine, glutamic acid, ω3-polyunsaturated fatty acids, lipidic prostaglandins, leukotrienes (22), all of which occur in pharmaceuticals and cosmetics.

Until now, the anti-photo damage activities of DM, especially skin barrier protection and melanin production inhibitory activities, have not been reported yet. This paper aimed at exploring the protective effects of DM on UVB-induced skin barrier damage and melanin pigmentation *via in vitro* and *in vivo* studies. In the animal model study, DM was applied topically on the UVB-irradiated dorsum skin of mice. The thickness and integrity of these irradiated skin were evaluated at definite time points. *In vitro* study, we added DM in the culture medium of UVB-irradiated HaCaT cells and observed the viability and protein expression. Meanwhile, B16 cells were applied to evaluate TYR activity and melanogenesis with or without DM after UVB-irradiated. Besides, the mechanisms of DM on UVB-induced skin barrier damage and melanin pigmentation were evaluated *via* a network pharmacology method. Overall, DM has considerable potential as a functional ingredient in food, cosmetic and pharmaceutical applications.

Materials and methods

Materials and reagents

DM was provided by Dong-E E-Jiao Co. Ltd (Shandong, China). B16 and HaCaT cell lines were from Kunming Institute of Zoology, Chinese Academy of Sciences. Dulbecco's modified Eagle's Medium (DMEM), penicillin and streptomycin solution and trypsin (0.25%) were obtained from HyClone (GE Health Care Life Science, Little Chalfont, Buckinghamshire, United Kingdom). Ascorbic acid (Vitamin C), tyrosinase, and L-dopa were purchased from Sigma (Sigma, United States). Fetal bovine serum (FBS) was from Gibco (Thermo Fisher, Waltham, MA, United States). Phosphate-buffered saline (PBS) was purchased from Zsbio Commerce CO (Zsbio, China). CCK-8 (Cell Counting Kit-8) was gained from Dojindo (Dojindo Laboratories, Kumamoto, Japan). Trizol reagent was acquired from Invitrogen Life Technologies (Carlsbad, CA). FLG primary antibody and corresponding secondary antibody (all from rabbit, 1: 2000) were procured from Abcam company (Abcam, United Kingdom). HE Stain assay kit was procured from Solarbio (Solarbio Inc., China). All other chemicals and solvents were of analytical grade.

Microplate spectrophotometer was Bio-Rad (Bio-Rad Inc., Hercules, CA, United States). Chromatography instruments were Agilent 7890A, Agilent ICP-OES5110, Agilent 1,200, and Thermo U3000, respectively. High-speed amino acid analyzer is Hitachi L-8900. Fluoro spectrophotometries are AFC062 and AFC045. Potentiometric titrator is AFC057.

Determination of main active ingredients in donkey milk

Total amino acids composition analysis

AAs concentrations in DM were analyzed by a Hitachi L-8900 AAs analyzer (Hitachi, Ltd., Japan). A mixture of basic, acid, and neutral AAs of known concentrations (Sigma Chemical Co., St. Louis, MO) was used as standard. The samples were hydrolyzed in 6 mol HCl at 110°C for 22 h and filtered through a filter (pore size, 0.22 μM). AAs were derived through reactions with the ninhydrin reagent and detected by the absorbances at 440 nm (proline and hydroxyproline) or 570 nm (total AAs except for proline and hydroxyproline).

Determination of fatty acids content

Fatty acids of DM were determined by Gas chromatography (GC) analysis. The fatty acids were obtained with sodium hydroxide in methanol and injected into an Agilent 7890A gas-chromatograph device (Agilent Technologies, United States), equipped with a flame ionization detector. The chromatographic column (Supelco SP-2560, China) was performed. Purified helium was used as a carrier gas with a split ratio of 1: 100. A 1.0 μl aliquot of each sample was injected at an initial temperature of 100°C and held constant for 13 min before being increased to 180°C at 10°C/min and held for 6 min, then ramped to 200°C at 1°C/min held for 20 min and then increased to 230°C at 4°C/min held for 10.5 min. The injector and detector temperatures were set at 270°C and 280°C, respectively.

Determination of mineral content

Determination of Ca, Fe, K, Mg, Na, and Zn was carried out with an inductively coupled plasma optical emission spectrometer (Agilent Technologies, United States). For plasma generation, nebulization, and auxiliary gas, argon with a purity of 99.996% was used. Digestion of samples was also performed using HNO_3 (5% v/v) in a microwave dissolver (MARS, USA). After the digestion procedure, clear solutions were obtained, and the analytes were determined by ICP-OES. The ICP-OES operating conditions are listed in Supplementary Table S1.

Determination of cholesterol content

The cholesterol content was determined according to the National Standards of the PRC. DM was saponified with methanolic potassium hydroxide, and the unsaponifiable matter was extracted by ligarine and diethyl ether, separated, and determined by HPLC. Analysis of cholesterol was performed by Agilent 1,200 (Agilent Technologies, United States) adapted a ZORBAX SB-C18 (4.6 mm × 150 mm, 5.0 μM) column and detected at 205 nm. The samples were filtered before injection (Millipore 0.45 μM). Injected volume was 50 μl, flow rate 1.0 ml/min, isocratic mode with methanol.

The determination of other chemical components (vitamin C, vitamin D2, vitamin D3, taurine, phosphorus, and chloride) of DM powder was provided in the section Supplementary Materials and Methods.

Cell viability assay

Cytotoxic effect of DM on B16 or HaCaT cells was determined by the CCK-8 assay. The B16 or HaCaT cells were seeded at $2–8 \times 10^4$ cells/well in 24 well plates and incubated in a humidified incubator at 37°C under 5% CO_2 for 24 h. The cells then were cultured for 24 h with or without DM (0.1–25 mg/mL). Cell survival was calculated as the percentages of that of control. Each sample was tested for three independent analyses.

Evaluation of donkey milk on melanin pigmentation *in vitro*

Determination of melanin content

B16 cells were seeded at a density of $2–5 \times 10^5$ cells/mL in 6-well plates and incubated for 24 h. Cells were then exposed to increasing doses of DM or ascorbic acid (VC) for 48 h in the presence or absence of 100 nM α-MSH. Then harvesting and centrifugation for 10 min at 4°C, the cells were dissolved in 1 M NaOH at 80°C for 1 h. The melanin content was gauged by the absorbance of microplate reader at 405 nm.

Assay of tyrosinase activity

The cells were seeded at a density of $2–5 \times 10^5$ cells/mL in 6-well plates and cultured for 24 h. Cells were then exposed to increasing doses of DM or VC for 48 h in the presence or absence of 100 nM α-MSH, Then, cells were washed twice with PBS and lysed in 1.0% Triton X in a refrigerator at-80°C for 30 min. 0.5% L-DOPA was added to each cell lysate and incubated at 37°C for 3 h. All the values of absorbance were gauged with a spectrophotometer at 475 nm. The inhibitory activity of TYR activity was expressed as inhibition ratios of that of control.

Tyrosinase, dopachrome tautomerase, tyrosinase-related protein 1, and microphthalmia-associated transcription factor mRNA expression assay

An amount of 1×10^5 B16 cells per well were cultured in 24-well plates for 24 h and then incubated with PBS after washing for twice. Cells were then exposed to increasing doses of DM for 48 h in the presence or absence of 100 nM α-MSH. The Trizol method was applied to extract total cellular RNA according to the manufacturer's instruction. NovoScript Kit (Novoproptein, China) was then used for the amplification with real-time PCR (Bio-Rad Inc., United States). The 2-ΔCT approach was performed to investigate gene Tyr, Dopachrome tautomerase (Dct), Tyrosinase-related protein 1 (TYRP1), MITF expression and β-actin mRNA served as an endogenous control to evaluate the relative expression levels of target mRNAs. The sequences of primers were listed in Table 1.

Evaluation of donkey milk on UVB-induced skin barrier damage

Filaggrin protein expression assay

An amount of 5×10^5 HaCaT cells per well were cultured in 6-well plates for 24 h. After PBS washing three times, the cells were covered with PBS and a dose of 20 mJ/cm^2 UVB irradiation. The cells were then cultivated in serum-free DMEM culture medium with DM added at varying concentrations for 24 h, or untreated (control， with neither

TABLE 1 The sequences of primers used for reverse transcription.

Gene	Nucleotide sequence	Size
TYR	F:5′-CCTTCTGTCCAGTGCACCAT-3′	20
	R:5′- TCCGCAGTTGAAACCCATGA-3′	20
DCT	F: 5′-CTTGGGGTTGCTGGCTTTTC-3′	20
	R:5′- CGCTGAAGAGTTCCACCTGT-3′	20
TYRP1	F:5′- GCTTCACTTGCTGGAACACA-3′	20
	R:5′-CGCAGGCCTCTAAGATACGA-3′	20
MITF	F:5′-TGCACTGGGGAGAAGTTGAT-3′	20
	R:5′-GCTGCGGACCATACAGAAAG-3′	20
β-actin	F:5′-ACAGCTGAGAGGGAAATCGTG-3′	21
	R:5′-AGAGGTCTTTACGGATGTCAACG-3′	23

F, forward primer; R, reverse primer.

UVB radiation nor DM supplement). The HaCaT cells were then acquired on an ice plate and added the lysis buffer to lyse for 30 min. Cellular extracts were then centrifuged at temperature 4°C for 15. The BCA assay (Beyotime, China) was then applied to evaluate collected total proteins' amount. Commercial SDS-PAGE gels (Beyotime, China) were utilized to separate whole proteins and protein bands, the proteins were then electro-transferred to PVDF membranes (Millipore, United States). After transferring, PVDF membranes were blocked for 30 min with the quick confining liquid (Beyotime, China). To probe corresponding target proteins, PVDF membranes were incubated with GAPDH and filaggrin (FLG) antibodies for 24 h at 4°C, subsequently incubated with secondary antibody for 1 h at 20°C. The iBright system (iBright FL1500, Thermo Fisher, USA) was employed to assess the protein bands in this study. Relative expression of objective protein (GAPDH as an internal control) was observed by electrophoresis bands' optical density and calculated with Image J (National Institutes of Health, Germany).

In vivo experiments

Six-week-old female C57BL/6 mice (Chengdu Dashuo Inc., China) were raised under standard animal husbandry conditions. This study was approved by the Ethical Committee of the West China Hospital of Sichuan University (Chengdu, China). The mice were separated randomly into five groups: a negative control group (n = 3), which was exposed to no UVB irradiation; a positive control group (n = 3), which received UVB irradiation and with no treatments; a hydrocortisone group (n = 3), which received UVB rays and treated with hydrocortisone cream; a concentration of 5 mg/ml DM treatment group (n = 3), which was exposed to UVB irradiation and treated with 5 mg/ml DM; a concentration of 10 mg/ml DM treatment group (n = 3), which was exposed to UVB irradiation and treated with 10 mg/ml DM. those external productions were applied once a day. After the treatment process, the animals were sacrificed on the 7th day, and skin lesion specimens were immersed in 4% paraformaldehyde. Hematoxylin and eosin (H&E) staining was used to demonstrate the general histopathological variations in the skin.

Network pharmacology study

Relevant targets data collection

The test report of DM ingredients was released as described above. GeneCards[1] (updated on December, 2019) (24), DrugBank[2] (updated on December, 2019) (25), and ChEMBL[3] (updated on Dec, 2019) were used. In order to acquire integrated and accurate data, substantial work of data mining and literature searching needed to be explored to ascertain the construction of the database.

Network analysis

The targets databases for ingredients of DM and UVB-induced skin barrier damage and melanin pigmentation were utilized to mine the potential UVB-protective targets. The ingredients of DM and relevant targets databases were utilized to mine the targets. To determine the connection between ingredients and target for DM, a network study was developed using STRING[4] (updated on August, 2019) and plotted using Cytoscape[5] (version 3.7.1) (26). We used Cytoscape 3.7.1 software to construct protein–protein (PPI) and component-target interaction networks. Target protein molecules were displayed by "nodes" and interrelationships by "edges." With excellent visual interface, the interaction between components and targets can be clearly shown. Pasted targets into the list of genes on the right and submitted them. We performed several gene ontology (GO) analyses ($p < 0.05$) and used Kyoto Encyclopedia of Genes and Genomes (KEGG) automatic annotation database[6] (KAAS) to analyze the obtained targets and related signaling pathways ($p < 0.05$).

Statistical analysis

The results were shown as the mean ± standard error (mean ± S). Data were determined by one-way analysis of variance (one-way ANOVA) and Kruskal-Wallis H rank sum test. A *value of p* less than 0.01 was considered statistically significant. IBM SPSS Statistics 23 was applied.

Results

Chemical composition analysis of main active ingredients in donkey milk

Table 2 presents the experimental data on the main active components content. As shown in Table 2, the content of mineral was the highest, followed by the amino acids and fatty acids. Of the 16 amino acids identified, the most abundant were glutamic acid (Glu), Aspartic acid (Asp), leucine (Leu), lysine (Lys), valine (Val), and Arginine (Arg), which accounted for over 66% of the total amino acids (Figure 1A). The results showed that 28 kinds of fatty acids were detected in DM (Figure 1B). The content of fatty acids in DM powder was 4.5%. The content of saturated fatty acids and unsaturated fatty acids was 2.16 and 2.34%, respectively (1.12% for unsaturated fatty acids and 1.22% for polyunsaturated fatty acids). The content of unsaturated fatty acids of DM, including myristoleic (C14:1), palmitoleic (C16:1), trans-elaidic (C18:1n9t), oleic (C18:1n9c), linoleic (C18:2-9c,12c), α-linolenic acid (C18:3; ALA), cis 11-eicosenoic acid (C20:1n11c), all cis-11,14-eicosadienoic acid (C20:2–11,14c), all cis-8,11,14-eicosatrienoic acid (C20:3–8,11,14c), all cis-5,8,11,14-eicosateraenoic acid (C20:4–5,8,11,14c; ARA), all cis-13,16-docosadienoic acid (C22:2–13,16c), nervonic (C24:1).

The determination of other chemical components of DM was provided in the section Supplementary Results.

Evaluation of whitening activities of donkey milk *in vitro*

The cytotoxicity of donkey milk in B16 cells

The cytotoxic effects of DM were evaluated by CCK-8 assay and light microscopic observation (Figures 2A,B). At DM concentrations

1 https://www.genecards.org/
2 https://www.drugbank.ca/
3 https://www.ebi.ac.uk/chembl/
4 https://string-db.org/
5 https://cytoscape.org/
6 https://www.kegg.jp/blastkoala/

10.3389/fnut.2023.1121498

TABLE 2 The main contents of DM.

Items	Unit	Testing methods	Molecular formula	Molecular weight	Values
MUFA	g/100 g	GC	–	–	1.6
PUFA	g/100 g	GC	–	–	0.25
SFA	g/100 g	GC	–	–	3.08
LA	g/100 g	GC	$C_{18}H_{30}O_2$	278.43	0.21
ALA	g/100 g	GC	$C_{18}H_{30}O_2$	278.43	0.08
linoleic acid	g/100 g	GC	$C_{18}H_{32}O_2$	280.44	1.12
AA	g/100 g	GC	$C_{20}H_{32}O_2$	304.46	ND
DHA	g/100 g	GC	$C_{22}H_{30}O_2$	328.48	ND
Vitamin C	mg/100 g	Fluoro spectrophotometry	$C_6H_8O_6$	176.12	48.1
Vitamin D_2	ug/100 g	HPLC	$C_{28}H_{44}O$	396.65	ND
Vitamin D_3	ug/100 g	HPLC	$C_{27}H_{44}O$	384.64	ND
P	mg/100 g	Fluoro spectrophotometry	–	–	580
Cl	g/100 g	Zeta	–	–	0.58
Ca	mg/kg	ICP-OES	–	–	$8.81*10^3$
K	mg/kg	ICP-OES	–	–	$8.27*10^3$
Na	mg/kg	ICP-OES	–	–	$2.59*10^3$
Mg	mg/kg	ICP-OES	–	–	826
Fe	mg/kg	ICP-OES	–	–	ND
Zn	mg/kg	ICP-OES	–	–	22.7
Cho	mg/100 g	HPLC	$C_{27}H_{46}O$	386.65	21.7
Tau	mg/100 g	HPLC	$C_2H_7NO_3S$	125.15	12.3
Glu	g/100 g	HPLC	$C_5H_9NO_4$	147.13	3.48
Gly	g/100 g	HPLC	$C_2H_5NO_2$	75.07	0.33
Ile	g/100 g	HPLC	$C_6H_{13}NO_2$	131.17	0.86
Tyr	g/100 g	HPLC	$C_9H_{11}NO_3$	181.19	0.55
Lys	g/100 g	HPLC	$C_6H_{14}N_2O_2$	146.19	1.33
Arg	g/100 g	HPLC	$C_6H_{14}N_4O_2$	174.20	0.9
Thr	g/100 g	HPLC	$C_4H_9NO_3$	119.12	0.72
Ser	g/100 g	HPLC	$C_3H_7NO_3$	105.09	0.91
Pro	g/100 g	HPLC	$C_5H_9NO_2$	115.13	1.41
Ala	g/100 g	HPLC	$C_3H_7NO_2$	89.09	0.61
Met	g/100 g	HPLC	$C_5H_{11}O_2NS$	149.21	0.41
Leu	g/100 g	HPLC	$C_6H_{13}NO_2$	131.18	1.62
Phe	g/100 g	HPLC	$C_9H_{11}NO_2$	165.19	0.81
Val	g/100 g	HPLC	$C_5H_{11}NO_2$	117.15	1.06
Asp	g/100 g	HPLC	$C_4H_7NO_4$	133.10	1.73
His	g/100 g	HPLC	$C_6H_9N_3O_2$	155.00	0.49

MUFA, monounsaturated fatty acid; PUFA, polyunsaturated fatty acid; SFA, saturated fatty acid; LA, linolenic acid; ALA, α-linolenic acid; DHA, docosahexaenoic acid; AA, arochidonic acid oil; Cho, cholesterol; Tau, taurine; Glu, glutamic acid; Gly, glycine; Cys, cystine; IIe, isoleucine; Tyr, tyrosine; Lys, lysine; Arg, arginine; Trp, tryptophan; Thr, threonine; Ser, serine; Pro, proline; Ala, alanine; Met, methionine; Leu, leucine; Phe, phenylacetic acid; Val, valine; Asp, aspartic acid; His, histidine; ICP-OES, inductively coupled plasma optical emission spectrometry; HPLC, high performance liquid chromatography.

of 25 mg/ml, light microscopy revealed significant toxicity as cells became round shaped and uniformly detached from the surface. CCK-8 assay demonstrated that the difference between 25 mg/ml DM and control group was statistically significant ($P<0.01$). Overall, a safe concentration of DM of under 10 mg/ml was used for the next stage of the experiment.

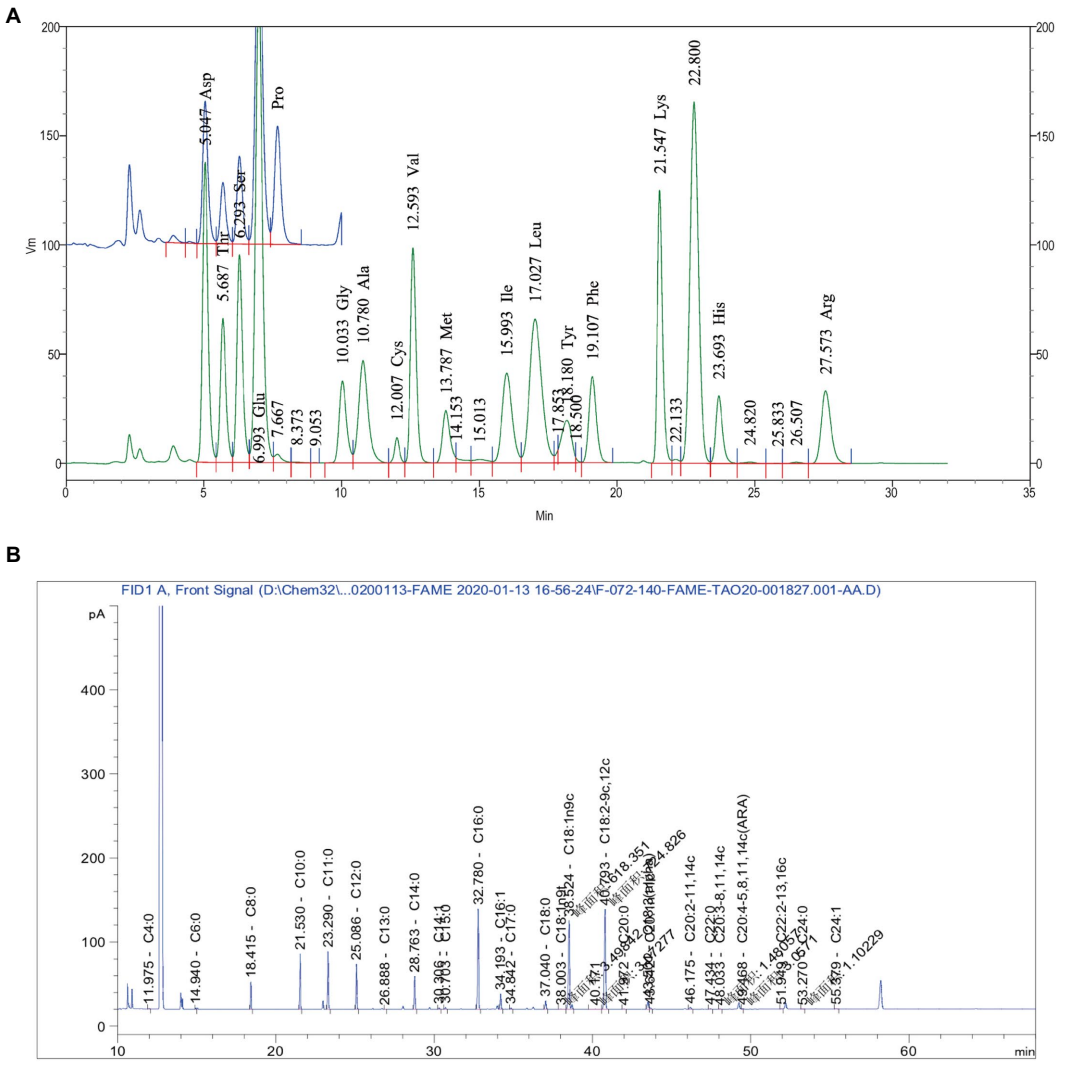

FIGURE 1
Main Active Ingredients in DM. **(A)** Main amino acids. **(B)** Main fatty acid.

Effect of donkey milk on melanin content in B16 cells

To explore the effect of DM, an experiment *in vitro* was applied to check whether DM activated or inhibited melanogenesis in cells that turn related-genes and proteins on and off. Treatment with various dosages of DM (0.1, 1, 10 mg/ml) showed inhibitory effect on melanogenesis in a dose-dependent manner in the B16 cells. The melanin content was 90.36% at 0.1 mg/ml, 68.67% at 1 mg/ml, and 52.81% at 10 mg/ml compared with the level of the 100 nM α-MSH group (Figure 2C). Meanwhile, B16 cells were treated with 1 mM VC as a positive standard (Figure 2C). The results indicated that DM had a potent inhibitory effect on melanin synthesis in B16 cells.

Effect of donkey milk on tyrosinase activity in B16 cells

As presented in Figure 2D, DM inhibited the TYR activity notably in a dose-dependent manner, by 81.78, 72.12, and 56.57% compared with 100 nM α-MSH at concentrations of 0.1, 1, and 10 mg/ml, respectively. Meanwhile, the TYR activity was decreased to 71.02% after the cells were exposed to 1 mM VC.

Effect of donkey milk on the expression of melanogenesis-related genes in B16 cells

As shown in Figure 2E, inhibition of Tyr, Trp1, Dct (Trp2), and Mitf expression with 1 mM VC was observed by 0.95-, 0.88-, 0.17-and 0.48-fold of 100 nM α-MSH, respectively. The inhibitory effects of DM (0.1,1, 1 mg/ml) on mRNA expression of Mitf were equivalent to the effects of 1 mM VC, which served as a well-known effective melanogenesis inhibitor, while the effects of 10 mg/ml DM was superior to that of 1 mM VC (P<0.01). DM (0.1, 1, 1 mg/mL) inhibited mRNA expression of Dct in a dose-dependent manner. In addition, the inhibitory effects of 0.1 mg/ml DM on TYR and TRP1 were inferior to the effects of 1 mM VC, while DM (1 and 10 mg/ml) on TYR and TRP1 was superior to the effects of 1 mM VC (P<0.01), further indicating that DM has a potential whitening effect.

10.3389/fnut.2023.1121498

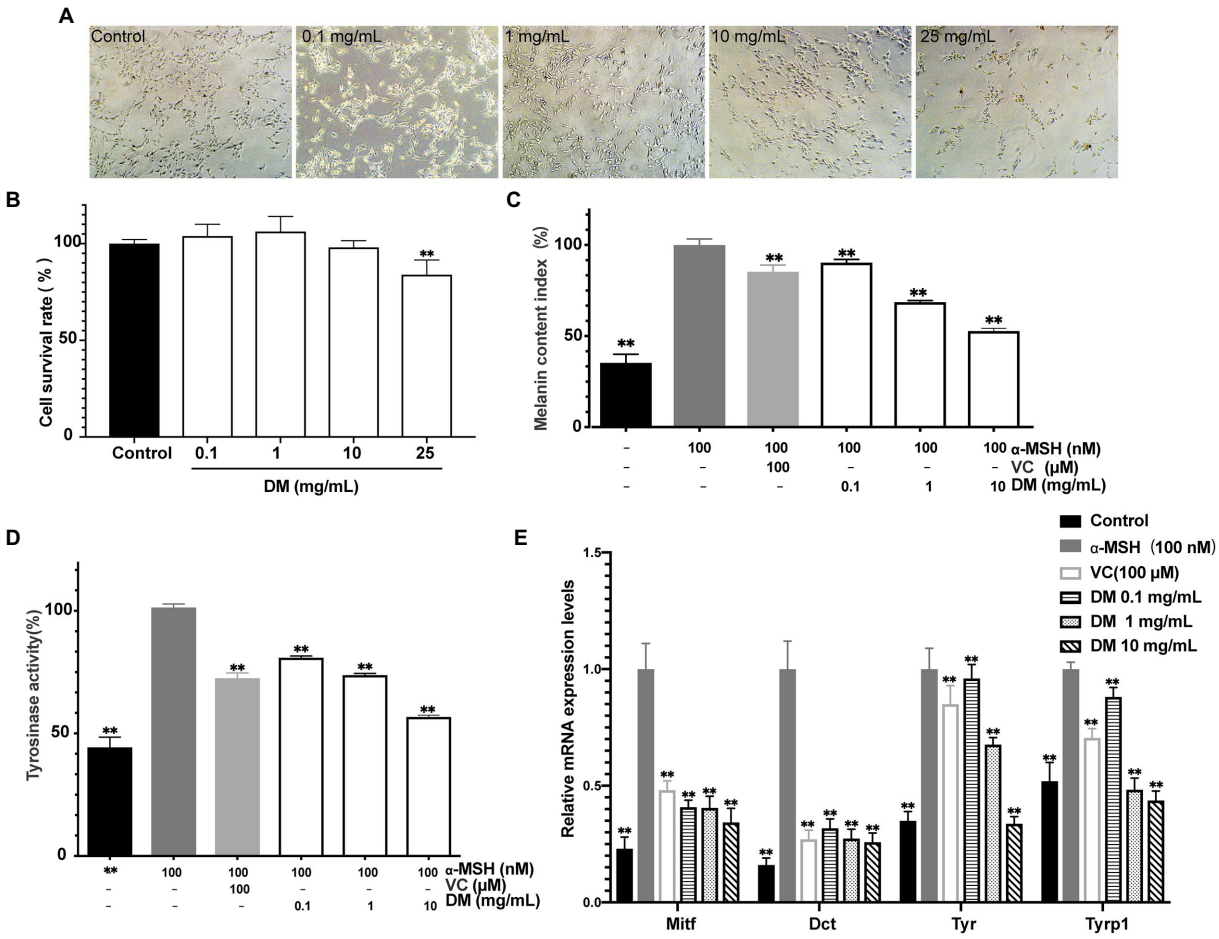

FIGURE 2
Whitening efficacy *in vitro*. **(A)** Light microscope image. **(B)** Effects of DM on B16 cell viability. **(C)** Effects of DM on melanin synthesis in B16 cells. **(D)** Effects of DM on TYR activity in B16 cells. **(E)** Effects of DM on expression of Mitf, Dct, Tyr, and Tyrp1 in B16 cells. The asterisk (**) indicated a significant difference ($p<0.01$) compared to the control of **(B)**. The asterisk (**) indicated a significant difference ($p<0.01$) compared to the 100nM α-MSH of **(C–E)**.

Effects of donkey milk on UVB-induced skin barrier damage

The protective effect on UVB-induced damage of donkey milk in mouse

After UVB irradiation, mice were topically treated with DM for 7 days. Figures 3A–F showed histological results of mouse skin exposed to UV and then treated with DM. After staining by hematoxylin and eosin (H&E), the control group demonstrated normal cutaneous histology which had the integrated epidermal structure and basement membrane zone without inflammatory cell infiltration. When exposed to UVB only, there was a significant acanthosis with liquefaction degeneration in basal cells, consistent with the exfoliation of epidermal and stratum corneum, severe inflammatory cells infiltration could be observed both in derma and epidermis. Hyperplasia of the spinosum and strata granulosum was illustrated as the histological alterations in UVB-irradiated skin. Compared to control group, there were significant differences when treated with DM from H&E photomicrographs. Considerable hyperplastic epidermis alterations were observed by after UVB radiation, and an increased thickness of epidermis in DM groups were observed, suggesting that DM provided a protective effect after UVB exposure *via* enhancing the structure of keratinocytes and the epidermal thickness. Compared to the group of hydrocortisone, the DM group showed less irritation.

Effect of donkey milk on cell viability after UVB irradiation in HaCaT cells

After UVB (20 mJ/cm^2) exposure, cell survival rate of HaCaT cells gradually declined to 36.2% after 24 h (Figure 3G). A concentration-dependent protective effect was indicated *via* analysis of cells survival while treated with DM. In comparison with control group (without UVB exposure), the amount of HaCaT cells after exposed to UVB was declined to exactly 73.1, 49.6 and 35.7%, after treated to DM for 1, 0.5 and 0.1 mg/ml, respectively. And the cell viability of UVB-exposed group without DM was only 36.2%. Compared to UVB group, the DM (0.1 mg/ml) group indicated no significant difference ($p > 0.05$). The results for viability of HaCaT cells after UVB exposure indicated that DM could play an important role in protecting keratinocytes against UVB injury.

10.3389/fnut.2023.1121498

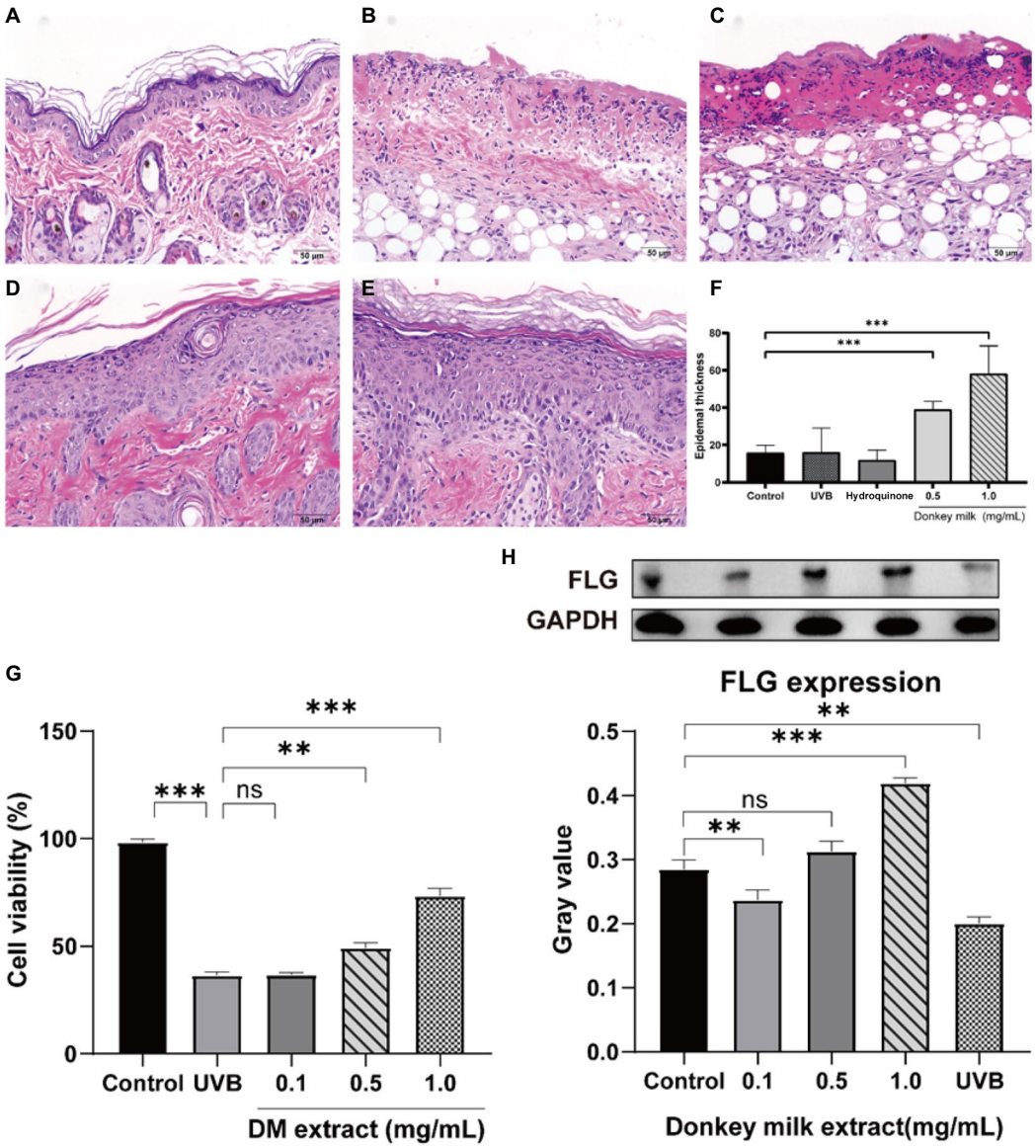

FIGURE 3
Effects of DM on UVB-induced skin barrier damage. The protective effect of DM in mouse through HE staining. **(A)** Control group. **(B)** UVB group. **(C)** Hydroquinone group. **(D)** 0.5mg/mL DM group. **(E)** 1mg/mL DM group. **(F)** Epidermal thickness. **(G)** Effects of DM on HaCaT cell viability after UVB exposure. **(H)** Effects of DM on expression of FLG in HaCaT cells. The asterisk (** and ***) indicated a significant difference ($p<0.01$ and $p<0.001$), the symbol (ns) indicated no significant difference.

Effect of donkey milk on the expression of filaggrin after UVB irradiation in HaCaT cells

After exposure to UVB (20 mJ/cm^2), HaCaT cells were incubated with 0, 0.1, 0.5 and 1 mg/ml DM for 24 h, then cells were collected. Filaggrin (FLG) expression, one of the key structural components of the epidermal barrier, was detected through Western blot. It illustrated that UVB irradiation led to down-regulation in FLG expression compared to untreated cells ($p<0.05$, Figure 3H). Usage of DM (0.5 and 1 mg/ml) up-regulated the FLG expression vs. UVB group ($p<0.05$). These results indicated DM inhibited UVB-induced injury and restored skin barrier function *via* up-regulating the expression of FLG.

Network pharmacology analysis

Donkey milk—target (ingredient) -melanin related targets network

To explore the relationship between DM and the effect of lightening pigmentations, a DM-target (ingredient)—melanin-related targets pharmacological network was used. A molecular target network was developed and validated to predict the melanogenesis regulators related to 64 melanin targets. Among the constructed and visualized target prediction database, 64 DM-related targets were observed, including TYR, TRP1, DCT (TRP2), and MITF which confirmed a high correlation with melanogenesis. There were several dozens of other proteins seemingly unrelated such as fatty acid

synthetase (FAS), catalase (CAT), KIT Proto-Oncogene, Receptor Tyrosine Kinase (KIT), and Lactoperoxidase (LPO). However, using Cytoscape to construct PPI network and component-target interaction network, we found that 53 PPI-related targets were mapped after 11 protein factors were excluded (Figure 4A). According to PPI enrichment $p < 1.0e\text{-}16$, three of the most interacting nodes were TYR, TRP1, DCT (TRP2), while MITF, FAS, CAT, KIT, LPO and killer cell immunoglobulin (Ig) like receptor, KIR3DL1 were the most potent factors. In accordance with the effect, the targets ranged from strong to weak. Component-target interaction network showed that 2 major categories of related active ingredients interacted with 53 gene targets. KEGG analysis was applied to enrich the related signaling pathways ($p < 0.05$), melanogenesis, cell adhesion molecules (CAMs), TNF signaling pathway, pathways in cancer tyrosine metabolism, gap junction, MAPK pathway, steroid biosynthesis, and cytokine-cytokine receptor interaction were dominant (Figure 4B).

To investigate the protective mechanism of DM on skin recovery after UVB exposure, a DM-target (ingredient)-UVB related targets pharmacological network was used. The potential targets data of DM were obtained from GeneCards. The potential targets data of UVB injury were obtained from mRNA sequencing of HaCaT cells after 20 mJ/cm^2 UVB exposure. There were 72 potential targets (score > 50) related to the protective effect of DM. The top 10 of them were APOA1, HADHA, HGF, LDLR, NPC1, F2, APOA2, APOB, IL10, APOE, which were related to lipid metabolism and inflammatory reaction. Ingredient-target gene interactions' network diagrams were plotted to employ Cytoscape (Figure 4C). As shown above, DM was rich in cholesterols, fatty acids, vitamins, minerals and amino acids. Component-target interaction network showed that 4 major categories of related active ingredients interacted with 72 gene targets, which were cholesterols, fatty acids, amino acids, and vitamins, respectively (Figure 4C).

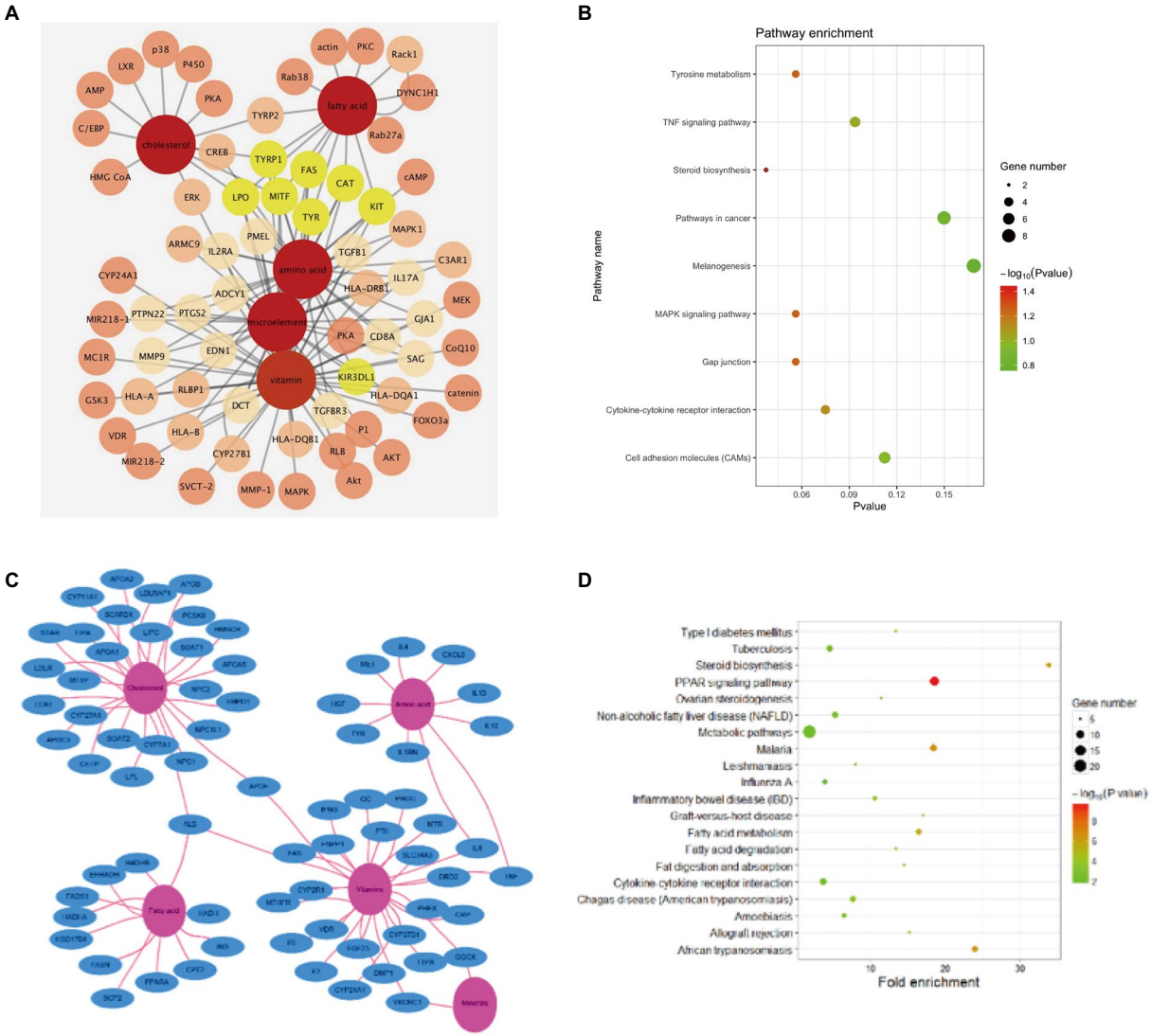

FIGURE 4
Network pharmacology analysis. **(A)** Components-melanin related targets interaction network. **(B)** Top 9 KEGG enrichment in DM components-melanin network pharmacology. **(C)** Components-skin barrier related targets interaction network. **(D)** Top 20 KEGG enrichment in DM components-skin barrier network pharmacology.

KEGG analysis was utilized to enrich the relevant signal pathways ($p < 0.05$), and the signal pathway analysis indicated that the protective effects of DM compound against UVB-induced changes might aim at the metabolic pathway, PPAR pathway, fatty acid metabolism, and steroid biosynthesis (Figure 4D). These signal pathways were associated with cell proliferation and metabolism.

Discussion

Exposure to UVB has psychological and physical benefits, especially in the synthesis of vitamin D_3 and the prevention of diseases like osteoporosis (27). However, UVB is responsible for photocarcinogenesis and sunburn response (28). Recent investigations have disclosed UVB-induced skin injury's pathology, like sunburn, photoaging, and skin cancer utilizing cells, animals, and human studies (4, 29, 30). Previous studies also have shown that UVB affected epidermal morphology, disrupted the skin barrier, increased transepidermal water loss, and decreased stratum corneum hydration (31). Initially, melanin pigmentation plays a dual role in skin:it is suggested to render photoprotection from the DNA-damaging effects of UV (32, 33) while leading to acquired hyperpigmentation disorders such as melasma (34, 35). In this context, consumers have an increasing requirement for quality natural cosmetic material. In this study, we found that DM protected against sunburn and tanning. Milk has been used to treat skin wounds for thousands of years (36, 37). In the past few years, researchers' attention has been attracted to milk products due to several bioactive components' plenteous presence (21). In this study, HPLC was employed to evaluate the composition of DM. A network pharmacology method was used to find out the potential mechanism and active compounds in DM for restoring skin barrier and pigmentation UVB-induced detriment.

By network prediction, we could find that DM was closely related to melanin metabolism. HPLC analysis revealed that DM is rich in cholesterol, fatty acids, vitamins and amino acids.DM is rich in leucine, lysine, glutamic, isoleucine, threonine, tyrosine, serine, and valine. It has been reported that alanine, glycine, phenylalanine, and aspartic acid were shown to have different effects against melanin contents and TYR activity in B16 melanoma cells according to their chemical structures or their combinations (38). Another study showed glycine hydroxamate downregulated melanin synthesis and TYR activity through activating cAMP/ PKA pathways (39). As a tripeptide component, glutathione serves long as an intravenous anti-pigmentation product by inhibiting TYR activity (40). Moreover, nicotinic acid hydroxamate inhibited the TYR activity and melanogenesis by downregulating the MEK/ ERK and AKT/ GSK3β pathways (41). Besides, the effect of cholesterol, fatty acids, and microelement in DM on lightening pigmentation has been controversial. Some reports demonstrated that fatty acids are able to regulate the post-Golgi proteasomal degradation in ubiquitinated TYR (42). Briefly, linoleic acid and docosahexaenoic acid (DHA) decrease melanin levels, while palmitic acid (PA) increases melanin levels (43). In addition, trace elements such as calcium (Ca), magnesium (Mg), copper (Cu) and zinc (Zn) are a kind of important nutrients, which participate in the body's metabolism as the components or activators of enzymes and receptors (44). Additionally, TYR with copper binding is the rate-limiting enzyme in melanin biosynthesis and first catalyzes hydroxylation (45). In the present study, a molecular target network was developed and validated to predict the melanogenesis regulators related to 64 melanin targets. DM was evaluated for TYR activity and melanogenesis *in vitro* with experimental validation. Thus, DM was considered to have the potential skin-whitening effect and may be supposed to develop as a safe potentially depigmented agent.

By network prediction, we could find that the nutritious ingredients of DM are the indispensable base of skin barrier reconstruction and keratinocytes survival from UVB exposure. The lipid fraction of DM consists of several nutritional significant components, such as phospholipids and polyunsaturated fatty acids. DM lipids' importance in skin structure and skin barrier function has been revealed by continued research. Researchers fed hairless mice with milk phospholipids, and discovered mice supplemented with more phospholipids showed higher concentrations of covalently-bound ω-hydroxy ceramides and an improved skin barrier function due to skin inflammation's suppression (19). Our results revealed that the efficiency of DM is dependent on the concentration, and the potential target genes are APOA1, HADHA, HGF, LDLR, NPC1, F2, APOA2, APOB, IL10, and APOE. Apolipoprotein A-II is the second most plenteous protein in high-density lipoprotein particles, and it is related to lipid metabolism (45). HADHA is related to mitochondrial function and phospholipid metabolism and HADHA's loss leads to long-chain fatty acid accumulation (46). In summary, APOA1, APOA2, APOB, APOE, HADHA, and LDLR are genes related to lipid metabolism, which is important for keratinocytes proliferation and stratum corneum lipids formation. The significant beneficial effect of DM on sunburn can be explained. Furthermore, we observed that DM can reduce UVB-induced injury by increasing HaCaT cells' survival. In addition, DM can restore the skin barrier function by increasing the expression of FLG in keratinocytes and epidermal thickness of C57BL/6 mouse skin after UVB exposure. Changes in epidermal structural proteins like FLG are frequently related to damage to cutaneous barrier function. FLG play a fundamental part in skin barrier function, and gene mutations of FLG are usually associated with the deterioration of atopic dermatitis and ichthyosis vulgaris (47, 48).Excessive exposure to sunlight can diminish epidermal FLG and result in an acquired filaggrin insufficiency (49), which is consistent with our results.

Conclusion

In this study, we suggested that DM help the skin restore after UVB exposure. We conducted *in vitro* tests to reveal that DM was protected against sunburn and tanning. The whitening effect was mainly reflected in the good inhibitory effect of DM on synthesis of melanin, tyrosinase activity, and related gene expression. DM could not only prevent UVB-induced adverse effects but also restore skin barrier function by increasing FLG's expression and regulating metabolism procedures such as lipid and steroid metabolism. Hence,

DM is desirable for skin care cosmetics against UVB-induced skin barrier damage and melanin pigmentation.

Data availability statement

The original contributions presented in the study are included in the article/Supplementary material, further inquiries can be directed to the corresponding authors.

Ethics statement

The animal study was reviewed and approved by Animal Ethical and Welfare, West China Hospital, Sichuan University.

Author contributions

AL, HH, and YC: data curation. JT and YF: formal analysis. FL: funding acquisition. LL (6th author) and LX: project administration, supervision, writing—review and editing, and conceptualization. AL, YC, and LX: investigation, validation, writing—original draft, and methodology. All authors have read and agreed to the published version of the manuscript.

Funding

We appreciatively acknowledge the financial support offered by China National Natural Science Foundation (No. 81673084) and 1.3.5 project for disciplines of excellence, West China Hospital, Sichuan University.

Conflict of interest

FL and YF were employed by Dong-E-E-Jiao Co. Ltd.

The remaining authors declare that the research was conducted in the absence of any commercial or financial relationships that could be construed as a potential conflict of interest.

The reviewer RD declared a shared affiliation with the authors LX, AL, HH, YC, JT, and LL to the handling editor at the time of review.

Publisher's note

Supplementary material

The Supplementary material for this article can be found online at: https://www.frontiersin.org/articles/10.3389/fnut.2023.1121498/full#supplementary-material

References

1. Wei, J, Shi, Q, Xiong, L, Xin, G, Yi, T, Xiao, Y, et al. Transcriptome profiling of cells exposed to particular and intense electromagnetic radiation emitted by the "SG-III" prototype laser facility. *Sci Rep*. (2021) 11:1–14. doi: 10.1038/s41598-021-81642-5

2. Mahmoud, BH, Ruvolo, E, Hexsel, CL, Liu, Y, Owen, MR, Kollias, N, et al. Impact of long-wavelength UVA and visible light on melano competent skin. *J Invest Dermatol*. (2010) 130:2092–7. doi: 10.1038/jid.2010.95

3. Fu, Y, Wan, R, Yang, L, Xiong, L, Hu, J, Tang, J, et al. Propolis inspired sunscreens for efficient UV-protection and skin barrier maintenance. *Nano Res*. (2022) 15:8237–46. doi: 10.1007/s12274-022-4434-z

4. Matsui, M, Tanaka, K, Higashiguchi, N, Okawa, H, Yamada, Y, Tanaka, K, et al. Protective and therapeutic effects of fucoxanthin against sunburn caused by UV irradiation. *J Pharmacol Sci*. (2016) 132:55–64. doi: 10.1016/j.jphs.2016.08.004

5. Nicolaou, A, Masoodi, M, Gledhill, K, Haylett, AK, Thody, AJ, Tobin, DJ, et al. The eicosanoid response to high dose UVR exposure of individuals prone and resistant to sunburn. *Photochem Photobiol Sci*. (2012) 11:371–80. doi: 10.1039/c1pp05272a

6. Nicolaou, A, Pilkington, SM, and Rhodes, LE. Ultraviolet-radiation induced skin inflammation: dissecting the role of bioactive lipids. *Chem Phys Lipids*. (2011) 164:535–43. doi: 10.1016/j.chemphyslip.2011.04.005

7. Vogeley, C, Esser, C, Tüting, T, Krutmann, J, and Haarmann-Stemmann, T. Role of the aryl hydrocarbon receptor in environmentally induced skin aging and skin carcinogenesis. *Int J Mol Sci*. (2019) 20:6005. doi: 10.3390/ijms20236005

8. Sklar, LR, Almutawa, F, Lim, HW, Hamzavi, IH, Uetsu, N, Miyauchi-Hashimoto, H, et al. Shining light on skin pigmentation: the darker and the brighter side of effects of UV radiation. *J Invest Dermatol*. (2014) 140:573–81. doi: 10.1046/j.1365-2133.1999.02754.x

9. Bernard, JJ, Gallo, RL, and Krutmann, J. Photoimmunology: how ultraviolet radiation affects the immune system. *Nat Rev Immunol*. (2019) 19:688–701. doi: 10.1038/s41577-019-0185-9

10. Huang, Y, Li, Y, Hu, Z, Yue, X, Proetto, MT, Jones, Y, et al. Mimicking melanosomes: Polydopamine nanoparticles as artificial microparasols. *ACS Cent Sci*. (2017) 3:564–9. doi: 10.1021/acscentsci.6b00230

11. Chang, NF, Chen, YS, Lin, YJ, Tai, TH, Chen, AN, Huang, CH, et al. Study of hydroquinone mediated cytotoxicity and hypopigmentation effects from UVB-irradiated arbutin and deoxyarbutin. *Int J Mol Sci*. (2017) 18:969. doi: 10.3390/ijms18050969

12. Ahmad, I, Simanyi, E, Guroji, P, Tamimi, IA, Delarosa, HJ, Nagar, A, et al. Toll-like receptor-4 deficiency enhances repair of UVR-induced cutaneous DNA damage by nucleotide excision repair mechanism. *J Invest Dermatol*. (2014) 134:1710–7. doi: 10.1038/jid.2013.530

13. Moriwaki, S, and Takahashi, Y. Photoaging and DNA repair. *J Dermatol Sci*. (2008) 50:169–76. doi: 10.1016/j.jdermsci.2007.08.011

14. Sun, X, Zhang, N, Yin, C, Zhu, B, and Li, X. Ultraviolet radiation and Melanomagenesis: from mechanism to immunotherapy. *Front Oncol*. (2020) 10:951. doi: 10.3389/fonc.2020.00951

15. Borkowski, AW, Kuo, IH, Bernard, JJ, Yoshida, T, Williams, MR, Hung, NJ, et al. Toll-like receptor 3 activation is required for normal skin barrier repair following UV damage. *J Invest Dermatol*. (2015) 135:569–78. doi: 10.1038/jid.2014.354

16. Ding, X, Willenborg, S, Bloch, W, Wickström, SA, Wagle, P, Brodesser, S, et al. Epidermal mammalian target of rapamycin complex 2 controls lipid synthesis and filaggrin processing in epidermal barrier formation. *J Allergy Clin Immunol*. (2020) 145:283–300.e8. doi: 10.1016/j.jaci.2019.07.033

17. He, H, Li, A, Li, S, Tang, J, Li, L, and Xiong, L. Natural components in sunscreens: topical formulations with sun protection factor (SPF). *Biomed Pharmacother*. (2021) 134:111161. doi: 10.1016/j.biopha.2020.111161

18. Schuch, AP, Moreno, NC, Schuch, NJ, Menck, CFM, and Garcia, CCM. Sunlight damage to cellular DNA: focus on oxidatively generated lesions. *Free Radic Biol Med*. (2017) 107:110–24. doi: 10.1016/j.freeradbiomed.2017.01.029

19. Verardo, V, Gómez-Caravaca, AM, Arráez-Román, D, and Hettinga, K. Recent advances in phospholipids from colostrum, milk and dairy by-products. *Int J Mol Sci*. (2017) 18:1–23. doi: 10.3390/ijms18010173

20. Dai, R, Hua, W, Chen, W, Xiong, L, and Li, L. The effect of milk consumption on acne: a meta-analysis of observational studies. *J Eur Acad Dermatology Venereol*. (2018) 32:2244–53. doi: 10.1111/jdv.15204

21. Vincenzetti, S, Polidori, P, Mariani, P, Cammertoni, N, Fantuz, F, and Vita, A. Donkey's milk protein fractions characterization. *Food Chem*. (2008) 106:640–9. doi: 10.1016/j.foodchem.2007.06.026

22. Cunsolo, V, Saletti, R, Muccilli, V, Gallina, S, Di Francesco, A, and Foti, S. Proteins and bioactive peptides from donkey milk: the molecular basis for its reduced allergenic properties. *Food Res Int*. (2017) 99:41–57. doi: 10.1016/j.foodres.2017.07.002

23. Witkowska-Zimny, M, Kamińska-El-Hassan, E, and Wróbel, E. Milk therapy: unexpected uses for human breast milk. *Nutrients*. (2019) 11:944. doi: 10.3390/nu11050944

24. Zeng, L, and Yang, K. Exploring the pharmacological mechanism of Yanghe decoction on HER2-positive breast cancer by a network pharmacology approach. *J Ethnopharmacol*. (2017) 199:68–85. doi: 10.1016/j.jep.2017.01.045

25. Qin, T, Wu, L, Hua, Q, Song, Z, Pan, Y, and Liu, T. Prediction of the mechanisms of action of shenkang in chronic kidney disease: A network pharmacology study and experimental validation. *J Ethnopharmacol*. (2019) 246:112128. doi: 10.1016/j.jep.2019.112128

26. Shannon, P. Cytoscape: A software environment for integrated models of biomolecular interaction networks. *Genome Res*. (2003) 13:2498–504. doi: 10.1101/gr.1239303

27. Young, AR, Narbutt, J, Harrison, GI, Lawrence, KP, Bell, M, O'Connor, C, et al. Optimal sunscreen use, during a sun holiday with a very high ultraviolet index, allows vitamin D synthesis without sunburn. *Br J Dermatol*. (2019) 181:1052–62. doi: 10.1111/bjd.17888

28. Shih, BB, Farrar, MD, Cooke, MS, Osman, J, Langton, AK, Kift, R, et al. Fractional sunburn threshold UVR doses generate equivalent vitamin D and DNA damage in skin types I–VI but with epidermal DNA damage gradient correlated to skin darkness. *J Invest Dermatol*. (2018) 138:2244–52. doi: 10.1016/j.jid.2018.04.015

29. Gaddameedhi, S, Selby, CP, Kemp, MG, Ye, R, and Sancar, A. The circadian clock controls sunburn apoptosis and erythema in mouse skin. *J Invest Dermatol*. (2015) 135:1119–27. doi: 10.1038/jid.2014.508

30. Moore, C, Cevikbas, F, Pasolli, HA, Chen, Y, Kong, W, Kempkes, C, et al. UVB radiation generates sunburn pain and affects skin by activating epidermal TRPV4 ion channels and triggering endothelin-1 signaling. *Proc Natl Acad Sci*. (2013) 110:E3225–34. doi: 10.1073/pnas.1312933110

31. Biniek, K, Levi, K, and Dauskardt, RH. Solar UV radiation reduces the barrier function of human skin. *Proc Natl Acad Sci*. (2012) 109:17111–6. doi: 10.1073/pnas.1206851109

32. Wang, C, Wang, D, Dai, T, Xu, P, Wu, P, Zou, Y, et al. Skin pigmentation-inspired polydopamine sunscreens. *Adv Funct Mater*. (2018) 28:1802127. doi: 10.1002/adfm.201802127

33. Chan, TK, Bramono, D, Bourokba, N, Krishna, V, Wang, ST, Neo, BH, et al. Polycyclic aromatic hydrocarbons regulate the pigmentation pathway and induce DNA damage responses in keratinocytes, a process driven by systemic immunity. *J Dermatol Sci*. (2021) 104:83–94. doi: 10.1016/j.jdermsci.2021.09.003

34. Lee, J, Jung, E, Lee, J, Huh, S, Boo, YC, Hyun, CG, et al. Mechanisms of melanogenesis inhibition by 2,5-dimethyl-4-hydroxy-3(2H)—furanone. *Br J Dermatol*. (2007) 157:242–8. doi: 10.1111/j.1365-2133.2007.07934.x

35. Serre, C, Busuttil, V, and Botto, JM. Intrinsic and extrinsic regulation of human skin melanogenesis and pigmentation. *Int J Cosmet Sci*. (2018) 40:328–47. doi: 10.1111/ics.12466

36. Kocic, H, Stankovic, M, Tirant, M, Lotti, T, and Arsic, I. Favorable effect of creams with skimmed donkey milk encapsulated in nanoliposomes on skin physiology. *Dermatol Ther*. (2020) 33:e13511. doi: 10.1111/dth.13511

37. Brumini, D, Criscione, A, Bordonaro, S, Vegarud, GE, and Marletta, D. Whey proteins and their antimicrobial properties in donkey milk: a brief review. *Dairy Sci Technol*. (2016) 96:1–14. doi: 10.1007/s13594-015-0246-1

38. Cha, JY, Yang, HJ, Moon, HI, and Cho, YS. Branched-chain amino acids complex inhibits melanogenesis in B16F0 melanoma cells. *Immunopharmacol Immunotoxicol*. (2012) 34:256–64. doi: 10.3109/08923973.2011.600764

39. Lin, YS, Wu, WC, Lin, SY, and Hou, WC. Glycine hydroxamate inhibits tyrosinase activity and melanin contents through downregulating cAMP/PKA signaling pathways. *Amino Acids*. (2015) 47:617–25. doi: 10.1007/s00726-014-1895-8

40. Chung, BY, Choi, SR, Moon, IJ, Park, CW, Kim, YH, and Chang, SE. The glutathione derivative, GSH Monoethyl Ester, may effectively whiten skin but GSH does not. *Int J Mol Sci*. (2016) 17:1–11. doi: 10.3390/ijms17050629

41. Niu, C, Yin, L, and Aisa, H. Novel furocoumarin derivatives stimulate melanogenesis in B16 melanoma cells by up-regulation of MITF and TYR family via Akt/GSK3β/β-catenin signaling pathways. *Int J Mol Sci*. (2018) 19:746. doi: 10.3390/ijms19030746

42. Ando, H, Wen, ZM, Kim, HY, Valencia, JC, Costin, GE, Watabe, H, et al. Intracellular composition of fatty acid affects the processing and function of tyrosinase through the ubiquitin-proteasome pathway. *Biochem J*. (2006) 394:43–50. doi: 10.1042/BJ20051419

43. Yamada, H, Hakozaki, M, Uemura, A, and Yamashita, T. Effect of fatty acids on melanogenesis and tumor cell growth in melanoma cells. *J Lipid Res*. (2019) 60:1491–502. doi: 10.1194/jlr.M090712

44. Okajima, S, Hamamoto, A, Asano, M, Isogawa, K, Ito, H, Kato, S, et al. Azepine derivative T4FAT, a new copper chelator, inhibits tyrosinase. *Biochem Biophys Res Commun*. (2019) 509:209–15. doi: 10.1016/j.bbrc.2018.12.105

45. Grabacka, M, Plonka, PM, Urbanska, K, and Reiss, K. Peroxisome proliferator—activated receptor α activation decreases metastatic potential of melanoma cells *in vitro* via down-regulation of Akt. *Clin Cancer Res*. (2006) 12:3028–36. doi: 10.1158/1078-0432.CCR-05-2556

46. Miklas, JW, Clark, E, Levy, S, Detraux, D, Leonard, A, Beussman, K, et al. TFPa/HADHA is required for fatty acid beta-oxidation and cardiolipin re-modeling in human cardiomyocytes. *Nat Commun*. (2019) 10:4671. doi: 10.1038/s41467-019-12482-1

47. Blunder, S, Rühl, R, Moosbrugger-Martinz, V, Krimmel, C, Geisler, A, Zhu, H, et al. Alterations in epidermal eicosanoid metabolism contribute to inflammation and impaired late differentiation in FLG-mutated atopic dermatitis. *J Invest Dermatol*. (2017) 137:706–15. doi: 10.1016/j.jid.2016.09.034

48. Brown, SJ, and McLean, WHI. One remarkable molecule: Filaggrin. *J Invest Dermatol*. (2012) 132:751–62. doi: 10.1038/jid.2011.393

49. Thyssen, JP, and Kezic, S. Causes of epidermal filaggrin reduction and their role in the pathogenesis of atopic dermatitis. *J Allergy Clin Immunol*. (2014) 134:792–9. doi: 10.1016/j.jaci.2014.06.014

frontiers | Frontiers in Nutrition

TYPE Original Research
PUBLISHED 27 March 2023
DOI 10.3389/fnut.2023.1153323

OPEN ACCESS

EDITED BY
Jinxuan Cao,
Beijing Technology and Business University, China

REVIEWED BY
Ishtiyaq Ahmad,
Sher-e-Kashmir University of Agricultural Sciences and Technology, India
Tao Huang,
Ningbo University, China

*CORRESPONDENCE
Li Lin
✉ linli@zhku.edu.cn

†These authors have contributed equally to this work

SPECIALTY SECTION
This article was submitted to Food Chemistry, a section of the journal Frontiers in Nutrition

RECEIVED 29 January 2023
ACCEPTED 03 March 2023
PUBLISHED 27 March 2023

CITATION
Li Q, Huang Y, Zhang X, Zou C and Lin L (2023) Improvement of muscle quality in tilapia (*Oreochromis niloticus*) with dietary faba bean (*Vicia faba* L.).
Front. Nutr. 10:1153323.
doi: 10.3389/fnut.2023.1153323

Improvement of muscle quality in tilapia (*Oreochromis niloticus*) with dietary faba bean (*Vicia faba* L.)

Qingqing Li[1,2†], Yao Huang[1†], Xingqian Zhang[1], Cuiyun Zou[1] and Li Lin[1,2*]

[1]Guangdong Provincial Water Environment and Aquatic Products Security Engineering Technology Research Center, Guangzhou Key Laboratory of Aquatic Animal Diseases and Waterfowl Breeding, College of Animal Sciences and Technology, Zhongkai University of Agriculture and Engineering, Guangzhou, Guangdong, China, [2]Guangdong Zhongshan Tilapia Science and Technology Backyard, Ministry of Education, Guangzhou, Guangdong, China

Tilapia (*Oreochromis niloticus*) is a freshwater fish which is farmed worldwide. Improving the muscle quality of fish has become a major goal while maintaining a sustainable aquaculture system. This research attempts to assess the effect of 0% (FB0), 40%(FB40), 50%(FB50), 60%(FB60) and 70% (FB70) faba bean on the texture parameter, histological analysis, proximate, amino acids, and fatty acids composition in tilapia fed 90days. The results showed that hardness, chewiness, and shear force of tilapia muscle fed FB60, and FB70 were considerably more in comparison to fish fed FB0 at 90days ($p<0.05$). Tilapia fed faba beans had higher muscle fiber density, wider spaces between muscle fibers and smaller fiber diameter, with the greatest difference in tilapia fed FB60. The total protein content in tilapia fed FB40 was considerably more in comparison to in fish fed FB70 ($p<0.05$), where the total protein content in muscle first increased and then reduced with increasing dietary faba bean level. The muscle ∑TAA, ∑EAA, valine, tyrosine, cysteine, aspartic acid, methionine, isoleucine, glutamic acid, leucine, arginine, and serine, contents in tilapia fed FB60 were much more in contrast to in fish fed FB0 ($p<0.05$), which initially increased and then reduced with increasing dietary faba bean level. The muscle ∑PUFA content in tilapia fed dietary faba beans was greater compared with fish fed FB0, whereas the ∑SFA contents in tilapia fed FB50 and FB60 were lower in contrast to in fish fed FB0. In summary, dietary faba beans can improve muscle texture, muscle fibers, amino acids content and fatty acids content in tilapia. The research's results make a contribution to the improved knowledge of the association among muscle quality in tilapia and dietary faba beans.

KEYWORDS

faba bean, texture, muscle fiber, amino acid, fatty acid, *Oreochromis niloticus*

1. Introduction

Tilapia (*Oreochromis niloticus*) is the second most common farmed fin fish group all over the world after carp (1), and its worldwide aquaculture production increased from 2.6 M tons in 2010 to 6.9 M tons in 2020 (2). This production is due to its excellent characteristics, such as rapid growth, high reproduction, resistance to high stocking densities, and high marketability (1, 3). Fish welfare may be impacted owing to increased stress brought on by growing production under intensive culture conditions, which will also have an impact on fish quality (4). The

muscle is the most interesting part of the fish body in terms of aquaculture products. Therefore, to improve muscle quality, more sustainable aquaculture needs to be formed, necessitating better technology and management (5).

The term "fish muscle quality" refers to a group of qualities including freshness, texture, wholesomeness, nutritional content, and integrity. The sensory interpretation and representation of a product's structure or inner construction, as well as its haptic qualities and reaction to stress, are all related to its texture (6). An essential aspect of fish muscle's freshness is its texture, which is influenced by a number of factors including its cohesiveness, hardness, chewiness, springiness, adhesiveness, and resilience (7). Along the fish value chain, textural criteria are widely used to measure fish quality, which primarily entails consideration of how processing as well as handling techniques affect fish products' shelf life as well as consumer preferences and satisfaction (7). Moreover, the quality of muscle is significantly impacted by composition and nutritional value (8). The fatty acid, protein, and amino acid content of fish represents its primary nutritional value (9). The precursors of a number of flavors are amino acids, which could alter the taste indirectly through the Maillard reaction, especially odor and flavor compounds. Through the process of oxidation, which also forms volatile molecules, lipids have a vital part in the cooked flesh of fish. Hence, the aquaculture industry's main problem is how to produce high-quality cultured fish.

Both internal and external elements, such as culture environment (5, 8), food nutrition (10, 11), and genetics (12) have an impact on the quality of fish muscle. Fish flesh quality can be improved through nutrient control, which has been shown to be beneficial (13). Fish muscle quality improvement defined as higher muscle hardness and crispiness by feeding faba bean (*Vicia faba* L.), has gained increasing research interest (14–17). Crisped fish is very popular in China and other countries due to its special flesh quality. A previous study reported that the chewiness, flesh hardness, adhesiveness, and elasticity of grass carp (*Ctenopharyngodon idella*) were significantly increased by feeding the fish faba beans (18). Faba bean supplementation obviously influenced muscle fatty acid composition in the grass carp (19). Therefore, faba beans may be an effective measure for improving fish muscle quality. Understanding the impact of faba beans on skeletal muscle quality is important for optimizing feed used for high-quality tilapia production.

This study aims to assess the impact of various dietary proportions of faba beans on the muscle texture, muscle histology, and nutritional composition of tilapia. The results will contribute to an understanding of the muscle quality affecting the tilapia crisping process.

2. Materials and methods

2.1. Experimental tilapias and diets

A 90-day rearing trial was conducted at the Laboratory of Aquaculture situated at Zhongkai University of Agriculture and Engineering. Faba bean was added to the diets at 0% (FB0, the control group) and 40% (FB40), 50% (FB50), 60% (FB60), and 70% (FB70) as shown in Table 1. When the faba beans content was increased in the diets, the soybean, rapeseed, wheat flour, and soybean oil contents were progressively decreased to maintain the crude protein (31.73% ~ 32.76%) and lipid content (7.52% ~ 7.60%). The dry ingredients of experimental diets were mixed, and oil and water (25% v/w) were added to the dry mixture to form a soft dough, then the mixed dough was extruded and air-dried.

TABLE 1 Ingredients and proximate composition of experimental diets (%, air dry basis).

Ingredients (% dry matter)	Diet 1	Diet 2	Diet 3	Diet 4	Diet 5
Fish meal	10.00	10.00	10.00	10.00	10.00
Soybean meal	25.30	13.70	10.80	7.90	5.00
Rapeseed meal	26.00	14.00	11.00	8.00	5.00
Wheat flour	29.00	13.00	9.00	5.00	1.00
Soybean oil	3.20	2.80	2.70	2.60	2.50
Fish oil	2.50	2.50	2.50	2.50	2.50
$Ca(H_2PO_4)2•H_2O$	1.00	1.00	1.00	1.00	1.00
Vitamin premix	1.50	1.50	1.50	1.50	1.50
Mineral premix	1.50	1.50	1.50	1.50	1.50
Faba bean meal	0.00	40.00	50.00	60.00	70.00
Total	100.00	100.00	100.00	100.00	100.00
Proximate composition					
Crude protein	32.76	32.17	32.03	31.88	31.73
Crude lipid	7.52	7.57	7.58	7.59	7.60
Ash	6.53	6.56	6.81	7.07	7.32
Moisture	6.12	6.11	6.13	6.12	6.14

The 300 tilapias (average initial body weight: 463.86 ± 16.51 g) were randomly and evenly assigned to the above five experimental diets, and triplicate for each experimental diet. The fish were cultured in 15 PVC tank (Φ108 × H120 cm) indoor circulating systems with a density of 20 tilapia/tank. A temperature of 28°C-29°C, dissolved oxygen ≥5 mg/l, pH 7.5, a light intensity of 100 lx and a photoperiod of 14 h in lightness and 10 h in darkness were maintained. The daily feeding amount were given ratios of around 3% of total fish biomass twice a day at 9:00 and 16:00, adjusted in accordance with satiation and residual feed.

2.2. Sample collection

Tilapia was monitored monthly until harvested at 90 days. The survival rate of tilapia in all groups has no significant difference and were greater than 90%. Every 30 days, three tilapias were randomly obtained from each tank. At each sampling point, the fish fasted for 24 h. Fish that were chosen at random were anesthetized rapidly in a 10 l plastic bucket with 20 mg/l clove oil (20). Each tilapia's body weight was measured employing a digital balance and recorded to the nearest 0.01 g. Tilapias were sacrificed by decapitation, peeled and dissected employing sterile scissors from the anus to the throat on ice, followed by removal of visceral mass. The 3 cm × 3 cm × 5 cm muscle samples were isolated for filet texture profile analysis (TPA), and the muscle filet (0.5 cm × 0.5 cm × 0.5 cm) at the junction of the fourth dorsal fin and lateral line scales was sampled with the aid of a scalpel blade, washed in phosphate-buffered saline (PBS) and fixed in 2.5 percent glutaraldehyde for 2 h at room temperature, and then transferred to 4°C for preservation and transportation for transmission

electron microscopy (TEM). The remaining muscle samples were swiftly separated, immediately frozen in liquid nitrogen, and then immediately kept at −80°C. Three muscle samples per group at days were dried used a vacuum freeze-dryer, ground to a fine powder with a mortar and pestle, then stored at −80°C until the proximate, fatty acid, and amino acid composition were determined.

2.3. Texture profile analysis

Texture profile analysis (TPA) of raw tilapia filets was carried out as explained by (21) with certain modifications. Three sampling points for TPA with a volume of 1 cm^3 in duplicate were chosen between the dorsal fin and tail above the lateral line. TPA was carried out utilizing a texture analyzer (TA-X plus, Stable Micro Systems, United Kingdom) fitted out an 8 mm cylinder probe. The muscle textural parameters (chewiness, firmness, resilience, springiness, shear force, and cohesiveness) were determined. At an initial force of 0.1 N and a constant speed of 30 mm/min, two sequent compression cycles were conducted to make sure that the original length of the muscle sample reached 60% deformation.

2.4. Transmission electron microscopy

The tissue blocks were washed with 0.1 M PB (pH 7.4) three times, for a total of 15 min, after the samples were sliced into 1 mm × 1 mm × 2 mm pieces. The tissue blocks were then placed for one to 2 h at room temperature in 1 percent OsO4 in 0.1 M PB (pH 7.4). The tissue blocks were then washed three times in 0.1 M PB (pH 7.4) for 15 min each, followed by 20 min in 30 percent ethanol, 20 min in 50 percent ethanol, 20 min in 70 percent ethanol, 20 min in 80 percent ethanol, and 20 min in 95 percent ethanol. Two washes with 100 percent ethanol for 20 min each were then performed, and then isoamyl acetate for 15 min. The following actions were then taken: Acetone:EMBed 812 = 1:1 for 2–4 h at 37°C; Acetone:EMBed 812 = 1:2 overnight at 37°C; pure EMBed 812 for 5–8 h at 37°C; The pure EMBed 812 was poured into the embedding models and the tissues inserted into the pure EMBed 812, and then left in an oven at 37°C overnight. The embedding models with resin and samples were placed in an oven at 65°C to polymerize for over 48 h. After being taken out of the embedding models, the resin blocks were set aside to cool. The resin blocks were cut into 60–80 nm sections utilizing an ultra-microtome, and the tissues were placed onto 150 mesh cuprum grids with formvar film. 2 percent uranium acetate saturated alcohol solution avoid light staining for 8 min, rinsed in 70 percent ethanol 3 times and then rinsed in ultra-pure water 3 times. 2.6 percent lead citrate avoids CO^2 staining for 8 min, followed by rinsing with ultra-pure water 3 times. The cuprum grids were placed in the grids board and allowed to dry overnight at room temperature after being dried with filter paper. The cuprum grids were observed under TEM (Hitachi, HT7800) and the images were recorded.

2.5. Proximate composition analysis

The fish muscle samples in each treatment group at 90 days was analyzed for moisture content (drying samples in a 105°C oven until constant weight), total lipid content (extracted with chloroform: methanol (2:1, v/v)), and total protein content (Kjeldahl method, utilizing 6.25 N as a protein conversion factor) in accordance with the technique of AOAC (22).

2.6. Amino acid analysis

Each muscle sample (about 0.2 g dry weight) was placed in a 10 ml hydrolysis tube. 10 ml of 6.0 M HCl solution was then added. The samples were left at −20°C for 5 min, filled with nitrogen and sealed, then hydrolyzed in a 110°C drying box for 22 h. The samples were transferred into hydrolysis solution in a 50 ml volumetric flask, rinsed with deionized water several times and the washing solution was pooled. After hydrolysis, 2 ml of the hydrolysate was taken out and evaporated at 60°C under vacuum to dryness in order to eliminate the HCl. In 5 ml of 0.02 N HCl, the hydrolysate was dissolved before being centrifuged used 2,237 x *g*, and then filtered through a 0.45 μm syringe filter. 1 μl of supernatant was employed for amino acid analysis, by means of pre-column orthophthalaldehyde and the 9-formic acid methyl ester of fluorine chlorine derivatization. The tryptophan content was analyzed separately, and pre-weighted samples were hydrolyzed at 5 M NaOH (containing 5% $SnCl_2$, w/v) in 110°C for 20 h. The hydrolysate was neutralized with 6 M HCl following hydrolysis, centrifuged used 2,659 x *g*, and filtered through syringe filter. The retention periods and peak areas of standard amino acids (AAS18-5ML, DCH (Shanghai) Co., Ltd. Shanghai, China) were compared to the identity and quantity of the amino acids. The amino acid contents of muscle were expressed as individual amino acids in gram per 100 grams of dry muscle (g/100 g dry weight).

2.7. Fatty acid analysis

According to Morrison and Smith (23) approach, fatty acid methyl esters (FAME) were created by transesterification with boiling 15% borontrifluoride/methanol (w/w). After injecting the sample into a Thermo trace 1,310 gas chromatograph equipped with an Agilent CP-sil88 fused silica capillary column (length 100.0 m, inner diameter 0.25 mm, film thickness 0.2 μm), the fatty acid content was analytically confirmed utilizing flame ionization detection (FID). The temperature of the injector and detector was maintained at 270°C. The column temperature was first set at 100°C for 13 min, 10°C/min to 180°C for 6 min, 1°C/min to 200°C for 20 min, and 2°C/min to 220°C for 6 min until all FAME were eluted. Helium was employed as the carrier gas, and the flow velocity was 40 ml/min. Individual fatty acids were quantified by making reference to the internal standard, and FAME in the sample was recognized by comparing retention durations with known standards. Fatty acid contents of muscle were expressed as individual fatty acids in milligrams per gram dry muscle (mg/g dry weight).

2.8. Statistical analysis

The mean ± standard error (SE) of the data was computed utilizing SPSS software (version 20.0). Duncan's multiple-range test and one-way analysis of variance (ANOVA) were employed for checking

for the considerable disparity between the treatment groups at the same time points. The linear and quadratic effects of increasing the dietary faba bean level were performed through orthogonal polynomial contrast at the same time points. Differences of $p < 0.05$ were deemed statistically significant.

3. Results

3.1. Texture parameters

The influence of various dietary faba bean levels on the texture parameters were presented in Table 2. The hardness of tilapia muscle fed FB40, FB50, FB60 and FB70 was considerably greater in comparison to that in fish fed FB0 at 30 days ($p < 0.05$), however, no substantial disparity exists in hardness between fish fed FB40, FB50, FB60, and FB70. The hardness of tilapia muscle fed FB60 and FB70 was substantially higher than that in fish fed FB0 at 60 days and 90 days ($p < 0.05$), however, no substantial disparity exists in hardness between fish fed FB0, FB40 and FB50. The chewiness of tilapia fed FB60 and FB70 was substantially higher than that in fish fed FB0 at 60 and 90 days ($p < 0.05$), however, no substantial disparity exists hardness between fish fed FB50, FB60, and FB70. The shear force of tilapia fed FB60 and FB70 was considerably greater in comparison to that in fish fed FB0 at 90 days ($p < 0.05$), but there was no substantially disparity at 30 and 60 days. No substantial impact of dietary faba beans exists on the springiness, cohesiveness, and resilience of tilapia.

3.2. Myofibrillar microstructure

The muscle TEM images of tilapia fed dietary faba bean were shown in Figure 1. The muscle fiber diameter significantly decreased with dietary faba bean in contrast to the control group, while muscle fiber density enhanced substantially with dietary faba bean, especially in fish fed FB60 and FB70. Wider intermyofibrillar spaces were also seen in muscle samples of fish fed faba beans comapred to the control group.

3.3. Proximate composition

The total protein content in tilapia fed FB40 was considerably greater in comparison to that in fish fed FB70 ($p < 0.05$), however, no substantial disparity exists in total protein content between fish fed FB50, FB60, and FB70. The total lipid content in tilapia fed FB40 was substantially less than that in fish fed FB0 ($p < 0.05$), however, there was no substantial disparity in total lipid content between fish fed FB40, FB50, FB60, and FB70. No considerable impact of dietary faba beans exists on the moisture of tilapia (Table 3). The total protein content in muscle initially enhanced followed by reduction with

TABLE 2 Effects of dietary broad bean levels on texture profile analysis in muscle of tilapia *Oreochromis niloticus*.

Items	FB0	FB40	FB50	FB60	FB70	Linear		Quadratic	
						P	R^2	*P*	R^2
30 days									
Hardness	647.75 ± 6.45^{b}	911.90 ± 41.11^{a}	976.30 ± 18.10^{a}	1011.65 ± 39.58^{a}	994.17 ± 10.35^{a}	0.000	0.834	0.000	0.891
Springiness	0.62 ± 0.01	0.60 ± 0.03	0.59 ± 0.01	0.66 ± 0.02	0.62 ± 0.02	0.343	0.100	0.450	0.181
Chewiness	355.04 ± 93.42	405.47 ± 96.32	391.31 ± 30.37	448.46 ± 26.11	418.71 ± 42.38	0.009	0.549	0.037	0.561
Cohesiveness	0.66 ± 0.01	0.59 ± 0.04	0.62 ± 0.02	0.62 ± 0.02	0.62 ± 0.02	0.306	0.116	0.414	0.198
Resilience	0.32 ± 0.01	0.30 ± 0.02	0.32 ± 0.01	0.30 ± 0.01	0.31 ± 0.01	0.672	0.021	0.767	0.064
Shear force	969.30 ± 129.15	1038.73 ± 194.24	1043.57 ± 53.61	950.73 ± 143.10	954.63 ± 14.34	0.807	0.007	0.956	0.011
60 days									
Hardness	688.13 ± 97.62^{b}	940.03 ± 124.04^{ab}	1039.40 ± 182.59^{ab}	1244.97 ± 218.20^{a}	1176.60 ± 87.34^{a}	0.027	0.401	0.098	0.403
Springiness	0.65 ± 0.03	0.68 ± 0.01	0.63 ± 0.01	0.66 ± 0.01	0.65 ± 0.01	0.020	0.436	0.062	0.461
Chewiness	308.80 ± 68.75^{b}	400.64 ± 51.78^{ab}	421.01 ± 25.23^{ab}	460.62 ± 17.14^{a}	456.76 ± 21.40^{a}	0.010	0.500	0.044	0.501
Cohesiveness	0.68 ± 0.02	0.66 ± 0.02	0.65 ± 0.01	0.64 ± 0.01	0.69 ± 0.02	0.643	0.022	0.377	0.195
Resilience	0.32 ± 0.02	0.30 ± 0.01	0.31 ± 0.02	0.32 ± 0.02	0.30 ± 0.01	0.555	0.036	0.698	0.077
Shear force	930.93 ± 58.56	1107.27 ± 90.84	1127.15 ± 26.95	1169.47 ± 111.17	1176.30 ± 129.04	0.342	0.091	0.652	0.091
90 days									
Hardness	707.27 ± 89.75^{b}	1097.87 ± 133.92^{ab}	1108.10 ± 170.80^{ab}	1393.00 ± 52.34^{a}	1329.43 ± 101.31^{a}	0.007	0.503	0.028	0.511
Springiness	0.66 ± 0.03	0.61 ± 0.03	0.64 ± 0.01	0.63 ± 0.02	0.65 ± 0.02	0.560	0.032	0.614	0.093
Chewiness	327.03 ± 58.67^{b}	541.47 ± 75.45^{b}	427.80 ± 64.96^{ab}	586.21 ± 32.90^{a}	550.36 ± 38.71^{a}	0.008	0.482	0.033	0.494
Cohesiveness	0.67 ± 0.02	0.63 ± 0.01	0.65 ± 0.02	0.65 ± 0.01	0.65 ± 0.02	0.152	0.177	0.366	0.182
Resilience	0.31 ± 0.01	0.31 ± 0.01	0.32 ± 0.01	0.32 ± 0.01	0.32 ± 0.01	0.004	0.540	0.016	0.654
Shear force	791.17 ± 95.17^{b}	1171.88 ± 184.93^{ab}	1202.18 ± 117.64^{ab}	1355.03 ± 186.91^{a}	1274.60 ± 69.03^{a}	0.030	0.360	0.105	0.363

Data are represented as mean ± SE ($n = 9$). Using one-way ANOVA, compared with the control, data at the same elapsed time with different letters are significantly different ($P < 0.05$) among treatments.

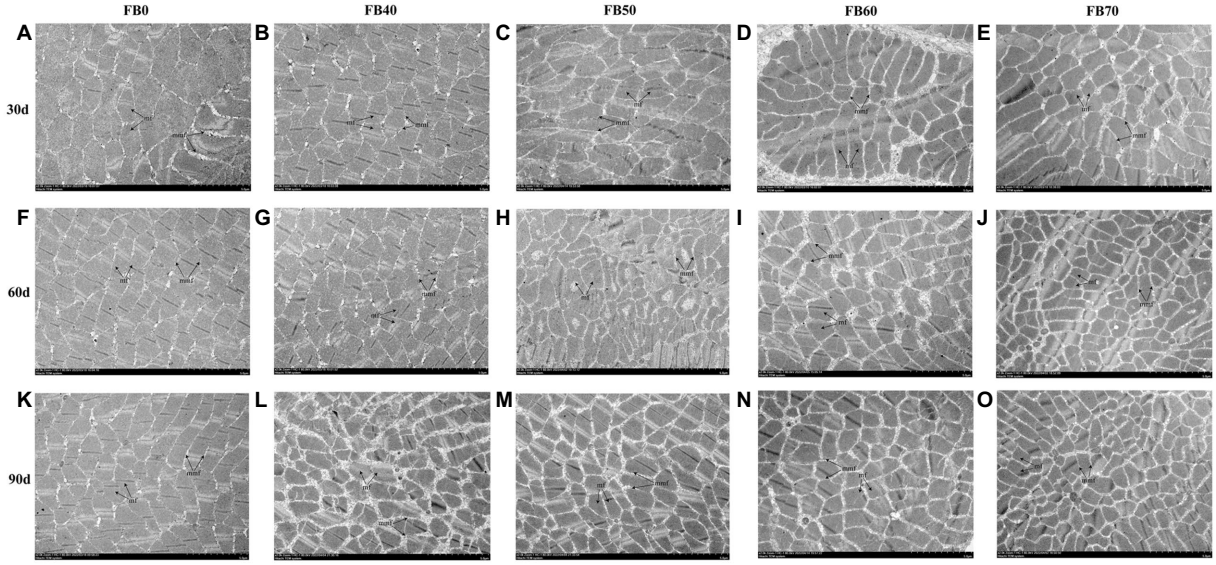

FIGURE 1
Effects of dietary faba bean levels on muscle transverse section microstructure by transmission electron microscope of tilapia *Oreochromis niloticus*. **(A)**, Control group on 30day **(D)**; **(B)**, 40% faba bean group on 30 d; **(C)**, 50% faba bean group on 30 d; **(D)**, 60% faba bean group on 30 d; **(E)**, 70% faba bean group on 30 d; **(F)**, control group on 60 d; **(G)**, 40% faba bean group on 60 d; **(H)**, 50% faba bean group on 60 d; **(I)**, 60% faba bean group on 60 d; **(J)**, 70% faba bean group on 60 d; **(K)**, control group on 90 d; **(L)**, 40% faba bean group on 90 d; **(M)**, 50% faba bean group on 90 d; **(N)**, 60% faba bean group on 90 d; **(O)**, 70% faba bean group on 90 d. mf, muscle fiber; mmf, matrix between muscle fibers.

TABLE 3 Effects of dietary faba bean levels on proximate composition (% dry weight) in muscle of tilapia *Oreochromis niloticus*.

Items	FB0	FB40	FB50	FB60	FB70	Linear		Quadratic	
						P	R^2	*P*	R^2
Moisture	74.85 ± 0.19	75.88 ± 0.27	75.69 ± 0.53	76.19 ± 1.00	75.89 ± 0.18	0.155	0.109	0.226	0.161
Protein	77.78 ± 0.92^{ab}	80.05 ± 0.56^{a}	78.38 ± 0.33^{ab}	78.50 ± 0.54^{ab}	77.58 ± 1.00^{b}	0.878	0.001	0.010	0.416
Lipid	3.88 ± 0.45^{a}	2.37 ± 0.34^{b}	2.68 ± 0.41^{ab}	2.67 ± 0.66^{ab}	2.67 ± 0.35^{ab}	0.222	0.082	0.015	0.392

Data are represented as mean ± SE ($n = 3$). Data with different letters are significantly different in the same tissues ($P < 0.05$) between treatments, and the no letters are not significantly different.

enhancing dietary faba bean level, while the total lipid content indicated the opposite trend.

3.4. Amino acid composition

The muscle ∑TAA content in tilapia fed FB60 was considerably greater in comparison to that in fish fed FB0 ($p < 0.05$), however, no considerable disparity exists in ∑TAA content between fish fed FB40, FB50, FB60, and FB70. The muscle ∑EAA content in tilapia fed FB60 was considerably greater in comparison to that in fish fed FB0 and FB70 ($p < 0.05$), however, no substantial disparity exists in hardness between fish fed FB40, FB50, and FB60. The ∑TAA and ∑EAA contents in tilapia first increased followed by reduction with increasing dietary faba bean level. Regarding valine, essential amino acids, methionine, cysteine, arginine, isoleucine, and leucine contents in tilapia fed FB60 were considerably higher in comparison to those in fish fed FB0 ($p < 0.05$), which first increased followed by reducing with increasing dietary faba bean level. Regarding aspartic acid, non-essential amino acids, serine, and tyrosine contents, and glutamic acid in tilapia fed FB60 were considerably higher in comparison to those in fish fed FB0 ($p < 0.05$), while no substantial impact of dietary faba beans exists on glycine, alanine, and proline contents in tilapia (Table 4).

3.5. Fatty acid composition

The impact of different dietary faba bean levels on the fatty acid contents were presented in Table 5. The muscle ∑SFA and ∑MUFA contents in tilapia fed dietary faba bean (FB40, FB50, FB60, and FB70) were slightly less than those in fish fed FB0, however, not significantly different. The C14:0 and C24:0 contents in fish fed FB40 were considerably lower in contrast to in fish fed FB0 ($p < 0.05$). The ∑MUFA content in muscle was generally not much impacted by dietary faba bean level, except that C16:1 and C18:1n9t decreased with increased dietary faba bean level. The ∑PUFA contents in tilapia fed FB50 and FB60 were slightly more in contrast to those in fish fed FB0, but not substantially different.

4. Discussion

Nutritional content, texture, and appearance are the crucial quality factors that must be determined in fish muscle. The "crisp taste" is the distinctive characteristic of crisp fish, and certain investigations have found indices reflecting this trait (17). Textural parameters (chewiness, hardness, and springiness) have been linked to the "crisp taste" (18, 24, 25). The mechanical processing

TABLE 4 Effects of dietary faba bean levels on amino acid composition (g/100g dry weight) in muscle of tilapia *Oreochromis niloticus*.

Items	FB0	FB40	FB50	FB60	FB70	Linear		Quadratic	
						P	R^2	*P*	R^2
Threonine	3.18 ± 0.03^{c}	3.33 ± 0.04^{ab}	3.37 ± 0.05^{a}	3.34 ± 0.07^{ab}	3.20 ± 0.05^{bc}	0.879	0.001	0.002	0.386
Valine	3.37 ± 0.03^{b}	3.57 ± 0.04^{a}	3.52 ± 0.07^{ab}	3.60 ± 0.07^{a}	3.45 ± 0.05^{ab}	0.412	0.026	0.027	0.250
Cystine	0.37 ± 0.02^{b}	0.40 ± 0.01^{b}	0.41 ± 0.01^{b}	0.48 ± 0.03^{a}	0.36 ± 0.02^{b}	0.635	0.009	0.036	0.233
Methionine	2.27 ± 0.05^{b}	2.38 ± 0.06^{ab}	2.41 ± 0.03^{ab}	2.49 ± 0.08^{a}	2.30 ± 0.06^{b}	0.514	0.017	0.042	0.223
Isoleucine	3.38 ± 0.04^{b}	3.55 ± 0.04^{ab}	3.50 ± 0.06^{ab}	3.68 ± 0.13^{a}	3.46 ± 0.06^{b}	0.292	0.043	0.070	0.191
Leucine	5.49 ± 0.05^{c}	5.83 ± 0.08^{ab}	5.76 ± 0.10^{ab}	5.97 ± 0.20^{a}	5.59 ± 0.10^{bc}	0.480	0.019	0.024	0.259
Histidine	1.78 ± 0.01	1.75 ± 0.05	1.81 ± 0.07	1.77 ± 0.03	1.70 ± 0.04	0.332	0.036	0.358	0.079
Arginine	4.31 ± 0.04^{b}	4.51 ± 0.05^{ab}	4.51 ± 0.07^{ab}	4.54 ± 0.10^{a}	4.40 ± 0.08^{ab}	0.448	0.022	0.036	0.234
Phenylalanine	3.32 ± 0.04^{ab}	3.31 ± 0.05^{ab}	3.29 ± 0.01^{ab}	3.37 ± 0.07^{a}	3.21 ± 0.06^{b}	0.229	0.055	0.322	0.087
Lysine	6.51 ± 0.07	6.79 ± 0.08	6.70 ± 0.12	6.82 ± 0.13	6.59 ± 0.11	0.627	0.009	0.112	0.161
∑EAA	33.96 ± 0.31^{b}	35.41 ± 0.34^{ab}	35.27 ± 0.58^{ab}	36.05 ± 0.88^{a}	34.25 ± 0.60^{b}	0.645	0.008	0.032	0.240
Aspartic acid	6.75 ± 0.08^{b}	7.21 ± 0.08^{a}	7.00 ± 0.09^{ab}	7.09 ± 0.12^{a}	6.82 ± 0.12^{ab}	0.853	0.001	0.030	0.245
Glutamic acid	10.49 ± 0.06^{b}	11.26 ± 0.16^{a}	11.05 ± 0.19^{a}	11.09 ± 0.20^{a}	10.76 ± 0.18^{ab}	0.609	0.010	0.012	0.297
Glycine	3.08 ± 0.04	3.23 ± 0.07	3.24 ± 0.05	3.22 ± 0.06	3.19 ± 0.11	0.372	0.031	0.226	0.112
Alanine	4.11 ± 0.05	4.27 ± 0.07	4.23 ± 0.07	4.25 ± 0.09	4.11 ± 0.06	0.830	0.002	0.104	0.166
Serine	2.81 ± 0.03^{c}	2.97 ± 0.04^{a}	3.04 ± 0.04^{a}	2.96 ± 0.05^{ab}	2.84 ± 0.05^{bc}	0.897	0.001	0.000	0.487
Tyrosine	2.74 ± 0.03^{b}	2.82 ± 0.04^{ab}	2.84 ± 0.02^{ab}	2.89 ± 0.07^{a}	2.81 ± 0.07^{ab}	0.168	0.072	0.089	0.176
Proline	2.27 ± 0.03	2.29 ± 0.08	2.28 ± 0.05	2.17 ± 0.01	2.16 ± 0.09	0.106	0.097	0.212	0.117
Tryptophan	0.42 ± 0.01^{a}	0.42 ± 0.01^{a}	0.35 ± 0.01^{b}	0.35 ± 0.00^{b}	0.32 ± 0.00^{c}	0.000	0.731	0.000	0.732
∑NEAA	32.67 ± 0.25^{b}	34.39 ± 0.44^{a}	34.03 ± 0.48^{ab}	34.00 ± 0.62^{ab}	33.00 ± 0.55^{ab}	0.928	0.000	0.022	0.264
∑TAA	66.63 ± 0.55^{b}	69.79 ± 0.77^{ab}	69.29 ± 1.05^{ab}	70.06 ± 1.50^{a}	67.25 ± 1.13^{ab}	0.772	0.003	0.024	0.258

Data are represented as mean ± SE ($n = 3$). Data with different letters are significantly different in the same tissues ($P < 0.05$) between treatments, and the no letters are not significantly different. ∑EAA: essential amino acids; ∑NEAA: non-essential amino acids; ∑TAA: total amino acids.

of filets and acceptance are both impacted by texture, a crucial quality attribute. Textural features, hardness especially, are linked to the intrinsic structure as well as the properties of components of the flesh and are closely related to the human fish products' visible acceptance (7). The hardness of tilapia fed FB60 and FB70 was considerably higher in contrast to that in fish fed FB0. The increased hardness of muscle because of feeding on faba bean has likewise been mentioned in European seabass (*Dicentrarchus labrax*) (26), Yellow River carp (*Cyprinus carpio haematopterus*) (27), and grass carp (19). When assessing the quality characteristics of a muscle, the shear force is a crucial measure. At 90 days, tilapia fed FB60 and FB70 had shear forces that were noticeably higher than fish fed FB0. Enhanced dietary faba bean levels significantly increased muscle shear force, which is consistent with earlier research on grass carp that found that a partial substitution from soybean to faba beans had an impact on muscle shear force (19). The faba bean contain a variety of anti-nutritional factors such as total phenolics, tannins, and trypsin inhibitor activity. The tilapia muscle texture changes after dietary faba beans might be because of anti-nutritional factors in faba bean.

While the microstructure and structure concentrate on minor alterations in internal features and offer increasing data and further interpret the textural modifications caused by external settings, the textural properties typically focus more on physical information about the fish freshness (6). Fish muscle texture is closely related to myofibrillar structure that is much impacted by rearing situations (7). The current research pointed out that dietary faba bean not only significantly increased hardness, but also significantly reduced muscle fiber diameter and increased muscle density in tilapia. Some studies have also highlighted that textural features have a substantial favorable association with the muscle fiber density (28, 29). Both connections between the density of muscle fibers and muscle hardness showed a clear positive correlation (13, 30). Tilapia muscle fiber density rose at appropriate levels of dietary faba bean, showing that these levels promoted muscle fiber growth and that the rise in density may be linked to hyperplasia.

The muscle's nutrient composition is a key measure for assessing fish meat quality, and the protein and amino acid contents and type can have an effect on value of nutrients, flavor and function of the fish muscle (9). In this study, the muscle ∑TAA content in tilapia fed FB60 was significantly higher than that of fed FB0, which may be the faba beans seeds are rich in protein and amino levels. When the hydrophobicity or acidity of the R group of the side chain of the amino acid is low, it exhibits an umami taste, whereas when the hydrophobicity is high, it exhibits a bitter taste. In the present study, the leucine and arginine contents in tilapia fed 60% faba bean were considerably higher in contrast to the control group, which may be the reason why faba bean transformed the amino acid content structure. Faba bean, with their higher levels of arginine, would supplement some of the ∑EAA compounds, thereby achieving a more balanced

TABLE 5 Effects of dietary broad bean levels on fatty acid composition (mg/g dry weight) in muscle of tilapia *Oreochromis niloticus*.

Items	FB0	FB40	FB50	FB60	FB70	Linear		Quadratic	
						P	R^2	*P*	R^2
C4:0	0.01 ± 0.00	0.01 ± 0.00	0.02 ± 0.00	0.01 ± 0.00	0.01 ± 0.00	0.605	0.021	0.756	0.046
C12:0	0.10 ± 0.01	0.04 ± 0.01	0.05 ± 0.02	0.06 ± 0.020	0.06 ± 0.02	0.178	0.135	0.078	0.346
C13:0	0.01 ± 0.00	0.00 ± 0.00	0.01 ± 0.01	0.01 ± 0.00	0.01 ± 0.00	0.278	0.090	0.430	0.131
C14:0	0.70 ± 0.13^{a}	0.22 ± 0.07^{b}	0.32 ± 0.13^{ab}	0.42 ± 0.13^{ab}	0.36 ± 0.11^{ab}	0.064	0.239	0.034	0.430
C15:0	0.07 ± 0.01	0.06 ± 0.01	0.10 ± 0.03	0.09 ± 0.01	0.09 ± 0.01	0.331	0.073	0.592	0.084
C16:0	7.32 ± 0.86	4.65 ± 0.72	6.00 ± 1.40	6.60 ± 1.12	5.75 ± 1.05	0.397	0.056	0.396	0.143
C17:0	0.07 ± 0.00	0.07 ± 0.01	0.13 ± 0.04	0.07 ± 0.04	0.11 ± 0.01	0.378	0.060	0.689	0.060
C18:0	2.53 ± 0.18	2.27 ± 0.19	2.96 ± 0.45	2.75 ± 0.04	2.57 ± 0.16	0.554	0.028	0.844	0.028
C20:0	0.07 ± 0.00	0.07 ± 0.01	0.12 ± 0.04	0.10 ± 0.02	0.09 ± 0.01	0.172	0.139	0.393	0.144
C21:0	0.01 ± 0.00	0.01 ± 0.00	0.02 ± 0.01	0.02 ± 0.01	0.01 ± 0.00	0.557	0.027	0.847	0.027
C22:0	0.03 ± 0.00	0.03 ± 0.01	0.04 ± 0.02	0.04 ± 0.01	0.03 ± 0.01	0.418	0.051	0.724	0.052
C24:0	0.16 ± 0.01^{a}	0.10 ± 0.01^{b}	0.12 ± 0.02^{ab}	0.12 ± 0.01^{ab}	0.13 ± 0.01^{ab}	0.087	0.208	0.026	0.456
∑SFA	11.07 ± 1.17	7.53 ± 1.04	9.90 ± 2.15	10.29 ± 1.32	9.23 ± 1.40	0.512	0.034	0.507	0.107
C14:1	0.03 ± 0.00^{a}	0.00 ± 0.00^{b}	0.00 ± 0.00^{b}	0.01 ± 0.01^{b}	0.01 ± 0.00^{b}	0.055	0.255	0.005	0.593
C16:1	0.98 ± 0.22^{a}	0.25 ± 0.09^{b}	0.38 ± 0.16^{b}	0.55 ± 0.21^{b}	0.43 ± 0.14^{b}	0.048	0.268	0.029	0.447
C18:1n9t	0.07 ± 0.01^{a}	0.03 ± 0.01^{b}	0.04 ± 0.01^{b}	0.05 ± 0.01^{b}	0.03 ± 0.01^{b}	0.035	0.300	0.034	0.430
C18:1n9c	6.92 ± 1.35	3.94 ± 1.07	5.66 ± 1.98	6.50 ± 1.61	5.15 ± 1.21	0.540	0.030	0.599	0.082
C20:1	0.33 ± 0.06	0.17 ± 0.04	0.29 ± 0.10	0.29 ± 0.06	0.22 ± 0.04	0.372	0.062	0.521	0.103
C22:1n9	0.02 ± 0.00	0.01 ± 0.01	0.02 ± 0.01	0.02 ± 0.01	0.02 ± 0.00	0.658	0.016	0.902	0.017
C24:1	0.01 ± 0.00	0.00 ± 0.00	0.01 ± 0.01	0.01 ± 0.00	0.01 ± 0.00	0.277	0.090	0.382	0.148
∑MUFA	8.36 ± 1.65	4.41 ± 1.22	6.41 ± 2.26	7.43 ± 1.91	5.88 ± 1.41	0.424	0.050	0.476	0.116
C18:2n6c	4.51 ± 0.43	4.80 ± 0.89	6.38 ± 1.83	6.74 ± 1.34	5.78 ± 1.22	0.223	0.112	0.490	0.112
C20:2	0.27 ± 0.03	0.27 ± 0.14	0.56 ± 0.12	0.54 ± 0.03	0.42 ± 0.04	0.073	0.226	0.213	0.227
C22:2	0.01 ± 0.00	0.01 ± 0.01	0.01 ± 0.01	0.02 ± 0.00	0.01 ± 0.00	0.343	0.069	0.406	0.139
C18:3n3	0.35 ± 0.03	0.26 ± 0.08	0.37 ± 0.15	0.41 ± 0.11	0.36 ± 0.10	0.733	0.009	0.830	0.031
C18:3n6	0.22 ± 0.05	0.15 ± 0.05	0.17 ± 0.05	0.22 ± 0.04	0.17 ± 0.05	0.623	0.019	0.705	0.056
C20:3n3	0.07 ± 0.01	0.08 ± 0.01	0.12 ± 0.04	0.12 ± 0.01	0.10 ± 0.01	0.139	0.160	0.342	0.164
C20:3n6	0.40 ± 0.03	0.27 ± 0.14	0.45 ± 0.06	0.51 ± 0.02	0.37 ± 0.05	0.673	0.014	0.815	0.033
C20:4n6	1.53 ± 0.06	1.44 ± 0.04	1.54 ± 0.08	1.52 ± 0.02	1.42 ± 0.15	0.520	0.033	0.803	0.036
C22:6n3	1.66 ± 0.15^{ab}	1.48 ± 0.08^{b}	2.16 ± 0.35^{a}	1.84 ± 0.04^{ab}	1.93 ± 0.20^{ab}	0.264	0.095	0.511	0.106
∑PUFA	9.02 ± 0.62	8.75 ± 1.32	11.77 ± 2.63	11.92 ± 1.50	10.56 ± 1.54	0.246	0.102	0.524	0.102
∑HUFA	3.20 ± 0.17^{ab}	2.92 ± 0.12^{b}	3.70 ± 0.39^{a}	3.37 ± 0.06^{ab}	3.35 ± 0.22^{ab}	0.429	0.049	0.715	0.054
∑n-3PUFA	2.08 ± 0.20	1.81 ± 0.17	2.65 ± 0.54	2.37 ± 0.16	2.38 ± 0.31	0.294	0.084	0.536	0.099
∑n-6PUFA	2.15 ± 0.13	1.86 ± 0.19	2.16 ± 0.17	2.26 ± 0.05	1.96 ± 0.25	0.828	0.004	0.930	0.012
n-6/n-3	1.05 ± 0.12	1.03 ± 0.09	0.87 ± 0.15	0.95 ± 0.01	0.82 ± 0.10	0.140	0.159	0.298	0.183

Data are represented as mean ± SE ($n = 3$). Data with different letters are significantly different in the same tissues ($P < 0.05$) between treatments, and the no letters are not significantly different. The fatty acids content less than 0.1 mg/g dry weight were not in the table. The fatty acids composition of less than 0.01 were not shown in the table. ΣSFA: total amount of saturated fatty acids; ΣMUFA: total amount of monounsaturated fatty acids; ΣPUFA: total amount of polyunsaturated fatty acids; ΣHUFA: highly unsaturated fatty acid; Σn-3PUFA: total amount of *n*-3 polyunsaturated fatty acids; Σn-6PUFA: total amount of n-6 polyunsaturated fatty acids; *n*-6/*n*-3: *n*-6/*n*-3 polyunsaturated fatty acids ratio.

and desirable amino acid profile (31). Prior investigations have claimed that the activity and release of a number of hormones is stimulated by arginine, such as insulin-like growth factor (IGF)-1 and insulin, which stimulate growth, and protein metabolism (32), and leucine has been documented to stimulate postprandial free amino acid synthesis and IGF-1 signaling. The amino acid content was increased in fish fed faba beans, suggesting that faba beans might enhance the flavor of fish muscle and its nutritional value.

The lipid content in muscle is closely associated with flesh's nutritional value, tenderness, and flavor (9), and present fatty acids in muscles of fish have an impact on the well-being of human (33). The total lipid content of the tilapia fed faba bean in the current

study was lower in comparison to control group. The drop in crude lipid content of fish muscle is typically thought to promote friction among muscle bundles, increase muscle hardness, and lessen muscle sensitivity (34). Previous studies have also reported a reduction in muscle lipid content in rainbow trout (*Oncorhynchus mykiss*) (34), Yellow River carp (27) and beluga (*Huso huso*) (35) fed faba bean. This may be attributed to the fact that when some anti-nutritional factors in faba bean goes to a specific level, they influence the process of the transportation of lipids leading to a reduction in fat deposition concentration in the muscle of fish. The species and contents of fatty acids have a significant influence on the nutritional value of lipids. According to the World Health Organization, reducing the amount of saturated fatty acids and rising amount of unsaturated fatty acids in the human diet can improve nutrition and help prevent chronic diseases (36). Tissue fatty acid content of farmed fish has been reported to be greatly to be greatly influenced by dietary nutritional composition. The faba bean are rich fatty acid and have particularly high unsaturated fatty acid levels (31). In the current investigation, the total ∑SFA content reduced and ∑PUFA content enhanced, suggesting that dietary faba bean might enhance the health effects of fish muscle.

5. Conclusion

The outcomes of the current investigation revealed that dietary faba bean increased hardness, shear force and muscle fiber diameter in tilapia. These outcomes indicate that the smaller size of the fiber and increased fiber density played a major role in the better filet texture of tilapia. Faba bean also influenced muscle amino acid composition, lipids, saturated and unsaturated fatty acid contents. The current investigation effectively showed that dietary faba bean levels significantly affected texture, histology, and amino acid composition in tilapia over the 90-days feeding experiment. To better understand how faba beans regulate the quality of the tilapia muscle, more research should be done.

Data availability statement

The raw data supporting the conclusions of this article will be made available by the authors, without undue reservation.

Ethics statement

The animal study was reviewed and approved by Committee on Animal Research and Ethics of Zhongkai University of Agriculture and Engineering.

Author contributions

QL was responsible for the conception and design of the experiments and writing the manuscript. YH was collected samples and performed the detection of nutrition index. XZ was organized the data and visualized part of the data. CZ was responsible for the visualization of figures and the revision of the manuscript. LL was provided supervision, validation, and funding support. All authors contributed to the manuscript and gave their approval for its submission.

Funding

This work was supported by the Guangdong Province Commissioner for Rural Science and Technology in Towns and Village [grant number KTP20210236]; the Key Research and Development Program of Guangzhou City [grant number 202103000067]; and the College Student Innovation and Entrepreneurship Training Program [grant number S202211347069].

Conflict of interest

The authors declare that the research was conducted in the absence of any commercial or financial relationships that could be construed as a potential conflict of interest.

Publisher's note

All claims expressed in this article are solely those of the authors and do not necessarily represent those of their affiliated organizations, or those of the publisher, the editors and the reviewers. Any product that may be evaluated in this article, or claim that may be made by its manufacturer, is not guaranteed or endorsed by the publisher.

References

1. Wang M, Lu MX. Tilapia polyculture: a global review. *Aquac Res.* (2016) 47:2363–74. doi: 10.1111/are.12708

2. FAO. *Fishery and Aquaculture Statistics in 2022: Sustaiable Development in Action*. Rome: FAO (2022).

3. Ng W-K, Romano N. A review of the nutrition and feeding management of farmed tilapia throughout the culture cycle. *Rev Aquacult.* (2013) 5:220–54. doi: 10.1111/raq.12014

4. Yilmaz S. Effects of dietary caffeic acid supplement on antioxidant, immunological and liver gene expression responses, and resistance of *Nile tilapia*, *Oreochromis niloticus* to *Aeromonas veronii*. *Fish Shellfish Immun.* (2019) 86:384–92. doi: 10.1016/j.fsi.2018.11.068

5. He JZ, Feng PF, Lv CF, Lv M, Ruan ZD, Yang HZ, et al. Effect of a fish–rice co-culture system on the growth performance and muscle quality of tilapia (*Oreochromis niloticus*). *Aquac Rep.* (2020) 17:100367. doi: 10.1016/j.aqrep.2020.100367

6. Coppes Z, Pavlisko A, Vecchi SD. Texture measurements in fish and fish products. *J Aquat Food Prod Technol.* (2008) 11:89–105. doi: 10.1300/J030v11n01_08

7. Cheng JH, Sun DW, Han Z, Zeng XA. Texture and structure measurements and analyses for evaluation of fish and fillet freshness quality: a review. *Compr Rev Food Sci Food Saf.* (2014) 13:52–61. doi: 10.1111/1541-4337.12043

8. Zhang X, Wang JW, Tang R, He XG, Li L, Takagi Y, et al. Improvement of muscle quality of grass carp (*Ctenopharyngodon idellus*) with a bio-floating bed in culture ponds. *Front Physiol.* (2019) 10:683. doi: 10.3389/fphys.2019.00683

9. Jiang WD, Wu P, Tang RJ, Liu Y, Kuang SY, Jiang J, et al. Nutritive values, flavor amino acids, healthcare fatty acids and flesh quality improved by manganese referring to up-regulating the antioxidant capacity and signaling molecules TOR and Nrf2 in the muscle of fish. *Food Res Int.* (2016) 89:670–8. doi: 10.1016/j.foodres.2016.09.020

10. Yang S-D, Wen Y-C, Liou C-H, Liu F-G. Influence of dietary l-carnitine on growth, biological traits and meat quality in tilapia. *Aquac Res.* (2009) 40:1374–82. doi: 10.1111/j.1365-2109.2009.02234.x

11. De Magalhaes CR, Schrama D, Fonseca F, Kuehn A, Morisset M, Ferreira SR, et al. Effect of EDTA enriched diets on farmed fish allergenicity and muscle quality; a proteomics approach. *Food Chem.* (2020) 305:125508:125508. doi: 10.1016/j.foodchem.2019.125508

12. Cai L, Tong F, Tang T, Ao Z, Wei Z, Yang F, et al. Comparative evaluation of nutritional value and flavor quality of muscle in triploid and diploid common carp: application of genetic improvement in fish quality. *Aquaculture*. (2021) 541:736780. doi: 10.1016/j.aquaculture.2021.736780

13. Dong M, Zhang L, Wu P, Feng L, Jiang W, Liu Y, et al. Dietary protein levels changed the hardness of muscle by acting on muscle fiber growth and the metabolism of collagen in sub-adult grass carp (*Ctenopharyngodon idella*). *J Anim Sci Biotechnol*. (2022) 13:109:109. doi: 10.1186/s40104-022-00747-7

14. Azaza MS, Wassim K, Mensi F, Abdelmouleh A, Brini B, Kraïem MM. Evaluation of faba beans (*Vicia faba* L. var. *minuta*) as a replacement for soybean meal in practical diets of juvenile Nile tilapia *Oreochromis niloticus*. *Aquaculture*. (2009) 287:174–9. doi: 10.1016/j.aquaculture.2008.10.007

15. Lun F, Leng XJ, Meng XL, Liu XM. Effect of feeding broad bean on muscle quality of tilapia. *J Shanghai Fish Univ*. (2007) 16:83–6. doi: 10.3969/j.issn.1004-7271.2007.01.015

16. Tian JJ, Fu B, Yu EM, Li YP, Xia Y, Li ZF, et al. Feeding faba beans (*Vicia faba* L.) reduces myocyte metabolic activity in grass carp (*Ctenopharyngodon idellus*). *Front Physiol*. (2020) 11:391. doi: 10.3389/fphys.2020.00391

17. Feng J, Lin WL, Li LH, Yang XQ, Wang JX, Huang H, et al. Advances in effects of broad bean on crispness in fish. *Sci Techno Food Ind*. (2016) 37:395–9. doi: 10.13386/j.issn1002-0306.2016.14.070

18. Yang S, Li L, Qi B, Wu Y, Hu X, Lin W, et al. Quality evaluation of crisp grass carp (*Ctenopharyngodon idellus* C. ET V) based on instrumental texture analysis and cluster analysis. *Food Anal Method*. (2015) 8:2107–14. doi: 10.1007/s12161-015-0101-2

19. Li XX, Chen SJ, Sun JJ, Huang XD, Tang HJ, He YH, et al. Partial substitution of soybean meal with faba bean meal in grass carp (*Ctenopharyngodon idella*) diets, and the effects on muscle fatty acid composition, flesh quality, and expression of myogenic regulatory factors. *J World Aquacult Soc*. (2019) 51:1145–60. doi: 10.1111/jwas.12671

20. Iversen M, Finstad B, McKinley RS, Eliassen RA. The efficacy of metomidate, clove oil, Aqui-S™ and Benzoak® as anaesthetics in Atlantic salmon (*Salmo salar* L.) smolts, and their potential stress-reducing capacity. *Aquaculture*. (2003) 221:549–66. doi: 10.1016/S0044-8486(03)00111-X

21. Xie X, Zhai XQ, Li F, Deng JC, Yang XQ, Liang SW, et al. Comparative analysis of physicochemical and nutritional properties between crisp and normal tilapia. *J Fish China*. (2021) 46:1439–48. doi: 10.11964/jfc.20211113162

22. AOAC. *Official Methods of Analysis of the Association of Official Analytical Chemists. 16th* ed. Arlington: Association of Analytical Communities International (1995).

23. Morrison WR, Smith LM. Preparation of fatty acid methyl esters and dimethylacetals from lipids with boron fluoride-methanol. *J Lipid Res*. (1964) 5:600–608. doi: 10.1016/S0022-2275(20)40190-7

24. Lin WL, Zeng QX, Zhu ZW. Different changes in mastication between crisp grass carp (*Ctenopharyngodon idellus* c.et V) and grass carp (*Ctenopharyngodon idellus*) after heating: the relationship between texture and ultrastructure in muscle tissue. *Food Res Int*. (2009) 42:271–8. doi: 10.1016/j.foodres.2008.11.005

25. Ma LL, Kaneko G, Wang XJ, Xie J, Tian JJ, Zhang K, et al. Effects of four faba bean extracts on growth parameters, textural quality, oxidative responses, and gut characteristics in grass carp. *Aquaculture*. (2020) Article 734620) 516:734620. doi: 10.1016/j.aquaculture.2019.734620

26. Adamidou S, Nengas I, Alexis M, Foundoulaki E, Nikolopoulou D, Campbell P, et al. Apparent nutrient digestibility and gastrointestinal evacuation time in European seabass (*Dicentrarchus labrax*) fed diets containing different levels of legumes. *Aquaculture*. (2009) 289:106–12. doi: 10.1016/j.aquaculture.2009.01.015

27. Song D, Yun Y, Mi J, Luo J, Jin M, Nie G, et al. Effects of faba bean on growth performance and fillet texture of Yellow River carp, *Cyprinus carpio haematopterus*. *Aquac Rep*. (2020) 17:100379:100379. doi: 10.1016/j.aqrep.2020.100379

28. Purslow PP. Intramuscular connective tissue and its role in meat quality. *Meat Sci*. (2005) 70:435–47. doi: 10.1016/j.meatsci.2004.06.028

29. Johnston IA, Alderson R, Sandham C, Dingwall A, Mitchell D, Selkirk C, et al. Muscle fibre density in relation to the colour and texture of smoked Atlantic salmon (*Salmo salar* L.). *Aquaculture*. (2000) 189:335–49. doi: 10.1016/S0044-8486(00)00373-2

30. Wang Y, Liang J, Miyazaki R, Sun HY, Zhao XX, Hirasaka K, et al. Influence of the interposition of pink muscle fibers in the dorsal ordinary muscle on the postmortem hardness of meat in various fishes. *J Text Stud*. (2021) 52:358–67. doi: 10.1111/jtxs.12587

31. Meng Z, Liu Q, Zhang Y, Chen J, Sun Z, Ren C, et al. Nutritive value of faba bean (*Vicia faba* L.) as a feedstuff resource in livestock nutrition: a review. *Food Sci Nutr*. (2021) 9:5244–62. doi: 10.1002/fsn3.2342

32. Mommsen TP. Paradigms of growth in fish. *Comp Biochem Physiol B*. (2001) 129:207–19. doi: 10.1016/S1096-4959(01)00312-8

33. Mekonnen MF, Desta DT, Alemayehu FR, Kelikay GN, Daba AK. Evaluation of fatty acid-related nutritional quality indices in fried and raw nile tilapia, (*Oreochromis niloticus*), fish muscles. *Food Sci Nutr*. (2020) 8:4814–21. doi: 10.1002/fsn3.1760

34. Ouraji H, Zaretabar A, Rahmani H. Performance of rainbow trout (Oncorhynchus mykiss) fingerlings fed diets containing different levels of faba bean (*Vicia faba*) meal. *Aquaculture*. (2013) 416-417:161–5. doi: 10.1016/j.aquaculture.2013.09.013

35. Soltanzadeh S, Esmaeili FA, Ouraji H, Khalili KJ. Growth performance, body composition, hematological, and serum biochemical responses of beluga (Huso huso) juveniles to different dietary inclusion levels of faba bean (*Vicia faba*) meal. *Aquac Int*. (2015) 24:100379:395–413. doi: 10.1007/s10499-015-9933-4

36. Li K, Sinclair AJ, Zhao F, Li D. Uncommon fatty acids and cardiometabolic health. *Nutrients*. (2018) 10:1559. doi: 10.3390/nu10101559

Frontiers in Nutrition

Explores what and how we eat in the context of health, sustainability and 21st century food science

A multidisciplinary journal that integrates research on dietary behavior, agronomy and 21st century food science with a focus on human health.

Discover the latest Research Topics

See more →

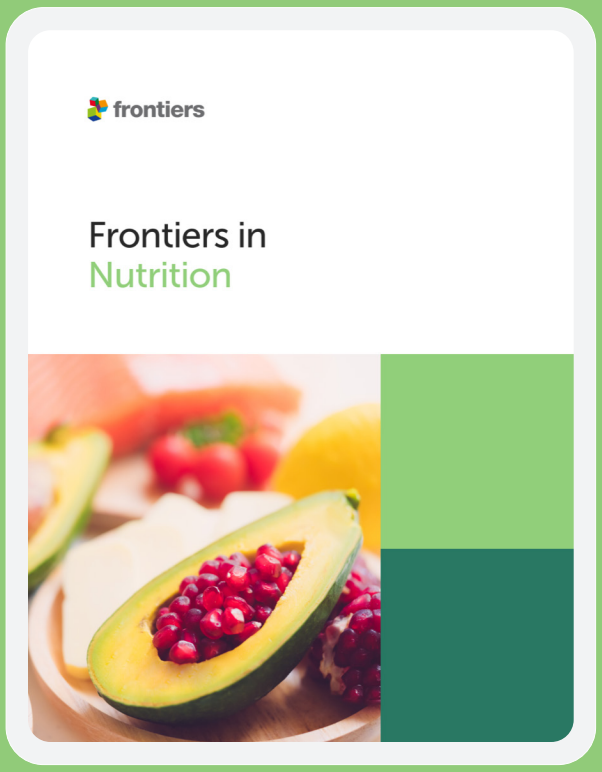

Frontiers

Avenue du Tribunal-Fédéral 34
1005 Lausanne, Switzerland
frontiersin.org

Contact us

+41 (0)21 510 17 00
frontiersin.org/about/contact